UNIVERSITE D'ABOMEY - CALAVI (UAC)

INSTITUT NATIONAL DE L'EAU

Registered under N°: **2769-20/UAC/VR-AA/SA**

A DISSERTATION

Submitted

In partial fulfillment of the requirements for the degree of

DOCTOR of Philosophy (PhD) of the University of Abomey- Calavi (Benin Republic)

In the framework of the

Graduate Research Program on Climate Change and Water Resources (GRP-CCWR)

by

Djan'na KOUBODANA HOUTETA

Public defense on: 02/27/2020

======

MODELING THE IMPACTS OF CLIMATE CHANGE, LAND USE CHANGE AND DAM MANAGEMENT ON WATER RESOURCE IN WEST AFRICA: CASE OF THE MONO RIVER BASIN, TOGO-BENIN

======

Supervisors

Julien G. ADOUNKPE, Associate Professor, University of Abomey-Calavi, Bénin
Bernd DIEKKRÜGER, Full Professor, University of Bonn, Germany
Kossi ATCHONOUGLO, Associate Professor, University of Lomé, Togo

======

Reviewers:

Benjamin N'GOUNOU NGATCHA	Full Professor University of Ngaoundéré, Cameroun	Reviewer
Masamaéya D. T.GNAZOU	Associate Professor, University of Lomé, Togo	Reviewer
Ernest AMOUSSOU	Associate Professor, University of Parakou, Bénin	Reviewer

======

JURY

Jean Bio CHABI OROU	Full Professor, University of Abomey-Calavi, Bénin	President
Benjamin N'GOUNOU NGATCHA	Full Professor, University of Ngaoundéré, Cameroun	Reviewer
Masamaéya D. T.GNAZOU	Associate Professor, University of Lomé, Togo	Reviewer
Ernest AMOUSSOU	Associate Professor, University of Parakou, Bénin	Reviewer
Albert Bi Tié GOULA	Full Professor, University of Nangui Abogoua, Côte d'Ivoire	Examiner
Kossi ATCHONOUGLO	Associate Professor, University of Lomé, Togo	Co-supervisor
Julien G. ADOUNKPE	Associate Professor, University of Abomey-Calavi, Bénin	Supervisor

Dedication

To the soul of my dears mother and father who have educated me a lot

Acknowledgements

A PhD thesis is a long journey like building a house. This cannot be achieved without material, financial assistance and encouragement of many people and organizations. Through these lines, I would like to express my gratitude to those who make this work possible by their assistance, encouragement and aids.

This thesis is realized in the framework of the West African Science Service on Climate Change and Adapted Land use (WASCAL) with the financing from by German Ministry of Education and Research (BMBF) in collaboration with the Benin Ministry of High Education and Scientific Research (MESRS). Therefore my sincere appreciation goes to the Federal Ministry of Education and Research (BMBF) and West African Science Centre on Climate Change and Adapted Land Use (WASCAL) for providing the scholarship and financial support during this thesis.

I am also grateful to the International Foundation for Science (IFS) Karlavägen 108, SE-11526, and Stockholm, Sweden for funding partly this work and for the next part of this study which will focus on modeling the impacts of land use, climate change and dam management on past and future scenarios extremes events.

This dissertation work has been possible through the generous contributions of many people.

My deepest gratitude goes to Professor Julien G. Adounkpe, the Director of my PhD thesis for his guidance and support throughout the three academic years.

I express my sincere gratitude to Prof. Dr. Bernd Diekkrüger Head of Hydrology Research Group (HRG), department of Geography at University of Bonn in Germany. He has supported me from the incept of my doctoral research to its end. His valuable guidance, supports, encouragements, and comments cannot be forgotten. I am also thankful to Prof Kossi Atchonouglo from university of Lomé in Togo for his advices and support during this long journey.

I also express my gratitude to the administrative team of WASCAL Graduate Research Program (GRP) of University of Abomey Calavi (UAC), Benin especially Prof Abel Afouda, the former director of the GRP under whom I started my PhD journey before the taking over by Professor Julien G. Adounkpe, the Deputy Director of WASCAL UAC program Prof Emmanuel A. Lawin for his advices and directives, staff of the GRP Mr Salem Kore and Mrs Imelda Djagoun.

I would also like the thank Professor Ernest Amoussou for his assistance and advices during this thesis for sharing his data with me and making criticism in my work. My best regard to Drs Hèou M. Badjana, Kossi Komi and Badabate Diwediga, Djigbo. F. Badou and Eliezer I. Biaou for their assistance, advices during this thesis. Particlary many thanks to Dr Hèou M.

Badjana who has introduced me to Prof .Dr Bernd Diekkrüger at the first hand and assists me from the proposal development to the end of this thesis.
Many thanks to the colleagues from HRG at University of Bonn in Germany that I met during my scientific visit particulaty, Mr Mouhamed Idrissou, Dr Thomas Poméon, Dr Kristian Naschen, Mrs Claudia Schepp, Dr Iken Rabbel, Mr Emmanuel Nkundimana and Dr Gregorian Haik for his administrative arrangement during my scientific visit at University of Bonn. It was a wonderful experience for being part of the team! I can remember the several times we hiked around Bonn areas.
I would like to thank my former supervisor of Master degree Dr Gael Alory at university of Paul Sabatier of Toulouse (France) for his support during the application to WASCAL program. Fellow students Mr Moustapha Tall, Mr Femi Adeyeri, Mr Isaac Larbi, Mr Abdou Boko, Mrs Oumou Diancoumba, Mr Abdelaziz Kouakou, Mrs Rita Houngue, Mrs Adama Jallow and Mrs Samiratou Oueremi thanks for the support and assistance we shared. I do not forget others GRP students and all my colleagues of Laboratoire d'Energie Solaire (LES) at University of Lomé (Togo).
Thanks to my colleagues and friends Dr Muhammad Mumtaz, Mr Koffi Worou, Mr Koba Afoudji, Mr Dambre Kougbanane, Mr Spéro Edikou, Mr Niyem Mawenbe Bawana, Mr Salima Dorouwa, Mr Hani Kpessou, Mr Thomas Barota, Ing. Padayô Kpekpassi and Mr Abalo Pekele.
My gratitudes to all the members of WASCAL GRP Togo and particularly to the former Director Prof Kokou Kouami, to the New Director Komi Agboka and to the staff Mrs Sefako Segbe, Mr Folly Kuevi and Mr Koudjo Akpene for their assistance during my stay in the institute
Thanks to Mrs Rosa N. A. Gómez, Dr Guely Isidore, and Mr Lekan Tobi for English proofreading some document sections or the whole.
To all my parents, brothers, sisters, uncle, friends and to all my family Koubodana, specialy Mrs Dida, Mrs Takélana, Mr Doguina, Mrs Loguina, Mr Alanda, Mr Kalintiga, Mr Nankourama, Mr Mawelabena, Tomwéna, Dissirama, Major Serge Hodba-Tolma, ect. In particular thank to my uncle Mr Faustin Kassawa Soka for the support and for driving from Lomé to Cotonou with family members to participate to my defense. Thanks for your encouragements, your supports and for being always with me during the difficult moments.
Many thank to my Dear Mrs Adjo Zognira for being available for me, supportive, patient, understanding and prayerfull.
Finally, for all people I did not mention here, please forgive me and accept my greetings.

Abstract

A good understanding of climate change, land-use change and dam management impacts on water balance components must enable the development of sustainable water resources strategies in West Africa. The Mono River Basin (MRB) in West Africa is a river basin shared with Togo and Benin Republics. Its contributions to the socio economic development of the region are needless to emphasize. But its course has been lately subject to several human activities such as dam construction that may have modified its functions. The present study objectives are to analyze the accuracy of CILSS, ESA and Globeland30 land cover datasets between 1975 and 2013, to investigate climate change detection via trend analysis on the hydro-climatic datasets over the period of 1961 to 2016, to simulate and compare discharge using empirical lumped, and to assess water balance component changes using semi- distributed hydrological models over two baseline periods in the Mono River Basin. The methodological approaches consist in land cover reclassification and accuracy evaluation. The three datasets were used to predict future LULC changes between 2020 and 2027 using the Terrset Land Change Modeler. Afterward, the non-parametric Mann Kendall (MK) trend analysis of historical hydro-climatic data was applied, and these data sets were used as inputs for the lumped models, GR4J (Génie Rural à 4 paramètres Journaliers), IHACRES (Identification of unit Hydrographs and Component flows from Rainfall, Evapotranspiration and Stream data) and SWAT (Soil, and Water Assessment Tool) simulations are undertaken. The results indicate for the accurate CILSS data set, there are an increase of 30.97% of cropland area, the losses of (6.91%) of forest area and the decrease of (25.59%) of savanna between 1975 to 2013 and are explained by the increase in population and their food demand. The climate change detection analysis reveals positive and negative trends of hydro-climatic data over MRB from 1961 to 2016. Mean temperatures increase at $\alpha = 0.01$ and 0.05 significance levels in the three stations investigated whereas a negative non-significant trend is noticed for average rainfall. Meanwhile, the discharge presents a significant seasonal and annual trend for three gauge stations investigated. An acceptable accuracy ($R^2 \geq 0.9$) of validated ensemble climate models allow the computation of extreme climate indices under RCP4.5 and RCP8.5 scenarios which shows a significant annual trend of some climate extreme indices of rainfall and temperature at three selected stations between 2020 and 2045. The hydrological modeling analysis indicates that the two lumped models discharge predictions are acceptable with evaluation efficiencies over pre-dam period (1964 – 1986) and more and less acceptable during post-dam period (1988-2010). IHACRES model was found to underestimating extreme high runoff in the downstream of MRB (1964-1986). Finally, the simulation with SWAT semi distributed model performances and uncertain-

ty analysis show that there are good model performances (Calibration_1964-1975; R^2> 0.60; KGE ≥ 0.70 et PBIAS ≤ ± 4.5; validation_1976 - 1986: KGE ≥ 0.50 and PBIAS ≤ ± 3.40) and acceptable parameters values range between 1964 and 1986. Conversely, there are poor model performances (calibration_1988-2000: KGE ≥ 0.60 and PBIAS ≤ ± 20); validation_2001-2011: KGE ≥0.24 and PBIAS ≤ ± 17.20) during the second period (1988-2010). An individual assessment of surface runoff, evapotranspiration and water yield components shows that its seasonal and annual variability depends on different land-use type change, climate conditions and also on the presence or not of reservoir in the watershed. This indicates that the implementation of the dam on the MRB in 1987 has affected the hydrological system of the river. Land use land cover change with the amplification of climate change are the others drivers accelerating this change. The study has proposed effective strategies for better planning and management of water resources in MRB such as land use management, climate change adaptation basin and Nangbéto reservoir reliable managements.

Keywords: Land covers change, climate change detection, sensitive analysis; dam management; hydrological modeling; Mono River Basin.

Synthèse de la Thèse

***Titre de la thèse**:* Modélisation des impacts du changement climatique, du changement d'occupation des terres et de la gestion d'un barrage sur les ressources en eau en Afrique de l'Ouest: cas du bassin versant du Mono, Togo-Bénin

Résumé

Une bonne compréhension des impacts du changement climatique, des changements d'occupation des terres (COCT) et de la gestion des barrages sur les composantes du bilan hydrique doit permettre l'élaboration des stratégies durables de la gestion des ressources en eau en Afrique de l'Ouest. Le bassin de la rivière Mono (MRB) en Afrique de l'Ouest est un bassin transfrontalier partagé par les républiques du Bénin et du Togo. Il est inutile de souligner sa contribution au développement socio-économique dans la région. Mais son cours a récemment fait l'objet de plusieurs activités humaines, telles que la construction de barrages, la déforestation et l'utilisation anarchiques des terres qui ont modifié les fonctions hydrologiques du bassin. Les objectifs de la présente étude sont d'analyser la précision des données d'occupation des terres de CILSS, de l'ESA et de Globeland30 entre 1975 et 2013 puis de développer des scenarios future entre 2020 et 2027, d'étudier l'analyse des tendances du changement climatique sur les données hydro-climatiques de 1961 à 2016, de prédire et de comparer les débits en utilisant des modèles hydrologiques empiriques individuel puis évaluer les modifications des composantes du bilan hydrique à l'aide d'un model semi-distribué pour deux périodes de référence, en tenant compte des changements d'occupation des terres ainsi que des impacts du changement climatique sur le bassin de la rivière Mono en Afrique de l'Ouest. Les approches méthodologiques consistent en une reclassification des cartes d'occupation des terres et une évaluation de leur précision. Les trois jeux de données ont été utilisés pour prédire les scenarios futurs COCT à l'aide de l'outil Terrset Land Change Modeler. Ensuite, l'analyse non paramétrique de la tendance de Mann Kendall (MK) des données hydro-climatiques historiques a été appliquée tant sur le bassin moyen ainsi qu'au niveau des stations individuelles de Tabligbo, Atakpamé et Sokodé. Ces jeux de données ont été utilisés comme données d'entrée pour la modélisation hydrologique à l'aide des modèles empiriques GR4J (Génie Rural à 4 paramètres Journaliers), IHACRES (Identification of unit Hydrographs and Component flows from Rainfall, Evapotranspiration and Stream data) et semi-distribué SWAT (Soil and Water Assessment Tool). Les résultats indiquent pour l'ensemble de données meilleures de CILSS une augmentation de 30,97% de la superficie des terres cultivées, engendrant des pertes de (6,91%) de la superficie forestière et la diminution de (25,59%) de la savane de 1975 à 2013 Ceci s'explique par l'augmentation de la population

togolaise/Béninoise entre 1975 et 2015 et de la demande alimentaire. L'analyse de détection du changement climatique révèle des tendances positives et négatives des données hydro-climatiques dans le bassin pour la période de 1961 à 2016. Les températures moyennes augmentent à $\alpha = 0,01$ et à 0,05 niveaux de significativité des stations de Tabligbo, Atakpamé et Sokodé étudiées, alors qu'une tendance négative non significative est observée pour les précipitations moyennes sur le bassin. Dans le même temps, le débit indique une tendance saisonnière et annuelle significative pour les trois stations de jaugeage étudiées. Ensuite une bonne précision ($R^2 \geq 0.50$) du modèle climatique après validation permet de calculer les indices climatiques des extrêmes selon les scénarios RCP4.5 et RCP8.5. Ceux -ci montrent une tendance annuelle significative de certains indices climatiques des extrêmes de précipitations et de température dans trois stations sélectionnées entre 2020 et 2045. L'analyse par modélisation hydrologique indique que les prévisions de débit des deux modèles empiriques sont acceptables, avec des efficacités d'évaluation sur la période antérieure à l'installation du barrage (1964-1986) et plus ou moins acceptables au cours de la période postérieure à l'installation du barrage (1988-2010). On a constaté que le modèle IHACRES sous-estimait le ruissellement extrême en aval du bassin (1964-1986). Enfin, les performances de la simulation avec le modèle semi-distribué SWAT et l'analyse de l'incertitude montrent qu'il existe de bonnes performances du modèle (Calage 1964-1975; $R^2 > 0,60$; KGE $\geq 0,70$ et PBIAS $\leq \pm 4,5$); cependant la validation_1976 - 1986: KGE $\geq 0,48$ et PBIAS $\leq \pm 3,40$) et les valeurs de paramètres acceptables pour la période entre 1964 et 1986. Les performances sont médiocres (calage_1988-2000: $R^2 > 0,25$; KGE $\geq 0,60$ et PBIAS $\leq \pm 20$; validation_2001-2011: KGE $\geq 0,24$ et PBIAS $\leq \pm 17,20$) au cours de la deuxième période de simulation (1988-2010). L' évaluation individuelle des composants de ruissellement, d'évapotranspiration et de débit d'eau montre que sa variabilité saisonnière et annuelle dépend de différents types de changement d'occupation des terres, de conditions climatiques ainsi que de la présence ou non de réservoir dans le bassin versant. Cela indique que la construction du barrage sur le bassin en 1987 a eu une incidence sur le système hydrologique du bassin versant du Mono. Le changement de couverture et d'occupation des terres en même temps que l'amplification du changement climatique en sont aussi d'autres facteurs. L'étude a proposé des stratégies pour améliorer la planification et la gestion des ressources en eau dans le bassin versant du Mono, telles que la gestion efficace de l'utilisation des terres, l'adaptation et l'atténuation des effets du changement climatique et la gestion des réservoirs de Nangbéto.

Mots-clés**:** changement de l'occupation des terres, détection du changement climatique, analyse sensible; gestion des barrages; modélisation hydrologique; Bassin du fleuve Mono.

Introduction

Les changements d'occupation et de couverture des terres combiné aux impacts du changement climatique et de la gestion du barrage de Nangbéto dans le bassin versant du Mono, localisé entre le Togo et le Benin ont entrainé d'énormes modifications du régime hydrologique de ce dernier en particulier sur les composantes du bilan hydrologique. Dans cette zone sub-tropicale où la population est en constante augmentation, la gestion des ressources en eau douce dans les bassins hydrologiques se trouve exposée à divers problèmes. Pour efficacement gérer ces bassins hydrologiques, il est donc nécessaire d'intégrer tous les processus tant aux échelles temporels que spatiaux intervenant dans le cycle hydrologique afin de proposer des solutions fiables et durables de gestion de l'eau. La connaissance du bassin versant du Mono est aussi mise à mal par une non-existence des données d'observation climatiques et hydrologiques fiables, ce qui affecte les études spatio-temporelles des différentes composantes du bilan hydrique et surtout la modélisation hydrologique. C'est pour ces diverses raisons que cette thèse s'est fixée comme objectif de mener une étude sur ledit bassin pour appréhender la répartition des précipitations en évapotranspiration réelle, ruissellement et recharge de la nappe souterraine avec différents types de données climatiques, de couverture du changement d'utilisation des terres, d'occupation des terres et de la gestion d'un barrage. Les objectifs spécifiques de l'étude sont de: (i) évaluer différentes bases de données d'occupation et d'utilisation des terres et de projeter les changements futurs d'occupation des terres à l'horizon 2020-2027dans le bassin versant, (ii) détecter les tendances de changement climatique sur les séries temporelles hydro-climatiques et déduire les indices d'extrêmes climatiques de précipitations, les températures avec les profils représentatifs d'évolution des concentrations RCP4.5& RCP8.5 à l'horizon 2020-2045, et (iii) évaluer l'impact des scénarios de changement climatique et d'occupation des terres sur les composantes du bilan hydrique dans le bassin versant du Mono à l'aide des modèles empiriques GR4J (Génie Rural à 4 paramètres Journaliers) et IHACRES (Identification of unit Hydrographs and Component flows from Rainfall, Evapotranspiration and Stream data) puis en utilisant le modèle semi-distribué SWAT(Soil and Water Assessment Tool) sur les périodes avant l'installation et après l'installation du barrage de Nangbéto pour évaluer les variation spatio-temporelle des composantes du cycle hydrologiques.

Zone d'étude

La zone d'étude est le bassin du fleuve Mono (MRB) entre les républiques du Togo le Bénin. C'est le fleuve principal au Togo en partage avec le Benin dans ses derniers kilomètres au

sud. Ce fleuve est situé entre 06 ° 16 'et 9 ° 20' de latitude nord et entre 0 ° 42 'et 1 ° 40' de longitude est. Avec un périmètre de 872.092 km, le bassin couvre la zone d'Athiémé sur une superficie de 22.014 km² (PCCP, 2008). D'une longueur de 308,773 km, le fleuve Mono tire son origine dans les montagnes d'Alédjo (Amoussou, 2010) au nord du Bénin avant de se jeter dans l'océan Atlantique par le système lagunaire entre les altitudes de 12 à 948 m. Le bassin versant abrite le plus grand barrage de Nangbéto qui produit 20% d'électricité totale utilisée par les deux pays. Le climat est subéquatorial au sud avec deux saisons de pluies et deux saisons sèches (1200 à 1500mm/an) et au nord le climat est tropical humide avec une saison de pluies et une saison sèche (1000 à 1200 mm /an) (PCCP, 2008). La population dans le bassin du Mono est d'environ 5,1 millions d'habitants (FAO, 2012; PCCP, 2008; SAWES, 2011). Les principales activités socio-économiques sont l'agriculture, le commerce, la pêche et l'élevage.

Matériel et méthodes

La figure 1 indique le diagramme synthétique des différentes étapes de cette étude. Dans un premier temps l'étude à évaluer les précisions de différente base de données historique d'occupation et d'utilisation des terres dans le Mono entre 1975 et 2013 puis projeter les scenarios d'occupation des terres entre 2020 et 2027 à l'aide de l'outil «Terrset Land Change Modeler». Il s'agit des bases de données de CILLS de 2km de résolution des années 1975, 2000 et 2013, des données de ESA de 300m de résolution des années 2000 et 2013 et des données de Globeland30 de 30m de résolution des années 2000 et 2010. Ensuite une analyse d'étude tendancielle de Man Kendall (MK) a été menée sur les données hydro-climatiques pour détecter le changement climatique sur ces séries temporelles sur l'ensemble du bassin et a des stations individuelles entre 1961 et 2016.

Les données d'observations de pluie et de température ont servi à la validation des sorties d'un ensemble de modèles climatiques entre 1980 et 2005. Ceci a permis d'utiliser le modèle climatique pour calculer et analyser les tendances (MK) des extrêmes climatiques de précipitations, les températures avec les profils représentatifs de l'évolution des concentrations (RCP4.5 & RCP8.5) à l'horizon 2020-2045. Les mêmes données hydro-climatiques évaluées par la suite ont été utilisées pour la modélisation hydrologique premièrement à l'aide de deux modèles empiriques GR4J et IHACRES sur deux sous-périodes différentes 1964-1986 (Période avant construction du barrage) et 1988-2010(Période après construction du barrage). L'évaluation des performances de ces modèles hydrologiques se fait à partir des critères de performance du modèle avec le coefficient de Nash-Sutcliffe (NSE), du coefficient de déter-

mination (R^2), Kling de Gupta Efficiency (KGE) et du pourcentage d'erreur (PBIAS). Ensuite les données hydro-climatiques entre 1961 et 2011, les données d'occupation et d'utilisation des terres au cours des années de référence 1975 et 2000, les données de relief et de la gestion des barrages ont servi de données d'entrée dans le modèle SWAT pour deux scenarios de simulation de 1964 à 1986 et de 1988 à 2011. Les performances des deux simulations du model SWAT ont été évaluées puis comparées par les mêmes critères de R^2, NS, KGE et PBIAS sur ces deux périodes puis utilisées pour déterminer les contributions des composantes du bilan hydrique et des changements tant temporelle et spatiale de chaque composante pour chaque sous-période précédente. La figure 1 montre les différentes structures artichesturales de cette étude.

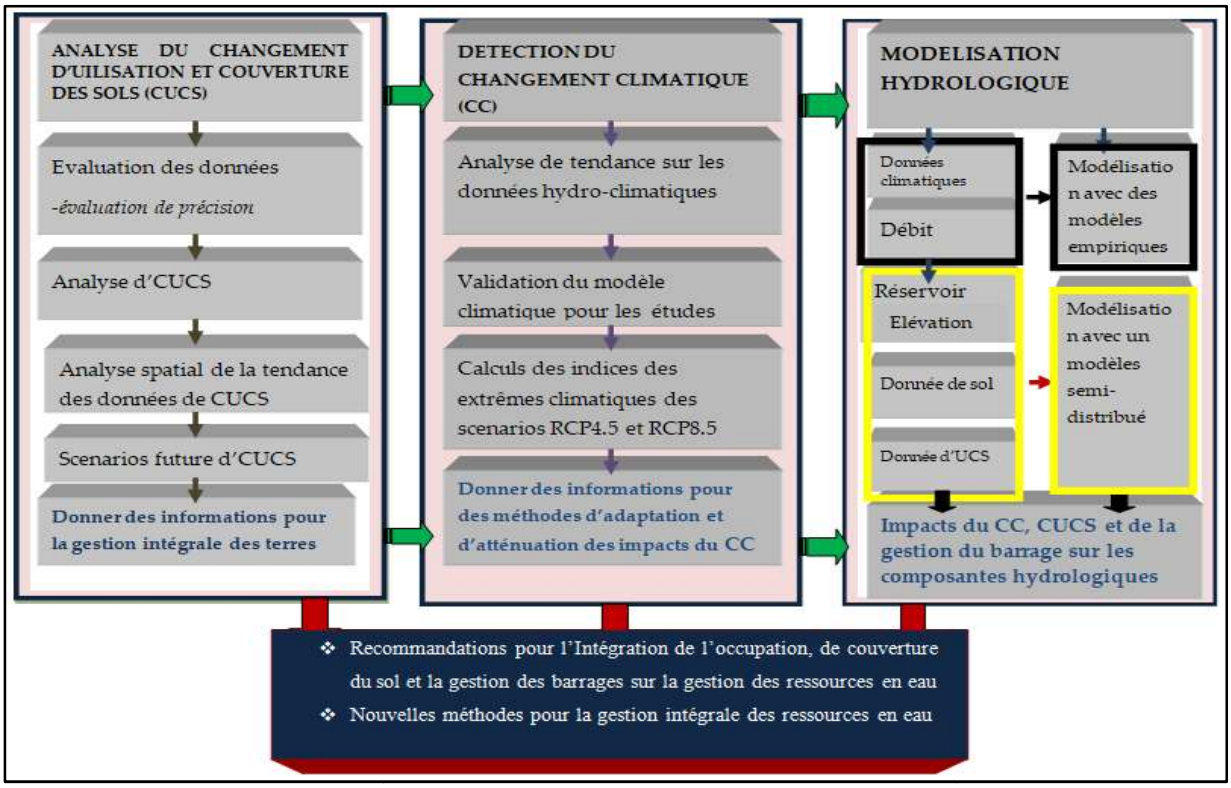

Figure. 1: Diagramme synthétisé des travaux de recherche

Résultats et discussion

Les résultats indiquent que les données de CILSS présentent une bonne précision d'occupation et d'utilisation des terres dans le bassin du Mono. En effet, le pourcentage de points de vérification au sol connu sous le nom de précision globale et de coefficients Kappa est respectivement de 83% et 68% pour le produit CILSS en 2013, 69% et 36% à l'aide des jeux des données ESA de 2013, 57% et 34% en utilisant l'ensemble des données de Globeland30 de l'année 2010. L'analyse des données du CILSS révèle que la couverture terrestre de

la savane est dominante, suivie des terres cultivées et de la forêt. En termes de pourcentage de la zone de couverture, la savane représente environ 75,94% en 1975, 63,75% en 2000 et 50,35% en 2013; les terres cultivées représentent 84% en 1975, 25,36% en 2000 et 39,82% en 2013 et les forêts environ 14,87% en 1975, 9,57% en 2000 et 7,96% en 2013, comme le montre le tableau 1. Ces résultats confirment de nombreuses analyses effectuées au Togo et au Bénin sur les changements dans la couverture et d'occupation des terres résultant principalement de la déforestation et de l'explosion démographique (Akinyemi et al., 2017; Kleemann et al., 2017). L'évaluation de la précision et le changement d'occupation des terres de ces ensembles de données ont eu un impact important sur les scénarios futurs d'occupation des terres projetées par CILSS, ESA et Globland30 entre 2020 et 2027.

Tableau 1: Couverture terrestre et changement de superficie

	Superficie d'occupation des terres [%]							**Changement de superficie d'occupation des terres [%]**				
Année/ Période	1975	2000			2010	2013		1975-2000	2000-2013		2000-2010	1975-2013
Source	CILSS	CILSS	ESA	GLC	GLC	CILSS	ESA	CILSS	CILSS	ESA	GLC	CILSS
Forêt	14,87	9,57	8,02	23.65	23,96	7,96	7,51	-5,31	-1,61	-0,51	0,32	-6,91
Savane	75,94	63,75	70,52	44.51	39,99	50,35	70,7	-12,19	-13,4	0,18	-4,52	-25,59
Welland	0,02	0,33	0,05	0.01	1	0,16	0,06	0,31	-0,16	0,02	0,99	0,14
Terre cultivée	8,84	25,36	20,66	30.69	33,88	39,82	20,91	16,51	14,46	0,25	3,19	30,97
Eau	0,02	0,51	0,68	0.68	0,67	0,49	0,63	0,49	-0,02	-0,06	-0,01	0,47
Habitations	0,31	0,49	0,07	0.48	0,5	1,22	0,19	0,18	0,73	0.12	0,02	0,91
Total	100	100	100	100	100	100	100	0,0	00	00	0,0	00

Les résultats de l'analyse de détection du changement climatique montrent des tendances positives et négatives des données hydro-climatiques de 1961 à 2016 (Figure 2 et Tableau 2). La température moyenne augmente de manière significative dans la plupart des stations, tandis qu'une tendance négative non significative est observée pour les précipitations. Pendant ce temps, le débit présente une tendance saisonnière et annuelle significative des stations de mesure de Corrokope, Nangbéto et Athiémé comme dans le Tableau 2. La validation des modèles climatiques d'ensemble révèle que le modèle sous-estime les observations aux stations de Sokodé, Atakpamé et Tabligbo, bien que les coefficients de régression linéaire et de corré-

lation spatiale soient supérieurs à 0,6. De plus, le pourcentage d'erreur entre le modèle climatique et les observations est inférieur à 15% dans la plupart des stations.

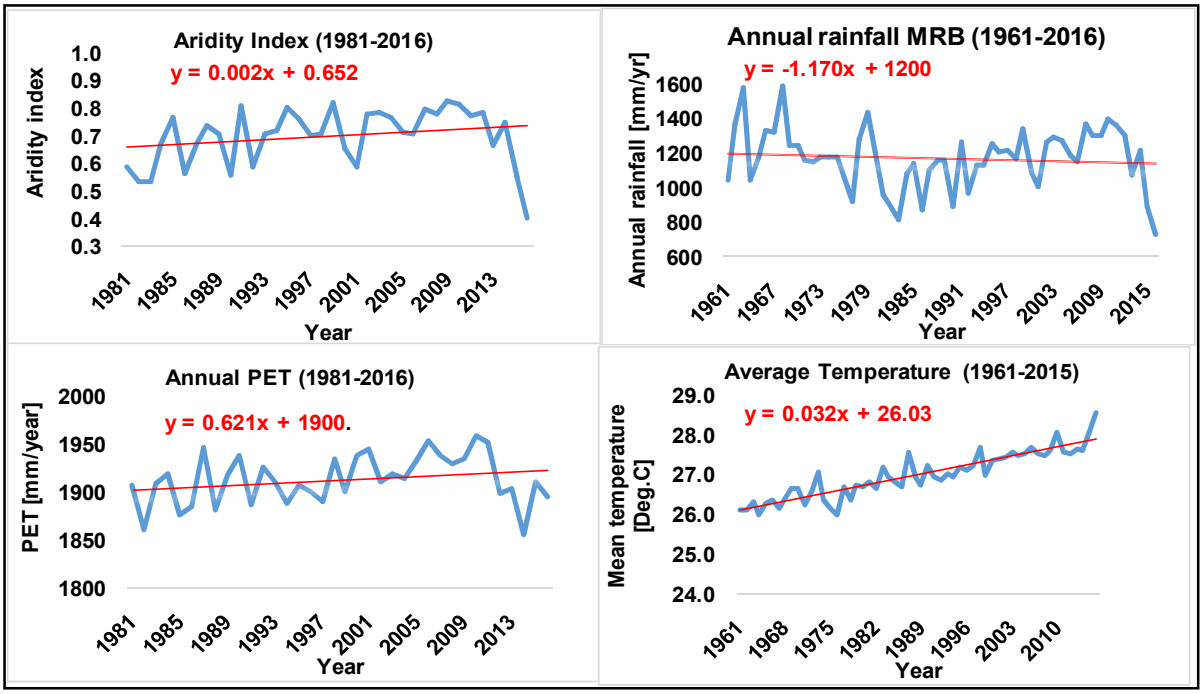

Figure 2: Sériés temporelles des différentes variables climatiques

Enfin, le calcul des indices climatiques extrêmes selon les scénarios RCP4.5 et RCP8.5 montre une tendance annuelle significative de certains indices climatiques extrêmes de précipitations et de températures dans certaines stations entre 2020 et 2045 dans le bassin.

Tableau 2: Statistiques de tendance annuelle et saisonnière

		PET	Precipitation	Temperature	Q Athieme	Q corro-kope	Q en-trant	Q sortant
n		36	36	56	50	38	24	24
MAM	Zs	-0.04	-0.91	6.47	1.63	0.72	1.02	1.07
	Sig			***				
	Qmed	-0.21	-1.43	0.030	4.578	0.149	4.06	20.66
JJA	Zs	0.86	-0.81	7.61	-2.37	-0.53	0.17	0.02
	Sig			***	*			
	Qmed	0.19	-2.68	0.028	-61.008	-15.075	15.27	2.52
SON	Zs	-0.48	-0.11	8.01	-2.01	-1.03	0.82	0.47
	Sig			***	*			
	Qmed	-0.049	-0.16	0.031	-92.319	-33.965	79.25	57.65

DJF	Zs	4.02	-0.20	7.47	3.66	-0.78	1.20	3.25
	Sig	***		***	***			**
	Qmed	0.72	-0.14	0.036	23.559	-0.184	2.00	44.13
Annuel	Zs	1.78	-0.52	8.38	-1.65	-1.03	0.57	0.97
	Sig	+		***	+			
	Qmed	0.83	-2.23	0.031	-26.267	-12.643	22.37	33.15

Les résultats de la modélisation hydrologique avec les modèles empiriques montrent que la génération de ruissellement n'est pas linéaire à la variabilité des précipitations dans le bassin à pas de temps journalier, le modèle GR4J surestime l'observation, tandis que le modèle IHACRES sous-estime les extrêmes des observations effectuées avant la construction du barrage (1964-1986). Cependant, au cours de la période postérieure au barrage (1988-2010), les prévisions d'observation sont faibles avec un décalage par modèle GR4J, tandis que le modèle IHACRES sous-estime les observations. L'étude a également testé le modèle d'ensemble (EM) moyen à l'échelle intra-annuelle indiquant une probable meilleure simulation du ruissellement à Athiémé entre 1964 et 1986 (Figure 3). Vu les performances faibles avec les modèles empiriques, il est claire que les processus de ruissellement dans le bassin est affecté par les propriétés des sols, les couches géologiques, le paysage, les changements climatiques et la gestion des barrages qui est pris en compte dans l'utilisation d'un model semi-distribué par la suite des travaux avec le modèle SWAT plus approprié.

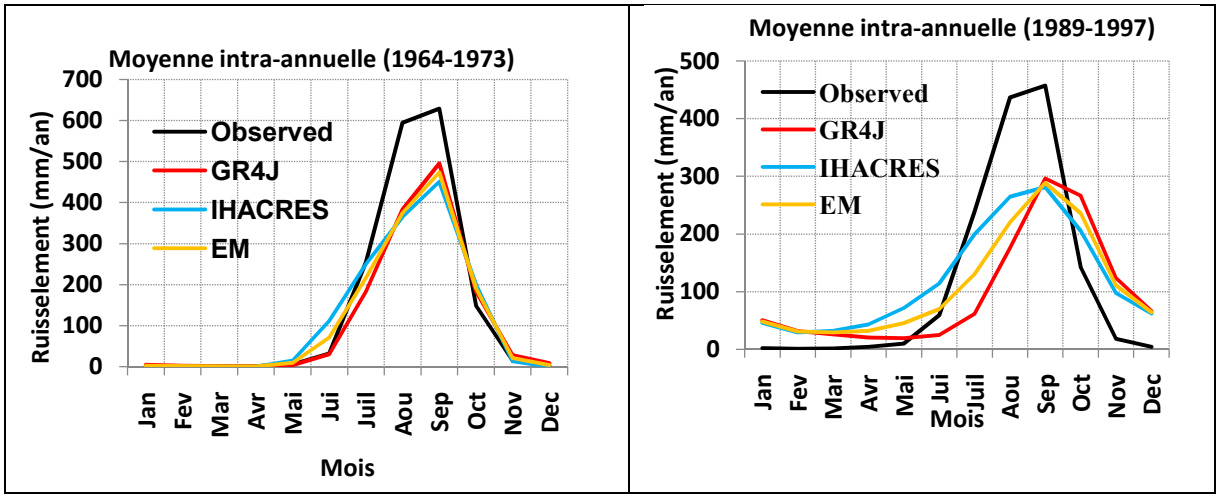

Figure 3: Variabilité intra- ruissellement simulé à Athiémé

Enfin, l'évaluation de la modélisation hydrologique à l'aide du modèle sémi-distribué SWAT montre que les variations du débit simulé dépendent de la période utilisée. En effet la procédure d'ajustement d'incertitude séquentielle (SUFI-2) pour l'analyse de sensibilité, l'étalonnage du modèle et la validation à un pas de temps journalier a été appliquée sur les

deux périodes (1961-1986 et 1988-2011). Les performances et l'incertitude obtenues lors de la simulation avant construction du barrage donnent (Calage_1964-1975: R^2> 0,60; KGE ≥ 0,70 et PBIAS ≤ ± 4,5; validation_1976 - 1986: R^2 ≥ 0,28; KGE ≥ 0,48 et PBIAS ≤ ± 3,40) et pour la simulation post-barrage (Calage_1988-2000: R^2> 0,25; KGE ≥ 0,60 et PBI ≤ ± 20; validation_2001-2011: R^2 ≥ 0,20; KGE ≥0,24 et PBIAS ≤ ± 17,20). Les performances du modèle montrent une plage de valeurs de paramètres acceptables lors de la première simulation et de mauvaises lors de la seconde simulation selon la Figure 4. Ceci s'explique d'une part par la présence du barrage et d'autre part aux limites du modèle SWAT.

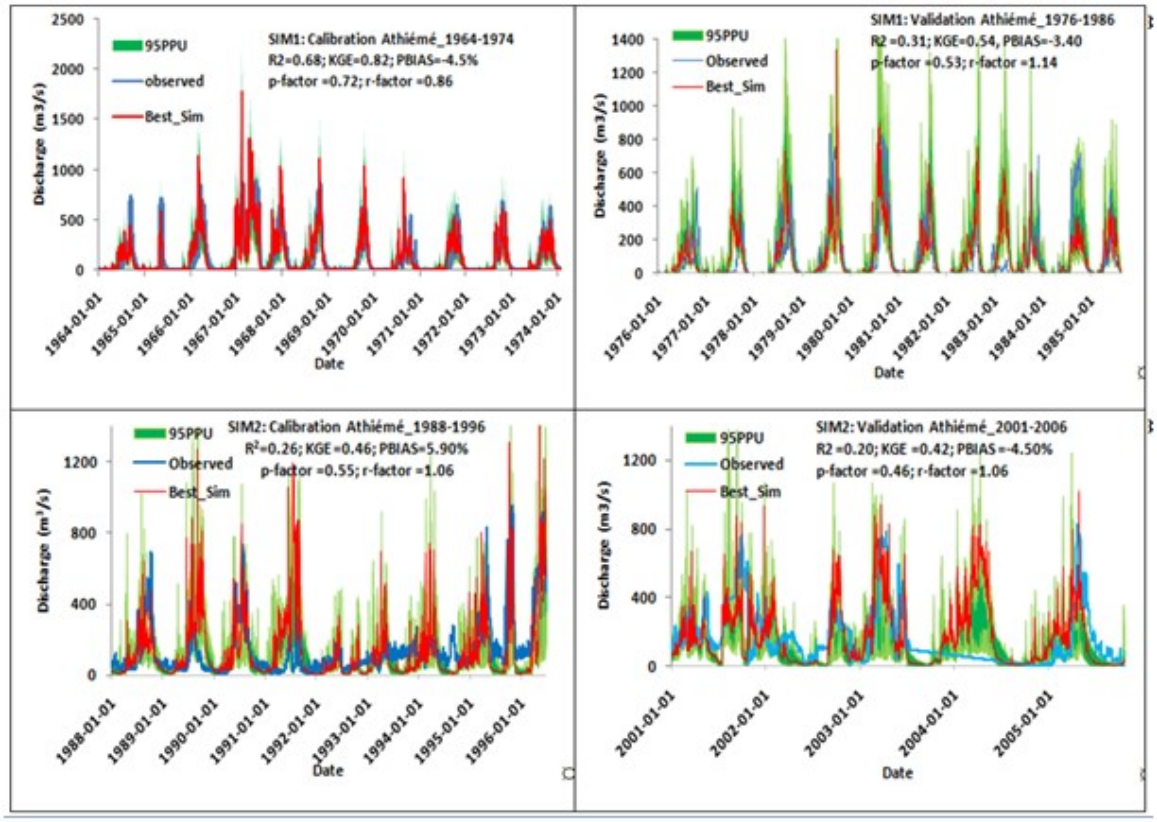

Figure 4**: Calage et validation du débit avec le model SWAT sur les deux sous-périodes**

Les composantes hydrologiques sur les deux périodes sont simulées et comparées. Par conséquent, l'écoulement, l'évapotranspiration et l'évolution des apports en eau dépendent des différents types d'utilisation des sols (Figure 5), des conditions climatiques ainsi que de la présence ou non de réservoir dans le bassin versant. Selon l'analyse des résultats pour deux périodes de simulation, le débit en amont (Corrokopé) entre 1964 et 1986 puis entre 1988 et 2011 dépend principalement des conditions climatiques, du changement d'utilisation des sols et du sol. A l'opposé en aval (Tététou et Athiémé), la variation du débit du cours d'eau est importante en deuxième période et est liée aux conditions climatiques, au changement de l'occupation des terres, et à la présence et la gestion du barrage.

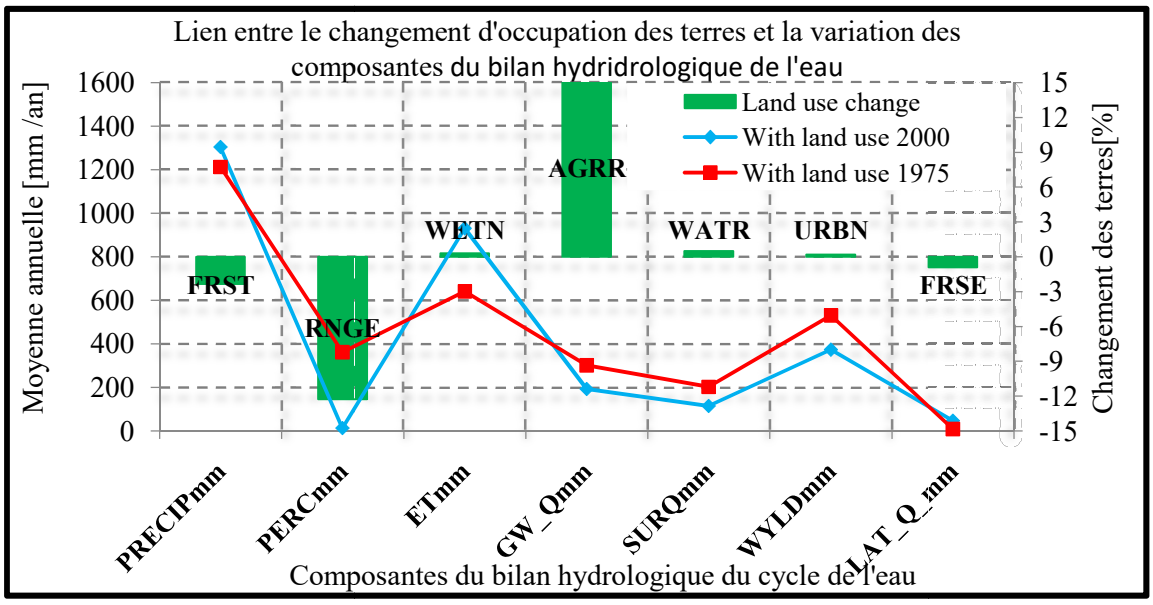

FRST= Foret, RNGE= Savane, WETN=wetland, AGRR= zone cultivée, WATR= eau, URBN= habitations and FRSE= foret claire, PRECIPmm= précipitation, PERCmm=percolation, ETmm=evapotranspiration, GW_Qmm= Eau souterraine, SURQmm=écoulement de surface, WYLDmm=Etendue d'eau, LAT_Q_mm= écoulement latérale

Figure 5: Changement d'occupation des terres et la contribution des composantes du bilan Du cycle de l'eau entre les sous-périodes (1964-1986) et (1988-2010)

Conclusion

Cette étude a permis d'avoir une bonne connaissance sur les facteurs intervenant dans le système hydrologique du bassin versant du Mono. L'étude approfondie sur les qualités des cartes d'occupation des terres plus représentative de CILSS montre une déforestation, une perte de la savane au profit des zones agricoles et d'habitation expliquée particulièrement par la croissance démographique dans la zone subtropicale. L'étude de détection du changement climatique sur les données hydro-climatiques a révélé une baisse des précipitations moyennes sur le bassin et une augmentation de la température moyenne et de l'évapotranspiration actuelle. L'intégration des variables climatiques, d'occupation du sol, du relief et données du sol dans la modélisation hydrologique à l'aide du modèle semi-distribué SWAT a donné des résultats plus ou moins acceptables des débits journaliers et des contributions des composants hydrologiques selon la période utilisée. Les impacts du changement d'occupation du sol, de la variabilité du changement climatique et de la gestion du barrage a montré, d'une part, que la déforestation, la perte de la savane et l'augmentation de la température moyenne jouent sur le système hydrologique de la rivière du Mono entrainant une augmentation des précipitations, de l'évapotranspiration réelle et écoulement latéral, et d'autre part, une diminution de la percolation, des eaux souterraines, du ruissellement , de surface et des apports en eau sont perceptibles. Les résultats indiquent que la mise en œuvre du modèle SWAT basé sur les systèmes d'information géographiques constitue un outil essentiel pour aider les autorités compétentes d'Afrique de l'Ouest et les décideurs à une gestion durable des ressources en eau au niveau des bassins versants.

Table of contents

List of acronyms

95PPU: 95% Prediction Uncertainty

AAT: All-At-a-Time

AE: Absolute Error

AI: Aridity Index

AMN: Agence de la Météorologie National

BMBF: German Ministry of Education and Research

BN: Benin

CA: Cellular Automata

CC: Climate Change

CCAFS: Climate Change Agriculture and Food Security

CCD: Consecutive Cool Days

CCI: Climate Change Initiative

CEB: Communauté Electique du Benin

CI: Confidence Interval

CILSS: Comité Inter-etats de Lutte contre la Secheresse au Sahel

CLIVAR: Climate and Ocean Variability, Predictability, and Change

CMD: Catchment Moisture Deficit

CN: Curve Number

CORDEX: Coordinated Regional Climate Downscaling Experiment model

CSDI: Cold Spell Duration Indicator

CUP: Calibration and Uncertainty Programs

CV: Coefficient of Variation

CWD: Consecutive Wet Days

DEM: Digital Elevation Model

DGEA: Direction Générale de l'Eau et Assainissement

DGEA: General Direction of Water and Sanitation in Togo (DGEA-Togo),

DGEau: Direction Générale de l'Eau

DGMN: Direction Générale de la Météorologie Nationale

DGSCN: Direction Générale de la statistique et de la Comptabilité Nationale

DTR: Diurnal TempeRature

ED: Euclidean Distance

EGCMs: Ensemble Global Climate Models

EM: Ensemble Model

ESA: European Space Agency

ESCO: Soil Evaporation Compensation Coefficient

ETCCDI: Expert Team on Climate Change Detection and Indices

ETP: Actual Evapotranspiration

FAO: Food and Agriculture Organization

FLASH: Atmospheric Analysis of Spectral Hypercube

GCMs: Global Climate Models

GHG: GreenHouse Gas

GIRE: Gestion Intégrée des Ressources en Eau

GIS: Geographic Information Systems

GLOWA: Globaler Wandel WAsserkreislauufes

GLUE: Generalized Likelihood Uncertainty Estimation method

GPG-LULUCF: Good Practices Guidelines for Land Use, Land Use Change and Forestry

GR4J: Génie Rural à 4 paramètres Journaliers

GRP: Graduate Research Program

GW_Q: groundwater flow

GWh: Giga Watt heur

HBV: Hydrologiska Byråns Vattenbalansavdelning

HRG: Hydrology Research Group

HRUs: Hydrologic response units

HWSD: Harmonized World Soil Database

HYCOS: Système d'Observation du Cycle Hydrologique

IHACRES: Identification of unit Hydrographs and Component flows from Rainfall, Evapo-transpiration and Stream data

IMPETUS: Integrative management project for an efficient and sustainable use of freshwater resources in West Africa

IPCC: Intergovernmental Panel on Climate Change

ITCZ: Inter-Tropical Convergence Zone

ITF: Inter-Tropical Front

IWRM: Integral Water Resources Management

KGE: Kling Gupta Efficiency

LAI: Leaf Area Index

LAT_Q: lateral flow

LCCS: Land Cover Classification System

LCM: Land Change Modeler

LES: Laboratoire d'Energie Solaire

LS: Length and Slope

LU: Land Use

LULC: Land Use and Land Cover

LULCC: Land Use and Land Cover Changes

MAE: Mean absolute error

MAM: March April May

MERF:Ministère de l'Environnement et des Ressources Forestières

MESRS: Ministry of High Education and Scientific Research

MK: Manna Kendall

MLP: Multi-Layer Perceptron

MNS: Modified Nash-Sutcliffe efficiency

ModHyPMA: Modèle Hydrologique basé sur le Principe de Moindre Action

MODIS: MODerate resolution Imaging Spectro-radiometer.

MOLUSCE: Modules for Land Use Change Evaluation

MPDAT: Ministère Auprès du Président de la République, Chargé de la Planification, du Développement et de l'Aménagement du Territoire

MRB: Mono River Basin

MW: Mega Watt

NASA: National Aeronautics and Space Administration

NCAR: National Center for Atmospheric Research

NCEP: National Center for Environmental Predictions

NGCC: National Geomatics Center of China

NOAA*:* National Oceanic and Atmospheric Administration

NSE: Nash-Sutcliffe Efficiency

OAT: One-At-a-Time

ONU: United Nations Organization

PANGIRE: Plan d'Action National de Gestion Intégrée des Ressources en Eau

PBIAS: Percent Bias

PCCP: Potential Conflict to Cooperation Potential

PERC: Percolation

PET: Potential EvapoTranspiration

PNSET:Programme National de Suivi de L'environnement au Togo

POK: Pixel-Object-Knowledge

PSO: Particule Swarm Optimization

QGIS: Quantum Geographic Information System

RCMs: Regional Climate Models

RCPs: Representative Concentration Pathways

REMO: REgional Model

RLCM: Rapid Land Cover Mapper

RMSE: Root Mean Squared Error

RS: Remote Sensing

SAWES: Sahelian Agency for Water, Environment and Sanitation

SCOS: Smoothed COS method

SCS: Soil Conservation Service

SMA: Soil Moisture Accounting

SMD: Soil Moisture Deficit

SMES: Small and Medium Size Enterprise

SOFRELEC: Société Française d'Etudes et de Réalisations d'Equipements Electriques

SON: September October November

SRTM: Shuttle Radar Topography Mission

SSQR: Ranked Sum of SQuares

STCHOICE: Stochastic Choice

STD: STandard Devaiation

SUFI: Sequential Uncertainty FItting

SURQ: Surface runoff

SW: Soil water content

SWAT: Soil and Water Assessment Tools

SWIM: Soil and Water IntegratedModel

TG: Togo

UCL: Université catholique de Louvain

UK: United Kingdom

UN: United Nations

UNEP: United Nations Environmental Program

UNESCO: United Nations Educational, Scientific and Cultural Organization United

UNOCHA: United Nations Office for the Coordination of Humanitarian Affairs

USA: United States of America

USAID: United State Agency for International Development

USD: United State Dollar

USGS: United State Geological Survey

UTM: Universal Transverse Mercator

VAR: VARiance

WAC: West African Craton

WASCAL: West African Science Service Center on Climate and Adapted Land Use

WaSiM: Water balance Simulation Model

WGS: World Geographic System

WSDI: Warm Spell Duration Indicator

WYLD: Water YieLD

List of figures

List of tables

Chapter 1 General introduction

This chapter gives a general overview on the thesis. It describes the project from its starting point, the gaps that have to be filled, the objectives, the literature review of the studies that have been achieved on the Mono River Basin (MRB), located between Togo and Benin Republics, along with their limits and finally the benefits of study results in the society as well for the countries.

1.1: Context and problem statement

1.1.1 Context

Water is a crucial resource in the world and particularly in Africa. It is crucial not only for the conservation of ecosystems but also for the development of agriculture, industry, power generation, livestock production, and other economic activities (Mango et al., 2011). However, water can also be dangerous to people when the overflow from the water bodies such as river or lake occur resulting in flooding of a basin, villages, cities, etc.. Understanding the hydrologic response of a watershed to land use and land cover (LULC) and climate changes is an important component for a sustainable water resource planning and management (Ali et al., 2012; Montenegro and Ragab, 2012). Land use and land cover changes (LULCC) are important factors that affect water temporal and spatial distribution in a watershed. LULCC in Africa is about the conversion of 75 million hectares of forest to agriculture and pasture between 1990 and 2010 (Ndulue et al., 2015). LULC conversion affects soil proprieties and the impacts of LULCC on river basin hydrology is interlinked with impacts of climate change (Kappelle et al., 1999). Climate change, reflected by a significant global warming, is seen as the changes in surface runoff, rainfall frequency and actual evapotranspiration. Therefore, tremendous efforts have been put on surface hydrology research in various relevant regions in the last decade (Herbst et al., 2009; Panthou et al., 2012). For example, it is widely conceived that with the increase of temperature, the water cycle process will be affected. This has as consequence a possible increase in the amount and intensity of precipitation. Many outputs from Global Climate Models (GCMs) and Regional Climate Models (RCMs) indicate the possibility of substantial increases in the frequency and magnitude of extreme daily precipitation that generates surface runoff (Paeth and Thamm, 2007; Sylla et al., 2013; Yang et al., 2012). According to Stocker (2014) climate change and climate variability constitute a global issue but its impacts are more local. For instance, over the West African sub-region, there have been severe disasters accelerated by the change in climate. Bilotta et al.(2007) and Bossio et al.(2010) also

argued that impacts of climate change led to land degradation that affects the quality of soil and reduces the infiltration rate of water by giving rise to high level of surface runoff. All these assumptions need to be verified in MRB, on which, to the best of our knowledge, no such study had been undertaken.

1.1.2**:** Problem statement

In the Gulf of Guinea and in the Mono watershed, located between Togo and Benin, rainfall regime modifications are becoming more frequent (Tramblay et al., 2014). The intensity and frequency of rainfall event are causing recurrent problems in an environment with rapid population growth (Tramblay et al., 2014). On this same river basin, Nangbéto dam was built in 1987 with primary objective hydroelectricity production, regulation of Mono river streamflow in the downstream, irrigation for agriculture and fisheries activities (Amoussou et al., 2017; Rossi, 1996). Nevertheless, some studies showed that most objectives were not met and dangerous environmental impacts on water resources such as flooding were observed (Ago et al., 2005; Ntajal et al., 2017). Flood has the potential to increase river flows and hydropower generation of the dam by retaining quantity of water upstream. However, in extreme cases, floods can also involve the destruction of the dams. Most of the past studies showed that Mono River at the downstream is vulnerable to flood event. According to some studies on the Mono river basin, the construction of Nangbéto dam during the year 1987 had created many modifications in Mono's hydrological lagoon system. Ago et al.(2005); Amoussou et al.(2014) and Rossi (1996) showed also that these modifications have caused permanent damages particularly in the downstream of the dam at Tététou and Athiémé sub-basin.

One of the Nangbéto dam utility is to generate hydropower that supports major industries in Togo, Benin, Ghana, and other countries (Owusu et al., 2008). The renewable energy focuses on the provision of sustainable energy for the society, combats energy shortages and provides clean energy from the perspective of the Kyoto directive towards global decarburization (Mohammed et al., 2013). Moreover, land use changes can modify the water cycle and control the transformation of the precipitation into runoff which is a parameter of hydropower production. For example, Oyerinde et al.(2016) have examined the impacts of climate change and land use change on hydroelectricity supply in the West African regions. Detailed assessment is important to understand how climate and land use change impact the Mono hydrology system and how in the downstream it can affect water balance components due also to dam management practices or land use and climate changes.

The United Nations Office for the Coordination of Humanitarian Affairs (UNOCHA) recently stated that environmental effects are becoming more severe within West Africa (references). Climate and land use changes are involving devastating natural hazards, affecting human lives and causing severe economic damage throughout the world (Zargar et al., 2011). Mono river basin is an important transboundary watershed and Nangbéto dam is one of the most hydroelectricity sources for Togo and Benin. During the last decade, most of studies done in this basin were related to its biodiversity; geology and forest change Akpagana, (1989); Gayibor, (1986) and Klassou (1996). Recently, Lawin et al.(2019a) and Tramblay et al.(2014) have assessed rainfall variability and hydro-sedimentary dynamics of the Mono basin. The same authors analyzed the runoff variability and sediment dynamics in the Mono-Ahéme-Couffo watershed over the period 1961-2000 in a context of integrated water resources management. As a result they found that there is excess or deficit of rainfall depending on the period and the sub-basin. They concluded that human activities, land use and geological bedrock and surface conditions equally play a key role. This explains the role of the dam on streamflow changes, flood event in the downstream of the basin. In this Mono river basin, it was also supposed that the increasing rainfall intensity based on climate variability could be the factor of increasing environmental crisis (Amoussou et al., 2014). Kissi et al. (2015) have worked on the social vulnerability of flood in the Bas Mono prefecture. Ntajal and Lamptey (2015) have investigated flood disaster risk mapping and analysis while Houngue (2018) has looked at the simulation of high discharge using hydrological and climate model in the small area of lower MRB. They concluded that the source of high discharge is not only due to climate change but also to the regulation of the Nangbéto dam and the social factors of the communities living in this area. The populations of African countries are exponentially increasing; consequently, more energy is needed for industry and household needs. Moreover, the better energy that can mitigate climate change is clean energies like hydropower that plays a dominant role in Africa's electricity use and in the world. More action is being made for additional hydroelectric development throughout Africa. For instance, the 147 MW Adjarala dam is the second largest hydropower dam that is being built on the Mono River to increase electricity production for industrial development and expand irrigation in the basin. Several studies have been conducted on the impacts of climate change on hydropower in West Africa and South Africa (Amoussou et al., 2014; Oyerinde et al., 2015; Yamba et al., 2011). Nevertheless, fewer researches have been conducted on climate, land cover change impacts and dam management impact on water balance components in West Africa and especially at the basin scale. Firstly, evaluation of land use change and future scenarios is important to be

assessed in Mono River Basin (MRB). Secondly, the simulation of the hydrological system of the Mono basin under climate and land use change impacts can allow estimating simulated discharge and water balance component seasonal and annual changes. Therefore a state of art in combination of climate change, land cover change impacts on hydrology is needed in order to fill the gap with past research.

1.2. Literature review

Since the 70s, climate change potential effects have been increasing on agriculture, socio-economy, energy, water resource and particularly at river basin level (Abdalla, 2001). Land use and land cover change induced by increase population in West Africa countries are some factors on global environmental changes (Leopold, 1968; Liu and Chen, 2006). In other side; dam development and managements affect many rivers' hydrological system in West Africa. Therefore modeling surface runoff variability and water balance components changes by reducing uncertainties in the river is very important for a sustainable water management. Many studies have analyzed the impacts of climate and land use change on water resources, biodiversity and globally on environmental resource (Amisigo et al., 2015; Kharel et al., 2016; Mbaye et al., 2015). Land use modeling and future scenarios projections are performed to give the future state of LULC and particularly in West Africa (Maria et al., 2014; Yira et al., 2016). Grimaldi et al.(2013) reviewed different methods of LULC modeling methods and propose a hybrid approach modeling for LULC future projection. Indeed LULC assessment have been evaluated through remote sensing data with manual digitalization classification and tools (Butt et al., 2015; Knauer et al., 2014; Olofsson et al., 2013). Olofsson et al.(2013); Pontius and Malanson (2014) have developed some methods for assessing LULC. Nevertheless, in the last years some algorithms have been developed for automatic classification in order to make land use data freely accessible. This automatic classification system can classify a large area and even with a long period of data processing in a short time consumption (Huth et al., 2012; Jiang et al., 2012). For example, the remote classified map of CILSS (CILSS, 2016), ESA (Gessner et al., 2015) and Globeland30 (Chen et al., 2017) are some of freely existing data sets with different spatial and temporal resolutions (Huth et al., 2012; Jiang et al., 2012). According to Jiang et al.(2012); Schneider and Pontius (2001), automatic remote sensing data need validation before any future use and decision making. This can be used to compare the classified map with field observation data using Olofsson et al.(2013); and Pontius and Millones (2011) new methodologies for land use accuracy assessment and validation. In

many cases, land use and land cover change are interlinked with climate change which are the factor mostly impacting river streamflow.

Concerning climate change detection on climate variables, it is recommended to use thirty (30) years minimum long period for analysis (Jaiswal et al., 2015; Tan et al., 2019).Some of the climate variables are air temperature, rainfall, wind speed and direction, evapotranspiration, solar radiation and humidity. But temperature and rainfall are the most important parameters used in several studies (Halimatou et al., 2017; Tan et al., 2019). Climate change impacts on hydrological system involve actually water scarcity in the future (Schewe et al., 2014; Thompson et al., 2014). To give valuable and sustainable guidelines for water resources management in West Africa, integration of climate change impacts and future scenarios is important. Some studies have focused on trend analysis of historical hydro climatic parameters and by providing an overview and changes of these parameters (Jain and Kumar, 2016; Soro et al., 2016; Thenmozhi and Kottiswaran, 2016). Other past researches have evaluated the modeling temperature and coupling river transport model for integrated water reservoir management in America (Li et al., 2014). In Togo, Mikemina (2013) has applied Ricardian approach to analyze climate change impacts on agriculture performances for the period of 1971-2004. To understand the spatial and temporal climate variability in local vulnerability in Togo, Badjana et al.(2014) and Djaman et al.(2017) have used temperature and rainfall to detect a significant changes with these variables over long period. Koutroulis et al.(2013) have used Global Climate Models (GCMs) and ensemble Regional Climate Model (RCMs) to analyze the impacts of climate change on water resources in Island. Regional or Global climate model impacts analysis with future scenarios have also been performed in West Africa (Osorio and Galiano, 2012; Paeth and Thamm, 2007). Sylla et al.(2016) analyzed the recent climate change trend and future projection based on observations and models data in West Africa while Gbobaniyi et al.(2013) examined the ability of an ensemble Regional Climate Models (RCMs), driven by ERA-Interim re-analysis to reproduce the key features on present-day precipitation and temperature (1990–2008) over West Africa. The analysis explores globally at different time scale, seasonal and annual climatology and the results showed a good reproduction by RCMs of temperature and precipitation. Akinsanola and Zhou (2018) and Tall et al. (2016) have used two Coordinated Regional Climate Downscaling Experiment models (CORDEX) for the projections of West African summer monsoon rainfall from and for RCP4.5& RCP8.5 future scenarios impacts studies on the hydro-climatology from 2070-2099. All these stu-

dies indicate the significant increase in temperature and precipitation anomalies over West Africa, two major parameters that govern hydrological cycle of the any river.

The simultaneous impacts of land cover and climate change are mostly influencing water resource in river basins. The lumped water balance equation is that the subtraction of evapotranspiration and infiltration out of precipitation gives runoff. So it is evident that modifications in precipitation, evapotranspiration or temperature will have impacts on runoff. Additionally, change in land use and land cover seriously affect leaf area index, evapotranspiration (Gessner et al., 2013), soil moisture content (Rosenbaum et al., 2012) and the soil infiltration capacity (Vereecken et al., 2013), surface and subsurface water content like base flow contribution to stream flow and recharge (Arnold et al., 1995). For these reasons, water resources assessments on the river have been the aims of many studies. These studies usually integrate lumped, semi-distributed or distributed model in the analysis (Devi et al., 2015; Trambauer et al., 2013). Lumped model considers the entire watershed as having the same land use/cover, climate and soil proprieties (Le Lay et al., 2007), semi distributed model divides the watershed in hydrological response unit (HRU) or sub-basins which have the same land use/cover, climate and soil proprieties So the runoff at the outlet is computed through the routing as a sum of the runoff from all the HRU. The distributed model is physical based model which divides the watershed in grids and considers a grid as a unit with same land use/cover, climate and soil proprieties. All the hydrological models have their strengths, weaknesses and their applications of the most appropriate depend on the data availabilities, objectives and the uncertainty analysis. From lumped model to distributed model, water balance components assessments performance depend on the inputs data and the category of hydrological model used (Ficchì et al., 2016; Rientjes et al., 2013). For instance, HBV, GR4J and IHACRES lumped models have been applied in West Africa for surface runoff predictions. These models utilized less climate and hydrological inputs data to predict runoff dynamic in the watershed at the gauging stations (Brirhet and Benaabidate, 2016; Liu et al., 2018). The lumped models are the simplification of the hydrological system to estimate the stream flow at selected gauged stations or for the whole watershed. They need minimum parameters for the calibration and validation of the models (Le Lay et al., 2007; Lee et al., 2007). To come out the lack of data in West Africa, a spatial empiric modeling approaches for hydrology is more required. These lumped model use less input data, take the watershed as a unique unit with the same spatial proprieties and can be used to evaluate the water resource assessment and climate change impacts. Devi et al.(2015) has reviewed many hydrological models and has pointed out their strengths and

weaknesses. Tegegne et al.(2017) by comparing two conceptual (IHACRES and GR4J) and one semi-distributed hydrological (SWAT) model to assess water resource in data - scare region in Nile river found that conceptual model are performing well stream flow but not better than SWAT model. Dye and Croke (2003) evaluated the stream flow prediction with IHACRES rainfall –runoff model in different catchments in South Africa. Results show good accuracy but with underestimation of quick flow events. Gaba et al.(2015) have used HBV (Lindström et al., 1997), GR4J and *ModHyPMA* (Modèle Hydrologique basé sur le Principe de Moindre Action) ensemble approach modeling to assess water management in Benin. Oyerinde et al.(2016) and Wagener et al.(2001) evaluate the performance of conceptual rainfall-runoff models of two-different basins. The acceptable results were obtained with these models and ensemble but the best ones were with mean-base ensemble modeling.

Recent studies on the Mono River basin have been focused, on flood dynamics modeling at Nangbéto station using GR4J lumped model (Amoussou et al., 2014). These past analyses focused on rainfall temporal variability in some particular gauges stations of discharge (Amoussou et al., 2017; Rossi, 1996; Houessou et al; 2016).

For the assessment of a complex environmental system by integrating land use, climate change and dam management in the river, the identification of sustainable tools, techniques and strategies such as Geographic Information Systems (GIS) and Remote Sensing (RS) are well known as information technologies and applied in many studies (Bárdossy and Schmidt, 2009; Rodriguez and Suarez, 2012). Indeed RS and GIS techniques have been extensively used in many applications like agriculture, forestry, water managements, hydrology, biodiversity, climate change and environment planning. For example, Liu (2009) has used GIS tools for modeling water-crop relation. The results indicate that there is a non-linear relationship between virtual water content and crop yield whereas Zhang et al.(1996) have integrated GIS for erosion modeling. GIS was used by Rodriguez and Suarez (2012) to develop a methodology for estimation of slope length and slope gradient factors (LS). The results have revealed the steps for accurate estimations of LS factors; provided algorithm and GIS packages to compute each parameter. In related study (Youssef et al., 2010) have estimated flash flood risk in Egypt using GIS based satellite images. GIS have been selected as a powerful tool for the assessment of natural hazard risk and management. By coupling RS data such as land use and land cover (Fohrer et al., 2005) have used SWAT model to provide sustainable strategies for water resource management in the catchment. Many hydrological models are available in GIS environment

and are used in many studies for integrated LULC in water management in the catchment. For example SWAT, SWIM, WaSiM, MIKE-SHE models that have been tested all over the world and particularly in West Africa (Fohrer et al., 2005; Gérard-Marchant et al., 2005; Jayakrishnan et al., 2005; Krysanova et al., 2015). Hydrological models are important tools to understand the characteristics of a river and the response of the stream flow. They are like a simple way of conceptual representation of river hydrology system of water cycle (Eshtawi et al., 2016; Haddeland et al., 2014).

In addition, to assess water resource management in the river, data are the most important variable that researchers deal with. Data availability is a challenge that researchers usually face particularly in West Africa (Bormann et al., 2012; Ndomba et al., 2008). To resolve these issues many hydrological and climate stations were installed during many projects implementation. Example, Innovation management using appropriate tools and measurements (IMPETUS) for Small and Medium Size Enterprise (SMES), GLOWA in Volta basin, Niger-Système d'Observation du Cycle Hydrologique (HYCOS) project, OROSTOM, PCCP in Togo (PCCP, 2008), GLOWA IMPETUS project (Speth et al., 2010), that investigate the effects of global change on the water cycle and water availability on a regional level. Most of hydro climate stations are abandoned or lack of maintenance (Idrissou et al., 2015). It is the case in Mono river basin, where several hydrometrics stations installed since 1960 have a long period of gaps. As consequences there are real challenges for water resource assessment and hydrological models calibration and validation. As alternative, reanalysis data is freely available at National Aeronautics and Space Administration (NASA) or others sites, but their data usually have to be validated with in situ data to see if these data represent the dynamic in the region. Poméon et al.(2017) evaluate the performance of remote sensing and reanalysis of different datasets over West Africa using Hydrologiska Byrans Vattenbalansavdelning (HBV) model and obtain different results depending to the source of reanalysis or remote sensing data. The results show that remote sensing dataset can be used for valuable information in hydrology unless there are in situ data for validation.

In order to give sustainable and adequate solutions on water resource pressed on by the above cited factors, a need of appropriate approaches that will take into account at least the most or the entirety of natural and social subsystems. Therefore, in science based tools are developed to assess hydrological processes by incorporating human activities like construction and operation of a reservoir, water withdrawal for population needs, agricultural developments, land use and land covert changes (Lahsen, 2005; Poff et al., 2003). Among

these tools, distributed hydrologic models are useful tools for the simulation of hydrologic processes, planning and management of water resources, investigation of water quality, and prediction of the impact of climate and land use changes worldwide (Breuer et al., 2009; Kankam-yeboah et al., 2013). Different hydrological models were used in West Africa and in the world for water management planning. For example HBV model is used by Poméon et al., 2018 (2017) to asses water availability in West African basin, Badjana et al., (2014) implemented IHACRES and J2000 models to assess water resource management in Kara river basin of Togo. Badou(2016) used four different models (HBV-light, UHP-HRU, SWAT and WaSiM) to simulate the streamflow in four non-sahelian basin of Niger basin in West Africa.

In fact, many studies have been done by using SWAT model in West Africa analyzing the effect of soil on sediment yield or on modeling the effect of crop and management on surface water and groundwater (Bossa et al., 2012) . Sintondji (2005) used SWAT model in Ouéme basin to assess erosion process. Awotwi et al.(2015) used SWAT model to predict the impact of climate and land use change in Volta basin in Ghana. SWAT model was used in Niger basin (Begou et al., 2016) to assess its performance and prediction uncertainties in Bani river and sub-basin. Hounkpe (2016) calibrates and validates two hydrological models WaSiM and SWAT for assessment of high discharge over the Zou catchment in Benin. For these reasons, SWAT model can be use for water resource management where data availability remains a big challenge.

1.3. Research questions

The following research questions are answered in the study:

- Are CILSS data sets the best land cover and land use available over MRB?
- What is the trend distribution of hydro-climate variables in MRB,
- What is the hydrological system response of the Mono river basin considering different lumped hydrological models?
- What are the impacts of climate, land use change and dam management on water cycle components over different periods?

1.4. Thesis objectives

1.4.1. Main objective

This study contributes for a sustainable water resources management in the MRB by integrating land use, climate change and dam management impacts on water balance components.

1.4.2. Specific objectives

The specific objectives are:

- to evaluate different land cover data sets, and predict future land cover mapping scenarios of the MRB;
- to investigate the spatial and temporal trend analysis of historical hydro-climate variables between 1961 and 2016 and compute and analyze RCP4.5 & RCP8.5 future scenarios climate extreme indices for near future (2020-2045);
- to test and to compare two different lumped rainfall-runoff models response for two sub-periods (1961-1986 and 1988-2011) in the MRB;
- to assess the impact of climate change, land use change and dam management on water balance components using semi-distributed model in the MRB for the two sub-periods.

1.5. Research hypothesis

In order to answer the research questions, some hypothesizes are formulated:

- CILSS data set are the best available over MRB and with population growth /human activities LULC will continue to change in near future;
- There are positive or negative trends on hydro-climate variables time series over MRB;
- Lumped models are sufficient for simulating surface runoff in the MRB;
- Land use change, climate change and dam management affect on water balance components changes.

1.6. Novelty

To the best of knowledge, no research has been conducted on the past in Mono river basin by combining land use/cover, climate change, dam management and climate scenarios RCP4.5 and RCP8.5 impacts in water resource management. Thus, the outputs of the

present study should be a new guideline for present and future integral water managements in the river and must be incorporated in the right way by the policy and decision makers for the Mono river basin particularly and in West Africa region as a whole.

1.7. Scope of the thesis

In West Africa, the trans-boundary River Basin of Mono, covering an area of 22,014 Km^2 between Togo and Benin Republics is the subject of this study. In the analysis, the impacts of climate, land use and dam management on water balance components over the river basin are assessed. Hydroelectricity data were not totally incorporated in the analysis because of its inaccessibility or lack of all the reservoir data. But the reservoir operation information such as the spillway conditions, the reservoir surface area, watershed area, the capacity of the reservoir storage capacity and principal spillway are incorporated. The study analysis period ranges between 1961 and 2016, with data available typically during this period. The period was divided into two sub-periods from 1961 to 1986 (period before dam installation) and from 1988 to 2016 (period after dam installation). The data used are meteorological data (daily minimum and maximum temperature, daily evapotranspiration, and daily precipitation), hydrological data (daily discharge), remote sensing data of land use and land cover from different database, Harmonized World Soil Database v 1.2 scale of *1:5 000 000* of Food Agriculture Organization (FAO) soil database and six different downscaled Global Climate Model aggregate into mean ensemble downscaled Global Climate Model over the MRB. Therefore, the simulated daily temperature and precipitation were validated with observed data from available gauging stations. They were used for future climate extreme indices scenarios and impact analysis on discharge for upstream–downstream gauge station of the river and for two sub-periods.

Land use and cover sample have been collected for validation with remote sensing data derived from land cover/use automatic classification. Different hydrological model (GR4J, IHACRES and SWAT models) are used to assess runoff temporal variability and spatial and temporal water balance component.

The analysis and models applied on the data results are:

- Three land cover database were analyzed, validated for the future land cover scenarios land cover accuracy assessment in the MRB.
- Land Change Modeler (LCM) software from Clark University (*https://clarklabs.org/terrset/land-change-modeler/)* was used for land cover analysis and future scenarios development.

- Thiessen Polygons interpolation (Thiessen, 1911) method has used to compute areal rainfall using 21 rain gauge stations over MRB.
- The Man-Kendall test statistic (Kendall, 1975; Mann, 1945) was used for trend analysis for a long period over the river and for rainfall, mean temperature, discharge and evapotranspiration gauging stations.
- Downscaled Global Climate Model outputs data were validated with observation data and trend analysis was performed on these time series (1961-2016).
- RClimDex was used for climate extremes indices computation for RCP4.5 and RCP8.5 in near future (2020-2045).
- GR4J and IHACRES lumped conceptual rainfall runoff models were used for runoff prediction and comparison for Athiémé gauging station over two sub-periods (1964-1986 &1988-2010).
- SWAT semi distributed model was used for streamflow prediction and water balance components prediction and comparison in the MRB over two sub-periods.

1.8. Expected results

At the end of this thesis, we expect:

- development of best land use and cover dynamic evolution and changes in the MRB from 1975 to 2013 and future land use scenarios between 2020 and 2027 from three different spatial resolution data sets;
- assessment of hydro-climatology trend analysis (1961-2016) and its response to RCP 4.5 &RCP8.5 extreme climate indices scenarios in near future (2020-2045);
- investigation of rainfall-runoff model response in the MRB for two sub-periods;
- Assessment of land cover, climate change and dam management impacts on water balance components in Mono river basin using semi-distributed model.

1.9. Outline of the thesis

The thesis is divided into eight following chapters:

- Chapter 1 presents the general introduction. This includes background, problem, statement and justification of the research, literature review, objectives, research question, hypothesis, novelty, scope of the thesis and expected results.

- Chapter 2 covers presentation of the study area with description of Mono River Basin (MRB), including climate, vegetation, soil, hydrology, demography, environmental, industrial installation, social and economic activities and water resources descriptions.
- Chapter 3 presents data, methods and material used to describe the study area. This chapter describes the data preparation, software used and methodology adopted to analyze these primary, secondary data such as observations data and climate and hydrological models.
- Chapter 4 shows the results on land use and land cover evaluation (1975-2013) and future scenarios development (2020-2027) in the Mono river basin
- Chapter 5 deals with ensemble climate model validation, spatial and temporal trend analysis of historical hydro-climates variables (1961-2016) and to compute RCP4.5 and RCP8.5 future scenarios climate extremes indices (2020-2045).
- Chapter 6 discusses runoff-rainfall modeling and comparison at Athiémé station using two conceptual lumped hydrological models.
- Chapter 7 looks at the results on modeling of water balance components and discharge simulation in the Mono River Basin under different scenarios of land cover, climate change and reservoir management over two sub-periods.
- Chapter 8 ends with a general conclusion, recommendations and perspectives.

Chapter 2: Presentation of the study area

This research was conducted in the largest river basin shared by Togo and Benin Republics, the Mono River Basin (MRB). This chapter provides a general description of the MRB at Athiémé outlet focusing on the whole MRB from Central region of Togo (Alédjo) to Atlantic Ocean in the South. The description encompasses location of the study, soil characteristics, land cover, climate, geology, topography, hydrography of the area, population characteristics and presents a brief description of the Nangbéto dam built on the course of the Mono River for hydro-electricity generation and irrigation.

2.1. Geographic location

The trans-boundary Mono River Basin (MRB) is shared by Togo and Benin Republics and accounted within the twenty five (25) cross-bordered river basins in West Africa. The MRB total surface area located in Togo Republic side represents 38% of the whole Togo'surface area, while its counterpart in Benin Republic side corresponds only to 3.14% of the territory. The Mono River is located between 06°16' and 9°20'Northern latitude and 0° 42'and 1° 40' Eastern longitude (Figure 2.1). Its basin encompasses the region from Alédjo to Athiémé an approximated surface area of 22,014 km² and a perimeter of 872, 092 km with its largest area in Togo (~ 87%). With a length of 527 km, the Mono river takes its source in the Alédjo Mountains in the north of Benin and drains into the Atlantic Ocean via "la bouche du roi"(ONU-SOFRELEC, 1964; PANGIRE, 2016; Rossi, 1996). The elevation of the basin is ranged from 11 to 948 meters. The biggest dam on the waterway of the Mono River is built at Nangbéto and produces 20% of the total electricity used by Togo and Benin Republics. The second dam, the one at Adjarala is built at the downstream of Nangbéto to increase the electricity production for the needs of the two countries.

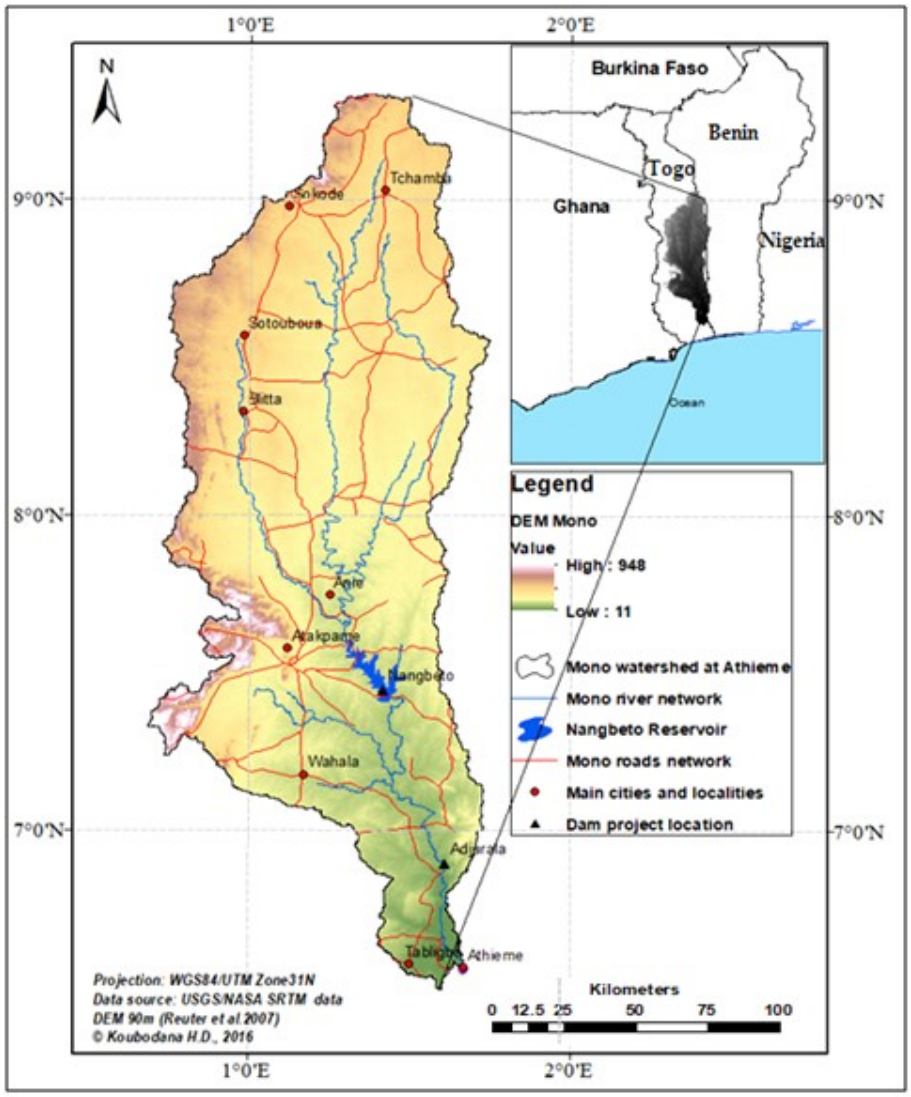

Figure 2.1: Location of the study area

2.2. Relief and geology

The Mono Basin is located in the biggest chain of Atakora. The topography is generally composed of the coastal floodplain littoral in the south, a sedimentary plateau and with the high mountain in the North-West and center-west of the basin (Amoussou, 2010; Klassou, 1996; PCCP, 2008), except for the massifs of the East and the North -East. The lower part of the basin, very narrow is found in the coastal sedimentary, often covered by alluvial deposits at Athiémé. The altitude in Mono river basin is between 11m and 948 m with the highest at Atilakoutse (Amoussou, 2010; ONU-SOFRELEC, 1964). For the first 35 kilometers from its source point in Benin, the Mono river has a relative slope between 1.5 to 3m/km (Affaton, 1990). The slope of the bed will becomes very low (0.04 to 0.06

m/km) and the river ends in a large meanders through flood zones before joining the lagoon system of the Gulf of Guinea (PCCP, 2008).

The geology in West Africa is dominated by the stable and precious unit West African Craton (WAC) comprising an Archean –Plaeoproterozonic lithosphere (Da Costa et al., 2013; Speth et al., 2010; Tairou et al., 2012). The geology of Togo Republic is largely composed of gneissesand graniticrocks of Proterozoicage in the central and southern part of the country (Speth et al., 2010). These are overlain in the coastal zone by Cretaceousand Cenozoic sediments. As MRB is about 38% of Togolese republicsurface aera, it lies in the same type of geological structure. The northern part of the country has a basement of Neo-proterozoicmetamorphic rocks and Paleoproterozoic granite. The south of the country is covered by sedimentary basins, covering 3,300 km^2 of lands. Togo mines gold, diamonds, and phosphate rock, with the largest of these being phosphate rock. The phosphate rock is found in Eocene deposits at the coastal basin. In addition to those easy–to-exploit locations, there are also hardened Neoproterozoic which have not been exploited.

The Mono River catchment area is spread over two large units geological phenomena (Klassou, 1996). According to Tairou et al.(2012), Mono river basin is laying in southeastern margin of the Pan-African-Dahomeyide belt. The geology is within the categories of Kyanite bearing micaceousquartzites, Buem structural unit, Meso-Cenozoic cover of the Gulf of Guinea Basin and Kandi fault mylonitic zone. The upper basin consists essentially of metamorphic rocks. More information can be found in (Da Costa et al., 2013; Tairou et al., 2012; Théveniaut and Thiéblemont, 2016).

2.3. Vegetation, fauna and flora

The vegetation is mainly savanna and is composed of the classified and gallery forests and various grassland grasses. The fauna consists of mammals (buffalo, warthogs, monkeys, deer, and various birds of prey, aquatic life, crocodiles and hippopotamuses (Amoussou, 2010; Klassou, 1996).There are some forests reserves in the Mono basin: the forest of Aboudoulaye, forest of Naglanou , the forest of Akissa and the forest of Togodo (Amoussou et al., 2017). Overall, the original dense vegetation has almost disappeared and has given way to oil palm and shrub plantations.

2.4. Climate

The watershed area encompasses two climate zones .The climate is a subequatorial climate from 0 to 8°N and with two rainy seasons and two dry seasons. It totals 1200 to 1500 mm/year in the mountainous area of the South-West and only, 800 to 1000 mm/ year on the coastal zone (example of Tabligbo climate station). From 8 to 10°N the climate is tropical humid (Case of Sokodé climate station) with one rainy season and one dry season (1000 to 1200mm/year). In the winter (December to March), there is an anti-cyclonic high-pressure area centered over the Sahara. It drives the harmattan, a desiccating, dusty wind that blows rather persistently from the northeast, drying out landscapes all the way to the coast (Ahmed et al., 2016).

The synoptic station of Atakpame is intermediate between the two climate zones (Figure 2.2). The distance between two successive synoptic stations is less than 150 km.

The Inter-Tropical Convergence Zone (ITCZ) is defined by the maximum water vapor convergence in a tropospheric column. The ITCZ is located between 6° and 10° latitude south of the Inter-Tropical Front (ITF) (Hamilton et al., 1945), governs the monthly rainfall distribution by a nearly east-west oriented zone of the zone of maximum precipitation (MERF, 2015; Speth et al., 2010). As far as temperatures are concerned, lowland areas have temperatures between 19 ° C and 34 ° C, while in mountain areas they vary between 18 ° C and 30 ° C. The mildest areas are the wooded mountains and plateaus, the warmest being the bare mountains and part of the plains.

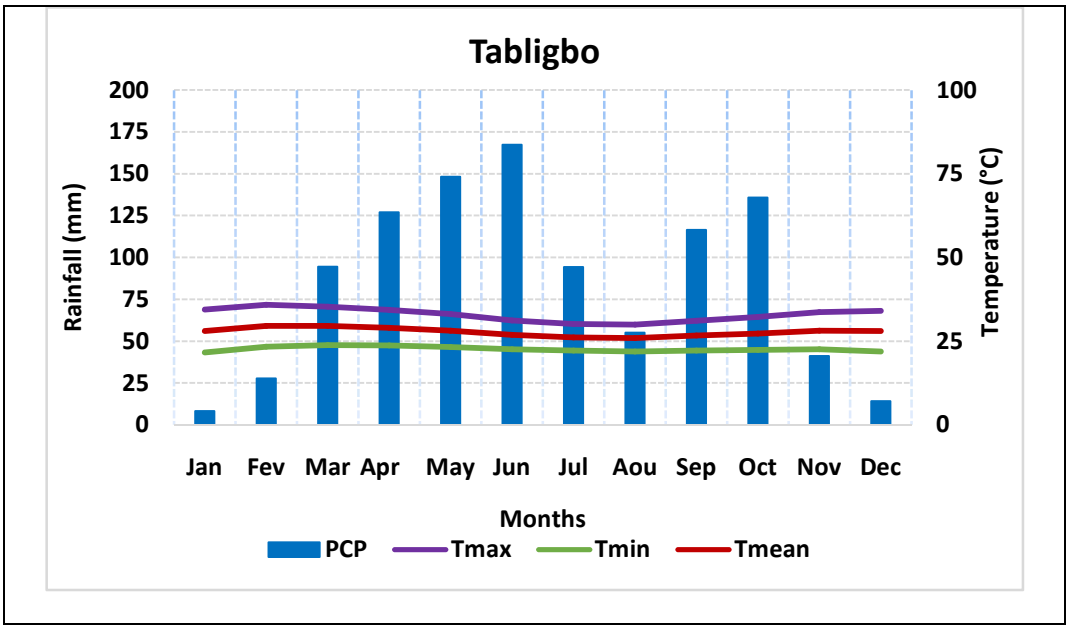

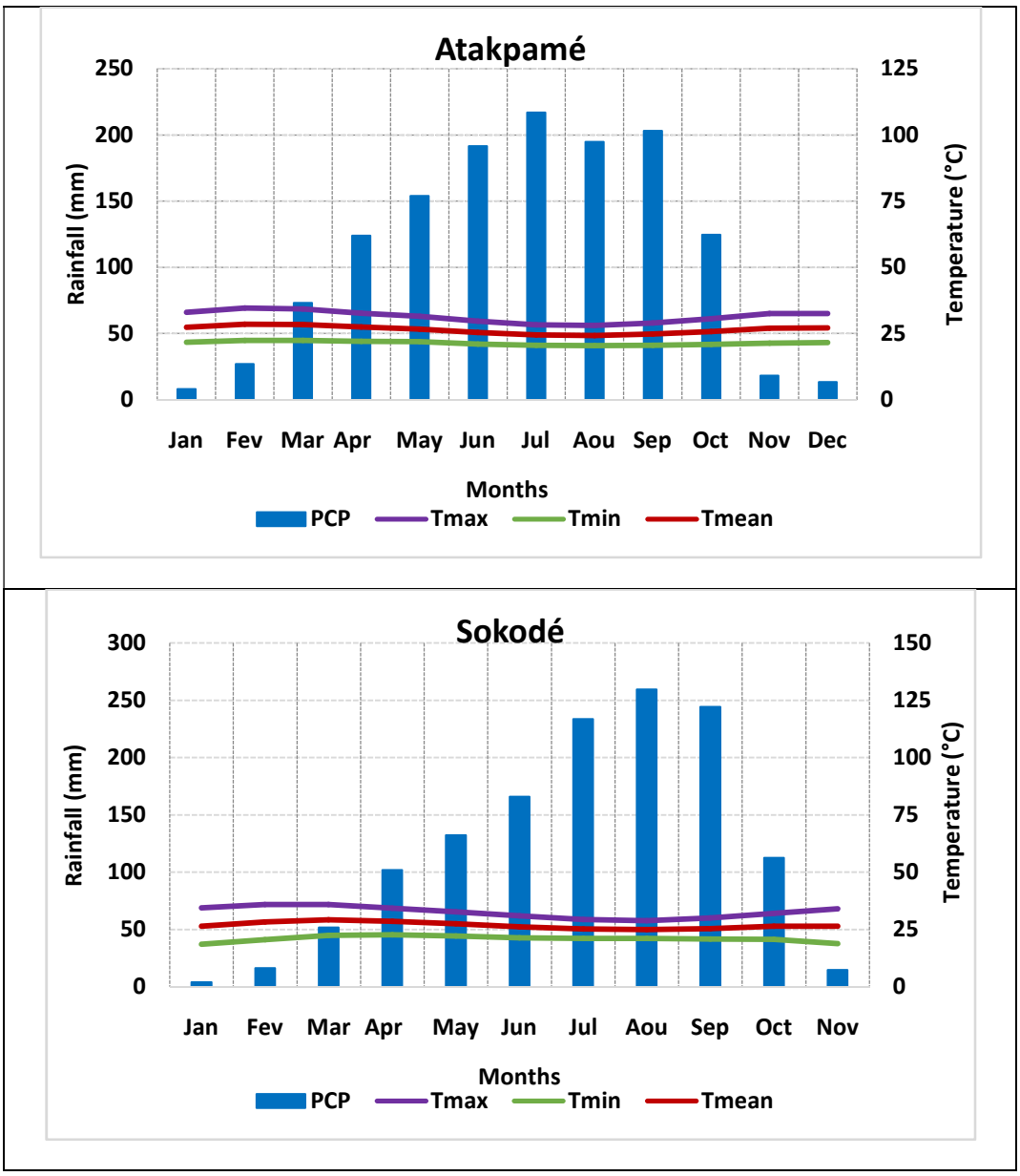

***Source**: DGMN-Togo, 2018.*

Figure 2.2: Climate diagram at different zone stations

2.5. Hydrography

The Mono River takes its source at Alédjo in the north of Benin Republic in the Koura Mountains. The river follows an East-West direction until the 8th latitude before changing eastwards direction to Athiémé outlet (Rossi, 1996).The river stream flow is originally from rainfall characteristic from Guinean regime in the Sudanian zone. Athiémé is the outlet where the river is joined by its mains tributaries. From the upstream to the downstream the main tributaries are Anié (161 km), Amou (114km), Amoutchou (62km), Kra (69km) and Ogou (207km). Mono River is at 90 m^3/s at Anié and around 125 m^3/s at the downstream of the river (ONU-SOFRELEC, 1964; PCCP, 2008).

The Mono has a tropical rainfall hydrologic regime but it is influenced by the sub-equatorial climate. In the average year, according to Le Barbé and Lebel (1997) the average annual flow of the Mono River is about 100 m^3 /s at the Athiémé station. Nevertheless, since 1988, when the Nangbéto dam is in operation, the Mono hydrological regime has undergone a major change, with a low water flow level of 40m^3/s. The reasons are explained in part by the dam reservoir water management. The river mostly presents one peak of discharge at Athiémé between August and October (Figure 2.3). The annual maximum discharge at Athiémé is around 389 m^3/s (ONU-SOFRELEC, 1964; PCCP, 2008).

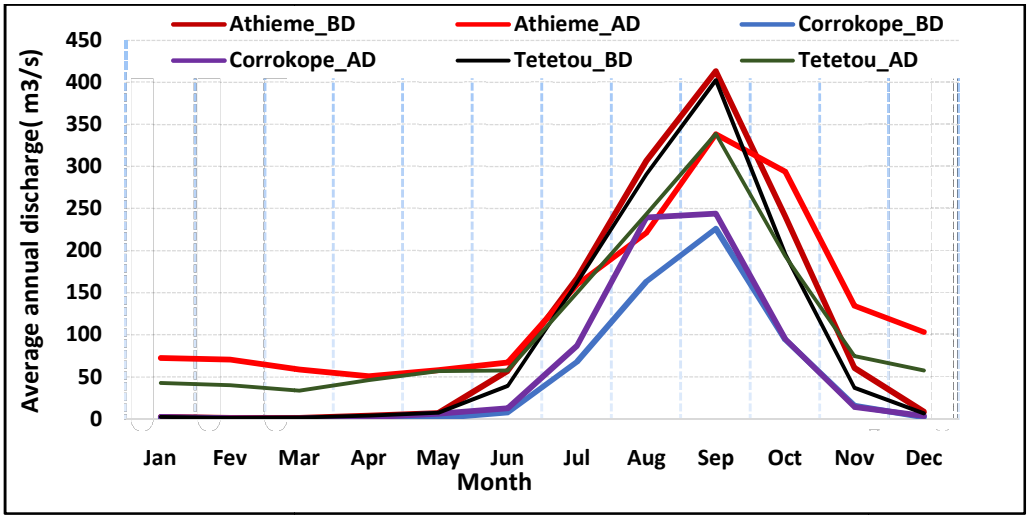

*[**BD** means before the dam construction (1961-1986) and **AD** after the dam construction (1988-2011)]*
***Source**: SIIEau-Togo, 2017 and DGEAU, 2016-Benin*

Figure 2.3: Average monthly discharge of MRB stations

2.6. Soil and land use

Soil proprieties play an important role in water infiltration and water runoff in the watershed (Kinnell, 2010). Mono river basin is composed of tropical soils type (http://www.fao.org/soils-portal). According to Faure (1985) and Lamouroux(1969) Togolese country contains a mosaic diversified type of soils generally of tropical characteristics. Mono river basin at Athiémé presents six (6) categories of soil (FAO-UNESCO, 1974) shown in Figure 2.4. All the soil type area is described in Table 2.1. Within the soils there are Gleysols, less represented soil which is located in the south-west of the basin covering 0.38% of the total area. Leptosols are the common soils along the Togo mountain chain, with shallow soils formed over hard rock (Faure and Volkoff, 1998). Leptosol soils represent 18.33% of the total area of the watershed. Lixisols are the dominant soils in Mono river basin which occupies 65.92% of the river area and are seen along the entire

basin specifically in the center east. They reflect a stable geological conditions and natural savanna vegetation (Lamouroux and Lamouroux, 1969; Soil Survey Staff USA, 1975). With 7.73% of total surface area, Nitisols are diversified in the basin but known to be more in the coastal plain in the southern Togo (Faure, 1985; Lamouroux, 196AD). As a minor soil in the Mono river basin, Plinthosols cover0.48% of the total area of Mono river basin and are only located in the north of the basin. Finally, vertisols (7.17%) are concentrated in the center of the basin and are the soil that flood quickly (Soil Survey Staff USA, 1975).

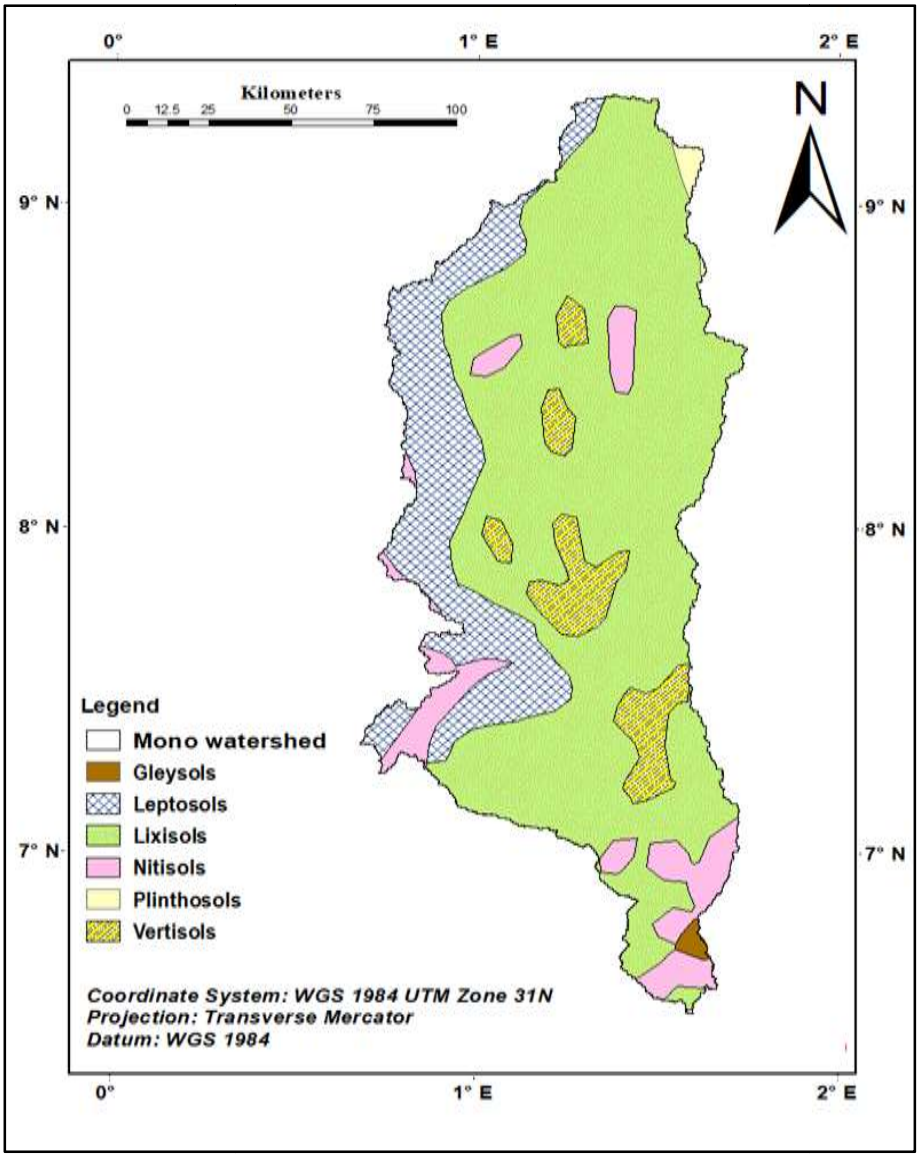

Source: *FAO-UNESCO, 1974*

Figure 2.4: Soil type Map in the Mono river basin

Table 2.1: Soil type description in the Mono river basin

FAO soil name	Soil symbol	Soil group description	Area [Km^2]	Area [%]
Leptopsols	LP	Very shallow soils over hard rock or in unconsolidated very gravelly material	4001.98	18.33
Gleysols	GL	Soils with permanent or temporary wetness near the surface	82.05	0.38
Lixisols	LX	Soils with subsurface accumulation of low activity clays and high base saturation	14390.10	65.91
Vertisols	VR	Dark-colored cracking and swelling clays	1564.31	7.17
Nitisols	NT	Deep, dark red, brown or yellow clayey soils having a pronounced shiny, nut-shaped structure	1687.08	7.73
Plinthosols	PT	Wet soils with an irreversibly hardening mixture of iron, clay and quartz in the sub-soil	104.24	0.48

Source: *FAO-UNESCO, 1974*

Land use and land cover in the MRB are characterized mainly by forest, savannah, bare soil, wetland, water body, cropland and settlements. The natural vegetation is dominated by savannah (grassland interspersed with shrubs and trees), forest (forest administrative park, mall dense and gallery forest). Cropland is an extensive practice in the Mono river basin.

2.7. Demography, environmental, social and economic activities

The population of Togo republic is estimated to 7.99 million (104th in the World) and 11.48 million in Benin in 2018 *(http://worldpopulationreview.com/countries/togo-population)* .The population is a rapidly growing one, compared to 6.3 million population in 2010. Between 1981 and 2010 censuses, the population has almost doubled in Togo. With globally 22,998 square miles of land in Togo, it is densely populated with 126 per square kilometers. The population growth rate in Togo is 2.48% and 2.77% in Benin in 2018 (DGSCN-MPDAT, 2014; MERF, 2015).

The Mono river basin population is 5,115,026 inhabitants or 34.92% of the total population of the two countries in 2010 (DGSCN-MPDAT, 2014; MERF, 2015; PANGIRE, 2016). The population in the MRB is evaluated to be about 24% of Togolese population in 2016 (PANGIRE, 2016; PNSET, 2012). The main activities in the MRB are agriculture, with extensive shifting cultivation followed by livestock and fishery. Agricultural activities are depended on rainfall. Globally in Togo about 29% of population is Christian, 20% is Muslim and 50% indigenous beliefs. More than49% of the population in Togo and Benin countries lives below the international poverty line of USD$1.90 per day (2011 indicator) *(http://www.worldbank.org).*

On Mono river basin settles the Nangbéto hydropower dam and located approximately at 45 km from Atakpamé city. The dam was built and has started operating in September 1987 to resolve the lack of electricity of Togolese and Beninese Republics. The realization of Nangbéto dam has lead to the displacement of 34 villages of 10600 inhabitants to others land (PANGIRE, 2016; PCCP, 2008). The characteristics of Nangbéto reservoir are shown in Table 2.2.

Table 2.2: Hydro-electricity production at Nangbéto

Designation	Creation	Capacity (MW)	Production (GWh)		
			1999	2000	2001
Nangbeto	1987	65	201	198	92
Characteristics of hydroelectricity planning					
Characteristics designation			Nangbéto planning		
General description			Buttress dam 48.0 m high and 517.0 m long		
Reservoir capacity			1485 millions of m^3		
Equipment discharge			2 ×120 m^3/s		
Total power			62 MW		
Power in the dry period			45 MW		
Average production			150 GWh		
Use factor			25%		

Source: (Houessou, 2016; PANGIRE, 2016; PCCP, 2008; Robert, 2013)

The other roles of the dam are irrigation, promotion of agriculture, fishery and the regulation of the stream flow at the downstream of the river at Athiémé (Bénin) and Yoto (Togo) localities. The hydrological regime of Mono is very irregular. The installation of the Nangbéto dam by Benin and Togo has led to a significant reduction of its floods. The height of fall created by the dam allows electricity production for both countries managed by Communauté Electrique du Benin in French (CEB) Company. Figure 2.5 indicates the topographic map in MRB.

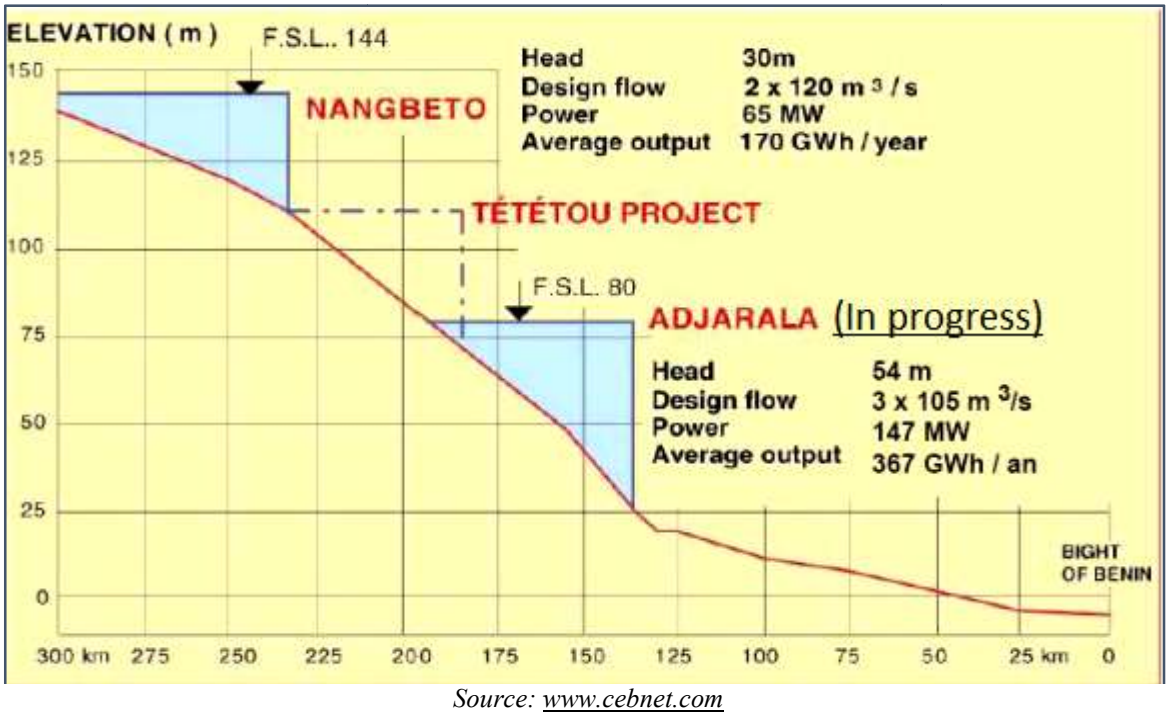

Source: www.cebnet.com

Figure 2.5: Topography map of the dam's position in the MRB

2.8. Conclusion of the chapter

Mono river basin is one of the main rivers in Togo which covers 38% of Togolese territory and 3.14% of Benin country's area. With the length of 308 km from its source to Athiémé, Mono river basin main tributaries are Anié, Amou, Amoutchou, Kra and Ogou. Nangbéto hydroelectric dam is the major hydraulic infrastructure in the basin producing 20% of electricity for the two countries. The second dam of Adjarala project is on the downstream of Nangbéto and it is located on the Benin territory. Mono river basin climate is generally from subequatorial climate in the south to tropical climate zone in the north of the basin. The rainy season globally is from May to October followed by the dry season. The annual total rainfall in the basin is between 1000 to 1500 mm and the mean temperature is about 26°C.The main socio-economic activities are agriculture, trade, fisheries and livestock husbandry.

Chapter 3: Data, materials and methods

In this study different types of material and methods are used both for data collection and data analysis. These materials are grid rater data, point data and tools that are described in this chapter. These data are collected at National meteorological and hydrological direction, freely online datasets and remote sensing, from literature, etc. All the data are used over MRB and over the period of the study for land use and land cover evaluation and scenarios, spatial and temporal trend analysis, climate extremes indices trend analysis and for runoff and water balance components prediction using different scenarios of hydrologic models.

3.1. Data

3.1.1. Land use and land cover data

In many papers, LULC assessment has been performed with data available from the U.S Geological Survey (USGS). These products are developed on a large, often global, scale and applying them to the local scale without any validation can significantly affect the model results (Mishra et al., 2014; Sun and Robinson, 2018). In the present study, different land cover data over the Mono River Basin (MRB) were used.

3.1.1.1.Permanent Interstate Committee for drought control in the Sahel (CILSS)

The United State Geological Survey (USGS) in West Africa Land Use Dynamics project worked in partnership with CILSS and the United State Agency for International Development/West Africa (USAID/West Africa) to map land use and land cover across the region for the years 1975, 2000, and 2013 with 2 km resolution (Cotillon, 2017)**.** Data can be downloaded on the West Africa land use and land cover dynamic website *(https://eros.usgs.gov/westafrica/data).*The images used to develop the maps are taken from Google Earth but the majority comes from one of the three sources LANDSAT, Corona, and the Moderate Resolution Imaging Spectro-radiometer (MODIS). CILLS data are aggregation of LANDSAT images information and local information. To classify the images, the Rapid Land Cover Mapper (RLCM) was used for the analysis, which is automated and semi-automated mapping method software. Based on manual photo interpretation techniques, tools facilitate mapping over larges area and through time and produce time–series of raster maps. These raster were classified according to the legend of CILSS into 22 land use and land cover types over West Africa including forest-savanna,

wetland, cropland, water and settlements and according to good practices guidance for land use, land cover change and forestry (Penman et al., 2003).

3.1.1.2. European Space Agency -Climate Change Initiative (ESA-CCI)

The European Space Agency by its Climate Change Initiative project (ESA-CCI) released the latest version of land use data in 2016, called CCI-Land Cover developed at Université catholique de Louvain (UCL) of Belgium. The products are freely available online through *(http://maps.elie.ucl.ac.be/CCI/viewer/index.php).* For the period 1992-2015, maps are available in annual time steps in a spatial resolution of 300m, which was the first freely available product at that high resolution. There are 10 generic land cover types across the world. The map legends are compatible with the United Nations (UN) Land cover Classification System (LCCS). It is based on an automated processing chain for a global land cover mapping. Data are available through the ESA-CCI website *(https://www.esa-landcover-cci.org).*

3.1.1.3.GlobeLand30 (GLC30)

The Globeland30 (GLC30) dataset is available at a 30 meters spatial resolution. The National Geomatics Center of China (NGCC) developed the land cover mapping products in 2014. The dataset covers land area from 80°N to 80°S and 60°W to 60°E latitude and longitude using 10 land cover types (Chen et al., 2017). The products are available only for the years 2000 and 2010.

The classification images used to generate Globeland30 are mainly 30m multispectral images from Landsat TM and ETM+ multispectral images downloaded from USGS *(www.landsat.usgs.gov/)* and those from the Chinese Environmental Disaster Alleviation Satellite *(www.cresda.com/).* After a geometric and radiometric correction, Landsat images are transformed to the WGS-84 coordinate system and the UTM projection. Line-of-Sight Atmospheric Analysis of Spectral Hypercube (FLASH), atmospheric correction and the Smoothed COS method (SCOS) topographic correction are applied to Landsat images before classifications. Auxiliary data like reference material are used to support sample selection, classifier training and accuracy assessment (Chen et al., 2017; Ren et al., 2018).

For the classification outline, the method used is based on Pixel-Object-Knowledge (POK). This method includes pixel classification, object filter and a human–computer interactive

check and verification step. More detailed information of the products can be found on *(http://tianditu.com).*

Table 3.1: Summary of land covers datasets description

Data sets	CILSS	ESA-CCI	Globeland30
Spatial resolution	2 km×2 km	300m×300m	30m×30m
Data periods	1975, 2000 and 2013	1992 to 2015	2000 and 2010
Coverage	West Africa	Worldwide	Worldwide
Inputs images for classification	Google earth, Landsat, Corona and MODIS	300 m MERIS, 1km SPOT-vegetation, 1km PROBA-V and 1km AVHRR	Landsat TM and ETM+
Classification type	automated and semi-automated	Automated	Pixel-Object-Knowledge (POK)
Number of initial LULC	22	22	10
Source	*https://eros.usgs.gov/westafrica/data*	*http://maps.elie.ucl.ac.be/CCI/viewer/index.php*	*http://www.globallandcover.com/*

3.1.2. Topography data (DEM)

For setting the ArcSWAT model, a digital elevation model (DEM) of 90 m resolution from the Shuttle Radar Topographical Mission (STRM) with an accuracy of about ±16 m (Reuter et al., 2007) was used *(source: http://srtm.csi.cgiar.org/)*. The DEM is used also for delineation including stream, outlets, inlets, slop definition and the calculation of the sub-basins parameters of the watershed of the Mono River basin (MRB) (Figure 3.1) and as an input driver in Land Change Modeler (LCM) during land cover prediction.

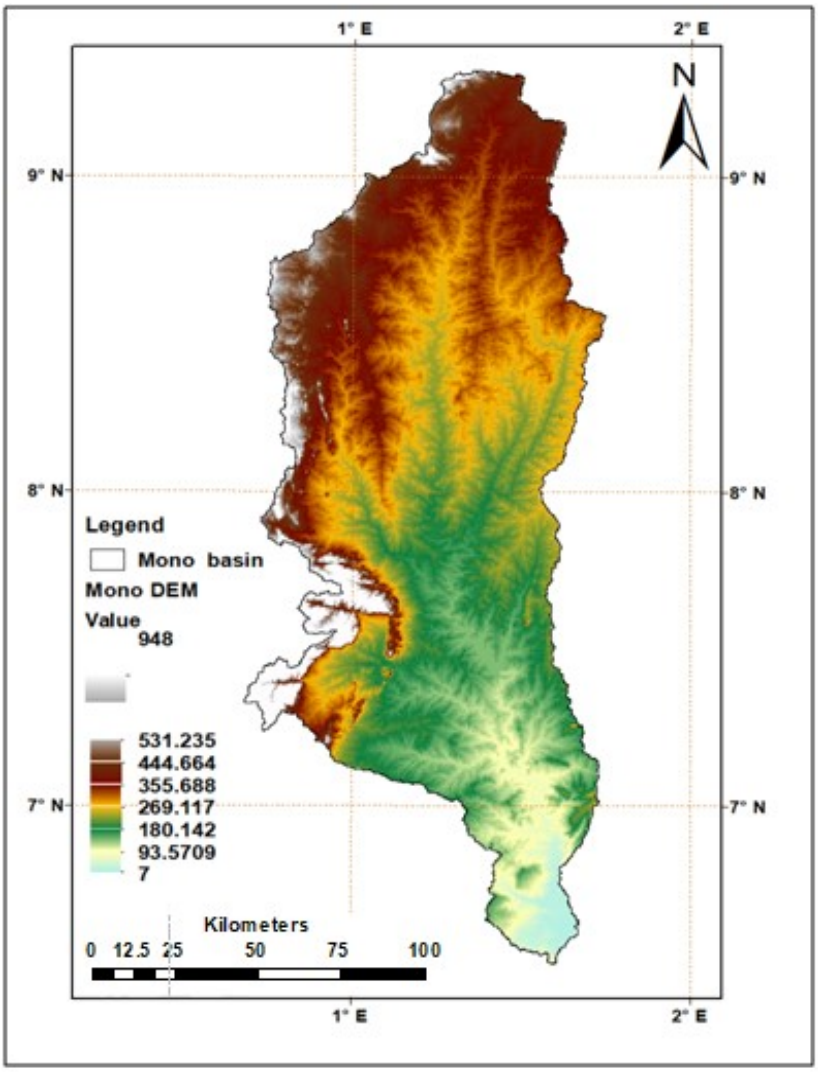

***Source**: DEM images of 2017(http://srtm.csi.cgiar.org/)*

Figure 3.1: Map of Mono River Basin at Athiémé outlet topography

3.1.3. Soil type data

Harmonized World Soil Database (HWSD) version 1.2 scale of 1:5 000 000 of FAO soil database was used for the study. Poméon et al.(2018) prepared HWSD SWAT soil data parameters for all West Africa. We extracted from the West Africa soil data the ones concerning the Mono watershed. Soil data in SWAT allows the determination of the soil texture, available water content, hydraulic conductivity, bulk density and organic carbon content for different layer depending on each type of soil. The missing parameters were estimated using pedotransfer function (Wösten et al., 2001) function. Pedotransfer functions are predictive functions which relate more easily measurable soil data such as soil texture (sand, silt and clay), bulk density, organic matter (or organic carbon) content and/or other data routinely measured or registered in soil surveys with hydraulic parameters such as the soil water retention curve . All soil in Mono watershed is given in Figure 3.2.

Table 3.2 and Table 3.3 indicate the Harmonized World Soil Database (HWSD) composition and type proprieties used during SWAT model simulation.

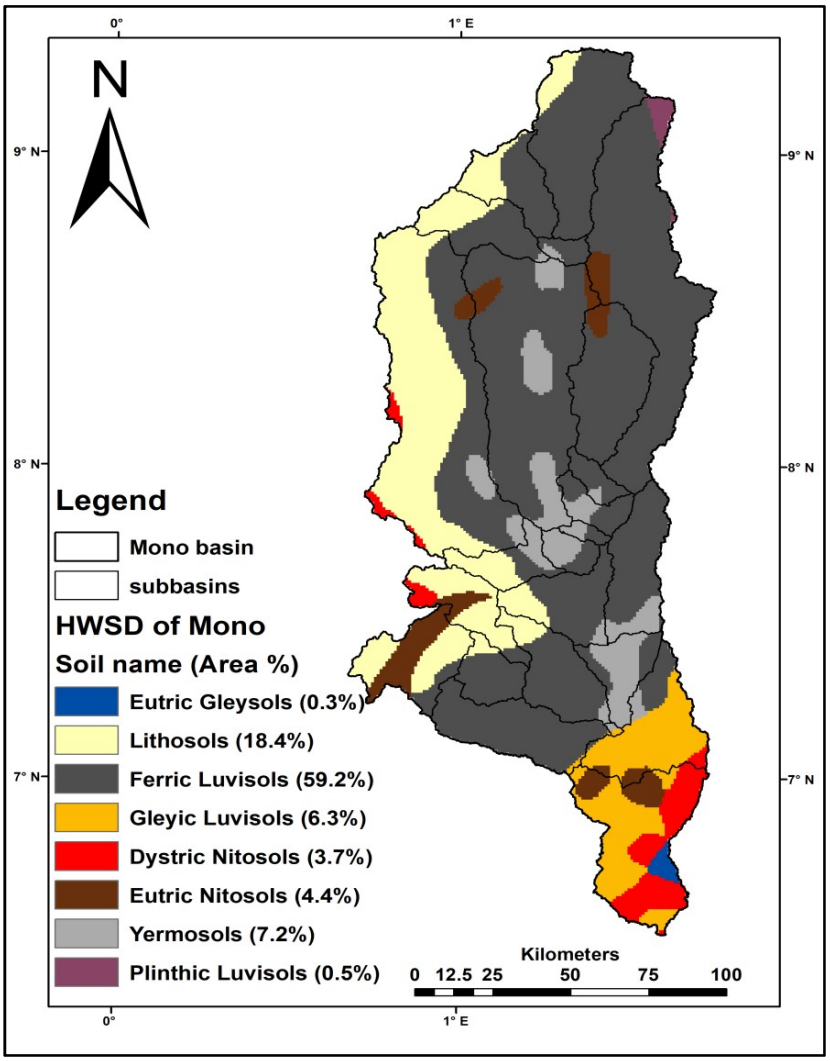

Figure 3.2: **HWSD data type Mono River Basin**

Table 3.2: HWSD of Mono types composition

Soil name	HWSD value	Area [%]	Nlayers	HYDGRP	SOL_ZMX	TEXTURE	CLAY1	SILT1	SAND1
Eutric Gleysols	1209	0.35	2	C	1000	9	23	40	37
Lithosols	1264	18.39	1	C	300	9	23	34	43
Ferric Luvisols	1458	59.46	2	B	1000	10	24	20	56
Gleyic Luvisols	1508	6.29	2	C	1000	9	22	36	42
Dystric Nitosols	1570	3.41	2	C	1000	9	23	33	44
Eutric Nitosols	1577	4.45	2	C	1000	9	23	28	49
Yermosols	1792	7.19	2	D	1000	3	55	29	16
Plinthic Luvisols	1956	0.46	2	C	1000	9	22	29	49

***Source** : HWSD (Pomeon, et al, 2018)*

Table 3.3: Soil properties used in SWAT model

Soil parameters	Description
NLAYERS	Number of layers in the soil(min=1, max=10)
HYDGRP	Soil hydrologic group(A, B, C, D)
SOL_ZMX	Maximum rooting depth of soil profile
ANION_EXCL	Fraction of porosity from which anions are excluded
SOL_CRK	Crack volume potential of soil [optional]
TEXTURE	Texture of soil layer [optional]
SOL_Z	Depth from soil surface to bottom of layer
SOL_BD	Moist bulk density
SOL_AWC	Available water capacity of soil layer
SOL_K	Saturated hydraulic conductivity
SOL_CBN	Organic carbon content
CLAY	Clay content
SILT	Silt content
SAND	Sand content
ROCK	Rock fragment content
SOL_ALB	Moist soil albedo
USLE_K	Soil crodability factor

***Source**: SWAT theorical document (Neitsch et al.,2011)*

3.1.4. Hydrological and meteorological data availability

MRB is the second main river of Togo Republic after Oti River (Volta river sub-basin). Many projects have been implemented in the past on the river for the climatology, hydrology and specifically water resource management. Some of these projects have made available climatic and discharge data (CEB, 2014; DGSCN-MPDAT, 2014; PANGIRE, 2016; PCCP, 2008; PNSET, 2012; SAWES, 2011). Beyond these projects many studies in different aspects on the MRB and published work can be used such as the one from (Ago et al., 2005; Amoussou et al., 2017, 2014; Klassou, 1996; PCCP, 2008; Rossi, 1996). In addition,

the Togolese and Beninese meteorological agencies collect hydrologic and climatic data specifically discharge rainfall, temperature, wind speed and evapotranspiration.

3.1.5. Climatic data

The rainfall database used are daily historical rainfall series from 21 gauging stations available from the General Direction of National Meteorology of TOGO (DGMN-Togo) and National Agency of Meteorology of Benin (METEO-Benin). We collected also minimum and maximum temperature of three synoptic stations (1961-2016) from Togo (Table 3.4). These stations are the unique synoptic stations available in MRB and distance between two successive stations is less than 150Km.The period of 1961 to 2016 is chosen because of the availability of the data with few gaps. There are some stations with missing values in daily rainfall but the percentage of the missing values is less than 10%.

Table 3.4: Detail of climatic data collected

No	Station name	Source	Long.(m)	Lat. (m)	Elevation(m	Daily Rainfall			Daily Mean Temperatu				Type
			East	North		Max	Std	CV [%]	Max	Min	Std	CV [%]	
1	Kara	DGMN-Togo	1.17	9.55	342.00	196.90	9.51	37.56					
2	Kpewa	DGMN-Togo	1.25	9.2	729.00	163.10	9.42	40.04					R
3	Tchamba	DGMN-Togo	1.42	9.03	360.00	160.50	9.69	33.53					R
4	Sokode	DGMN-Togo	1.12	8.98	400.00	142.60	9.67	38.35	34.3	20.4	1.9	7	R & M
5	Malfacassa	DGMN-Togo	0.96	8.98	405.97	146.40	8.79	41.85					R
6	Bassila	METEO-Benin	1.67	9.02	384.00	129.10	9	34.17					R
7	Sotouboua	DGMN-Togo	0.98	8.57	380.00	145.00	10.37	36.30					R
8	Blitta	DGMN-Togo	0.98	8.32	307.26	120.00	8.92	39.45					R
9	Yegue	DGMN-Togo	0.65	8.17	594.35	108.90	7.61	41.6					R
10	Akaba	DGMN-Togo	1.04	7.95	225.87	142.50	8.28	38.44					R
11	Tchetti	METEO-Benin	1.72	7.63	353.00	118.00	10	33					R
12	Anie	DGMN-Togo	1.25	7.75	160.00	149.50	9.29	33.47					R
13	Agouna	METEO-Benin	1.70	7.55	240.00	162	10.29	31.32					R
14	Atakpame	DGMN-Togo	1.12	7.58	400.00	157	10.53	35.70	35	12	1.8	7	R & M
15	Amou	DGMN-Togo	0.87	7.386	291.60	104	8.47	36.47					R
16	Wahala	DGMN-Togo	1.16	7.176	144.69	118	8.9	35.02					R
17	Lonkly	METEO-Benin	1.65	7.15	110.00	118	10.12	31.87					R
18	Notse	DGMN-Togo	1.18	6.95	150.00	157	10.14	32.81					R
19	Adjarala	METEO-Benin	1.61	6.90	52.00	185	11.02	39.7					R
20	Tabligbo	DGMN-Togo	1.51	6.59	51.00	117	9.04	31.77	35.1	19.3	1.7	6.3	R & M
21	Afanyangan	DGMN-Togo	1.63	6.49	72.19	192	8.66	31.3					R

R = rain gauge station, M=meteorological stations

***Source**: DGMN-Togo, METEO-Benin, 2018*

The missing rainfall values were corrected by using Pearson correlation with a neighboring station (Ficchì et al., 2016). The values of potential evapotranspiration collected at DGMN- Togo are available only for the stations of Tabligbo, Sokodé and Kara and from 1981 to 2016 at daily step. Potential Evapotranspiration (PET) are estimated by Hargreaves

methods (Hargreaves and Samani, 1982) which requires only minimum and maximum temperature (Tabari et al., 2012; Xie et al., 2012). The equation (3.1) is used for PET computation.

$$\lambda E_0 = 0.0023 \times H_0 \times (T_{max} - T_{min})^{0.5} \times (\overline{T}_{av} + 17.8) \quad (3.1)$$

Where λ is the latent heat of vaporization in MJ/kg , E_0 is the potential evapotranspiration in mm, H_0 is extraterrestrial radiation in MJ/m^2, T_{max} is maximum air temperature in °C, T_{min} is the minimum air temperature in °C, and $\overline{T}_{av}$ is the average air temperature in °C (Neitsch et al., 2011.).

3.1.6. Discharge data

Daily discharges were analyzed for the trend analysis and model calibration and validation. The data are from four discharge gauges stations in the Mono river basin measured for different length of periods. Discharge data stations are shown in Figure 3.3. The sources of climatic data are from the General Direction of Water and Sanitation in Togo (DGEA-Togo), General Direction of Water in Benin (DGEau-Benin) and at Communauté Electrique du Benin (CEB). The maximum daily flow at Athiémé is 951m^3/s. This maximum usually occurs between August and September corresponding to the maximum rainfall in the basin. The following Table 3.5 is showing the characteristics and hydrologic data source.

Table 3.5: Discharge station used in the Mono river basin

N$_o$	**Station Name**	**Source**	**Long. (m)**	**Lat. (m)**	**Elevation (m)**	**Discharge (m^3/s)**	**Area (km^2)**	**Period**
			East	**North**		**Max**		
1	Corrokopé	DGEA-Togo	1.36	7.78	196	844	9904	1961-1998
2	Nangbéto inflow	CEB	1.52	7.67	150	2133	1560	1988-2011
	Nangbéto outflow					1428.55		
3	Tététou	DGEA-Togo	1.54	7.01	69	1350	20469	1961-2011
4	Athiémé	DGEau-Benin	1.67	6.57	11	951	22014	1961-2011

Source: *DGMN-Togo, METEO-Benin DGEau and CEB*

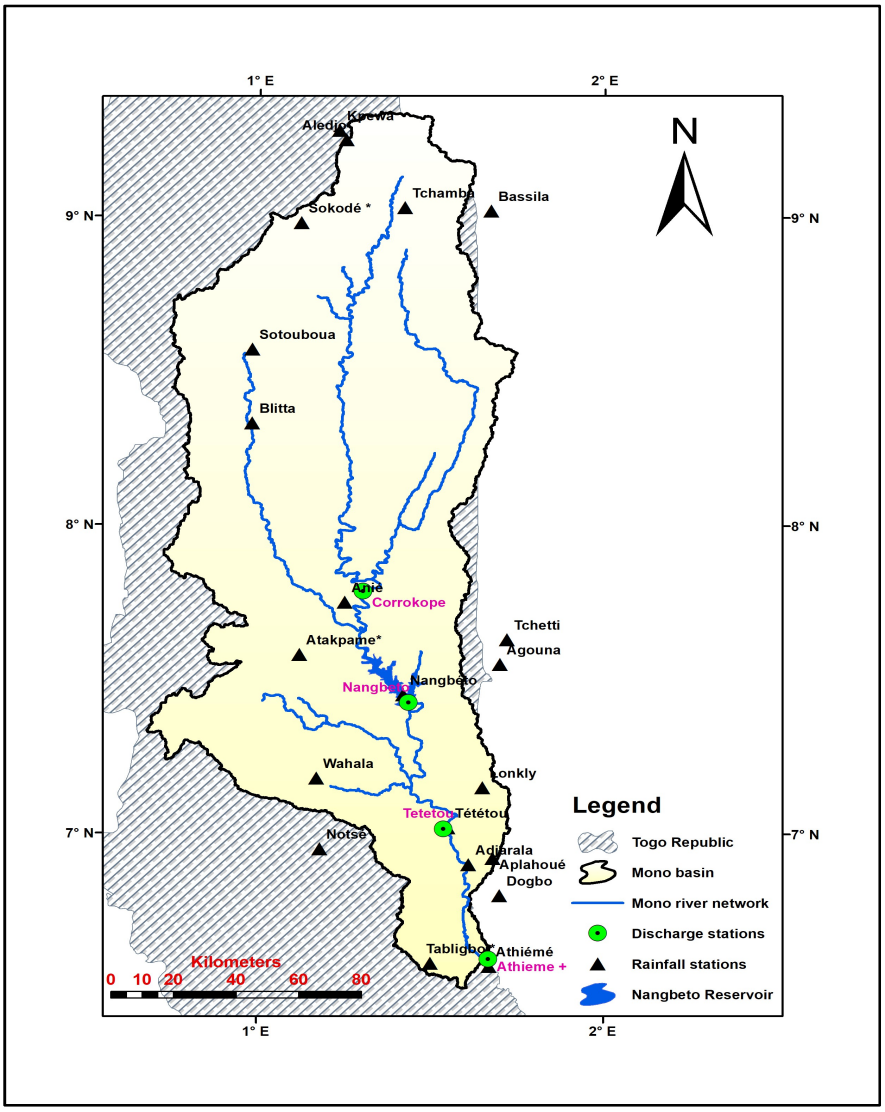

Source: *DGMN-Togo, METEO-Benin DGEau and CEB*

Figure 3.3: Climatic and discharge station used for the study

3.1.7. Climate Models and Ensemble Climate Models generation

In this study, downscaled and bias corrected daily historical minimum, maximum temperature and rainfall (1980-2005) and projected data (2020-2045) generated by Climate Change Agriculture and Food Security (CCAFS) *(http://ccafs-climate.org/data_bias_correction/)* were used. The model data are obtained from Global Climate Model which is derived by Princeton Reanalysis Princeton is a meteorological forcing dataset that can be used to drive Global Climate Models (GCMs) for land surface hydrology studies (Table 3.6). The dataset is constructed by combining a suite of global observation-based datasets with the National Center for Environmental Predictions/ National Center for Atmospheric Research (NCEP/NCAR) reanalysis. Four different models were used to blend on Ensemble Global Climate Models (EGCMs). The ensemble model is the average of climate variables in the same time, location and for a unique RCP.

Table 3.6: Climate models used description

Region	Model Centre	Models	Resolution (Lon&Lat)	References
China	Beijing Climate Center, China Meteorological Administration	BCC_CSM1_1	2.79 × 2.80	(Wu et al., 2014)
Germany	Max Plank Institute for Meteorology	MPI-ESM-MR	1.87 × 1.88	(Giorgetta et al., 2013)
Japan	Japan Agency for Marine-Earth Science and Technology, Atmosphere and Ocean Research Institute	MIROC_ESM	2.79 × 2.81	(Watanabe et al., 2011)
USA	NOAA Geophysical Fluid Dynamics Laboratory	GFDL-ESM2M	2.00 × 2.50	(Heuzé et al., 2013)

***Source**: http://ccafs-climate.org/data_bias_correction/*

3.1.8. Nangbéto dam data

The biggest dam on the waterway of the Mono River is at Nangbéto and produces 20% of the total hydroelectricity used by Togo and Benin (Figure 2.1). Nangbéto dam reservoir was integrated in the development of SWAT model. SWAT requires data about the reservoir characteristics and the reservoir management for the simulation of water balance. Data on Nangbéto reservoir characteristics and management was collected from the literature and at the CEB Company managing the dam (Amoussou et al., 2016; CEB, 2014; Houessou, 2016; ONU-SOFRELEC, 1964). Table 2.87 and Table 3.7: summarized the characteristics of Nangbéto dam.

Table 3.7: Nangbéto dam characteristics

SYMBOL	DESCRIPTION	VALUE	UNIT
MORES	Month the reservoir became operational	September	-
IYRES	Year of the simulation the reservoir became operational	1987	-
RES_ESA	Reservoir surface area when the reservoir is filled to the emergency spillway	180	ha
RES_EVOL	Volume of the water needed to fill the reservoir to the emergency spillway	263.34×10^6	M^3
RES_PSA	Reservoir surface area when the reservoir is filled to the principal spillway	-	ha
RES_PSOL	Volume of the water needed to fill the reservoir to the principal spillway	212.4×10^6	M^3
RES_VOL	Initial reservoir volume	1715×10^3	M^3

Source : *CEB, 2014*

3.1.9. Population data

Demographic data of Togo and Benin Republics was derived from literature and also from FAO population database. In 2011, the Mono river basin is populated by about 5.1 Million inhabitants (FAO, 2012; PCCP, 2008; SAWES, 2011). According to FAO *(http://worldpopulationreview.com/countries/togo-population),* the population in Togo has tripled since 1975 and it is predicted to constantly increase in future as shown in Table 3.8.

Table 3.8: Population scenarios (millions of inhabitants) in Togo from 1975 to 2050.

Year (Million)	**1975**	**2000**	**2010**	**2015**	**2020**	**2025**	**2030**	**2035**	**2040**	**2045**	**2050**
Population (P)	2.4	4.9	6.5	7.4	8.34	9.41	10.5	11.66	12.86	14.08	15.29
Growth rate *	-	2.86	2.83	2.59	2.39	2.41	2.19	2.1	1.96	1.8	1.66

Source: *World Population, 2018 (http://worldpopulationreview.com/)*

*Growth rate estimated from reported population data assuming exponential growth as given in equation (3.2)

$$P = P_0\, Exp(\frac{K}{100}\Delta t) \qquad (3.2)$$

Where K (%) is population growth rate estimated from reported population data assuming exponential growth as given in Equation (3.2) and P is the population value at time$t_0 + \Delta t$, P_0 is the initial population value at t_0 .

3.1.10. Tools and software

The tools and software used in this study are:

- **ArcGIS 10.6** used for map generation and during Kriging interpolation methods.
- **QGIS 2.0** used in land cover analysis and rainfall regionalization
- **EXCEL spreadsheet** use in the preparation of hydrometric and climate data of the SWAT model, GCMs and for some elementary analysis.
- **Google Earth** used during land cover reclassification and localization of points.
- **GPS** utilize to detect the geographic coordinate of some identified points.
- **Rstudio** used for statistical analysis and in Mann Kendall (MK) trend analysis in the basin and for SWAT model outputs visualization and analysis.
- **RClimDex version 1.0** used to compute climate extremes indices of temperature and rainfall which and for evaluation of non parametric Mann Kendall test under Rstudio

  Source: *https://www.wcrp-climate.org/extremes-risk-summer-school-overview*

- **MAKESENS version 1.0** application applied for MK test and slope estimation.
- **Land Change Modeler** of TerrSet Geospatial Monitoring and Modeling System integrated in the IDRISI, robust software for land use and land cover analysis and modeling.
- The **IHACRES** model used as lumped model for steam flow prediction in R
- The **AirGR** model is used for GR4J model simulation under R package
- **GR4J** model used as lumped model for steam flow prediction in Excel
- **ArCSWAT** used for SWAT modeling and watershed delineation
- **SWAT-CUP** used for SWAT model calibration and validation
- **SWAT Output Viewer** for a quickly view outputs from a SWAT model

3.2. Methods

This section summarizes the methodology as represented by the flowchart bellow (Figure 3.4). The methodology in general is divided in three parts: (1) land use, land cover change analysis and future scenarios, (2) climate change detection analysis and (3) hydrological

modeling using two lumped models and a semi-distributed model over different time periods.

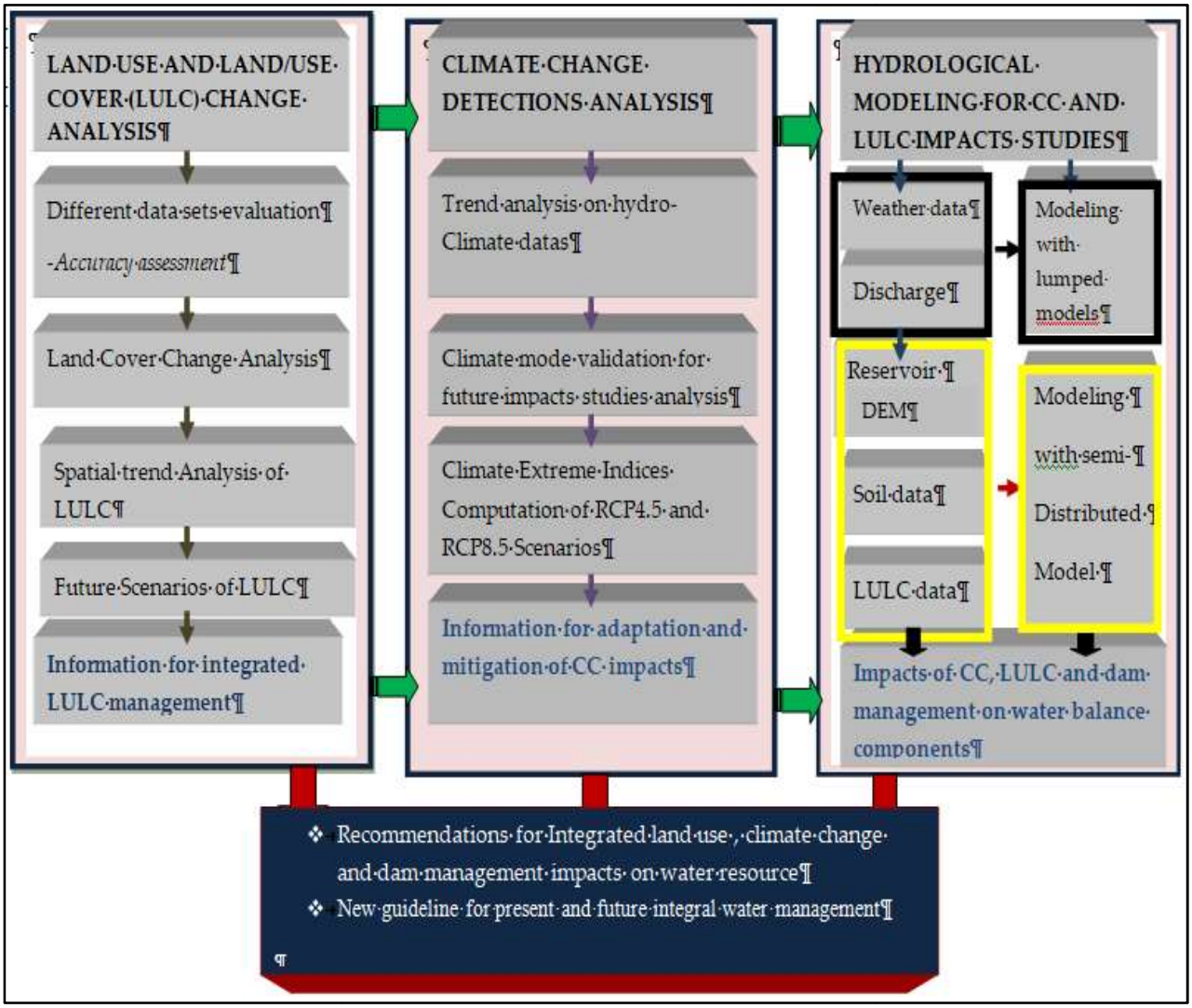

Figure 3.4. Flowchart of the thesis and interactions between the sections

3.2.1. Land use land cover evaluation and future scenarios development

3.2.1.1.Pre-analysis and harmonization of land use/ cover type

After extraction of Mono watershed in CILSS, ESA-CCI and Globeland30 datasets, only ten land cover types are represented (Table 3.9). The pre-analysis consists first; to the reclassification of the different then land cover types into six common land cover classes using ArcGIS 10.5 tools. Secondary the spatial resolution of CILSS and ESA-CCI maps were resampled to the 30 meters same spatial resolution of Globeland30 (Thibaut et al., 2011)to be able to superpose the maps for further comparison (Bárdossy and Schmidt, 2009).

Table 3.9: Land covertypes in the MRB and reclassification scheme.

N_o	Land cover type	Description	Land cover reclassified
1	Forest	Forests and woody vegetation land (> 75% trees/ha), dense, closed canopy formation of evergreen	Forest
2	Gallery forest and riparian	Corridor of dense permanent vegetation, forest bordering the edges of streams and rivers	
3	Degraded forest	Immature forest, or forest in various stages of regrowth after disturbance	
4	Woodland	Open formations of small to medium height trees, tree cover generally between 50%- 75%	
5	Savanna	Land with trees (< 75% trees/ha) with mixture of shrub and grass undergrowth, with some dominance of grass or shrub	Savanna
6	Wetland and floodplain	Permanent wetlands and swamps	Wetland
7	Agriculture	Cultivated areas with seasonal crops dependent on rainfall.	Cropland
8	Cropland and oil palm	Crop field and fallow land, farms with crops and harvested croplands	
9	Water	Rivers, open water, inland waters and small reservoirs	Water
10	Settlements	Cities and villages, roads, and other buildings	Settlements

***Source** : CILSS, 2016*

The six major classes which were selected in Table 3.9 after resampling and reclassification are similar to those proposed by Penman et al.(2003) in the International Panel on Climate Change (IPCC) guidelines according to the Kyoto Protocol of 2001 and the Good Practices Guidelines for Land Use, Land Use Change and Forestry (GPG-LULUCF). Because all land cover categories existing in CILSS, ESA-CCI, and Globeland30 are similar it is easy to select the common reclassified land cover from the three data sets as shown in column 4 of Table 3.9.Figure 3.5 shows the flowchart of land cover analysis.

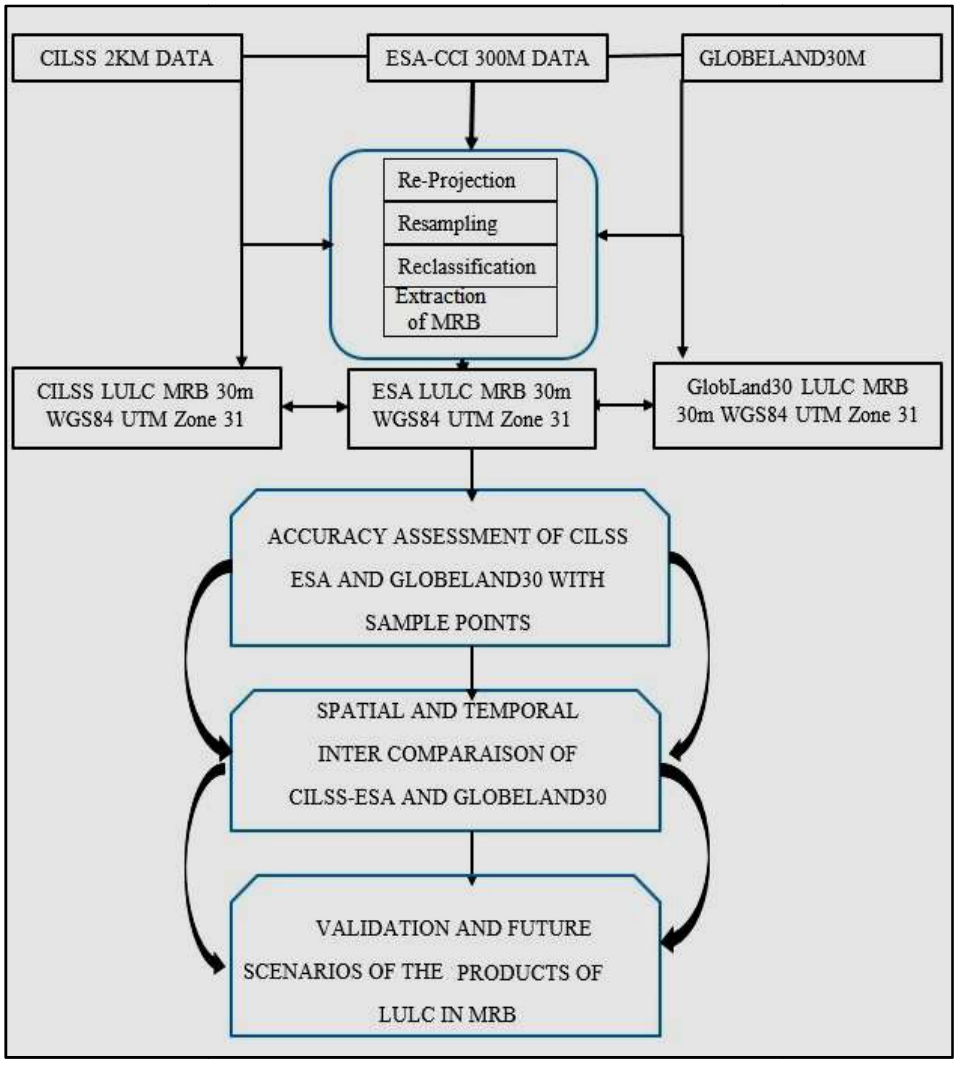

Figure 3.5: Flow chart of land use/cover processing.

3.2.1.2.Accuracy assessment, land use area and change analysis

According to Sitthi et al.(2016) a land cover accuracy assessment is required in any study using remote sensing data. Land cover map accuracy is quantified by creating an error matrix or a confusion matrix, which compares the classified map with a reference classification or a true map. These matrices can be used as a measure of agreement between model algorithm predictions and the references points (Congalton, 1991). Following the guidelines of the Food and Agriculture Organization (FAO), the tables of accuracy estimates were produced for the three data sets. This was followed by confidence intervals for area estimation and comparison of area estimation derived from map data to reference data. Finally the estimated area was adjusted using both map and reference data (FAO-ONU, 2016). Many past studies have estimated how accurate is the observed land cover map with modeled one by using a Kappa coefficient user and overall accuracies (Chen et al., 2015; Lunetta et al., 2006; Ren et al., 2018).

The methodology described by Olofsson et al.(2013); Pontius and Malanson (2014) to detect or to compare LULCC often used in the generation of LULC maps can also be applied for evaluating the results of different scenarios. The analysis of Pontius and Millones (2011) discussed the limitations of comparing two maps using the Kappa coefficient and proposed a new methodology for comparison namely "quantify disagreement and allocation disagreement". Nevertheless, Kappa coefficient is still considered a vital tool for accuracy assessment measurement in a number of studies (Ren et al., 2018; Sitthi et al., 2016).

Table 3.10: Number of land cover reference points

Land cover reference points							
Land cover type	Forest	Savanna	Wetland	Cropland	Water	Settlements	Total
Year 2013	23	665	10	289	8	5	1,000
Year 2010	140	527	17	286	13	17	1,000

Source: Google earth points, 2018

For accuracy assessment, 1,000 reference points were randomly taken from high-resolution satellite images for the years 2010 and 2013 provided by Google Earth. These reference points were distributed over the six classes (Table 3.10).

The accuracy assessment and an error matrix for each category of dataset were generated by following the guidelines of Congalton(1991)and the method proposed and described by Olofsson et al.(2013). According to this method, an error matrix can be computed. In addition, from this error matrix statistics such as Kappa coefficient and the overall and user accuracies are generated.

The overall accuracy ($\hat{O}$) indicates the overall proportion of area correctly classified. It is the sum of all pixels on the diagonal in the adjusted error matrix.

$$\hat{O} = \sum_{i=1}^{n} \hat{P}_{ii} \tag{3.4}$$

User's accuracy ($\widehat{U}_i$) of class *i* is the proportion of the area mapped as class *i* that has reference class *i,* and producer's accuracy ($\hat{P}_j$) of class *j* is the proportion of the area of reference class *j* that is mapped as class *j*. They are estimated by equation (3.5) and (3.6)

$$\widehat{U}_i = \frac{\hat{P}_{ii}}{\hat{P}_{i+}} \tag{3.5}$$

$$\hat{P}_j = \frac{\hat{P}_{jj}}{\hat{P}_{j+}} \tag{3.6}$$

$$K = \frac{N \sum_{i=1}^{n} \hat{P}_{ii} - \sum_{i=1}^{n} (\hat{P}_{i+} \hat{P}_{j+})}{N^2 - \sum_{i=1}^{n} (\hat{P}_{i+} \hat{P}_{j+})} \tag{3.7}$$

The percent error can only be found if the true value is known. It has been computed by the absolute error (δX) defined as:

$$\delta X = \left|\frac{x_0 - x}{x_0}\right| \quad (3.8)$$

Where x_o is the number of reference pixels, x is the number of observed pixels.

According to Fitzgerald and Lees (1994) Kappa statistic (K) is considered to be statistically significant at p <0.001 at level of confidence for the following intervals values:

- Poor if K <40
- Good if 40 ≤ K <75
- Excellent if K ≥ 75

3.2.1.3. Area of change estimation and precision

Following the approach suggested by Olofsson et al.(2013) the adjusted error matrix was used to elaborate an area estimator based on theproportion of the area of category j. Equation (3.9) gives the area of category j ($\widehat{A}_j$).

$$\hat{A}_j = Atot \times \hat{P}j \quad (3.9)$$

Where $\widehat{P}j = \Sigma_{i=1}^{q} Wi \frac{nij}{ni+}$and A_{tot} the total area of the watershed

This area estimator is an error-adjusted estimator of area that includes the area of map omission error of category j and removes the area of map commission error (Olofsson et al., 2013). Its standard error ($\widehat{A}_j$) was computed as follows.

$$S(\hat{P}j + 1) = \sqrt{\sum_{i=1}^{q} \frac{Wi\hat{}ik - \hat{P}ik^2}{ni+1 - 1}}^{-} \quad (3.10)$$

The use of$\hat{P}+j$ (estimated from the reference samples) instead of $\hat{P}i+$ (map areas) is because it allows the assessment of uncertainty of the area estimates in the form of sampling variability that can be computed as confidence interval. For$\hat{}j$the approximate 95% confidence interval (CI) was derived as:

$$CI = \widehat{A}_j \pm z \times S(\widehat{A}j) \quad (3.11)$$

Where z corresponds to the percentile from the curve of the standard normal distribution, and for 95% confidence, z = 1.96.

LULCC was computed for three periods (1975-2000, 2000-2013 and 1975-2013). LULC transition matrices as well as land use change maps are now produced. For LULCC, year to year Modules for Land Use Change Evaluation (MOLUSCE) tools was used. It is a user-friendly plug-in for Quantum Geographic Information System(QGIS 2.0) and above which offers an easy-to-use interface with specific modules and functions for land use area estimate on changes between two period and for future land use scenarios. Information about basic modules in MOLUSCE can be obtained at *(https://plugins.qgis.org/plugins/molusce/)*.

3.2.1.3.Absolute error and mean absolute error between the datasets

The classified land use maps from CILLS, ESA-CCI and Globeland30have are to be compared. This is done by calculating the mean absolute error and spatial regression coefficient between CILSS, ESA-CIC or Globeland30.

The absolute error *(AE)* is the total error between two measurements or objects. It is computed as:

$$AE = |X - Xo|, \tag{3.12}$$

Where *Xo* is the number of pixel of the first land use map and X for the second map. The mean absolute error (MAE) is the average of absolute error and is expressed as:

$$MAE = \frac{1}{n}AE = \frac{1}{n}|x - x_o| \tag{3.13}$$

With n = number of land use categories. Its value is six (6) in this study. Bennett et al.(2013)used *AE* and *MAE* to compare observations and model data in their studies

3.2.1.4.Land use validation and scenarios prediction

For land cover change analysis and future scenario prediction, a number of models have been developed like the GeoMod, the Cellular Automata (CA) and Stochastic Choice (ST-CHOICE) (Arsanjani et al., 2013) and applied in a number of studies (Herbst et al., 2006; Mishra et al., 2014). A comparison of four statistical approaches of these models (Markov chain, logistic regression, generalized additive models, and survival analysis) was done by Sun and Robinson (2018) to detect their ability to quantify land use change and to perform prediction. The results show that the generalized additive model performs well for overall accuracy and is good for land use validation and modeling. For example, Pontius and Neeti (2010); Pontius and Spencer (2005) analyzed the uncertainty of future LULC scenarios and discussed techniques to quantify the meaningful differences between future scenarios using

the GeoMod model. A number of studies of LULCC analysis used computation of transition potentials, the spatial trend change analysis and land cover change prediction using the Land Change Modeler (LCM), a tool in the TerrSet Geospatial Monitoring and Modeling System integrated in the IDRISI software (Du et al., 2012; Eastman, 2006). The LCM software provides a robust set of tools for change analysis and spatial trend analysis utilizing different variables for future scenarios computation (Eastman, 2006; Mishra and Singh, 2010). LULC maps are required for the analysis of the past but also for developing LULC scenarios (Rounsevell et al., 2006). For that, validated maps are used to analyze the drivers of change in the past and to project them for the future (Pontius et al., 2001). Land cover scenarios development steps are showed in Figure 3.6.

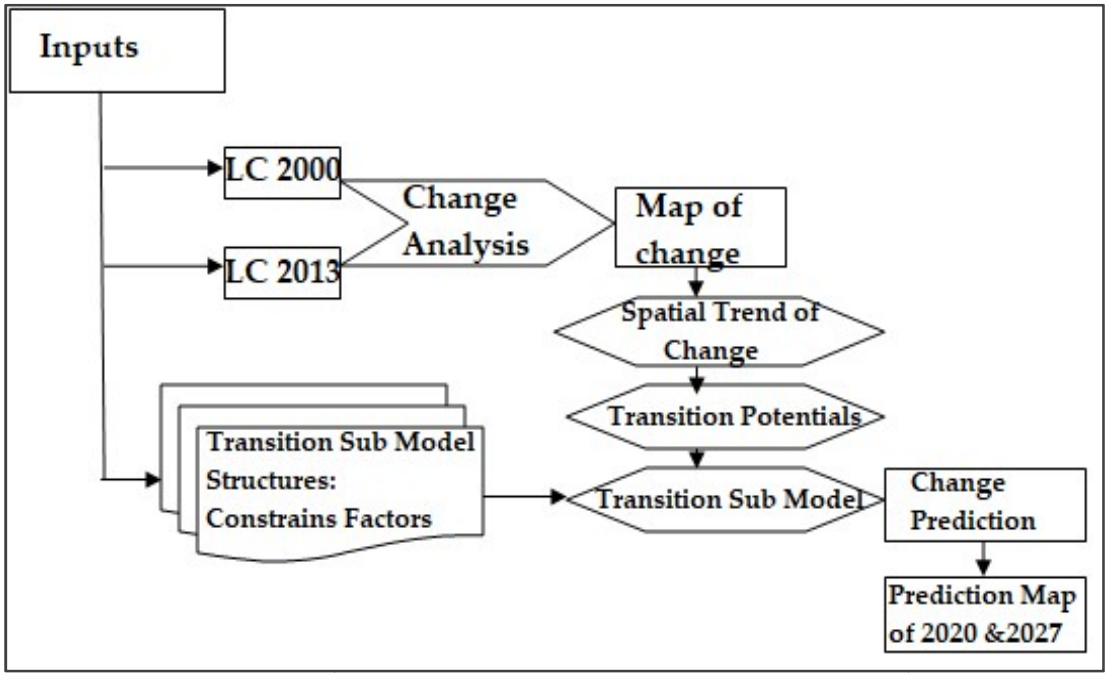

Figure 3.6: Flowcharts for land cover modeling

Developing future LULC maps consists of two steps. In the first step, the rate of change has to be estimated while in the second step it has to be computed where the change will take place (Verburg and Veldkamp, 2002).

The spatial trend change analysis was performed for each data set of CILSS, ESA-CCI and Globeland30 for the periods 1975-2000, 2000-2010 and 2000-2013. Spatial trends per land cover category were computed as 9^{th} order polynomial. Low spatial trend are represented by negative value (in black) and high trend by positives value (in red) in the spatial trend map legend (Eastman, 2006; Václavík and Rogan, 2009).

The results are used to compute spatial transition probabilities for every land cover category. In this study, population growth, elevation, and distance to roads were used as drivers for calculating the main transitions from forest to savanna, from forest to cropland, from savanna to cropland, and from savanna to forest. Road network and elevation are static drivers while population is a dynamic driver. The factors of reforestation in Togo/Benin as projected in Intended Nationally Determined Contribution (INDC-Togo, 2015) data were not incorporate in the model because of data availability.

These transition probabilities are based on a Multi-Layer Perceptron (MLP) neural network (Eastman, 2006). This MLP neural network uses only few parameters for modeling. The parameters which are the driving forces of change are assume to be the same (Eastman, 2006). Many studies have shown that MLP is useful and a good tool for prediction, function approximation and classification (Gardner and Dorling, 1998).

We adopted Markov Chain prediction process and a transition probability bias transitions potential maps to model the future land cover maps (Eastman, 2006). The transition probability file is a matrix that records the probability that each land cover category will change to any other category. The quality of the prediction can be evaluated using an observed map not used for calculating the transition potentials (Eastman, 2006). Computing the rate of change between 1975 and 2000 and comparing the projected land cover of 2013 with the observed one allows validation of CILSS data sets. This step was performed for the periods of 2000-2013 (CILSS and ESA-CCI) and 2000-2010 (Globeland30) before predicting land cover for the years 2020 and 2027.

3.2.2. Climate changes detection and extreme indices trends analysis

Change detection or trend analysis of different weather variables is the common assess by which hydrologists and climatologists. From global to local scales, Global Climate Models (GCMs) and Regional Climate Models (RCMs) are mostly used for these analyses. However, the impacts studies rarely used GCM output without downscaling directly because the errors are from the limited spatial resolution, simplified physics, thermodynamic processes and numerical schemes. GCMs are more global and coupled with atmospheric and oceanographic model which reflect the earth climate system. The errors are large in GCMs (Navarro-Racines et al., 2015). Thus, statistical downscaling and bias correction of GCMs to small grids are more representative of local agriculture, biodiversity or hydrological modeling analysis. There are many downscaled bias correction methods such as bias correction with variability; bias correction with no variability, change factor with variabili-

ty, change factor with no variability, quantiles mapping and raw data (Berg et al., 2012; Maraun, 2013; Navarro-Racines et al., 2015). Many studies showed the better performances of quantiles mapping for rainfall data and bias correction with variability for temperature (Haerter et al., 2011; Onyutha et al., 2016; Teutschbein and Seibert, 2012).

The present study analyzes the last fifty years historical climate and hydrological data of twenty one (21) stations available on the MRB in order to detect climate change on stream flow, rainfall, potential evapotranspiration and mean temperature.. This will be followed by a validation ensemble mean model and two different RCPs scenarios extremes indices calculation. Thus this chapter aim to assess the long-term temporal (1961-2016) and spatial trend analysis of hydro-climatic variables in the MRB; to validate an ensemble mean climate model and to compute twenty two (22) climate extreme indices for two futures RCP4.5 & 8.5 scenarios (2020-2045).

The study consists in multi- validation methods, estimation of the spatial and temporal trend analysis in MRB and the impacts of climate scenarios in hydrology in the future using different scenarios for extreme indices analysis. The method adopted here is the Man-Kendall (MK) test trend on historical and extremes index computation using RclimDex package. MK method was used around the world and has been shown to be the most reliable for trend analysis on hydro-hydrological time series (Wilson et al., 2010). For example, Robson et al.(2004) reviewed several studies on trend detection analysis of rainfall, temperature and have discovered that the significant trend was observed when using MK method. The climate models used are from Climate Change Agriculture and Food Security (CCAFS) downscaled at 0.25° fine spatial resolution and bias corrected GCMs, which is acceptable for local studies for adaptation and mitigation with climate change impacts.

3.2.2.1.Spatial and temporal distribution and rainfall indexes

A primary analysis is conducted using the average PET, rainfall over the MRB. Rainfall was obtained by computing Thiessens polygons (Allchin and Déry, 2017) with 21 stations of MRB.

In order to achieve accurate estimation of the spatial distribution of rainfall, it is necessary to use interpolation methods. This method assigns weight at each gauge station in proportion to the catchment area that is closest to that gauge. The method of constructing the polygons implies the following steps:

(i) Gauge network is plotted on map of the catchment area of interest.

(ii) Adjacent stations are connected with lines

(iii) Perpendicular bisectors of each line are constructed (perpendicular line at the mid-point of each line connecting two stations)

(iv) The bisectors are extended and used to form the polygon around each gauge station

(v) Rainfall value for each gauge station is multiplied by the area of each polygon

(vi) All values from step 5 are summed and divided by total basin area.

The average rainfall over the basin was computed and used to estimate: Aridity index (AI) which was defined by the United Nations Environmental program (UNEP) as the ratio of annual rainfall (PCP) by potential evapotranspiration (PET) and totals rainfall variability index ($_{\delta j}$) as the standardized rainfall:

$$\delta j = \frac{P_j - m}{\sigma} \quad (3.14)$$

Where δ_i is the rainfall variability of the year i, P_j is annual rainfall for the year j, m is the mean of annual rainfall and σ is the standard deviation during the period from 1961 to 2016

The aridity index is a quantitative indicator of water deficiency over a given region or location. It has used in many studies (Li et al., 2017; Sahin, 2012). Normally aridity index is a function of rainfall, temperature and evaporation. The use of rainfall and potential evapotranspiration only means that we ignore the importance of temperature and evaporation.

3.2.2.2.Test of correlation adapted and trend analysis methods.

The parametric or non–parametric trend analysis methods under statistical approach are frequently used for trend detection by fixing a certain level of confidence. Many studies have been assessing trend analysis of hydro climate variables at the whole watershed. For example in china the studies found the decrease and increase of flood precipitation and non-flood precipitation between 1969 to 2011 (Yan and Bai, 2017),whereas over West and South Africa the trend analysis of daily climate extremes showed an evident warming over most of the region(Gosling et al., 2011). Oguntunde et al.(2006) determined an increase of runoff trend with significant by analyzing the long-term trend hydro-climatology of Volta river basin in West Africa from 1901 to 2002. In china, Gocic and Trajkovic (2013) ob-

tained a negative and positive trend of stream flow for the past 50 years and compared factors due to human activities and climate change. Diallo et al.(2012) analyzed the inter-annual variability using multiple models over Sahel region. Amoussou et al.(2017) reviewed hydro-climatic variability and flood risk in two small forests located in the MRB. Lawin et al. (2019a); (2019b) studied climate extremes trend of MRB of temperature and rainfall with Coordinated Regional Downscaling Experiment (CORDEX) and Regional MOdel (REMO) at few stations. They only focused on the trend analysis using few stations on the watershed (1981-2010) and (2018-2050). These studies have found an increase of temperature and high variability of rainfall for historical and future baselines. As most of the analysis in the region, more focus in trend and all hydrology cycle components were not taken in account. Most of the studies in the region were done annually and inter annually (Lawin et al., 2019a; Sanogo et al., 2015).

Initially, auto-correlation test is applied on hydro-climatic time series for determining the randomness of the data. This criterion involves using parametric and non-parametric methods for trend analysis. Therefore, depending on the correlation coefficient values ranges ($0 \leq r1 \leq 1$), parametric or non-parametric MK test is used (Memarian et al., 2012) . For this analysis two methods, MK and Sen's estimator were used to evaluate the variables trend for a long period.

3.2.2.3.Climate variability analysis

The method consists of computing climatic index and applying Non-parametric Mann-Kendall test for trend detection analysis with MAKESENS version 1.0, application developed by Finnish Meteorological Institute (Salmi et al., 2002) for MK test and slope estimation. The method was applied in many studies around the world with success (Akpovi et al., 2016; Attogouinon et al., 2017; Oguntunde et al., 2006; Rana et al., 2014). In this study, analysis was applied on four hydro climatic and 21 rainfall stations over the Mono river basin.

The Mann Kendall test analysis S (Kendall, 1975; Mann, 1945) is computed as:

$$S = \sum_{i=1}^{n-1} \sum_{j=i+1}^{n} sgn(X_j - X_i) \quad (3.15)$$

With n the number of data point, Xi and X_j are the data values in the time series i and j (j>i), and Sgn (X_j-X_i) is the sign of the following system:

$$sgn(X_j - X_i) = \begin{cases} +1, if X_j - X_i > 0 \\ 0, if X_j - X_i = 0 \\ -1, if X_j - X_i < 0 \end{cases} \quad (3.16)$$

This statistics computes the number of positives differences minus the negatives difference for all the differences considered.

The variance is computed as:

$$Var(S) = \frac{n(n-1)(2n+5) - \sum_{i=1}^{m} t_i(t_i-1)(2t_i+5)}{18} \quad (3.17)$$

Where n is the number of data point available, m is the number of tried groups in the series and t_i denotes the number of ties of extent i. A tried group is defined as the set of sample data that have the same value. If no ties between observations are present and no trends in the time series, the test statistic is asymptotically normal distributed with:

$$Var(s) = \frac{n(n-1)(2n+5)}{18} \quad (3.18)$$

For the case where the size of the sample data is bigger than 10 (n>10), the standard normal test statistic Z_s is computed using the flowing equations:

$$Zs = \begin{cases} \frac{S-1}{\sqrt{Var(S)}}, if S > 0 \\ 0 \quad if S = 0 \\ \frac{S+1}{\sqrt{var(S)}}, if S < 0 \end{cases} \quad (3.19)$$

A positive value of Zs shows the increase in the trend while a negative value indicates the decrease in the trends. To test the trend, α significant level can be used. When $|Z_s| > Z_{1-\alpha/2}$, the null hypothesis is rejected and a significant trend exists in the time series. $Z_{1-\alpha/2}$ is computed by from the standard normal distribution table. In this study we used α =0.01 and α = 0.05. So at 5% significance level the null hypothesis of no trend is rejected if $|Z_s| > 1.96$ and rejected if $|Z_s| > 2.576$ at 1% significance level.

3.2.2.4. Sen's slope estimator

Sen and Niedzielski(2010) have developed the non-parametric procedure in order to estimate the slop of trend in the sample of N pair of data.

$$Qi = \frac{X_{j-X_k}}{J-k} for i = 1, \dots, N, \quad (3.20)$$

Where X_j and X_k are the data value at tiles j and k (j>k), respectively.

If there is only one datum in each time period, the N= $\frac{n(n-1)}{2}$, (3.21)

Where n is the number of periods. If there are multiple observations, the N values of Q are ranked from smallest to largest and the median of slop or Sen's estimator is computed as

$$Q_{med} = \begin{cases} Q_{\left[\frac{N+1}{2}\right]}, & if N is odd \\ \frac{Q_{\left[\left(\frac{N}{2}\right)\right]} + Q_{\left[\frac{N+2}{2}\right]}}{2}, & if N is even \end{cases} \quad (3.22)$$

The Q_{med} sign indicates data trend reflection, while its value indicates the steepness of the trend. To determine whether the median slope is statistically deferent from zero, one should obtain the confidence interval of Q_{med} at specific probability.

The confidence interval about the tile slope (Gilbert, 1987) can be defined as :

$$C_{\alpha} = Z_{1-\alpha/2}\sqrt{Var(S)} \quad (3.23)$$

Where Var (S) is defined in equation (3.18) and $Z_{1-\alpha/2}$ is obtained from the standard normal distribution table. In this study, the confidence interval was computed at two significance level (α =0.01 and α =0.05).

Then, $M1 = \frac{N-C\alpha}{2}$ and $M2 = \frac{N+C\alpha}{2}$ are computed. The lower and upper limits of the confidence interval, Q_{min} and Q_{max} are the M_1^{th} largest and the $(M_2+1)^{th}$ largest of the N ordered slope estimates.

The slope Q_{med} is statistically deferent from zero if the two limits (Q_{min} and Q_{max}) have similar sign. Sen's slope estimator has been widely used in hydro-meteorological time series (Tabari et al., 2012).

3.2.2.5.Climate model validation with observation data

Validation of a model means to compare the model output with observations data. It gives the fitness between model outputs and observations data and indicates the confidence of future scenarios results. A very good fit of the model with the observation data allows using the model for future scenarios and changing impacts in the region. In the present study downscaled and bias corrected GCM is validated with the observation data obtained from the meteorological services of Togo and Benin. Daily, monthly and annual data from the observation are plotted against model value and by determining the coefficient of determi-

nation values between observations and model. Additionally the difference between ensemble model output and observed data ratio (Bias) was performed during the same period to determine if the change is sensitive to observations or not as well monthly and annual time steps (Onyutha et al., 2016). The period chosen for validation is from 1980 to 2005, the period was chosen where the model outputs and observations data are both available and without gaps. The linear regression coefficient of observations against model output was computed at each station for mean temperature and rainfall.

The spatial representation of ensemble model rainfall against observations data were mapped for two periods:

- ✓ June-July -August (JJA) corresponding to the maximum of rainfall over MRB
- ✓ December-January-February (DJF) corresponding to the minimum of rainfall.

Kriging interpolation method developed in ArcGIS 10.5 was used for rainfall spatial distribution (Bogena et al., 2010; Gudmundsson and Seneviratne, 2016; Maraun et al., 2010; Martinez-Casanovas, 2003). Kriging is a linear interpolation method which allows estimating areal value as a weighted mean of observations (Laurent et al., 1998)

3.2.2.6.Data quality control and extremes indices computation

The important key for indices concept is the calculation of the temperature and indices with a fixed threshold. The indices calculation aims is to monitor climate change and climate change detections. Initially 27 cores indices are recommended by CCI/CLIVAR Expert Team for Climate Change Detection Monitoring and Indices (ETCCDI). RClimDex allows a rapid analysis of data quality before indices calculation. Data quality corrects all the unreasonable values, missing values, negatives precipitation and temperature identifying outliers of daily values outside of user region. All no valid data were replaced by -99 known to RClimDex as missing value. More information about the indices and its computation developed by Expert

Table 3.11: Climate extreme indices used

TN = minimum temperature and TX = maximum temperature, p = daily precipitation, and PRCP = annual total precipitation

ID	Indicator	Definitions	Units
Mean Temperature			
TXx	Max Tmax	Monthly maximum value of daily maximum temperature	°C
TNx	Max Tmin	Monthly maximum value of daily minimum temperature	°C
TXn	Min Tmax	Monthly minimum value of daily maximum temperature	°C
TNn	Min Tmin	Monthly minimum value of daily minimum temperature	°C
TN90p	Warm nights	Percentage of day when TN >90th percentile	%
TX90p	Warm days	Percentage of day when TX >90th percentile	%
WSDI	Warm spell duration indicator	Annual count of days with at least 6 consecutive days when TX >90th percentile	days
DTR	Diurnal temperature range	Monthly mean difference TX and TN	°C
Precipitation			
SDII	Simple daily intensi-ty index	Annual total precipitation divided by the number of wet day (defined as PRCP >= 1.0 mm) in the year	mm/day
R10	Number of heavy precipitation days	Annual count of day when PRCP >= 10mm	days
R25	Number of days above 25 mm	Annual count of day when PRCP >= 25mm	days
CDD	Consecutive dry days	Maximum number of consecutive days with RR<1mm	days
CWD	Consecutive wetdays	Maximum number of consecutive days with RR>1mm	days
R95P	Very wet days	Annual total PRCP when RR>95th percentile	mm
R99P	Extremely wetdays	Annual total PRCP when RR>99th percentile	mm
PRCPTOT	Annual total wet day precipitation	Annual total PRCP in wet days(RR>1mm)	mm

***Source**: Zhang et al., 2018*

Team on Climate Risk and Sector-specific Climate Indices can be found on *http://www.wmo.int/pages/prog/wcp/ccl/opace/opace4/expertteam.php*

In this study, we used the RClimDex (Version 1.9) package in R environment (version 1.1.463) developed by (Zhang et al., 2018) to compute sixteen (16) indices of temperature (08) and rainfall (08) which were evaluated by non parametric Mann Kendall test and annual trend analysis for two climate RCP4.5 and RCP8.5 by selecting three representatives climate stations in Mono River Basin. Table 3.2.2.6 shows the selected indices and definition. RClimDex is available through *http://cccma.seos.uvic.ca/ETCCDI/*. In this analysis RClimDex was applied for RCP4.5 and RCP8.5 for the future period of 2020-2045. The trend change was considered significant if the estimated p _value is less than or equal to 0.05.

3.2.3. Discharge prediction and comparison using IHACRES and GR4J models

3.2.3.1.Rainfall -runoff models description

- **GR4J model**

The GR4J model is a daily four parameters rainfall–runo lumped conceptual model. The model is part of soil moisture accounting (SMA) family models. The model uses daily precipitation, evapotranspiration, and observed discharge to simulate daily runoff at the basin outlet. Figure 3.7 shows a schematic representation the model. P is the rainfall depth and the potential evapotranspiration (PE) considered as inputs in the model. P is the areal catchment rainfall, which is estimated by an interpolation method using the rain gauges stations in the basin. In this analysis, Thiensen polygons interpolation is used to obtain the areal rainfall. E represents the average value of PE. The input and output variables are in millimeter (mm).

Determination of net rainfall and PE

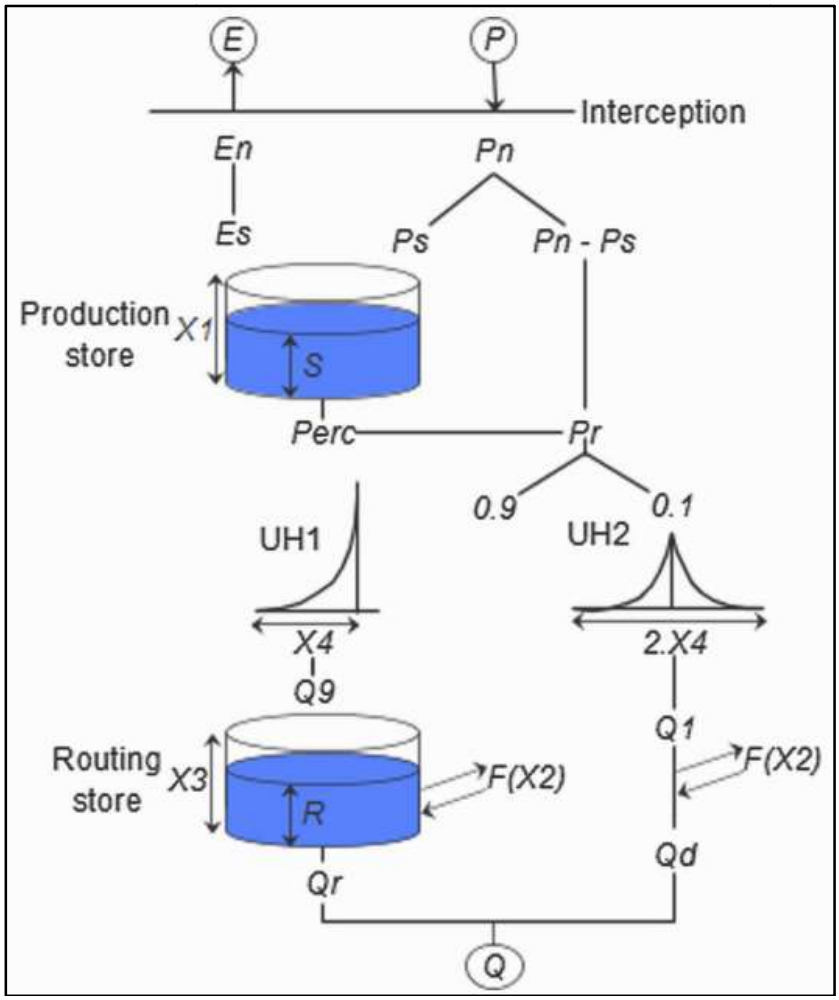

***Source**: Perrin et al., 2003*

Figure 3.7: Schematic diagram of the GR4J model.

The first operation is to subtract E from P to determine the net rainfall Pn or net evapotranspiration capacity En. In GR4J model, this operation is computed as if there were interception storage of zero capacity.

Pn and En can be obtained with the following conditions

$$\text{If } P_k > E, \text{ then } Pn = P_k - E \text{ and } En = 0$$

$$\text{Otherwise } Pn = 0 \text{ and } En = E - P_k$$

Production (SMA) store. In case Pn ≠ 0, a part Ps of Pn fills the production store. It is determined as a function of the level S in the store by:

$$Ps = \frac{x_1\left[\left[(1-(\frac{sk}{x_1})^2\right]\tanh(\frac{Pn}{x_1})\right]}{1+\text{ta}\quad(\frac{Pn}{x_1})} \tag{3.24}$$

Where: X1, the maximum capacity of the production store (mm); Eq (3.24) and Eq (3.25) result from the integration over the time step of the differential equation that have a parabolic form with terms in $(Sk/x_1)^2$, as detailed by Michel (1989).

In the other case, when En is not zero, an actual evapotranspiration rate is determined as a function of the level in the production store to compute the quantity Es of water that will evaporate from the store by:

$$Es = \frac{Sk\left[(2-\frac{sk}{x_1})\tanh(\frac{En}{x_1})\right]}{1+\left(1-\frac{sk}{x_1}\right)\tanh(\frac{En}{x_1})} \tag{3.25}$$

The water content in the production store is then updated with

$$S = Sk - Es + Ps \tag{3.26}$$

Note that S can never exceed X1. The schematization of the rating curves obtained with Eqs. (3.24) and (3.25) is shown in Figure. 3.7.

A percolation leakage Perc from the production store is then calculated as a power function of the reservoir content:

$$Perc = S\left\{1 - \left[1 + \left(\frac{4}{9}\frac{s}{x_1}\right)^4\right]^{-1/4}\right\} \tag{3.27}$$

Perc is always lower than S. The reservoir content becomes:

$$S = Sk - Perc \tag{3.28}$$

The percolation function in Eq. (3.27) occurs as if it originated from a store with a maximum capacity of $9/4x_1$. Given the power law of the mathematical formulation, this means that the percolation does not contribute much to the streamflow and is interesting mainly for low flow simulation.

Linear routing with unit hydrographs. The total quantity Pr of water that reaches the routing functions is given by:

$$\mathrm{Pr} = Perc + (Pn - Ps) \tag{3.29}$$

Pr is divided into two flow components according to a fixed split: 90% of Pr is routed by a unit hydrograph UH1 and then a non-linear routing store and the remaining 10% of Pr are

routed by a single unit hydrograph UH2. With UH1 and UH2, one can simulate the time lag between the rainfall event and the resulting stream flow peak. Their ordinates are used in the model to spread effective rainfall over several successive time steps. Both hydrographs depend on the same time parameter X4 expressed in days. However, UH1 has a time base X4 days whereas UH2 has a time base of 2X4 days. X4 can take real value and greater than 0.5 days.

In the discrete form, unit hydrographs UH1 and UH2 have n and m ordinates respectively, where n and m are smallest integer exceeding X4 and 2X4, respectively. This means that the water is staggered into n unit hydrograph inputs for UH1 and m inputs

For UH2. The ordinate of both unit hydrographs are derived from the corresponding S-curves (cumulative proportion of the input with time) denoted by SH1 and SH2, respectively. SH1 is defined a long time t by:

$$\begin{cases} \text{For } t \leq 0, SH1(t) = 0 \\ For\ \ 0\ < t < X4, SH1(t) = (\frac{t}{X4})^{5/2} \\ \text{For } t \geq X4, > SH1(t) = 1 \end{cases} \quad (3.30)$$

SH2 is similarly defined by:

$$\begin{cases} \text{For } t \leq 0, SH2(t) = 0 \\ For\ \ 0\ < t \leq X4, SH2(t) = \frac{1}{2}(\frac{t}{X4})^{5/2} \\ ForX4\ < t < 2X4, SH2(t) = 1 - \frac{1}{2}(2 - \frac{t}{X4})^{5/2} \\ \text{For } t \geq X24, > SH2(t) = 1 \end{cases} \quad (3.31)$$

UH1 and UH2 ordinates are then calculated by:

$$\begin{cases} UH1(j) = SH1(j) - SH1(j-1) \\ UH2(j) = SH2(j) - SH2(j-1) \end{cases} \quad (3.32)$$

Where j is an integer. If $0.5 \leq X > 4 \leq 1$, UH1 has a single ordinate equal to one and UH2 has only two ordinates.

Catchment water exchange. A groundwater exchange term F that acts on both flow components, is then calculated as:

$$F = X2(\frac{R}{X3})^{7/2} \quad (3.33)$$

Where R is the level in the routing store, X3 it's 'reference' capacity and X2 the water exchange coefficient. X2 can be either positive in case of water imports, negative for water exports or zero when there is no water exchange. The higher the level in the routing store, the larger the exchange. In the absolute value, F cannot be greater than X2: X2 represents the maximum quantity of water that can be added (or released) to (from) each model flow component when the routing store level equals X3.

Nonlinear routing store. The level in the routing store is updated by adding the outputs Q9 of UH1 and F as:

$$R = \max(0 ; R + Q9 + F) \quad (3.34)$$

The outflow Qr of the reservoir is thus computed as:

$$Qr = R\left\{1 - \left[1 + (\frac{R}{X3})^4\right]^{-1/4}\right\} \quad (3.35)$$

Qr is always lower than R, as shown in Figure 4. The level in the reservoir becomes:

$$R = Rk - Qr \quad (3.36)$$

Note that although the reservoir can receive a water input greater than the saturation deficit X3 – R at the beginning of a time step, the level in the reservoir can never exceed the capacity X3 at the end of a time step, as shown in Figure 3.7. Therefore, the capacity X3 could be called the 'one day ahead maximum capacity'. This routing store is able to simulate long stream flow recessions, when necessary.

Total stream flow. Like the content of the routing store, the output Q1 of UH2 is subject to the same water exchange F to give the flow component Qd as follows:

$$Qd = \max(0; Q1(k) + F) \quad (3.37)$$

Total stream flow Q is finally obtained by:

$$Qk = Qr + Qd \quad (3.38)$$

X2, the groundwater exchange coefficient (mm); X3, the maximum capacity of the routing store (mm); and X4, the time peak ordinate of hydrograph unit UH1 (day). The production store (X1) is storage at the surface of the soil that holds rainfall. Evapotranspiration and percolation occur in this store. The storage capacity depends on the types of soil in the riv-

er basin. Low porosity in the soil can increase the size of the production store. The groundwater exchange coefficient (X2) is a function of groundwater exchange, which influences the routing store.

When X2 has a negative value, water infiltrates to the aquifer; when it has a positive value, water exits the aquifer and adds to the routing storage. Routing storage (X3) is the amount of water that can be stored in soil porosity. The value of X3 depends upon the type and the humidity of the soil. The time peak (X4) is the time when the ordinate peak of the flood hydrograph is created during GR4J modeling (Perrin et al., 2003).

Table 3.12.: Parameters description and ranges in GR4J model

Parameters name	Unit	Range	Description
GR4J			
X1	mm	50-50,000	Maximum capacity of production store
X2	mm	-15 to 4	Groundwater exchange coefficient
X3	mm	10-1,300	1-day ahead maximum capacity of routing store
X4	day	0.5-5	Time base of the Unit Hydrodraph, UH1

***Source**: Perrin et al., 2003*

- **IHACRES model**

IHACRES (Identification of unit Hydrographs And Component flows from Rainfall, Evapotranspiration and Stream data) model is a lumped parameters conceptual model. The model is a Soil Moisture Accounting model (Jakeman and Hornberger, 1993).The model is dependent of inputs data specially rainfall data and is focused on top-down, spatial lumped, empirical approach to environmental hydrology. The model predict stream flow from rainfall and evapotranspiration/temperature inputs time series (Andrews et al., 2011; Dye and Croke, 2003). The model has two components: A nonlinear module that transforms the measured precipitation into effective rainfall, and a linear transfer function module computing the modeled stream flow as a linear combination of previous stream flow and effective rainfall (Figure 3.8). This model does not consider land use change in stream flow prediction. IHACRES have been applied in different catchments from 490 Km^2 to 10,000 Km^2 in China and UK (Littlewood et al., 1997). The version of Soil Moisture Defi-

cit (SMD) of IHACRES model with more physical meaning for the parameters has been applied here.

The nonlinear model is computed by:

$$U_k = [C(S_k - l)]^p r_k \tag{3.39}$$

where r_k is the observed rainfall; C is the mass balance factor, l is the soil moisture index threshorld and p is the power on soil moisture. S_k is the soil moisture, which can be written as:

$$S_k = r_k + (1 - \frac{1}{\tau_k})S_{k-1} \tag{3.40}$$

Where τ_k the drying is rate, and can be detailed as:

$$\tau_k = \tau_w \exp\,[0.062 f(t_r - t_k)] \tag{3.41}$$

Where τ_w is the drying rate at the reference temperature, f is the temperature dependent of drying rate,t_r is the reference temperature, and t_k is the observed temperature.

The linear module assumes that there is a linear relationship between the effective rainfall and runoff. Two components in the module (quick flow and slow flow) can be connected in parallel or series. In this study, two storages were used in the linear module to observe the basin conditions and runoff (q_k) at time step k, and as follows:

$$q_k = q_k^f + q_k^s \tag{3.42}$$

$$q_k^f = \beta_f U_k - \alpha_k q_{k-1}^f \tag{3.43}$$

$$q_k^s = \beta_s U_k - \alpha_k q_{k-1}^s \tag{3.44}$$

Where $q_k^f and\ q_k^s$ are the quick and slow flow, respectively and α and ß are the recession rate and peak response, respectively. The relative volume of quick and slow flow is given by:

$$V_f = 1 - V_s = \frac{\beta_f}{1+\alpha_f} = 1 - \frac{\beta_s}{1+\alpha_s} \tag{3.45}$$

The IHACRES model assumes that the partitioning of effective rainfall into quick and slow flow components is constant, and thus does not depend on rainfall amount or intensity, or catchment conditions. The model consists of only a few parameters (five parameters) associated with temperature, soil moisture, rainfall, etc. Consequently, the model can be used in the watershed with sparse data about land surface change.

In the present study, the inputs data used in IHACRES model included daily data of precipitation, mean temperature and daily discharge from 1961 to 2011 devised into two sub period: 1961-1986 and 1988-2011.

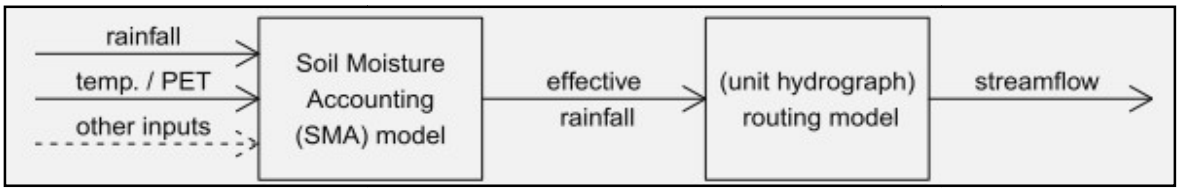

***Source**: Andrews et al., 2011; Dye and Croke, 2003.*

Figure 3.8: Conceptual schema of the IHACRES model

Table 3.13 gives the description of all parameters in the two rainfall-runoff models. The parameters ranges are the same, as described in GR4J (Perrin et al., 2003) and IHACRES (Andrews et al., 2011; Dye and Croke, 2003) models.

Table 3.13: Parameters description and ranges in IHACRES model

Parameters symbol	Unit	Range	Description
IHACRES			
f	-	0.5-1.3	CMD stress threshold as a proportion of d
e	-	1(fixed)	Temperature to PET conservation factor
d	mm	50-550	CMD threshold for producting flow
Ts (tau_s)	day	10-1,000	Time constant for slow flow store
Ts (tau_q)	day	0-10	Time constant for quick flow store
υ 8 (v_8)	-	0-1	Fractional volume for slow flow

***Source**: Andrews et al., 2011; Dye and Croke, 2003.*

- **Model's inputs**

As mentioned above GR4J and IHACRES models use daily areal rainfall, temperature or evapotranspiration to simulate runoff in the catchment outlets. Discharge is used for models calibration and validation. For IHACRES or GR4J models, areal rainfall at Athiémé was computed using Thiesen polygon method (Thiessen, 1911) using the 21 available rainfall stations in the catchment (Koubodana et al., 2019a).

3.2.3.2.Models calibration-validation and performances

Model calibration and validation is performed with daily discharge of Athiémé. The study period was divided first into two-sub period with equal length of dry and wet year as rainfall breakpoint in 1987 (Koubodana et al., 2019b): the pre-dam period (1964-1986) and post-dam period (1988-2011) (Table 3.14). One year was used as model warm-up period in each sub period. In IHACRES model the entire period of study were also use for verification after calibration and validation in each sub period. Calibration was performed for 10 years in each sub period and the same parameters from calibration were used for validation and compared models sensitivity analysis. The sensitive analysis of IHACRES and GR4J models leading to selected optimization parameters and ranges was based on the literature of the past studies done in the region (Badjana et al., 2017a; Biao et al., 2015; Gaba et al., 2015; Kodja et al., 2018; Le Lay et al., 2007; Oyerinde et al., 2016).

Table 3.14: Calibration and validation periods

Sub-period	Warm up period	Calibration period	Validation period
Pre -dam	1964-01-01 to 1964-12-31	1965-01-01 to 1968-12-31	1969-01-01 to 1973-12-31
Post -dam	1988-01-01 to 1988-12-31	1989-01-01 to 1992-12-31	1993-01-01 to 1997-12-31

We use different criteria to evaluate the model performance: coefficient of determination (R^2), the Nash-Sutcliffe coefficient (NSE) (Nash and Sutcliffe, 1970), Root Mean Squared Error(RMSE), Kling Gupta Efficiency (KGE) and Percent Bias (PBIAS). These criteria were used after calibration and validation in each sub catchment and for each sub period (Adeaga et al., 2012; Vansteenkiste et al., 2014).

- R^2 explains the ratio of the variance for observed data, which were correctly modeled by the model. It value are between 0 and 1 and higher value shows that the error is less. Usually value bigger than 0.5 are considered as acceptable result (Adamowski, 2000; Lebel and Ali, 2009).

$$R^2 = \frac{[\sum_{i=1}^{n}(Q_{obs}-mea\ (Q_{obs}))((Q_{sim}-mean(Q_{sim}))]^2}{\sum_{i=1}^{n}(Q_{obs}-mean(Q_{obs}))^2 \times \sum_{i=1}^{n}(Q_{obs}-mea\ (Q_{obs}))^2} \quad (3.46)$$

- NSE is a normalized statistic that determines the relative amplitude of the residual variance deviated to the observed data variance and can be computed by equation (3.47).

$$NSE\ (Q) = 1 - \frac{\sum_{i=1}^{n}(Q_{obs} - Q_{sim})^2}{\sum_{i=1}^{n}(Q_{obs} - mean(Q_{obs}))^2} \quad (3.47)$$

WhereQ_{obs},Q_{sim} and mean (Q_{obs}) are the observed data, simulated data and mean observed data value, respectively; while n is the total number of data record. NSE value shows the accuracy of the model prediction base on observations. It ranges between 0 and 1. The model performance is considered satisfactory for NSE ≥ 0.5; adequate for 0.5 < NSE< 0.65 and very good when NSE ≥ 0.65 (Moriasi et al., 2007).

There are also some other objective functions to use for performance comparative analyses: the objective functions like logarithm-transformed steam flow value NSElog, particularly NSE objective function focuses on the high flow whereas the NS log objective relative function focuses on the fitting low flow because of the log transformation of the time series values (Krause and Boyle, 2005)and 0.5(NSE +NSElog) hybrid function which focuses on the fitting medium flow by giving equal weight on NSE and NSlog

- RMSE is computed base to statistical bias. The function calculates the error criterion based on the mean squared error (Gupta et al., 2009).

This estimator allows comparing two variables and it is formulated as:

$$RMSE = \sqrt{\frac{1}{N}\sum_{i=1}^{N}(Sim\ i - Obs\ i)^2} \quad (3.48)$$

N is the number of time steps, *Obs* and *Sim* are observed and simulated flows, respectively, at time step i.

- KGE can assess the performance of GR4J model by simulating high discharge at Athiéme outlet. Gupta et al.(2009)has proposed KGE (equation 3.49) as a criterion that combines an equal weighting of three components of correlation, bias and variability measure. The optimized values of KGE show that except correlation, the two components lead to their ideal values (Andréassian et al., 2014):

$$KGE = 1 - EDandED = \sqrt{(r-1)^2 + (\alpha - 1)^2 + (\beta - 1)^2} \quad (3.49)$$

ED = Euclidean distance from ideal point; r = Pearson correlation coefficient;

$\alpha = \frac{\sigma_s}{\sigma_o}$: $is the$ratio between the standard deviation of simulated values and the standard deviation of observed ones; $\beta = \frac{\mu_s}{\mu_o}$ is the bias and also the ration between the mean of the simulated values and the mean of the observed ones.

- PBIAS measures the error between the observed and simulated values. It can be computed as:

$$PBIAS = \frac{\sum_{i=1}^{n}(Q_{obs} - Q_{sim}) \times 100}{\sum_{i=1}^{n} Q_{obs}} \quad (3.50)$$

With Q_{obs} and$Q_{sim}$are the observed and simulated streamflow respectively. PBIAS values between ±10 and ±15 indicate a good model prediction, whereas value greater than ± 25 indicates an unsatisfactory model simulation (Moriasi et al., 2007).

3.2.3.3.Comparison of GR4J and IHACRES simulated discharge

The monthly and annual averages of discharge have been computed and we plotted the monthly and annual evolution of discharge from GR4J and IHACRES model for the sub periods at each discharge gauges station. The coefficient of determination between simulated and observed discharges from GR4J and IHACRES gives the degree of correlation between the daily simulated and observation discharges. A coefficient of determination higher than 0.7 shows that the simulated discharges from GR4J and IHACRES are perfect match with observations while a value smaller than 0.5 shows an acceptable simulated discharge whereas above 0.7 is an excellent simulated discharge.

3.2.4. Land cover, climate changes and dam impacts on water balance components

In order to determine the impacts of land use , climate change and dam management on hydrological components in the Mono river basin, CILSS land cover data reclassified by (Koubodana et al., 2019a) were used for land cover change assessment. Two different scenarios of land use and land cover were developed and used during SWAT model simulation. Indeed Land use and land cover map of 1975 was selected for the first period of simulation between 1961 and 1986 and land use and land cover map of 2000 integrated in the second simulation between 1988 and 2011. The second simulation incorporates Nangbéto dam information and management in SWAT model. Two simulations using different climate and land use data scenarios were run. The first of simulation named SIM1 (pre-dam period) is forced with climate data from 1961 to 1986 with land use layers of the year

1975. The second simulation SIM2 (post-dam period) has used climate data from 1988 to 2011 with land use map of the year 2000. The second simulation incorporates Nangbéto reservoir management data into SWAT model. Land use of 1975 and 2000 were used to reflect land use pattern for SIM1 and SIM2 respectively because of the significant changes of land use and land cover classes within this period (see Figure 3.9). Figure 3.9 illustrate de schematic diagram of the methodology in this study.

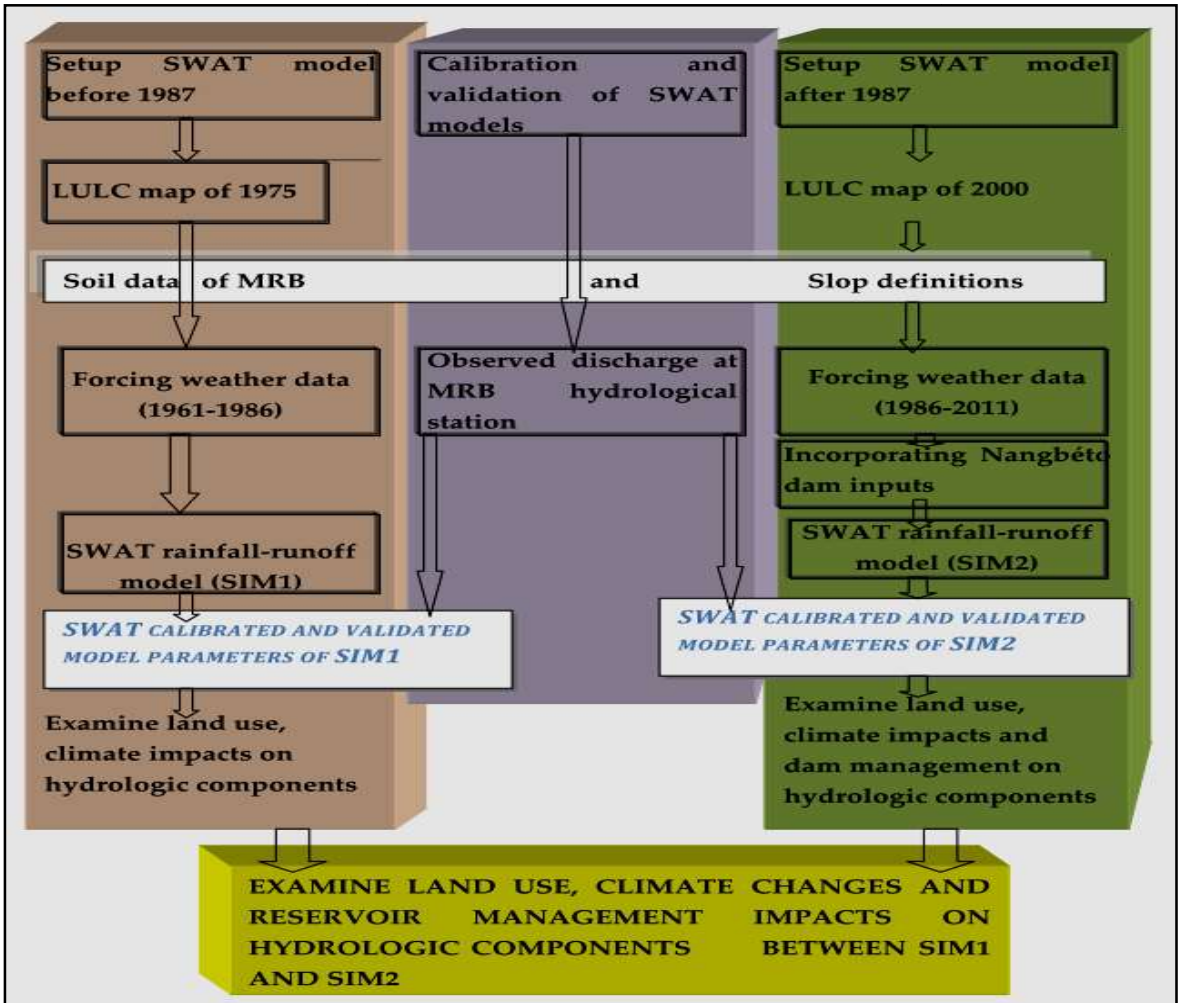

Figure 3.9: SWAT modeling steps

These significant changes are forest, savanna and cropland between 1975 and 2000 which were indicated in Koubodana et al.,(2019a). The Nangbéto dam put in operation in 1987 was selected as a turning point of the climate data in conformity with the results of Koubodana et al., (2019b) for negative decanal rainfall variability index between 1981-1990 over the MRB. This year was used because the significant change of land use and climatic variable will play an important role on hydrological components (Tan et al., 2015). The hydrological components considered were streamflow, evaporation (EV), eva-

potranspiration (ETP), soil water content (SW), percolation (PERC), surface runoff (SURQ), groundwater flow (GW_Q), water yield (WYLD) and lateral flow (LAT_Q) .

3.2.4.1.SWAT model description

To simulate discharge under LULCC; CC and dam management in MRB SWAT "Soil and Water Assessment Tool" (Arnold et al., 1998) was selected for the study. SWAT is a semi-distributed and comprehensive model which is easily handled by the user and developed for complex watershed over long period studies (Arnold et al., 2012; Gassman et al., 2007; Moriasi et al., 2012). The model used at daily time step to predict the impact of land cover, dam management and climate on water, sediment, agriculture and chemical yield in a complex river (Gassman et al., 2007; Mango et al., 2011). SWAT model even integrates reservoir management interface. The model is process based, computationally efficient, and able for a continuous simulation over long periods. Some components of SWAT model are weather, hydrology, soil temperature and properties, plant growth, nutrients, pesticides, bacteria, land management and reservoir management. More information can be found in (Arnold et al., 2012, 1998).

For this study, the latest version in ArcGIS graphical user interface for SWAT model (ArcSWAT2012) was used to build the hydrological model for MRB. In SWAT, a watershed is divided into multiple sub-basins and each sub-basin is further discretized into hydrologic response units (HRUs). An HRU is a small virtual region in a given sub-basin assumed to have the dominant land use (LU), management, topographical/slop, and soil characteristics. Soil water content, surface runoff, nutrient cycles, sediment yield, crop growth and management practices are computed for each HRU and then aggregated for the sub-basin by a weighted average. Physical characteristics, such as slope, reach dimensions, and climatic data are taken into account for each sub-basin. For climate, SWAT uses the data from the nearest station to the centroid of each sub-basin. Calculated flow, sediment yield, and nutrient loading obtained for each sub-basin are then routing through the river system. Channel routing is simulated by using the variable storage or Muskingum method (Kim and Lee, 2010). More information is available on official web site of SWAT *(https://swat.tamu.edu/)*.

3.2.4.2.SWAT model inputs data

In this study, we use several datasets to set up, calibrate and validate SWAT model. These data are:(1) a 1:5,000,000 Harmonized World Soil Database v 1.2 map extracted for Mono

watershed (Figure 3.10); (2) land-use land cover maps 2 km×2 km spatial resolution for the 1975 and 2000 from CILSS database used by Koubodana et al.(2019a) for land use assessment of MRB; (3) a 90 m Digital Elevation Model (DEM); (4) daily minimum and maximum temperature, rainfall and discharge (Table 3.15). We converted the geospatial datasets of different resolutions into a common spatial projection of World Geographic System Universal Transverse of Mercator (WGS 84 UTM) zone 31.

Table 3.15: SWAT Mono inputs data set

Data description and sources used for SWAT Mono			
Data type	Resolution	Period	Sources
DEM	90m	-	Shuttle Radar Topography Mission(SRTM) http://www2.jpl.nasa.gov/srtm/
Soil			http://www.fao.org/soils-portal/soil-survey/
Landuse	2km	1975-2000	https://eros.usgs.gov/westafrica
Weather data	daily observed	1961-2011	METEO-BENIN & DGMN-TOGO
Discharge	5 stations-daily	1961-2011	Direction Générale de l'Eau et de l'Assainissement (DGEA) du Togo Direction Générale de l'Eau (DGEau) du Bénin Comminauté Electrique du Benin(CEB)
Agricultural management	Planting, harvesting	Yearly	FAOSTAT http://faostat.fao.org/site/339/default.aspx
Water resource		country	http://www.fao.org/nr/water/aquastat/water_res/index.stm AQUASTAT, FAO
Management and operation	Reservoir	season	CEB (http://www.cebnet.org)
inflow, outflow		daily	
surface area and		season	
spillway conditions			

- **Land use and land cover:** Human activities in the MRB mainly include land use/cover change, the construction and operation of Nangbeto dam, water withdrawal for population growth, agricultural development and irrigation. Two different land cover map of 1975 and 2000 were used in SWAT model set up (Table 3.16 and Figure 3.11c &d). The type of land use and land cover database used were reclassified assessed by Koubodana et al.(2019a) over MRB and conclude to be more realistic compare to other databases.

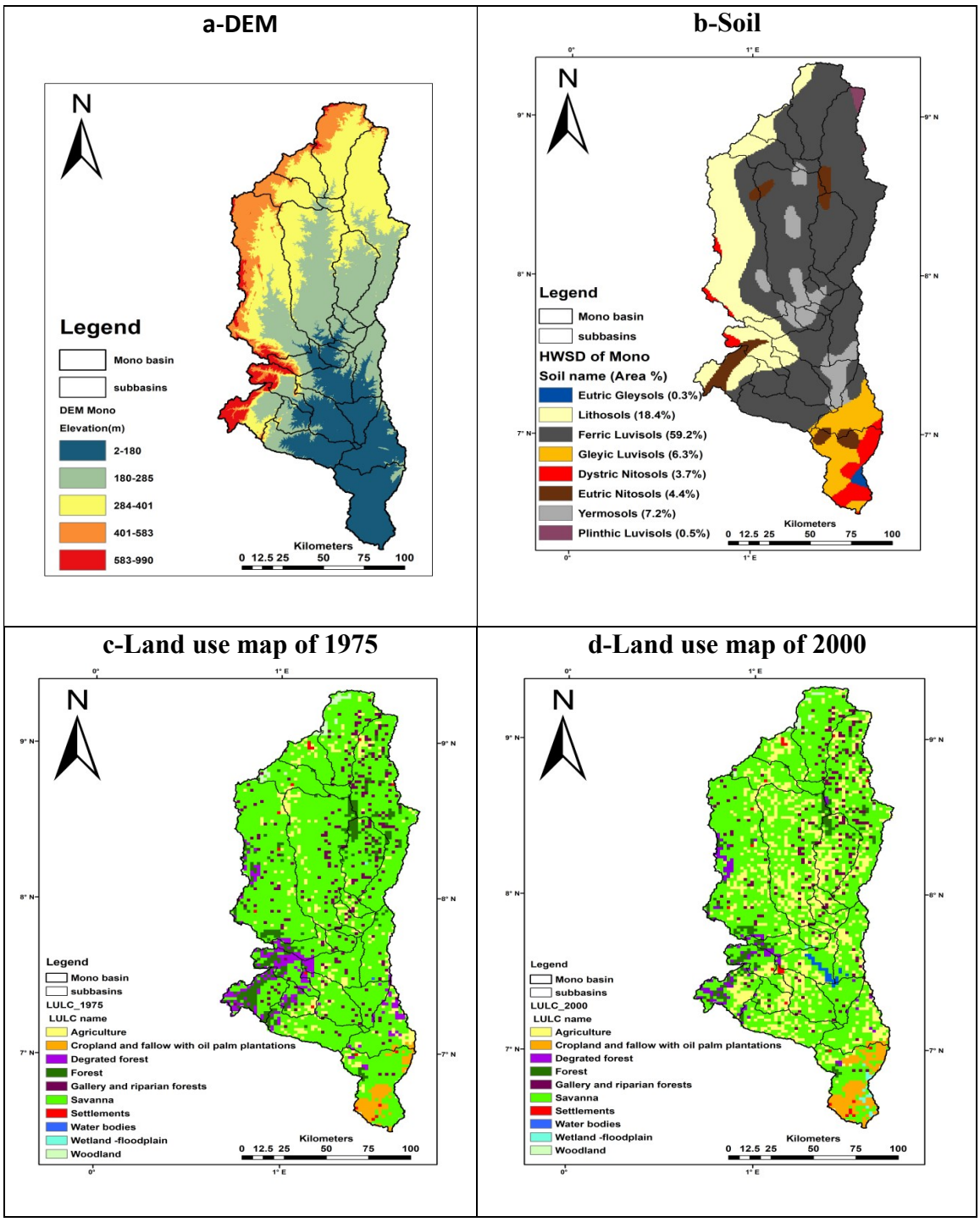

***Source**: DEM-2017, HWSD-2018, CILSS-2018*

Figure 3.10: Input data sets used in SWAT model

Table 3.16: SWAT land cover inputs description

N_o	**SWAT LU code**	**Land use /cover name**	**Land use area [%](1975)**	**Land use area [%](2000)**
1	FRST	Forest	5.38	3.03
2	RNGE	Savanna	76.03	63.76

3	WETN	Wetland-floodplain	0.02	0.33
4	AGRR	Plantation/Agriculture	6.48	21.83
5	WATR	Water bodies	0.02	0.52
6	URBN	Settlements	0.31	0.49
7	FRSE	Gallery forest and riparian forest	5.20	4.28
8	RNGB	Degraded forest	3.91	1.98
9	FRSD	Woodland	0.43	0.27
10	OILP	Cropland and fallow with oil palms	2.22	3.51

***Source**: CILSS dataset*

- **Reservoir management information and operation**

The reservoir management inputs information consists to daily inflow and outflow from 1988 to 2011. There are also the spillway conditions, the reservoir surface area, watershed area, the reservoir storage capacity and a height of 143m in principal spillway. We obtained all the information for the dam from local managers of the reservoir and from literature (Ago et al., 2005; Amoussou et al., 2012; Houessou, 2016; PCCP, 2008) and CEB institution *(www.cebnet.com)*. SWAT model also required the date of the reservoir operation (Figure 3.11).

SWAT input variables that pertain to reservoirs.

Variable name	Definition	File Name
RES_ESA	SA_{em}: Surface area of the reservoir when filled to the emergency spillway (ha)	.res
RES_PSA	SA_{pr}: Surface area of the reservoir when filled to the principal spillway (ha)	.res
RES_EVOL	V_{em}: Volume of water held in the reservoir when filled to the emergency spillway (10^4 m^3 H_2O)	.res
RES_PVOL	V_{pr}: Volume of water held in the reservoir when filled to the principal spillway (10^4 m^3 H_2O)	.res
RES_K	K_{sat}: Effective saturated hydraulic conductivity of the reservoir bottom (mm/hr)	.res
IRESCO	Outflow method	.res
RES_OUTFLOW	q_{out}: Outflow rate (m^3/s)	resdayo.dat
RESOUT	q_{out}: Outflow rate (m^3/s)	resmono.dat
RES_RR	q_{rel}: Average daily principal spillway release rate (m^3/s)	.res
STARG(mon)	*starg*: Target reservoir volume specified for a given month (m^3 H_2O)	.res
IFLOD1R	$mon_{fld,beg}$: Beginning month of the flood season	.res
IFLOD2R	$mon_{fld,end}$: Ending month of the flood season	.res
NDTARGR	ND_{targ}: Number of days required for the reservoir to reach target storage	.res
OFLOWMN(mon)	$q_{rel,mn}$: Minimum average daily outflow for the month (m^3/s)	.res
OFLOWMX(mon)	$q_{rel,mx}$: Maximum average daily outflow for the month (m^3/s)	.res

***Source:** Neitsch et al., 2011*

Figure3.11: SWAT input variables necessary for the reservoir

3.2.4.3.Hydrology of SWAT model

The hydrologic cycle is climate driven and provides moisture and energy inputs, daily precipitation, maximum/minimum air temperature, solar radiation, wind speed, and relative humidity that control the water balance. This water balance relation is mathematically represented in Arnold et al.(2012) by:

$$SW_t = SW_o + \sum_{i=1}^{t}(R_{day} - Q_{surf} - ET_a - W_{pec} - Q_{gw})i \quad (3.51)$$

Where SW_t is the final soil water content (mm); SW_o is the initial soil water content on day (mm);R_{day}, Q_{surf}, ET_a, $W_{pec}$and Q_{gw} are the daily amounts (in mm) of precipitation, surface runoff, evapotranspiration, percolation, and the amount of return flow on day i respectively.

Figure 3.12 exhibits the components of the hydrologic cycle for SWAT model based on the water balance equation (3.51). Runoff amounts are predicted for each sub-basin and computed for the channel. The SWAT model different layers are defined bas on the soil used for the model initialization in the regions. No matter what type of problem studies SWAT, water balance is driving force behind everything that happens in the watershed. Therefore SWAT simulation is divided into two major divisions (Figure 3.12). The first division is the land phase of the hydrologic cycle which controls the amount of water, sediment nutrient and pesticide loading to the main channel in each sub basin. The second division is the water or routing phase of hydrologic cycle which is the movement of water, sediment, etc through the channel network of the watershed outlet (Arnold et al., 2012)

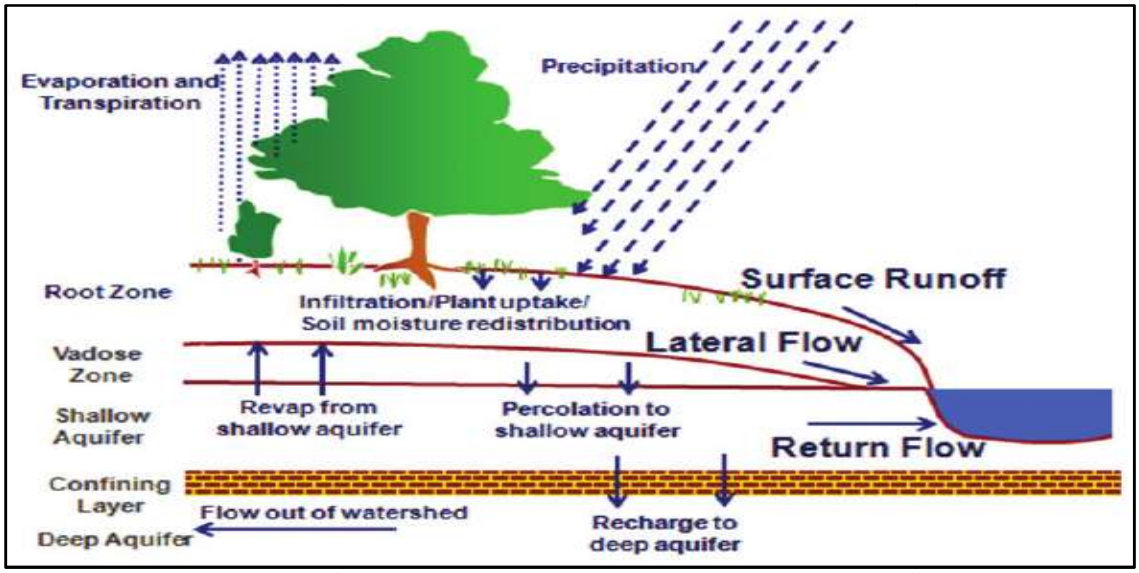

***Source**: Arnold et al., 2012*

Figure 3.12: Schematic representation of SWAT hydrology cycle

Table 3.17: SWAT model hydrological component factors

SWAT component	Process description	Considered factors
Hydrology		
Surface runoff	SCS-CN equation, Green & Amp infiltration method	Hourly or daily rainfall, soil and land use properties
Percolation	Storage routing, travel time, up and downward flow	Available water capacity, hydraulic conductivity
Lateral flow	Kinematic storage model, up and downward flow	Slope, porosity, flow length, soil water
Groundwater flow	Linear storage model, up and downward flow	Topography exerts
Potential evapotranspiration	Priestley-Taylor, Permann-Monteith or Hargreaves	Minimum and maximum air temperature, solar radiation, relative humidity, wind velocity
Actual evapotranspiration	Soil evaporation	Soil depth, water content, ET_{pot}, LAI
Transmission	Lane's method	Channel dimensions, flow duration

Source: *Hiepe, 2008*

- **Surface runoff**

SWAT model uses the Soil Conservation Service (SCS) curve number method for rainfall daily data or Green &Ampt infiltration method for hourly rainfall data (Arnold et al., 1998). SCN depends on retention parameters, which depend on soil water content (Neitsch et al., 2011) to perform the estimation of surface runoff. It is used to predict the approximate amount of runoff from a given rainfall event and based on soil properties, land use and hydrologic conditions. The SCS curve equation is given by:

$$Q_{surf} = \frac{(R_{day} - Ia)^2}{(R_{day} - Ia + S)} \quad (3.52)$$

Where $Q_{surf}$the daily surface runoff (mm), R_{day} is is the rainfall depth for the day (mm), Ia is the initial abstractions which includes surface storage and S is the retention parameter (mm). The retention parameter S and the prediction of lateral flow by SWAT model are determined in the following equation.

$$S = 25.4(\frac{1000}{CN} - 10) \quad (3.53)$$

Where S = drainable volume of soil water per unit area of saturated thickness (mm/day); CN = Curve Number (Arnold et al., 2012). The initial abstraction, Ia is commonly approximated as 0.2S and Equation (3.52) becomes:

$$Qsurf = \frac{(Rday - 0.2S)^2}{(Rday + 0.8S)} \quad (3.54)$$

Thus, Runoff will occur when $R_{day} > Ia$

SWAT calculates the peak runoff rate, the time of concentration for overland and channel flow, the surface runoff lag and the runoff volume for each HRU and sub-basin individually. The peak runoff rate is the maximum runoff flow rate that occurs within a given rainfall event. It is an indicator of the erosive power of a storm and can be used to predict sediment loss. The peak runoff rate is calculated using the modified rational method as a function of surface runoff, sub-basin area, time of concentration and the fraction of daily rainfall during time of concentration:

$$qpeak = C.i.\frac{Area}{3.6} = \frac{Qsurf}{Rday}.\frac{Rtc}{tconc}.\frac{Area}{3.6} = \frac{\alpha tc.Qsuf\ ..Area}{3.6.tconc} \quad (3.55)$$

q_{peak} : peak runoff rate [m^3/s]

C: runoff coefficient [-], quotient of Q_{surf} and Rday

i : rainfall intensity [mm/h], ratio Rtc and tconc

Area: sub-basin area [km^2]

R*tc* : rainfall during time of concentration [mm]

Rday daily rainfall [mm]

t_{conc} time of concentration for the sub-basin [h]

Atc fraction of daily rainfall that occurs during the time of concentration [-]

Qsurf surface runoff [mm].

The time of concentration is the amount of time from the beginning of a rainfall event until the entire sub-basin area contributes to flow at the outlet. It is calculated as a function of sub-basin slope length, average flow channel length, overland flow velocity and the average channel velocity estimated from Manning's n. For large sub-basins with a time of concentration greater than one day, SWAT incorporates a surface runoff storage feature to lag a portion of the surface runoff release to the main channel.

- **Potential evapotranspiration according to Hargreaves**

Potential evapotranspiration (PET) includes evaporation from plant canopy, transpiration, sublimation and evaporation from the soil. SWAT uses all the plant growth as a single plant to simulate land cover and makes a difference between annual and perennial plants. Plants growing invert in evapotranspiration by transpiration process, and biomass production. Many methods have been developed inside the model to compute potential evapotranspiration (PET): the Penman-Monteith method (Monteith, 1965; Penman, 1956), the Priestley-Taylor method (Priestley and Taylor, 1972) and the Hargreaves method (Hargreaves and Samani, 1982). The two first methods need climate variables such as wind speed, radiation, temperature, precipitations and relative humidity to compute evapotranspiration. As our study area is limited by weather data, the Hargreaves method is preferable. Therefore, potential evapotranspiration was computed using the Hargreaves method, which requires the climatic input of daily precipitation, and minimum and maximum temperature. This method has been successfully applied in many studies in West Africa (Komi et al., 2016; Poméon et al., 2018; Schuol et al., 2008).Actual soil evaporation computed by using exponential functions of soil depth and water content. Plant water evaporation simulated by a linear function of PET, leaf area index (LAI), and root depth, and can be limited by soil water content. More detailed descriptions of the model can be found in (Arnold et al., 2012).

- **Actual evapotranspiration**

Once the total potential evapotranspiration is determined, actual evaporation must be calculated. SWAT assumes that the daily soil heat flux G is equal to zero. The aerodynamic resistance is calculated as a function of the height of wind, humidity and temperature. The maximum storage capacity varies as a function of LAI. SWAT first evaluates any rainfall intercepted by the plant canopy. Next, SWAT separately calculates the maximum amount of transpiration and soil evaporation using a modified approach of (Ritchie, 1972). Transpiration is determined as a function of LAI and ETpot using equations (3.56) to Maximum transpiration is calculated as a function of ETpot , aboveground biomass, residue and two terms defining the upper and lower limits. The upper limit is defined as 80% of the plant-available water on a given day. If an evaporation demand for soil water exists, SWAT first partitions the evaporative demand between the different layers. SWAT does not allow a different layer to compensate for the inability of another layer to meet its evaporative de-

mand. The depth distribution used to determine the maximum amount of water allowed to be evaporated is:

$$Esoil, z = E_s^{II} \frac{z}{z + \exp(2.374 - 0.0713.z)} \quad (3.56)$$

$E_{soil,\,z}$: evaporative demand at depth z [mm]
E_s^{II}: maximum soil water evaporation on a given day [mm]
z : depth below the surface [mm]

The coefficients in (Eq. 3.57) were chosen so that 50% of the evaporative demand is extracted from the top 10 mm of soil and 95% from the top 100 mm of soil. This assumption can be modified by the soil evaporation compensation coefficient (ESCO). As the value of the ESCO is reduced, the model can extract more of the evaporative demand from lower levels. The actual amount of transpiration in a day equals the plant water uptake for the day, which depends on the amount of water required by the plant for transpiration and the amount of water available in the soil. The depth distribution used to determine the maximum amount of water uptake from the soil surface to a depth z is:

$$W_{up,z} = \frac{E_t}{[1 - \exp(-\beta_w)]}.[1 - \exp(\beta_w.\frac{z}{z_{root}}] \quad (3.57)$$

As default, βw is set to 10, so that 50% of water uptake will occur in the upper 6% of the root zone. This assumption can be modified by the plant uptake compensation coefficient (EPCO). As the value of the EPCO is increased, the model allows more of the water uptake demand to be met by lower layers in the soil.

- **Percolation**

Water can flow in the soil under saturated or unsaturated conditions. SWAT records the water contents of the different soil layers but assumes that the water is uniformly distributed within a given layer. Unsaturated flow between layers is indirectly modeled with the depth distribution of plant water uptake and that of soil water evaporation (Eq. 3.56). Water is allowed to percolate if the water content of a soil layer exceeds the field capacity of the layer. The amount of water that moves from one layer to the underlying layer is calculated using the storage routing technique (Eq. 3.58).

$$W_{perc,Jy} = SW_{Jy,excess}\left[1 - e^{\frac{-\Delta t}{TT_{perc}}}\right] = SW_{Jy,excess}\left[1 - e^{\frac{-\Delta t - K_{sat}}{SATly - FCly}}\right] \quad (3.58)$$

If infiltration is explicitly modeled using the Green-Ampt approach, a crack-flow model allows bypass flow to be considered.

- **Lateral flow**

SWAT uses a kinematic storage technique to compute subsurface flow as a function of drainable volume of water, saturated hydraulic conductivity, soil slope, hill slope length and drainable porosity, as follows:

$$q_{lat} = 24.H_0 \cdot v_{lat} = 0.024.\left[\frac{2.SW.K_{sat}.slp}{\phi_d \cdot L_{hill}}.\right] \quad (3.59)$$

where

$q_{lat:}$ lateral flow [mm/d]

$H_{0:}$ is saturated thickness normal to the hillslope at the outlet expressed as a fraction of total thickness [mm/mm]

$v_{lat:}$ velocity of flow at the outlet [mm/h]

24: conversion factor hours to days

SW: drainable volume of soil water [mm]

Slp: slope [m/m]

Φd: drainable porosity [mm/mm]

$K_{sat:}$ vertical saturated hydraulic conductivity [mm/h]

$L_{hil:}$ hill slope length [m]

For times of concentration greater than one day, SWAT incorporates a lateral flow storage feature to lag a portion of lateral flow release to the main channel

- **Groundwater flow**

In each sub-basin, SWAT simulates an unconfined aquifer that contributes to the flow in the main channel (shallow aquifer) and a confined, deep aquifer. Water that enters the deep aquifer is assumed to contribute to stream flow somewhere outside the catchment. Water leaves groundwater storage either by discharge into rivers and lakes, by upward movement from the water table into the capillar fringe or by seepage to the deep aquifer. Equation (3.60a) shows the daily water balance for the shallow aquifer. The shallow aquifer storage is recharged by percolation from the unsaturated zone and reduced by baseflow, deep aquifer recharge, upward flows into the soil zone and withdrawal. Baseflow is implemented as a linear storage with a specific recession coefficient (cf. Eq. 3.60b).

$$aq_{sh,i} = aq_{sh,i-1} + w_{rchrg} - Q_{gw} - w_{revap} - w_{deep} - wu_{sa} \quad (3.60a)$$

$$Q_{gw,i} = Q_{gw,i} \cdot e^{-\alpha \Delta t} + w_{rchrg}(1 - e^{-\alpha \Delta t}) \quad (3.60b)$$

where

$aq_{sh,i}$ Shallow aquifer storage on the day i [mm]

$aq_{sh,i-1}$ Shallow aquifer storage the day before [mm]

w_{revap} Recharge entering the aquifer [mm]

Q_{gw} Groundwater flow or base-flow into the main channel [mm]

w_{deep} Amount of water moving into the soil zone as response to water deficiencies [mm] amount of water percolating from the shallow aquifer into the deep aquifer [mm]

wu_{sa} : Water use from the shallow aquifer [mm]

α base flow recession constant [-], describes the lag flow from the aquifer, estimation by base flow filter techniques. Besides several specific groundwater coefficients, SWAT defines minimum thresholds for the shallow aquifer for the occurrence of return flow and water flow to the unsaturated zone or deep aquifer.

- **Water yield**

WYLD: Water yield (mm H_2O).The net amount of water that leaves the sub-basin and contributes to streamflow in the reach during the time step. It is computes as WYLD = SURQ + LATQ + GWQ – TLOSS – pond abstractions.

3.2.4.4.Set up of Mono SWAT

The DEM is the first input data for beginning any SWAT project. DEM is used to delineate the stream network. Threshold drainage area of 500 km^2 was selected to discretize automatically and adding manually where streamflow gauging station exist in the MRB. The watershed was divided into 24 sub-basins for the first period of simulation (1961-1986) and 23 for the second period (1986-2011). The threshold of 20% of LU, 10% of soil and 20% of slop within a sub-basin are neglected within a single HRU for the two simulations, This involves a subdivision into 109 HRUs (1961-1986) and 111 HRUs (1986-2011) based on same soil, land use, and slope (Arnold et al., 1998). We run two different simulations (1961-1986 &1988-2011) based on different land use and climate data since the dam started operating in 1987. For all the simulation, the same criterions were use in the set up process. For simulation one (SIM1) and Simulation two (SIM2), 3 and 2 years are chosen for model warm up period. It is the period for initial conditions for equilibration and miti-

gation, this period does not appear in the outputs (Setegn et al., 2010). For the SIM1, the river was at natural state without any perturbation of industrial installation. However, for SIM2 Nangbéto reservoir operating since September 1987 was taken into account in the implementation of SWAT model by inputting reservoir management operation and information, in the model set up, calibration and validation processes (Arnold et al., 1998; Cho et al., 2012).

3.2.4.5.Model Sensitivity analysis

Sensitivity analysis is to identify the most important influencing factors which have a significant impact on a specific model outputs (Ghoraba, 2015). Sensibility analysis provides information on the most important process in the region and helps to decrease the number of parameters in the calibration procedure (Abbaspour et al., 2017). As mentioned by Ma et al. (2000), it is necessary to select the key parameters and its ranges for calibrations analysis. Usually, two types of sensitivity analysis are available in SWAT model: One-at-a-time (OAT) or local sensitivity analysis, and all-at-a-time (AAT) or global sensitivity analysis. In OAT, all parameters are maintained constant while varying one to identify its effect on some model output or objective function (Arnold et al., 2012). The two methods can lead to different results. The first method parameters always depend on the value of other related parameters. Nevertheless, the weakness is that the corrected value is unknown. The second method disadvantage is the high number of simulation needed. However, the two methods are necessary for a best calibration (Muleta and Nicklow, 2005; van Griensven et al., 2006; White and Chaubey, 2005).

Table 3.18: SWAT model parameters ranking.

N_o	Parameters	Descriptions	Min	Max	Differ by	Method
1	SLSUBBSN.hru	Average slope length	-0.5	0.5		R
2	OV_N.hru	Manning's "n" value for overland flow	0.01	30		V
3	ESCO.hru	Soil evaporation compensation factor	-0.5	0.5	Landuse	R
4	EPCO.hru	Plant uptake compensation factor	-0.5	0.5		R
5	CANMX.hru	Maximum canopy storage	-0.5	0.5		R
6	CN2.mgt	SCS runoff curve number f	-0.5	0.5	Landuse	R
7	BIO_INIT.mgt	Minimum plant biomass for plant	-0.5	0.5		R
8	BIO_MIN.mgt	Minimum plant biomass for plant	-0.5	0.5		R
9	GW_REVAP.gw	Groundwater "revap" coefficient	0.02	0.2		V
10	ALPHA_BF.gw	Baseflow alpha factor (days)	0	1		V
11	GW_DELAY.gw	Groundwater delay (days)	0	400		V
12	GWQMN.gw	Treshold depth of water in the shallow aquifer (mm)	0	4000		V
13	SOL_AWC().sol	Available water capacity of the soil layer	-0.5	0.5	Soil texture	R
14	SOL_BD().sol	Moist bulk density	-0.5	0.5	Soil texture	R
15	SOL_K().sol	Saturated hydraulic conductivity	-0.5	0.5	Soil texture	R
16	SOL_ALB().sol	Moist soil albedo	0	0.25		V
17	SURLAG.bsn	Surface runoff lag time	0.05	24		V
18	ALPHA_BNK.rte	Base flow alpha factor for bank storage	-0.5	0.5		R
19	CH_K1.sub	Effective hydraulic conductivity in tributary channel alluvium	-0.5	0.5		R
20	RES_ESA.res	Reservoir surface area in emer-gency spillway	-0.5	0.5		R

***Source**: Neitsch et al., 2011*

"V" in Method implies a replacement of the initial parameter value with the given value in the final range, whereas an "R" indicates a relative change to the initial parameter value.

In this study, we used AAT sensitivity analysis for Mono watershed SWAT model by choosing first, 56 parameters according to SWAT manual (Arnold et al., 2012; Neitsch et al., 2011.) and studies literature in the region (Badou, 2016; Begou et al., 2016; Bossa et al., 2012; Hounkpe, 2016; Näschen et al., 2018; Poméon et al., 2018; Sintondji et al., 2014). This analysis have performed 1,500 simulations of AAT sensitivity analysis which come finally to 20 parameters out of 58 parameters (Table 3.18) which are used after 2,000

simulations for calibration and one best simulation for validation of the model during SIM1 and SIM2.

3.2.4.6.Model calibration process

Calibration is the process by which the modeler parameterizes a model to make it representative of local conditions. Calibration involve to minimize the uncertainties or to have "realistic model". For a better model calibration, it is important to select the main important parameters in the best ranges that influence the system hydrology (Arnold et al., 2012). Based on the sensitivity analysis or the expert judgments of the area, the user determines which parameters will be adjusted by calibration process (Arnold et al., 2012). The predicted variables or output by the model can now be compared with the observed data to see if it is representative. There are usually manual and automatic calibrations. Manual calibration allow the model to respond at certain condition and automatic calibration is set by the model itself after giving it a range and number of parameters with selected objective function.

In 2019, many tools have been tested for calibration/validation and uncertainty analysis around the world. For example Beven and Binley (1992) described the Generalized Likelihood Uncertainty Estimation method (GLUE) methodology for calibration and uncertainty estimation incorporating many observations into the calibration with multiples parameters. The Sequential Uncertainty Fitting procedure (SUFI-2) by (Abbaspour et al., 2004); Parameters Solution (ParaSol) by (Van Griensven and Meixner, 2006) and Particule Swarm Optimization (PSO) by Kennedy and Everhart (1995) are well known and also used. Some studies have compared all these methods of calibration. Wu and Chen (2015) by comparing tree different methods suggested that SUFI-2 method is more sustainable for hydrological calibration and validation, Kouchi et al.(2017) added some conclusions using SUFI-2 in SWAT-CUP Version 5.1.6.2 (Abbaspour, 2015) interface for sensitivity of parameters using different optimization algorithms and objective function to asses water management in two basins.

We used both manual and automatic calibration in our study. Manual calibration was set in land cover/ plant growth management and give estimated BLAI (maximum leaf area), plant/ begin growing for seasonal plants in term of LAI_INIT (LAI Initial), biomass initial (BIO_INIT), ESCO, EPCO, CANMX and dam reservoir operation, because plant growth days and biomass production impact considerably affect water balance, erosion and nutrient yield in local and regional scale (Arnold et al., 2012).The value sets were chosen

according to in situ data or satellite data. SUFI-2 semi-automatic tools for calibration – validation-sensitivity-uncertainty analysis were then used. In SUFI-2, uncertainty of input parameters is depicted as uniform distributions, while model output uncertainty is quantified by the 95% prediction uncertainty (95PPU) calculated at the 2.5% and 97.5% levels of the cumulative distribution of output variables obtained through Latin hypercube sampling. Abbaspour et al. (2004) and Schuol et al (2008) proposed p-factor and r-factor providing the model strength in capturing uncertainties. The p-factor is related in the capacity to tale all the process taking place in basin and should be between values from 0 to 1(perfect value). Hence, r-factor indicates the quality of the calibration by showing a thickness of 95PPU. The value must be near to zero for ideal result. Both p-factor and r-factor are complementary and indicate the strength of model uncertainty.

Observed discharge is used for two calibration implementations (1964-1975) and (1988-2000) using KGE as objective function. The calibration is performed at Athiémé, Tététou and Corrokopé station for the first period (SIM1) and at Athiémé, Tététou, Nangbéto and Corrokopé stations for the second period (SIM2) by selecting the parameters of Table 3.18.

3.2.4.7.Model validation process

Validation means to run the model with the best ranked parameters during the calibration period. According to Gan et al.(1997), a good calibration and validation must have a same length with similar wet, dry day and average water balance year. Many tools were created for calibration and validation in the last years. It included manually and auto-calibration tools in SWAT (Van Griensven and Bauwens, 2003) or the most used in most studies SWAT-CUP (Abbaspour et al., 2007). The analysis requires running the best iteration with the same number of simulations as in the last calibration iteration. Similar to calibration, validation results are also quantified by the p-factor, r-factor, and the objective function value.

The same parameters (Table 3.19) used during calibration are run for validation steps. Automatic calibration and uncertainty analysis were used in many studies for the last year by using SWAT-CUP proposed by Abbaspour et al.(2007) for multi-objective calibration and validation of a watershed in Switzerland. Schuol et al.(2008) applied the same method in entire Africa to calibrate and validate green and blue water. A SWAT-CUP tool was performed on validation step. As calibration, two validation periods are chosen (1976-1986; and 2001-2011), at the same stations and selecting the same objective function.

Table 3.19: SWAT Mono calibration and validation periods

Simulation	Warm-up period	Calibration period	Validation period
SIM1	1961-1963	1964-1975	1976-1986
SIM2	1986-1987	1988-2000	2001-2011

Source: *Table base on observation data (DGEau, CEB, DGMN)*

3.2.4.8.Model performance and uncertainty analysis

Objective function allows modeler to know if the simulated and the observation values are closer. In this analysis we use many objective functions used in most of hydrologic studies. It is the case of the coefficient of determination (R^2), Nash-Sutcliffe efficiency (NSE), modified R^2 (bR^2), Modified Nash-Sutcliffe efficiency (MNS), ranked sum of squares (SSQR), percent bias (PBIAS), King-Gupta efficiency (KGE) (Gupta et al., 2009) and ratio of standard deviation of observation or root mean quart error (RSR, and MNS.

Table 3.20: General performance rating for recommended statistics

Performances	R^2	NSE	KGE	PBIAS
Very good	$0.75<R^2<1.00$	0.75<NSE<1.00	0.75<KGE<1.00	PBIAS<±10
Good	$0.65<R^2<0.75$	0.65<NSE<0.75	0.65<KGE<0.75	±10<PBIAS<± 15
Satisfactory	$0.50<R^2<0.65$	0.50<NSE<0.65	0.50<KGE<0.65	±15<PBIAS<± 25
Unsatisfactory	$R^2<0.50$	NSE<0.50	KGE<0.50	PBIAS≥±25

Source*: Kouchi et al., 2017a*

3.2.4.9: Climate, land use and dam management impacts on hydrological components

To establish the impacts of change in land use, climate variables and dam management on hydrological components, SWAT model simulation is divided into two periods: SIM1 period (1961-1986) for which land use 1975s is used as input and with climate variables extended between 1961 and 1986; SIM2 period (1988-2010) for which land use 2000s, climate variables extended between 1988-2011 and Nangbéto reservoir is incorporated are used as input data. Based on the model performances and uncertainties during SIM1 or and SIM2, modelers could be able to deduce the impacts of land use change, climate change

and dam management on streamflow and hydrological components. Thus, temporal, spatial distribution and related statistics of water component over MRB for SIM1 and SIM2 respectively are generated. The impacts climate, land use change and dam management on water cycle components are deduced by comparing the results from SIM1 and SIM2 statistics. Furthermore, the changes between the two periods of hydrological cycle components are computed and comparative methods allow giving sustainable information for water resource management.

Partial conclusion

This chapter described the different types of data collected, the materials and methods used in analyzing the data to achieve the objectives. The different types of data used in this study include land cover, climate data, and outputs from climate models, soil maps and discharge data. The data were analyzed using different tools and land cover evaluation, for climate change detection and extreme indices analysis, and for water hydrological modeling using lumped and semi- distributed model for water balance components simulations.

Chapter 4: Land use,land cover evaluation and future scenarios results

Introduction

Land use and land cover (LULC) change in West Africa (Giertz et al., 2005; Kleemann et al., 2017; Ouedraogo et al., 2010; Reid et al., 2000; Turner et al., 1994) is mostly caused by population growth, although locally other drivers may be of importance (Atsri et al., 2018; Giertz et al., 2005; Kleemann et al., 2017; Reid et al., 2000). With increasing population, demand for food, energy, and water is also increasing (Lambin et al., 2003; Ruelland et al., 2008), which causes land use and land cover changes (LULCC). West Africa is a region facing severe LULCC, particularly in the Republic of Togo (TG) and the Republic of Benin (BN), which are experiencing environmental and social degradation due to increasing subsistence farming. This causes an acceleration of the depletion of the natural resources and the increase of agricultural area due to rapid population and economic growth (Koglo et al., 2018; Turner et al., 1994).

Land use refers to, "man's activities on land which are directly related to the land," while land cover is "the vegetation and artificial constructions covering the land surface" (Anderson et al., 1976). LULCC in West African countries are driven by natural and anthropogenic factors. The anthropogenic factors are mainly related to demographic growth (Brink and Eva, 2009) while the natural factors are linked to climate variability and climate change (Brink and Eva, 2009; Oguntunde et al., 2006). LULCC influence hydrological processes as agricultural intensification results in increased surface runoff, reduced groundwater recharge, and transfer of pollutants (Veldkamp and Lambin, 2001). Knowledge about LULC dynamic at the watershed scale is indispensable for water and land resource management (Ouyang, 2012; Wisser et al., 2010).

Land cover products from remote sensing are often the input for environmental modeling and analysis. This is the case in hydrologic modeling and trend analysis (Wisser et al., 2010), biomass and energy modeling (Eisfelder et al., 2012), population density modeling (Sutton, 1997) as well as risk and hazard analysis (Arsanjani et al., 2013; Herbst et al., 2006).

One important research interests is to analyze land cover change in the MRB from 1975 to 2013 using different data sources and to project future changes using scenarios. The aim of this study is therefore to assess past and future land cover changes in the MRB using different data sets. We have analyzed the past land cover change in the MRB using three dif-

ferent data, have projected future land cover considering population growth as the main driver and have determined how the choice of the data set will influence projected future land cover.

4.1. Results of LULC evaluation and future scenarios

4.1.1. Land cover data sets accuracy assessment

The assessment of accuracy of land cover maps was done using the latest available land cover maps of the years 2010 (Globeland30) and 2013 (CILSS and ESA-CCI). The percentage of ground-true points estimated correctly known as overall accuracy and Kappa coefficients were respectively of 83% and 68% for CILSS in 2013 product, 69% and 36% using the ESA-CCI 2013 data set, 57%, and 34%using the Globeland30data set. The Kappa coefficient from CILSS is considered good while being poor for ESA-CCI and Globeland30 data sets (Chen et al., 2004; Fitzgerald and Lees, 1994). The overall accuracy of CILSS is excellent while good for ESA-CCI and Globeland30data set. Detailed producer and user‘s accuracy computed for each land cover type and each product is shown in Table 4.1 and Appendix 4.1.

Table 4.1:.User and producer accuracy values

	CILSS 2013		**ESA 2013**		**Globeland30 2010**	
	User	Producer	User	Producer	User	Producer
Land cover type	Accuracy [%]					
Forest	62.9	95.7	3.9	8.7	37.0	52.9
Savanna	98.3	76.5	78.6	81.1	69.8	55.2
Wetland	81.8	90.0	7.6	50.0	0.0	0.0
Cropland	65.8	95.8	70.8	45.3	56.5	66.8
Water	63.6	97.5	100.0	87.5	88.9	61.5
Settlements	100.0	80.0	80.0	80.0	66.7	11.8

According to this table, CILSS dataset shows acceptable results with all user and producer accuracies higher than 60%. User and producer accuracy for ESA-CCI for forest and wetland are very poor especially for wetland and settlements in Globeland30 data set. Particularly for the land cover categories of forest, savanna, cropland and water the accuracies are

acceptable in both ESA-CCI and Globeland30. In the three data sets user and producer accuracies for savanna and water are acceptable while forest is good in CILSS and Globeland30 datasets.

Although the spatial resolution of the ESA-CCI and the Globeland30data is high, the accurate mapping of some land cover types in the study area may explain the fact that CILSS local information from West Africa is used during the automated and semi automated classification (CILSS, 2016; Cotillon, 2017). It may be also due to the number of reference points and random spatial reparations used for the validation.

4.1.2: Land cover area and change estimation

The analysis of the CILSS data reveals savanna land cover as dominant followed by cropland and forest. In term of area coverage percentage, savanna was about 75.94% in 1975, 63.75% in 2000 and 50.35% in 2013; cropland was 84% in 1975, 25.36% in 2000, and 39.82% in 2013 and forest was about 14.87 % in 1975, 9.57% in 2000 and 7.96% in 2013 as shown in Figure 4.1. It appears a decrease in the Savanna and Forest between 1975 and 2013, but there is an increase in settlement and crop land from 1975 to 2013. These results confirm many analyses performed in Togo and Benin about land cover change mainly derived by deforestation, cropland expansion and losses of savanna (Akinyemi et al., 2017; Kleemann et al., 2017). The ESA-CCI results are different for land cover data; contrary to the CILSS data the savanna surface area was 70.52% in 2000 and 70.70% in 2013. The area of cropland was 20.66% in 2000 and 20.91% in 2013.The forest area decreased from 8.02% in 2000 to 7.51% on 2013. This means there is an increase of savanna and of cropland over time. Thus, deforestation still exists, which result in an increase of cropland area in the MRB. Figure 4.1 shows the decrease of forest of 0.51% from 2000 and 2013 and an increase of 0.18% of savanna from 2000 to 2013 for the ESA-CCI dataset. However, all the changes are slight and there is not significant for the study area. The results of Koglo et al.(2018) revealed an important deforestation; losses of savanna because of cropland and settlements in south and north of Togo Republic. In the Fazao-Malfacassa National Park near the MRB, Atsri et al.(2018) found that forest and savanna are degraded which could be explained by agriculture expansion, bush fire, timber extraction all linked to population growth. By assessing land use change process in the North of Togo, Polo-akpisso et al.(2019) has confirmed that savanna and forest have decreased annually at the rate more than 2% whereas there is gain of cultivated area and settlements in the region.

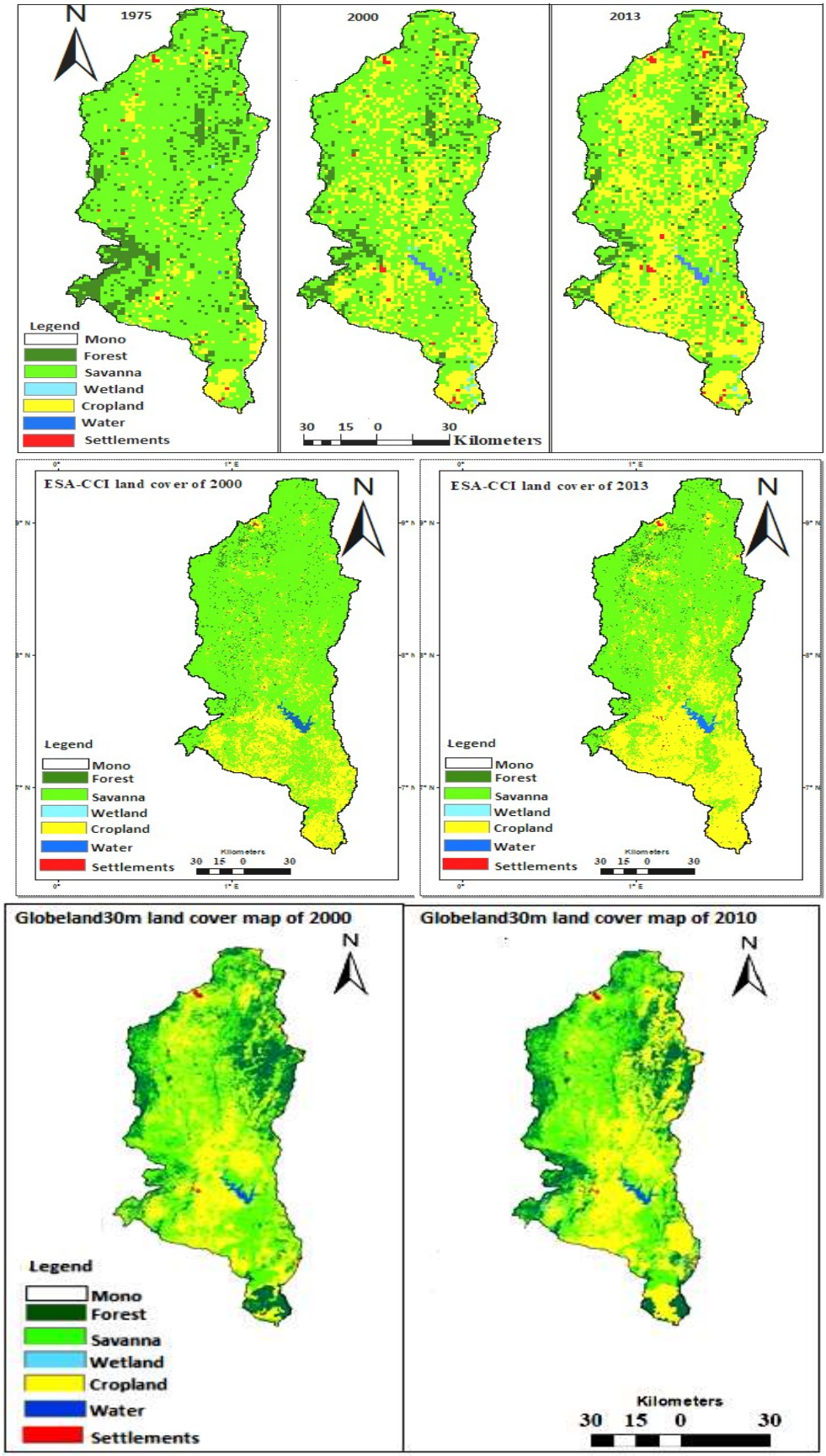

Figure 4.1: CILSS (upper), ESA-CCI (middle) and Globeland30 (bottom)maps

Table 4.2: Land cover area and area change

	Land cover category area [%]							Land cover category area change [%]				
Year	1975	2000			2010	2013		1975-2000	2000-2013		2000-2010	1975-2013
Sources	CILSS	CILSS	ESA	GLC	GLC	CILSS	ESA	CILSS	CILSS	ESA	GLC	CILSS
Forest	14.87	9.57	8.02	23.65	23.96	7.96	7.51	-5.31	-1.61	-0.51	0.32	-6.91
Savanna	75.94	63.75	70.52	44.51	39.99	50.35	70.7	-12.19	-13.4	0.18	-4.52	-25.59
Wetland	0.02	0.33	0.05	0.01	1	0.16	0.06	0.31	-0.16	0.02	0.99	0.14
Cropland	8.84	25.36	20.66	30.69	33.88	39.82	20.91	16.51	14.46	0.25	3.19	30.97
Water	0.02	0.51	0.68	0.68	0.67	0.49	0.63	0.49	-0.02	-0.06	-0.01	0.47
Settlemens	0.31	0.49	0.07	0.48	0.5	1.22	0.19	0.18	0.73	0.12	0.02	0.91
Total	100	100	100	100	100	100	100	0.0	0.0	0.0	0.0	0.0

However, savanna is the major land cover with positive trend category in the ESA-CCI map between 2000 and 2013, followed by cropland. However, forest has negative trend. Considering the user and the overall accuracy by categories (Table 4.2), it is clear that forest and wetland are not accurately classified in the ESA-CCI data sets. Cropland spatial representation is more in the south of the basin; which does not reflect the agriculture activities in the study area when comparing CILSS and Globeland30 results. The Globeland30 maps for 2000 and 2010 are shown in Figure 4.1. The forest area was around 23.65% in 2000 and 23.96% in 2010. For savanna, it was 44.51% in 2000 and 39.39 % in 2010 while cropland was 30.69% in 2000 and 33.68% in 2010.Based on these results; it appears an increase of 0.32% in forest area and 3.19% in cropland. In the case of savanna, the area decrease of about 4.52%. Together with Table 4.2, it appears that ESA-CCI, forest and wetland are not well mapped, but the classification of water category is good for the three data sets (CILSS; ESA and Globeland30) because the user and producer accuracy in Table 4.2 is higher than 60%. The findings indicate that savanna and agriculture are the dominant land cover classes in the study area over all the evaluated years; this is in accordance with other studies. For example (Badjana, 2016) analyzed LULC change in the Kara river basin, and found that savanna was dominant.

This was also observed by Diwediga et al.(2015) in the Mono river basin a small tributary of Oti river in central region of Togo. Accordant to Koglo et al.(2018), savanna and forest are the most important land cover categories that are being converted in cropland in Kloto, a small district in the south of the MRB. Nevertheless, the increase of the water bodies between 1975 and 2000 can be explained by the building of the Nangbéto reservoir in 1987 and rainfall variability in this region (Badjana, 2016). As the consequences of climate change and climate variability, there is a reduction of precipitation resulting in a decrease of the water body of the reservoir from 2000 to 2013. This directly affects the hydroelectricity production as mentioned by Houessou (2016). Climate variability, especially the droughts between 1970s and 1980s, negatively affected grassland due to over grazing. The increase of settlement is also realistic because of population growth (Table 3.8).

4.1.3: Comparison between land cover data sets

Because CILSS showed the highest accuracy, it was taken as reference for the comparison with the other maps. Figure 4.2 shows the area of each land cover class from CILSS, ESA-CCI and Globeland30. Therefore, from each land cover area percentages were computed; absolute error and mean absolute error of 2000 and 2013 are also calculated respectively. The Absolute Error (AE) for each data class from CILSS and ESA is small in 2000 and 2013; except for savanna and cropland in 2013 with an error more than 18%.

Table 4.3: Absolute error and mean absolute error [%]

Land cover types	2000			2013
	CILSS &ESA-CCI	CILSS& Globeland30	ESA-CCI &Globeland30	CILSS&ESA-CCI
Forest	1.55	14.08	15.63	0.45
Savanna	6.77	19.24	26.01	20.35
Wetland	0.28	0.32	0.04	0.10
Cropland	4.70	5.33	10.03	18.91
Water	0.17	0.16	0.01	0.14
Settlements	0.42	0.02	0.40	1.03
MAE [%]	2.31	6.53	8.69	6.83

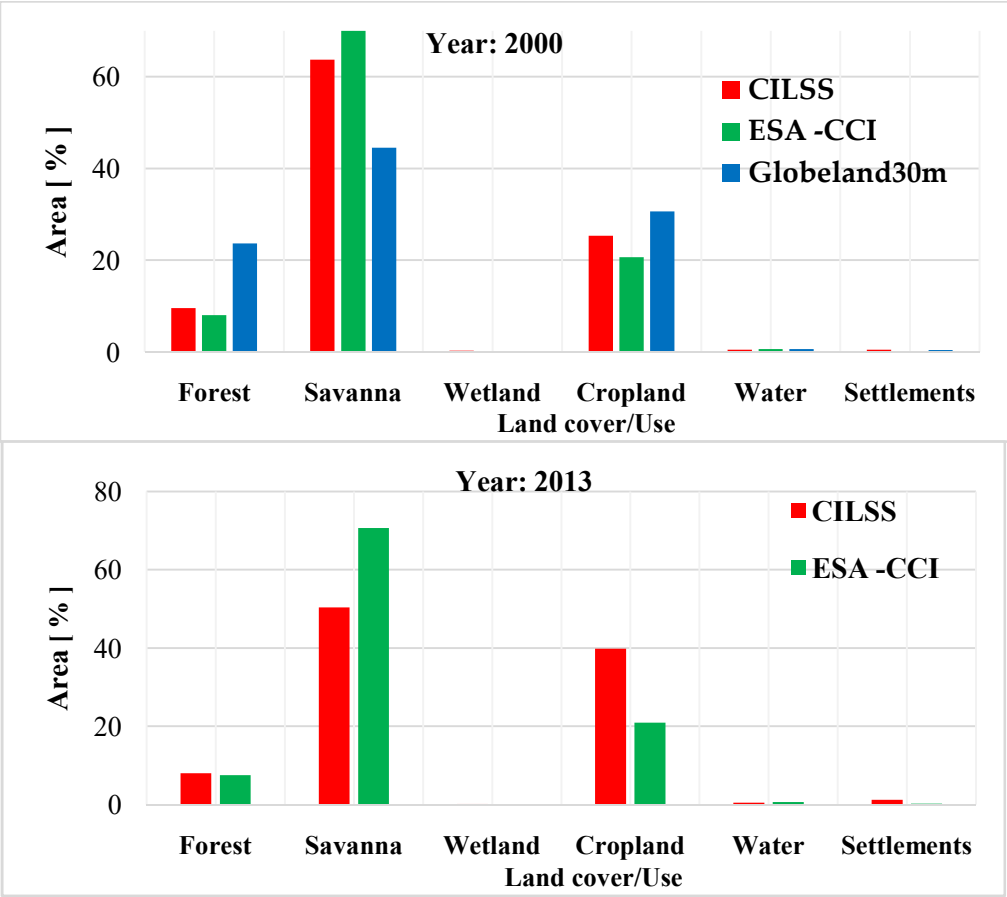

Figure 4.2: Land cover area comparison

4.2: Land covers data modeling using the Land Change Modeler

4.2.1: Land cover spatial trend of change

The spatial trend of change computed for the CILSS, ESA-CCI and Globeland30data sets are shown in Figure 4.3. CILSS data show a spatial trend during the period of 2000 to 2013 from forest to savanna in the south-west of the basin. The forest trend change is more intensive in the south–west and in the north-east. These are the locations of the cities of Sokode, Blitta, Anié, Atakpamé and the roads network as shown in Figure 2.1.The trend of change from savanna to cropland is high in the center of the basin. This indicates that there was 16.51% of the total area that become cropland between 1975 and 2000, 14.46% between 2000 and 2013. So, the total trend was about 30.97% from 1975 to 2013. There are some similarities of the spatial trend of the transition forest to savanna between 2000 and 2013 using CILSS and ESA-CCI data sets. The path is the same for the transition of savanna to cropland between 2000-2013 and 2000-2010 using the three data sets (Appendix 4.2). The trend direction and location is approximately the recharge zone located on the main cities in the basin. Therefore, the spatial trend in land cover change might be ex-

plained by population activity and growth in the south district of Mono river basin (Koglo et al., 2018).

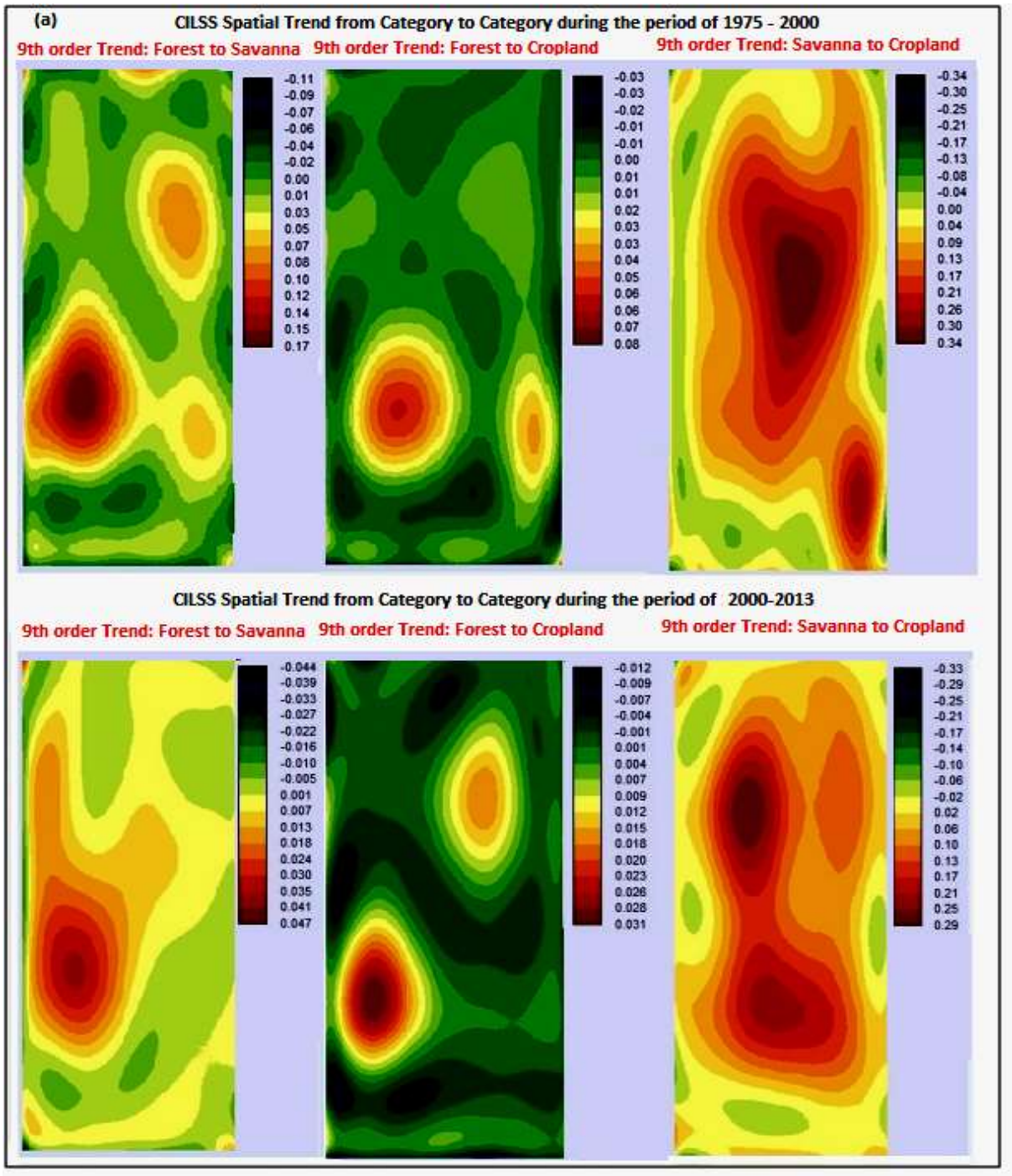

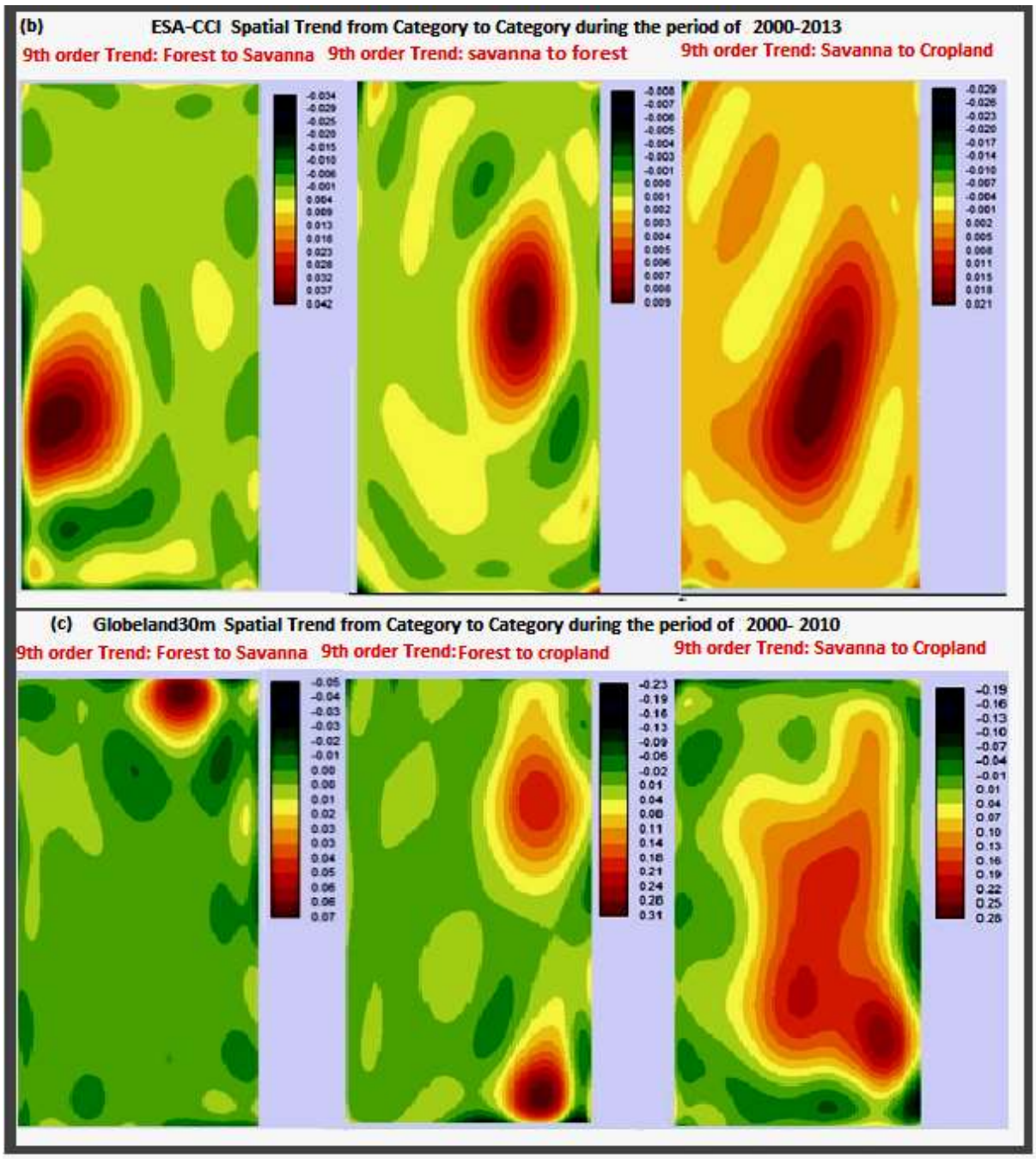

Negative values represent a reverse spatial development for the analyzed trend, whereas increasing positive numbers characterize an increasing intensity for the analyzed trend.

Figure 4.3: spatial trend maps of land cover changes over MRB

4.2.2: Quantifications, locations of land cover change and driving forces

Land cover modeling requires information about how much change occurs in the land, where it happened and why. Therefore, quantification of historical land covers change allows knowing the past state of land cover in the MRB, and the drivers involving change are useful for future land projection.

Table 4.4: Changes in land cover in the MRB

Areal changes [km^2]	2000 to 2013		2000 to 2010
	CILSS	ESA-CCI	GLC30
Forest to Savanna	108.00	72.00	76.50
Savanna to cropland	252.00	13.50	9.00
Water to wetland	36.00	27.00	28.80
Forest to cropland	54.00	180.00	25.00
Total change area	450.00	292.5	139.3

Table 4.4 shows the main changes in land cover in the study area as derived from CILSS, ESA-CCI, and Globeland30. The largest changes are savanna to cropland (252 km^2), forest to savanna (108 km^2), and forest to cropland (54 km^2) using the CILSS data set. The land cover change using ESA-CCI and Globeland30 is underestimated compared to CILSS. The land cover changes can be explained by the population growth in the region as from 2000 to 2015, the population in Togo increases from 4.9 Million to 7.4 Million inhabitants (*Table 3.8* http://worldpopulationreview.com/).

The hot spot of the change from forest to savanna is in the south-west of the basin while forest to cropland change is also important in the north–east. Changes of savanna to cropland are occurring over the entire basin, but densely centered in the basin from south to north. The change from forest to savanna with CILLS datasets is located in the south and west in the basin where probably rural population has access to wood for their domestic needs such as fire for cooking, charcoal.

4.2.3 Model assumptions, constraints and factors of prediction

The variables loaded in sub-model executed the model, which by the neural network can create random sample of cells experiencing each of the transitions selected in the modeling. We use the default value of 10000 iterations of training for testing the accuracy and the result has given acceptable accuracy of 50.94% for CILSS, 40.04% for ESA-CCI and 20.13% for GLC30 (Table 4.5). Then the transitions potential maps of CILSS, ESA-CCI and GLC30 were obtained (Appendix 4.3). But Markov Chain determines the amount of using the earlier and later land cover map along with the data. That prediction specified with two numbers of future scenarios was modeled respectively for the year 2020 and 2027. A Markov Chain is a random process that depend on the current state and the initial drivers defined for the modeling (Eastman, 2006). The procedure for extracting exactly how much land use will be in the future is based on the projection of the transition's

potential into a future and also by generating land cover transitions potential file. The transitions potential file is a matrix (Table 4.5) that save the probability that each land cover class may change to every other class.

Table 4.5: CILSS probability of transitions potential (2020-2027).

2020						
Given :	Probabilty	of	changing	to		
Class	Forest	Savanna	Wetland	Cropland	Water	Settlements
Forest	0.723	**0.171**	0.000	**0.103**	0.000	0.004
Savanna	0.003	0.598	0.000	**0.391**	0.000	0.008
Wetland	0.000	0.412	0.255	0.330	0.000	0.003
Cropland	0.000	**0.185**	0.000	0.785	0.000	0.030
Water	0.000	0.006	0.048	0.004	0.942	0.000
Settlements	0.000	0.005	0.000	0.111	0.000	0.885
2027						
Given :	Probabilty	of	changing	to		
Class	Forest	Savanna	Wetland	Cropland	Water	Settlements
Forest	0.656	**0.083**	0.004	**0.257**	0.001	0.001
Savanna	0.141	0.516	0.011	**0.327**	0.004	0.001
Wetland	0.563	0.060	0.001	0.143	0.234	0.000
Cropland	0.090	0.431	0.013	0.459	0.005	0.003
Water	0.075	0.052	0.001	0.028	0.844	0.000
Settlements	0.019	0.054	0.006	0.111	0.002	0.809

As shown in Table 4.5 the probability of transition predicted for land use of 2020 from forest to savanna is 0.171, from savanna to cropland 0.39 and from forest to cropland is 0.1. Then, the prediction for 2027 indicates that from Forest to Savanna is 0.0825, forest to cropland is 0.257 and savanna to cropland is 0.3268. The transitions in Table 4.5 are the major transitions; because the diagonal probabilities are high and stables transitions such as forest-to-forest, savanna-to-savanna or water to water, etc. for 2020 as for the 2027. However, for minor transitions we used negligible probability.

4.2.4: Land cover validation and change predictions

Because of limited data availability, validation was performed only for CILSS data set. For that, after assessing land cover change between 1975 and 2000, we generated a land cover map for the year 2013 using the Land Change Modeler (Appendix 4.4). The model performance explains the change in land cover for CILSS and ESA-CCI 2000-2013 as well as for Globeland30 2000-2010/ RMSE: Root Mean Squared Error. Then, we compared the estimated map with the observed land cover map. As a result, the validation was ranked as acceptable in an accuracy rate higher than 50% (Table 4.6).

After analyzing land cover change, future land cover was predicted for all data sets using population growth as the main driver.

Table 4.6: MLP parameters and performances

	CILSS	**ESA-CCI**	**Globeland30**
Input layer neurons	2	2	2
Hidden layer neurons	3	2	3
Output layer neurons	6	5	5
Requested samples per class	10,000	10,000	10,000
Final learning rate	0.0001	0.0001	0.0005
Momentum factor	0.5	0.5	0.5
Sigmoid constant	1	1	1
Acceptable RMSE	0.01	0.01	0.01
Iterations	10,000	10,000	10,000
Training RMSE	0.2890	0.3482	0.4000
Testing RMSE	0.2890	0.3482	0.4000
Accuracy rate	**50.94%**	40.04%	20.13%
Skill measure	0.4113	0.2406	0.0017

Change in land cover for CILSS and ESA-CCI 2000-2013 and Globeland30 2000-2010
RMSE: Root Mean Squared Error.

The predicted land cover maps for 2020 and 2027 using the CILSS data set are shown in Figure 4.4 together with the related statistics. According to this projection, forest and savanna land cover decrease with a change rate of 0.45% and 5.64% respectively. The opposite occurred on cropland and settlements because is constantly increasing with a rate of 5.26% and 0.83% between 2020 and 2027. Wetland and water bodies did not show significant change.

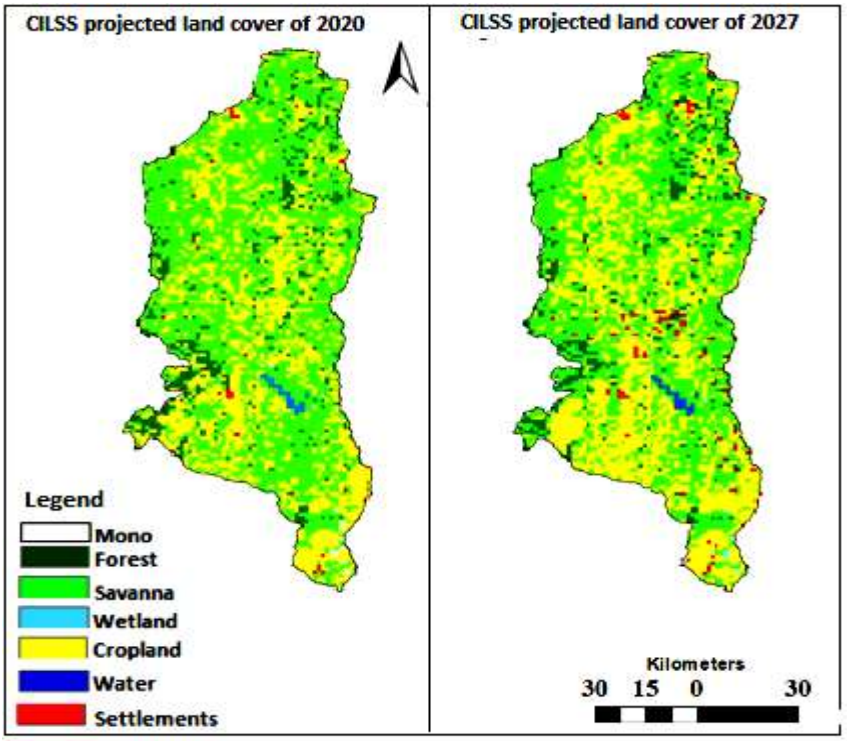

	Land cover area [%]		Change area [%]
Classes	2020	2027	2020-2027
Forest	7.56	7.11	-0.45
Savanna	45.13	39.49	-5.64
Wetland	0.07	0.07	0.00
Copland	45.72	50.98	5.26
Water	0.47	0.47	0.00
Settlements	1.05	1.88	0.83
Total	100.00	100.00	0.00

Figure 4.4: CILSS projected land cover maps and areal changes (2020 and 2017)

ESA-CCI and Globeland30 land cover data sets confirmed that there is a weak representation of prediction accuracy less than 50% (Table 4.6) for 2020. Furthermore, Figure 4.5 indicates the low prediction accuracies, where the projected land covers maps of 2020 is almost similar to the earlier land cover map 2013 and 2010 respectively for ESA-CIC and Globeland30.

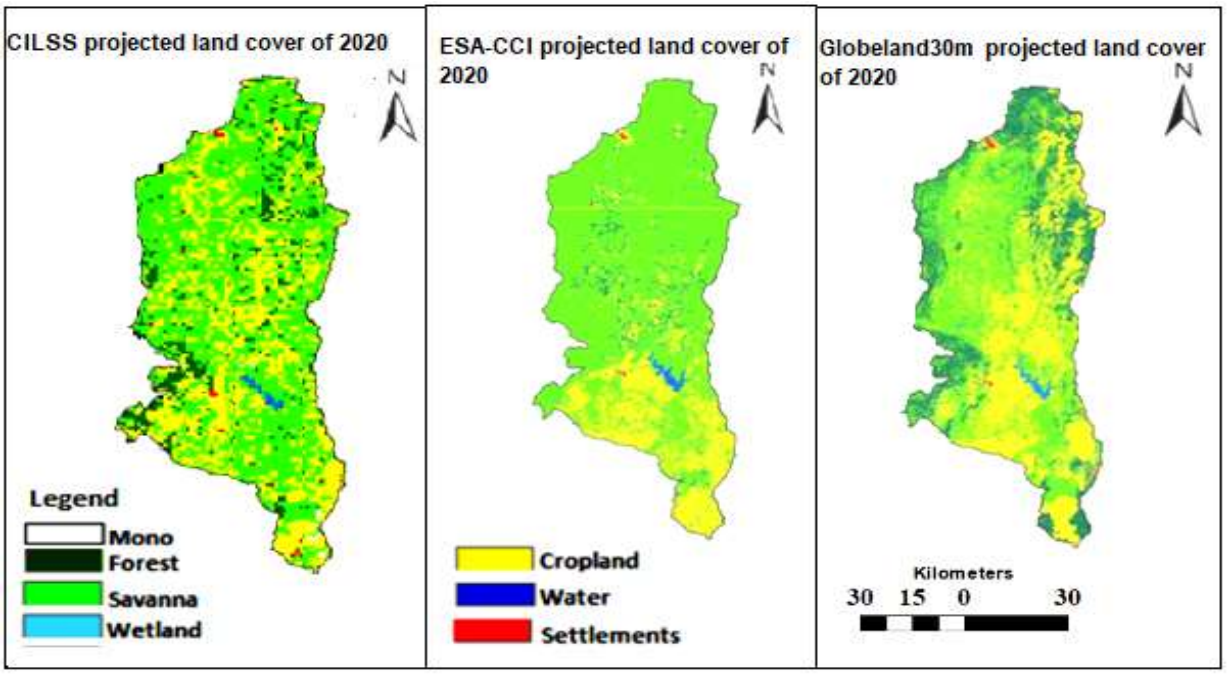

Predicted land cover in 2020 area [%]						
Data sets	Forest	Savanna	Wetland	Cropland	Water	Settlements
CILSS	7.56	45.13	0.07	45.72	0.47	1.05
ESA-CCI	7.61	70.30	0.07	21.19	0.64	0.20
Gloeband30m	23.96	39.99	1.00	33.88	0.67	0.50

Figure 4.5:.Comparison of the projected land cover maps and areal changes

For the reason of weak representation of land cover using ESA-CCI and Globeland30confirmed by the prediction accuracy of less than 50% (Table4.6) the projection was performed only for the year 2020. In Figure 4.5, CILSS, ESA-CCI, and Globeland30, land cover maps of 2020 are shown. We noticed that the projected land cover map of 2020 is almost similar to the earlier land cover map 2013 and 2010 respectively for ESA-CIC and Globeland30 (Figure 4.1). These similarities can be explained by the low prediction accuracies.

The predicted land cover maps in 2020 depend strongly on the accuracy of each land cover source and category. Our results show that the temporal change of land cover in the basin is best reproduced by CILSS dataset. Beyond CILSS data set, Globeland30 data performs better than spatial representation on forest, savanna, cropland and water categories; Because of its fine resolution the Nangbéto dam area and some protected forests such as Malafacassa (Amoussou et al., 2017; Atsri et al., 2018)were well delimitated.

A summary of CILSS land cover change in MRB from 1975 to 2027 is given in Figure 4.6.Savanna, cropland, and forest are the dominant land cover classes in the region. From 1975 to 2027, there is a decrease of forest and savanna, and an increase of cropland and settlements in the Mono river basin.

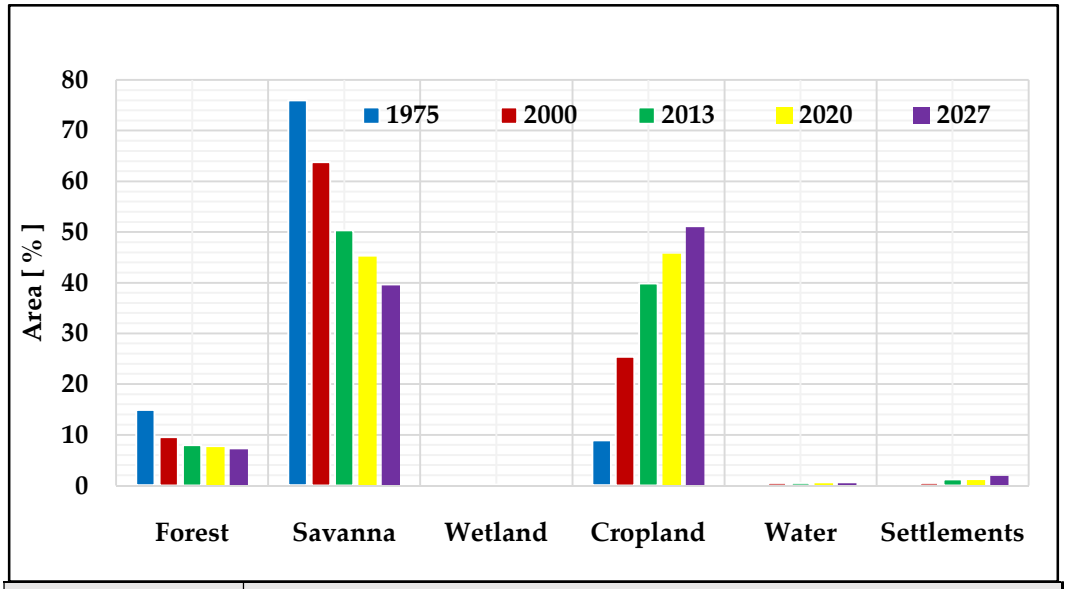

	Land cover area [km^2]				
Land cover type	1975	2000	2013	2020	2027
Forest	3262.98	2098.62	1746.11	1133.84	1068.35
Savanna	16660.10	13986.14	11045.72	6767.38	5932.63
Wetland	4.04	71.76	35.82	10.90	10.88
Cropland	1940.32	5563.12	8735.81	6855.82	7783.05
Water	4.04	112.04	108.00	70.03	69.94
Settlements	67.90	107.70	267.92	157.71	157.52
Total	21939.38	21939.38	21939.38	14995.69	15022.38

Figure 4.6: Development of CILSS land cover from 1975 to 2027.

The result of the current study show that deforestation is increasing over the whole period. According to Kokou et al.(2005) more than 80% of the rural communities in Togo are using wood for cooking causing significant losses of forest as the same situation in Benin. Therefore, decision makers need to take measures to reduce forest degradation, sensitizing the local communities concerning the advantage of reforestation, and the negative impacts to the climate due to losses of forests. Measures must be also taken concerning demographic policies.

4.3: Discussion

4.3.1: Accuracy assessments and past land cover change

Although the spatial resolution of the ESA and the Globeland30 data is high, the two data sets do not accurately map some land cover types in the study area, which may be explained by the fact that for CILSS local information are used during the automated and semi- automated classification (CILSS, 2016; Cotillon, 2017). It may be also due to the number of reference points spatial repartition used for the accuracy assessment. Indeed the selected random points size from Google earth imagery can affect on the spatial distribution depending if the resolution of 2-km than 300-m or 30-m (Congalton, 1991; Stehman, 2009). More the resolution is great more it is easy to a visual interpretation the land cover type identified in these points.

The findings that savanna and agriculture are the dominant land cover classes in the study area during the period of study are in accordance with other studies. For example, (Badjana 2015) analyzed LULC change in the Kara River basin, and showed that savanna was dominant. This was also observed by Diwediga et al.(2015) in the Mo River basin, a small tributary of Oti river in central region of Togo. It was also concluded by Koglo et al.(2018) that savanna and forest are the most important land cover type that are being converted by cropland in Kloto, a small district in the south of the MRB.

The results of CILSS land cover change in MRB confirm many analyses performed in Togo and Benin about land cover change mainly due to deforestation, cropland expansion, and losses of savanna (Akinyemi et al., 2017; Kleemann et al., 2017). The results from Badjana et al.(2017b) and Koglo et al.(2018)have revealed that deforestation and savanna changed to cropland and settlements are observed in south and north of Togo. In Fazao-Malfacassa National Park, in the northern part of the MRB, Atsri et al.(2018) found that forest and savanna are degraded, which could be explained by agriculture expansion, bush fire, timber extraction and linked by population growth. By assessing the land use change process in the northern Togo, Polo-akpisso et al.(2019) confirmed that savanna and forest have decreased annually at the rate of more than 2%, whereas cropland and settlements have increased in the region at an average of 108.13% and 5.45%, respectively, from 1987 to 2000.According to Kokou et al.(2005) more than 80% of the rural communities in Togo (Benin) are using wood for cooking, causing significant losses of forest. Therefore, decision makers need to take measures to reduce forest degradation, sensitizing the local com-

munities concerning the advantage of reforestation, and the negative impacts to the climate due to losses of forests. Measures must be also taken concerning demographic policies.

The increase of the water bodies between 1975 and 2000, can be explained by the building of the Nangbéto dam in 1987 and rainfall variability in this region (Badjana 2015). As the consequences of climate change and climate variability, is less precipitation causing a decrease of the water body of the reservoir from 2000 to 2013 which had consequences for hydroelectricity production as mentioned by Houessou (2016). Climate variability, especially the droughts between 1970s and 1980s, negatively affected grassland due to overgrazing. The increase of settlement is also realistic and can be explained by demography explosion in Togo and Benin Republics (see Table 3.5).

4.3.2: Land cover scenarios accuracy and assessment

The trend direction and location are approximately the locations of the main cities in the basin, therefore, spatial trend in land cover change can be explained by population activity and growth as Koglo et al.(2018) has mentioned in the south district of MRB land use analysis. Because of its fine resolution, the Nangbéto dam area and some protected forests such as Malafacassa (Amoussou et al., 2017; Atsri et al., 2018) are well delimited. It can also due to low albedo factor of water which plays a role during data collection by satellite sensors. CILSS land cover scenarios positive area change of cropland and settlements; negative area change of forest and savanna can be explained by the same factors cited above.

Difference between future land cover scenarios is due to the poor and better Kappa coefficients obtained and which prove the importance of land cover validation. Therefore validation or land cover based on supervised classification are preferable as an input in land use and land cover future scenario studies (Foody, 2002).

Land cover scenarios rate have been strongly impacted by the accuracy assessment and land cover change of CILSS, ESA and Globeland30 data sets. Furthermore, the low accuracies obtained from the modeling can also been explained by the fact that all the drivers of land cover change were not used. It can be due to the weakness of LCM software or the error from user (Camacho Olmedo et al., 2015; Mas et al., 2014). The simulation can allow understanding, forecast and anticipating the future evolution of environment coverage. Nevertheless it is important to know the validity of LCM outputs based on local expertise (Zoungrana et al., 2015).

4.3.3: Partial Conclusion

This work focused on land cover changes in the Mono river basin (MRB) and future scenarios over the period 1975 to 2027 using three different data sets. The results show that the CILSS data set is the most reliable for the MRB with acceptable accuracy assessment efficiencies (higher than 75%). In the MRB, savanna, cropland, and forest are the major land cover classes with decreasing (forest and savanna) and increasing (cropland, settlement) trends. The expansion of agriculture due to population growth occurs at the expenses of savanna. In the tropical zone of West Africa, people use wood for their life hood timber as an energy source is another cause of deforestation. Land cover change must be taken seriously by the authorities and population themselves. It is very important to know the evolution of land cover in order to develop strategies for planning of an integral water resources management (IWRM) in general.

The study assessed scenarios of future land cover by mapping and analyzing the situation for two time steps (2000 and 2013).The maps obtained from this analysis can be used as inputs in hydrological modeling for assessing the impacts of land use and climate changes on water yield and surface runoff in Mono river basin.

Future scenarios of land cover depend significantly on the source of the underlying data set. The high spatial resolutions of Globeland (30 m) and ESA-CCI (300 m) are attractive but it is shown that the quality is limited to specific land cover categories. The resolution of CILSS is rather coarse and therefore users often prefer other data set. Nevertheless, because CILSS data were produced with local knowledge, the quality is convincing and out pass the others. Using the data sets for scenario analysis results in completely diverging futures, what may significantly affect and management strategies.

Chapter 5: Climate change detection and future scenarios climate extremes indices

Introduction

A Hydrologic model to analyzing the impact on water resource requires hydro-climate historical data as inputs. These data need a primary analysis to capture its variability or change over time and spaces, to understand the current and historical hydro climatology for a future development and sustainable water managements (Jaiswal et al., 2015; Oguntunde et al., 2011; Panthou et al., 2012). According to the Intergovernmental Panel on Climate Change 2014 (Pachauri et al., 2014), climate change is due to natural and anthropogenic or human factors. Human causes can be listed as deforestation (land use), burning of fossil fuels, increase of population and industrialization (Koubodana et al., 2019a). The emissions of greenhouse gas (GHG) from anthropogenic activities increases temperature and precipitations frequencies (Leblanc et al., 2012; Yan and Bai, 2017; Zhang et al., 2010). Therefore an increase of earth temperature affects the spatial and temporal distribution of rainfall leading to extremes events such as flooding and drought. According to historical analysis of series of monthly and annually mean temperature in many regions in the world, the year 2005 was the warmest year in the historical series (Jaiswal et al., 2015; Schoof and Robeson, 2016). Thus, it is important to evaluate the long-term change of hydro climatic variables to track their impact on natural water resource and biodiversity.

The set of historical and present state of hydro-climatology can be analyzed through climate model followed with Representative Concentration Pathways (RCPs) scenarios impact studies. Many previous studies already demonstrated that West Africa have suffered from extreme events (Mishra and Singh, 2010; Regh et al., 2014). For example, West Africa has experimented drought of 1970s and 1980s and recently flood events (Nicholson, 2013). Ciais et al., (2013) also proved a dry trend over West Africa in a long period from 1951 to 2012.

5.1:Inter-annual variability of hydro-climatologic time series

A brief summary of the statistical value of annual cumulative sum of rainfall (PCP), mean potential evapotranspiration (PET), mean temperature and cumulative value of discharge is shown in Table 5.1Table 5.1: Descriptive statistics of hydro-climate variables in MRB.

	Period	Min	Max	Mean	STD	CV
PET (mm/yr)	1981-2016	1854.00	1975.14	1913.13	25.77	1.35
PCP (mm/yr)	1961-2016	727.53	1584.77	1166.60	175.03	15.00
Mean Tempature (°C)	1961-2016	25.97	28.50	26.96	0.58	2.15
Q_Athieme (m^3/yr)	1961-2011	235.63	8117.08	2931.82	1737.96	59.10
Qint_Nangbeto (m^3/yr)	1988-2011	1098.83	5525.45	3268.46	1071.68	32.79
Qout_Nangbeto (cm^3/yr)	1988-2011	1472.34	5592.22	3018.22	1026.19	34.00
Q_ Corrokope (m^3/yr)	1961-1998	191.76	3720.28	1604.28	825.11	51.43
AI	1961-2016	0.40	0.82	0.69	0.10	14.89
δj	1961-2016	-2.85	2.45	0.00	1.00	-

PET (mm/yr) means Potential Evapotranspiration in mm/year; PCP (mm/yr) is the amount of precipitation in mm/year; Q_Athieme (m3/yr) is discharge at Athiéme station; Qint_Nangbéto is inflow at Nangbéto reservoir; Qout_Nangbéto is outflow at Nangbéto reservoir discharge; Q_ Corrokope is discharge at Corrokopé; AI means Aridity Index and δi rainfall variability index

It shows that in the MRB, PET CV is 1.35% and PET is ranged between 1854mm/yr to 1975mm/yr with a mean value of 1913.13±25.77mm/yr. The annual cumulative rainfall is varied between 227.53mm/yr and 1581mm/yr with a CV =15% and annual mean of 1166.6±175.03mm/yr. With a range between 25.97°C and 28.50°C, the mean temperature is 26.96±2.15 and a CV of 15%. Roughly discharge varies similarly at Athiémé (CV=59.10%) and Corrokope (51.43%) with a mean value of 3268.46±1737.9 mm/yr and 1604.28±825.11 respectively. With the same local conditions, the inflow and outflow at Nangbéto stations looks near similar; CV=32.76% for inflow and 34% for outflow. Annual discharge minimum and maximum are between 191.76 and 5592.22mm/yr while the annual mean is 3268.46±1071.68mm/yr for inflow and 3018.22±1026.19mm/yr. The AI shows that there is a balance between 0.4 and 0.82with a means of 0.69±0.1, while δi is in the range of -2.85 and 1.08.

The long-term cumulative PET time series, mean temperature and annual rainfall given in Figure 5.1, shows a positive trend of each variable for the period of study. Annual rainfall globally decrease rather for the whole period but at sub series level there is decrease and increase of annual rainfall separated by the year 1981. For PET, there is a real increase only from the sub period 2012-2016 where the PET is under the mean value.

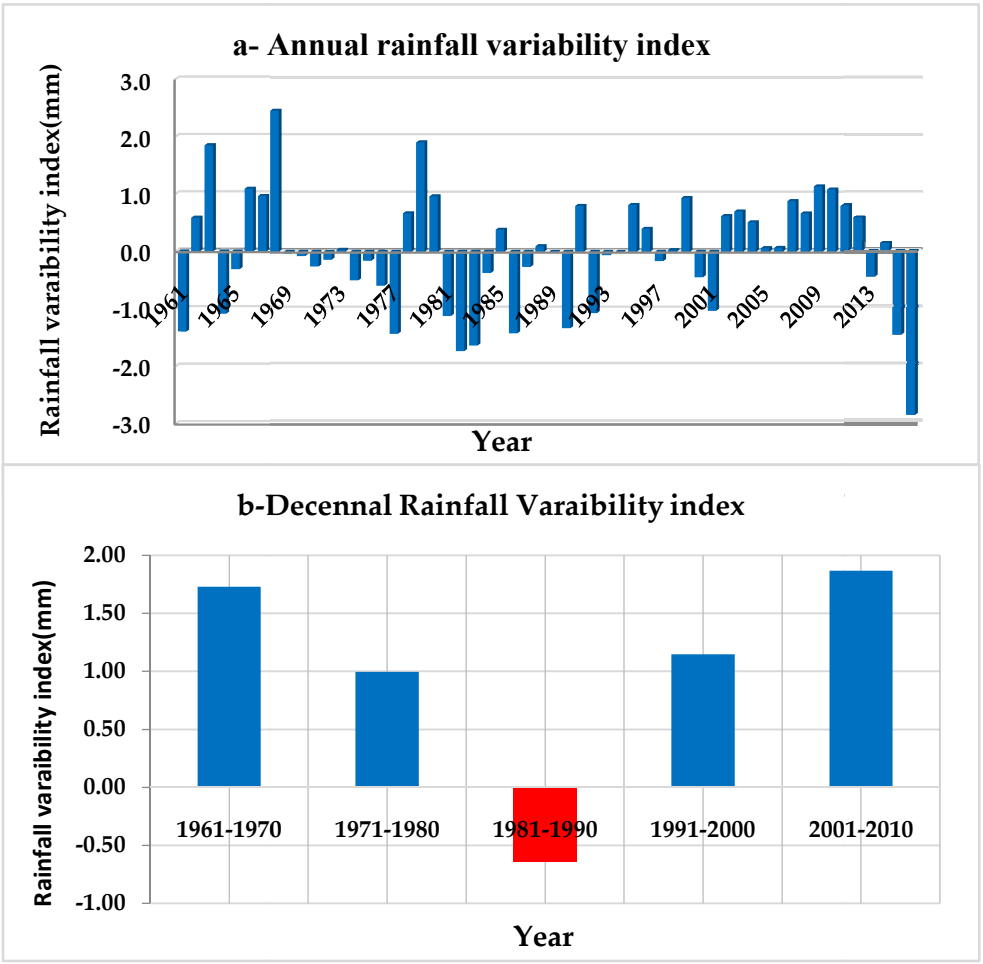

Figure 5.1: Rainfall variability index over the MRB

In figure 5.2, the Annual time series indicate that there is a slight decrease of annual rainfall between 1961and 2016.Nevertheless, over the sub-periods series between 1961 -1987 and 1988 -2014 reveal a decrease and increase respectively of the rainfall. An in-depth analysis of the annual rainfall shows that from 1981 to 1990 the total rainfall received by the basin was under the mean. This corresponded exactly to the drought period, which has occurred within West African countries and particularly in Togo and Benin.

The aridity index as defined by United Nations Environmental program (UNEP) was estimated during the period of means PET 1971 to 2016 and presents a slight positive slop (Figure 5.2). The driest years during this period are 1981-1982-1983-1984-1986-1990-1992-2000 confirming that there were drought years between 1981 and 1991.

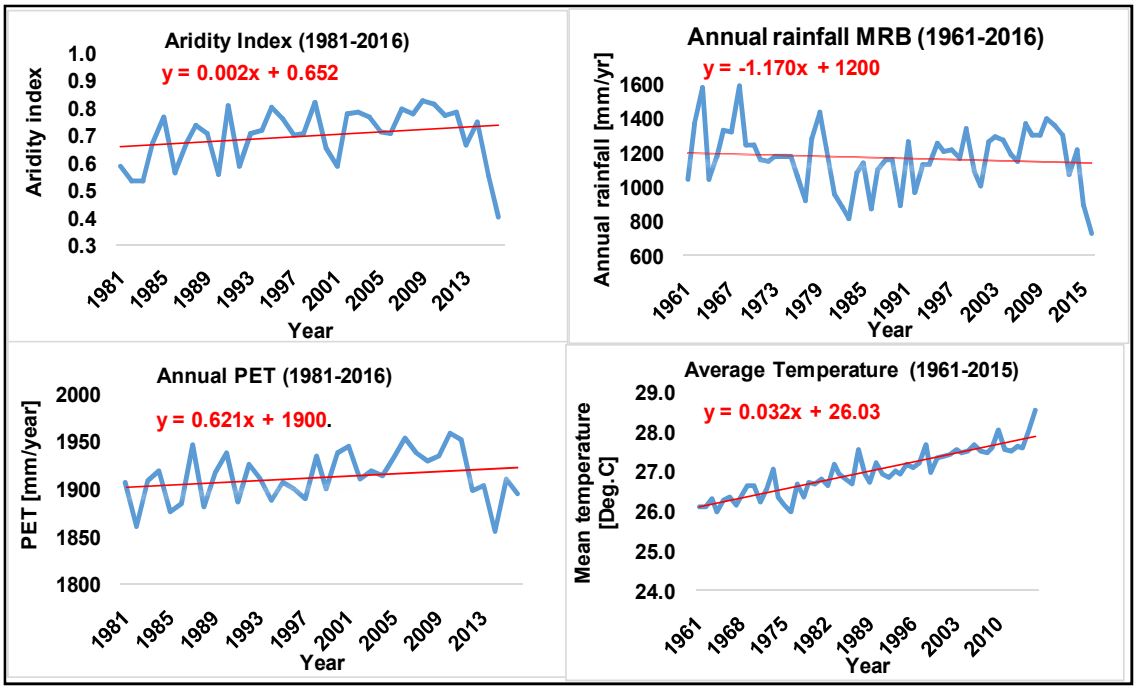

Figure 5.2: Annual hydro-climate time series over the MRB

A complementary analysis by estimating rainfall variability index over MRB and aridity index were performed in order to understand the pattern. This is shown in the figure 5.2. So, the annual time series of rainfall variability index between 1961 and 2012 shows the negative values between 1981-1990 except for the years 1985, 1988 and 1991 where aridity index (δj) is positive. While in the period from 1968 to 1997 was also another less dried period with δj negative for annual and decanal value between 1961 and 2012. An analysis of the 21 rainfall stations shows that the majority of the stations have a negative rainfall variability index except for the year of 1988 and 1991 where the data of the stations show a positive rainfall variability index.

5.2: Annual and seasonal trend of average hydro-climatic time series over MRB

The results of annual trend applying MK statistical test at four hydro climatic average values of 21stations (whole basin) in MRB (Table 5.2) show that all discharge at Corrokopé and Nangbéto (inflow and outflow) had a trend, but not significant: except for Athiémé where there is negative trend at 0.1significance level. At Corrokopé there is a negative trend while positive trend at Nangbéto is obtained. Rainfall has a negative trend but not significant while potential evapotranspiration (PET) a positive trend at 0.1 significance levels and positive trend for mean temperature at 0.05 and 0.01 significance levels.

Table 5.2: Results of Statistical tests of averagevariables in MRB

		PET	PCP	Mean Tem-perature	Q Athieme	Q corro-kope	In-flow	Out-flow
n		36	36	56	50	38	24	24
MAM	Zs	-0.04	-0.91	6.47	1.63	0.72	1.02	1.07
	Sig			***				
	Qmed	-0.21	-1.43	0.030	4.578	0.149	4.06	20.66
JJA	Zs	0.86	-0.81	7.61	-2.37	-0.53	0.17	0.02
	Sig			***	*			
	Qmed	0.19	-2.68	0.028	-61.008	-15.075	15.27	2.52
SON	Zs	-0.48	-0.11	8.01	-2.01	-1.03	0.82	0.47
	Sig			***	*			
	Qmed	-0.049	-0.16	0.031	-92.319	-33.965	79.25	57.65
DJF	Zs	4.02	-0.20	7.47	3.66	-0.78	1.20	3.25
	Sig	***		***	***			**
	Qmed	0.72	-0.14	0.036	23.559	-0.184	2.00	44.13
AN-NUAL	Zs	1.78	-0.52	8.38	-1.65	-1.03	0.57	0.97
	Sig	+		***	+			
	Qmed	0.83	-2.23	0.031	-26.267	-12.643	22.37	33.15

Zs: Mann-Kendall test, Qmed: Sen's slope estimator, Sig: significant indicator, - delineate negative trends based to the MK test, n= length of the time series

**Statistically significant trend at α = 0.05 significance level*

*** Statistically significant trend at α = 0.01 significance level*

*** * Statistically significant trend at α = 0.01 and 0.05 significance levels*

+ Statistically significant trend at α = 0.1 significance level

At seasonal (MAM, JJA, SON and DJF), the trend can be found on all the variables. Particularly the mean temperature is increasing at 0.05 and 0.01 significant level.

During MAM period, there is negative trend in PET and PCP but not significant, mean temperature over MRB is increasing at 0.05 and 0.01 significant levels. In opposite at discharge station of Athiéme, Corrokope and Nangbéto, the trend is positive but not significant. A similarity in the trend can be seen during JJA and SON. Indeed, there is a positive (negative) trend during JJA (SON) of PET and negative trend in PCP without significant level. Discharge at Athiéme is decreasing at 0.05 significant levels during JJA and SON. A positive trend is noticed during the same periods in inflow and outflow at Nangbéto dam station. Finally, during the period of DJF, a positive trend is found in PET discharge of Athiéme and mean temperature at 0.1 significance levels at 0.01 and 0.05 significant levels. Rainfall (PCP) and discharge Corrokope showed a negative trend while inflow and outflow at Athiéme showed a positive trend not significant except for the outflow significant at 0.01 levels.

5.3: Annual and seasonal trend of climate variables by stations

5.3.1: Mean temperature and potential evapotranspiration

Mean Kendall statistic trend applied to the mean temperature at Tabligbo, Atakpame and Sokode stations over the period of 1961-2016 is summarized in Table 5.3. There is at Tabligbo, Atakpame and Sokode stations positive trend at 0.05 and 0.01 significant levels for the mean temperature variables in MAM, JJA, SON, DJF and annual period. This is similar to results of mean temperature over the basin. For potential evapotranspiration (PET), during MAM at Kara (negative), Sokode (positive) and Tabligbo (positive) trends are detected but not significant. During JJA at Kara the trend is negative, Sokode no trend, and Tabligbo positive trend at 0.1 significance level. At Kara, the trend is negative and not significant, Sokode negative trend not significant and Tabligbo positive trend significant at 0.1levels. During DJF the trends are positive in all the three stations at 0.05 or/and 0.01 significant level. For annual period, the trend is all positive with no significance except for Tabligbo where it seems significant at 0.05 levels.

Table 5.3: Statistical tests for seasonal and annual mean temperature and PET.

		Mean temperature			PET		
n=56		Tabligbo	Atakpame	Sokode	Tabligbo	Sokode	Kara
	Zs	5.53	5.77	6.88	0.37	0.74	-0.45
	Sig	***	***	***			
MAM	Qmed	0.03	0.03	0.04	0.07	0.25	-0.31
	Zs	6.71	7.31	7.27	1.78	0	-0.4
	Sig	***	***	***	+		
JJA	Qmed	0.03	0.03	0.03	0.24	0.01	-0.15
	Zs	7.13	7.48	7.40	1.7	-0.37	-1.01
	Sig	***	***	***	+		
SON	Qmed	0.03	0.03	0.03	0.26	-0.08	-0.2
	Zs	5.62	6.62	8.06	3.96	3.09	3.41
	Sig	***	***	***	***	**	***
DJF	Qmed	0.03	0.03	0.05	0.81	0.75	0.61
	Zs	7.05	8.01	8.57	2.44	1.05	0.26
	Sig	***	***	***	*		
ANNUAL	Qmed	0.03	0.03	0.04	1.36	0.89	0.29

Zs: Mann-Kendall test, Qmed: Sen's slope estimator, Sig: significant indicator
**Statistically significant trend at α=0.05 significance level*
*** Statistically significant trend at α = 0.01 significance level*
*** * Statistically significant trend at α = 0.01 and 0.05 significance levels*
+ Statistically significant trend at α = 0.1 significance level

5.3.2: Rainfall of Mono river basin

The seasonal and annual MK test analysis where performed at each rainfall gauge stations used to compute the mean rainfall of the basin. Results are displayed in Table 5.4. According to these results there is positive or negative trend at all stations but not significant for annual rainfall. On seasonal scale, there were positive trend at Sotouboua and negative trend at Blitta at 5% significance level in MAM. Positive and negative trend are also detected respectively at Akaba and Yegue stations in JJA at 5% significant level. During SON, Notse is the only station where there is positive trend at 5% significant level while at other stations the trend is not significant. In DJF, a decreasing trend at 5% significant level is detected at the stations of Bassila, Blitta and Yegue.

Table 5.4: Rainfall station trend statistical analysis at MRB stations.

		MAM			JJA			SON			DJF			ANNUAL		
1	n = 56	Zs	Sig	Qmed	Zs	Sig	Qmed	Zs	Sig	Qmed	Zs	Sig	Qmed	Zs	Sig	Qmed
	Kara	-1.05		-0.76	-0.93		-1.05	1.24		1.17	0.82		0	-0.08		-0.204
2	Kpewa	-1.24		-0.95	-2.01		-2.54	-2.47		-2.7	1.37		0.1	-2.72		-6.9
3	Tchamba	-1.09		-1.68	-0.04		-0.03	-0.46		0	-1.44		-0.21	-0.93		-0.755
4	Sokode	-0.88		-1.18	-0.36		-0.08	-0.55		0	-1.16		-0.34	-2.21		-1.183
5	Malfacassa	-1.78		-1.72	-2.10		-3.04	1.18		0.067	-2.13		-0.41	1.78		1.304
6	Bassila	-1.04		-1.58	-1.19		-1.34	0.87		0.14	-1.06	*	-0.35	-1.08		-0.95
7	Sotouboua	0.32	*	0.70	0.20		0.51	0.62		0.029	-0.09		-0.011	-0.4		-0.37
8	Blitta	-0.94	*	-0.45	0.25		0.23	1.26		0.17	-0.06	*	-0.042	0.59		0.38
9	Yegue	-0.38		0.00	-0.22	*	0.00	-0.18		0	-0.13	*	-0.063	0.41		-0.33
10	Akaba	1.35		1.2	1.31	*	4.07	0.28		0.011	1.92		0.53	1.15		0.78
11	Tchetti	-1.13		-0.762	-0.2		-0.346	0.31		0.39	-1.14		-0.229	-0.54		-1.207
12	Anie	0.11		0.19	1.36		1.85	-0.04		0	0.95		0.19	-0.7		-0.8
13	Agouna	0.19		0.272	2.54		2.25	-1.05		-0.189	1.39		0.364	1.16		0.98
14	Atakpame	-0.28		-0.42	1.17		0.86	-1.12		-0.32	0		0	1.11		1.04
15	Amou	-0.7		-0.8	0.11		0.194	1.36		1.85	-0.04		0	1.27		3.107
16	Wahala	-1.17		-1.084	0.233		0.377	-0.96		-0.65	-0.899		-0.31	-0.5725		-1.133
17	Lonkly	1.63		2.95	1.6		1.31	-1.77		-0.5	1.04		0.25	-0.18		-0.17
18	Notse	-0.87		-0.97	2.49		3.27	1.15	*	1.47	-2.11		-0.75	1.07		3.52
19	Adjarala	-1.07		-1.39	-1.89		-2.3	0.01		0	-2.24		-0.4	-1.37		-0.78
20	Tabligbo	-0.8		-0.6	0.25		0.2	1.55		1.39	-0.61		-1.68	0.42		0.851
21	Afanyangan	0.19		0.27	2.54	+	2.25	-1.05		-0.18	1.39	*	0.36	1.16		0.98

*Zs: Mann-Kendall test; Qmed: Sen's slope estimator; Sig: significant indicator; - delineate negative trends based to the MK test; *statistically significant trend at α = 0.05 significance level*

5.3.3: Spatial distribution of hydro-climatic data at seasonal and annual scale

In Figure 5.3 is shown the spatial trend distribution of PET. This explain thatduring MAM all the hydrological stations show an increase of discharge, except in JJA and SON there are two stations of three decreasing. Only at Nangbéto the discharge is increasing when it is the rainy season. During the period of DJF and at annual scale the upstream stations of

Corrokopé has a decrease of discharge while at Nangbéto there is an increase, especially, during DJF at the outlet and decrease at annual time scale. At the downstream, the PET is increasing during all seasonal and annual periods. In the upstream of the basin the station outside of the river shows a decrease trend during MAM, JJA and SON while increase during DJF and annual time scale. The stations being outside PET is connected with the river hydrology because of land and atmosphere exchange. Finally, the second stations at the upstream indicate a positive trend for MAM, DJF and annual, however; no trend is detected during JJA, while there is a negative trend in SON.

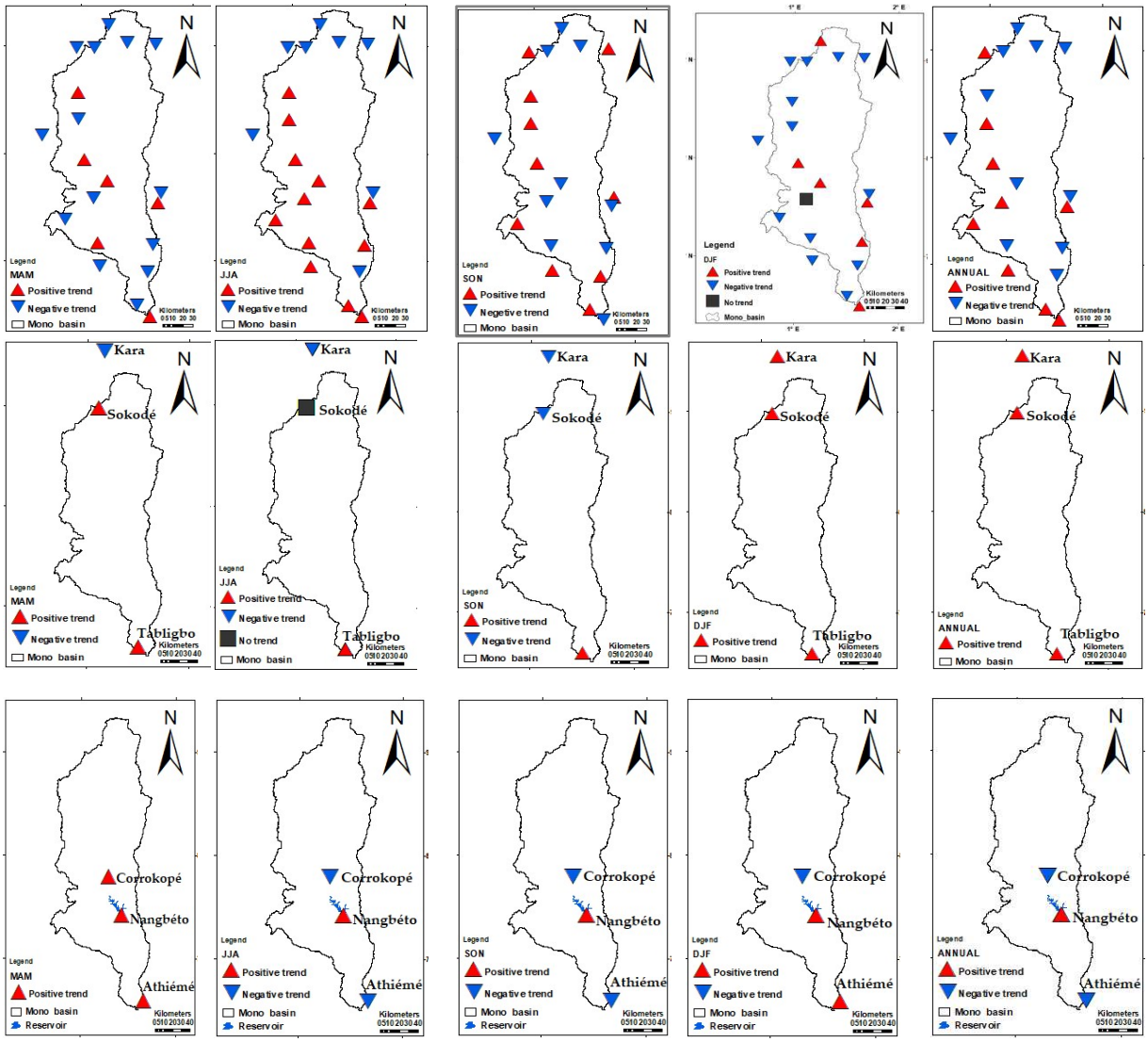

Figure 5.3: The spatial distribution of rainfall (above), PET (middle) and discharge (bottom)

The spatial distribution of rainfall from 21 stations over the MRB displayed in Figure 5.3 shows an increase, decrease or no trend during the seasonal and annual period between 1961 -2016. At annual period, nine of twenty-one stations show an increase trend of rain-

fall and one of them decreased. All the stations with increase rainfall are in the West from North to South, located at the high slope of mountain, except Tchetti station that it is in the East where other factors may explain the trend .Similar situations are observed during JJA and SON with some exceptions. During MAM and DJF, 6 stations are with positive trends of rainfall.

5.4:**Multi-ensemble model temperature time series validation (1980-2005)**

Table 5.5 shows the Pearson correlation and bias between ensemble model outputs and observations time series using mean temperature at three major stations. There is an excellent correlation coefficient (> 0.95) between model and observation at each station. The bias is less than ± 25% in the three stations at monthly and annually scale, but in November at Tabligbo station the bias is equal to zero. The ensemble model slightly underestimates the observations with a small positive deviation and confirmed with bias values.

Table 5.5: Correlationcoefficient and biasof temperature

Bias [%]	R^2	Jan	Feb	Mar	Apr	May	Jun	Jul	Aug	Sep	Oct	Nov	Dec	Annual
Tabligbo	0.96	1.30	2.60	2.18	1.36	0.94	0.61	2.20	1.28	1.05	0.50	0.00	-0.15	1.16
Atakpame	0.98	3.06	3.96	3.71	4.54	4.67	5.07	5.63	5.62	5.71	4.61	3.19	3.12	4.41
Sokode	0.97	4.72	3.15	0.98	1.65	3.13	3.78	4.62	5.24	4.70	3.27	3.48	5.14	3.66

There is a strong (or robust) trend regression at Tabligbo (0.96), Atakpame (0.98) and Sokode (0.97) with coefficient of regression between the model outputs and observations. At seasonal variability between 1980 and 2005, it seems that the seasonality is well represented in the stations. Therefore, the model outputs are much representing observation data in the Mono river basin.

The bias or error between model and observation are too low and is balanced between -1% and 6% at Sokode, Atakpame and Tabligbo station at mean annual scale between 1980 and 2005.

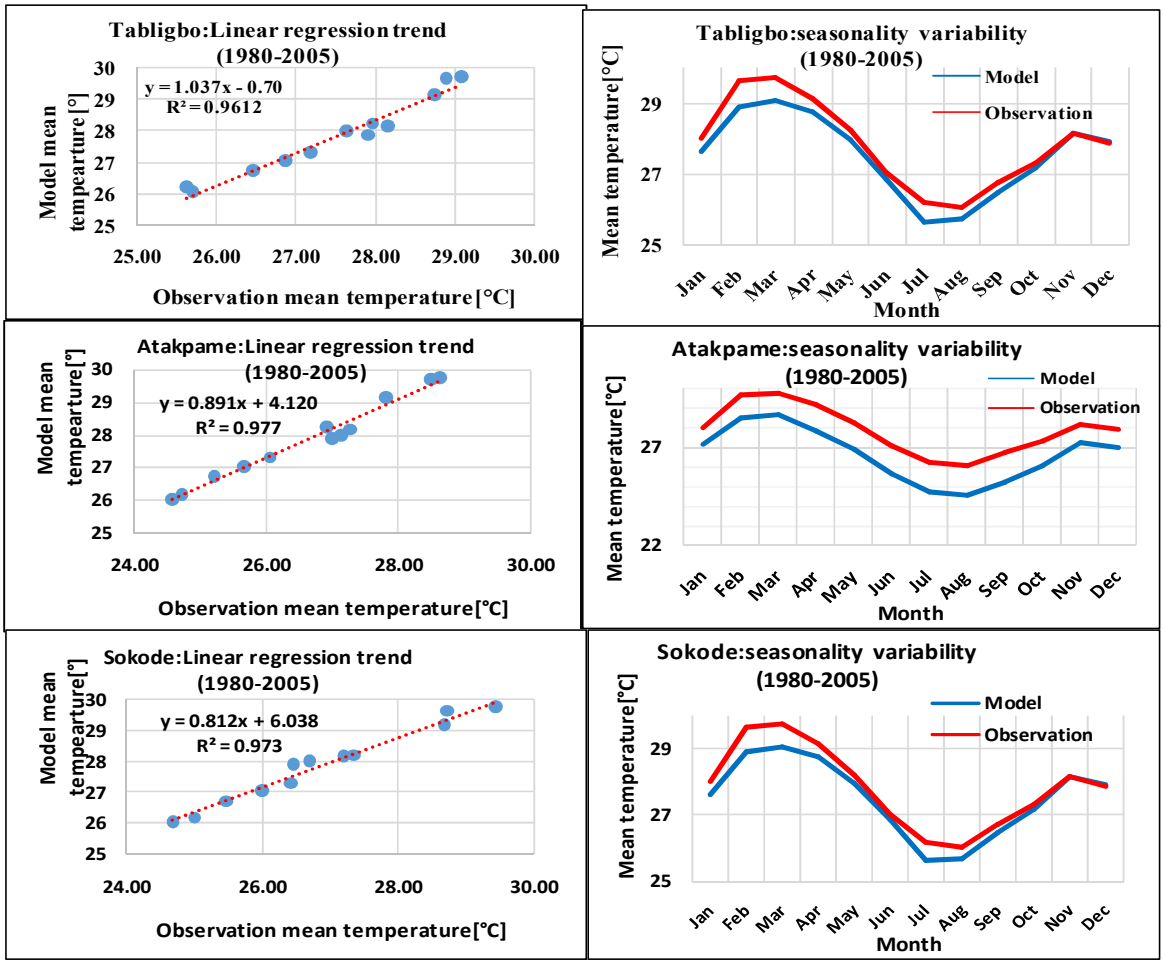

Figure 5.4:Comparison of temperature with climate model output

5.5: Ensemble model temporal and spatial validation of rainfall (1980-2005)

The validation of monthly rainfall over MRB was performed using 21 gauged stations. Figure 5.5 and Table 5.6 show the bias between the ensemble model outputs, coefficient of determination and observations respectively. The correlation between the two datasets show strong positive correlation while the bias was computed as subtracting model value in three major stations, where it was found a high bias at Tchamba and Adjarala stations in July, August and September. The bias in others stations are quite acceptable because low than 50%. Undoubtedly the model underestimates the observation globally in the stations and this can be explained by the type of model or primitives equations weakness.

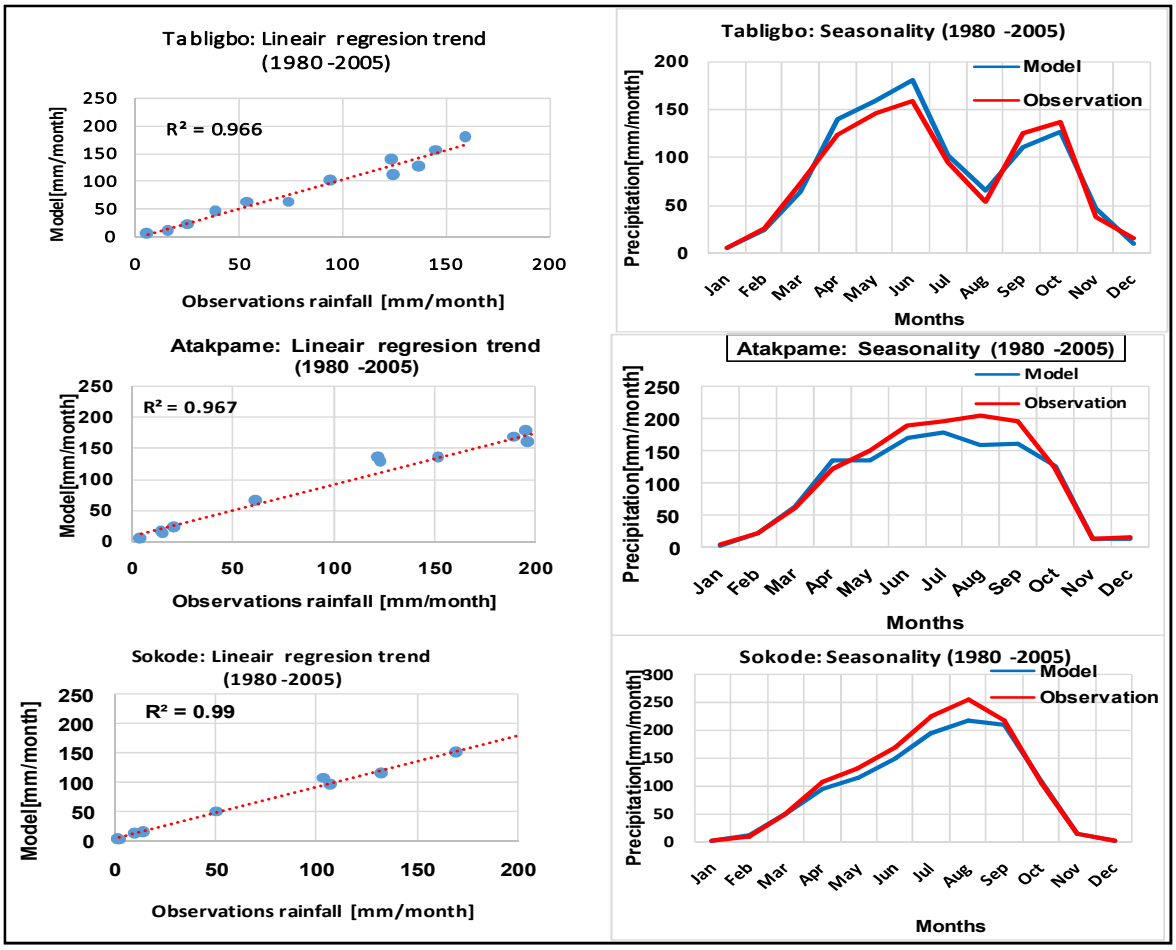

Figure 5.5: Comparison between climate modelsand observations rainfall

In Table 5.6, the results of the comparison of ensemble model rainfall and observations indicate high bais (bias value ≥ ± 25%) globally at 12% of 252 grids evaluated, at Sotouboua, Yegue, Tchetti, Anié, Agouna, Lonkly and Afanyangan., with the highest bias at Yegue in November (71.8%). The rest of the stations, the value never exceed ±25%.However, the bias in March, June and July is lower than ± 25%. Globally, the annual bias is acceptable for the 21 stations, but the highest bias obtained might be due to downscaling methods.

Those differences between ensemble model and observation were computed using spatial interpolation representation of rainfall in DJF and JJA in Figure 5.6. In the whole basin, DJF the dry season occurred when the rainfall is minimized, while in JJA the rainy season was present when the rainfall is at the maximum. The contrary occurred in the south west and east of the basin in January, the model and observation show a maximum rainfall.

Table 5.6: Bias[%] between ensemble model rainfall and observations

Annual and monyhly bias betweem ensemble model and observations (1980-2005)															
No	Station	R^2	Jan	Feb	Mar	Apr	May	Jun	Jul	Aug	Sep	Oct	Nov	Dec	Annual
1	Kara	0.993	19.6	-5.8	2.1	8.5	15.6	14.8	2.5	2.5	10.5	7.8	0.7	16.0	7.9
2	Kpewa	1.00	11.1	**-25.0**	20.7	4.7	21.4	17.8	14.0	12.5	9.1	10.7	24.6	17.6	11.6
3	Tchamba	0.97	-10.0	1.0	-19.3	12.1	-13.1	-6.0	21.1	9.9	4.9	1.8	15.5	15.7	2.8
4	Sokode	0.97	-17.0	-2.1	-10.5	11.0	**25.4**	24.4	1.3	-1.7	4.1	-10.9	**-33.1**	-7.8	-1.4
5	Malfacassa	0.91	**27.8**	-1.6	-7.6	**-27.8**	**-31.9**	-21.5	19.0	20.4	4.1	3.1	20.8	2.8	0.6
6	Bassila	0.99	-0.9	0.3	11.1	-0.4	-3.3	-18.1	4.4	-13.5	-4.2	8.4	-11.2	17.3	-0.8
7	Sotouboua	0.99	3.4	-10.0	8.9	14.0	17.8	7.0	13.5	1.6	-9.4	-4.7	**61.9**	0.1	8.7
8	Blitta	0.96	-12.2	-18.3	-24.6	1.4	3.6	-4.8	-0.2	13.3	**25.5**	14.3	11.0	0.0	0.8
9	Yegue	0.96	19.3	**25.6**	-10.8	6.7	6.1	10.7	-13.9	9.7	10.3	**25.7**	**71.8**	**42.6**	17.0
10	Akaba	0.98	-1.7	-4.1	17.6	-2.5	-14.6	8.8	3.9	13.8	3.8	-4.8	-7.4	-9.0	0.3
11	Tchetti	0.97	1.6	-14.0	-9.9	4.2	12.5	16.7	14.4	24.3	2.6	**-41.2**	13.4	0.1	2.0
12	Anie	0.97	**-50.0**	-6.4	3.0	-10.5	1.1	9.6	-1.1	14.1	-0.7	**-28.3**	-13.1	**30.8**	-4.3
13	Agouna	0.99	-6.2	18.3	8.7	0.1	-4.2	8.3	11.5	12.7	4.6	6.7	**-41.3**	-18.1	0.1
14	Atakpame	0.96	**-25.3**	-1.2	-20.8	7.2	18.4	15.9	-8.9	5.1	17.2	-10.9	-0.3	17.3	1.1
15	Amou	0.99	19.6	**28.8**	20.9	13.1	4.2	11.9	10.6	18.3	18.5	2.1	-3.5	-2.6	11.8
16	Wahala	0.91	24.7	-16.3	-10.8	0.1	**-29.1**	-21.1	19.8	9.9	14.8	6.1	23.5	-7.4	1.2
17	Lonkly	0.97	3.8	0.9	0.4	18.0	-8.4	-5.6	-3.8	10.2	5.8	-0.1	-6.1	**65.5**	6.7
18	Notse	0.89	**29.3**	5.3	0.1	-18.4	**-29.5**	-5.5	19.6	19.3	19.5	-7.6	-4.6	**29.8**	4.8
19	Adjarala	0.96	-9.4	-3.7	0.4	-21.4	6.1	22.8	-0.8	21.3	-1.9	8.2	11.7	-1.2	2.7
20	Tabligbo	0.96	2.7	-5.2	14.2	-14.3	-6.3	-4.6	-23.8	-1.7	6.8	9.7	-0.1	18.6	-0.3
21	Afanyangan	0.92	**-65.1**	-6.8	-17.1	**-47.4**	**-44.6**	-18.5	-24.8	**-32.6**	11.1	-12.1	**-43.9**	-5.7	**-25.6**

*Note: High value of bias (**bias** $\geq \pm$ **25%**) in bolt*

However, the maximum rainfall in the model and observations during august is located in the North of MRB. But the south of the basin presented the minimal rainfall for the two datasets. As a result, the coefficient of determination between observation and ensemble model are 0.62 and 0.68 in January and August respectively which are quite acceptable values. However, the extreme value from the model and observation are similar in January and August. In other words, the rainfall variability over seasonal presents a better pattern for both model and observations. While for the south in Tabligbo, the model predicted two peaks of maximum rainfall for June and October and for the center and north in Atakpame and Sokode one peak of maximum rainfall in August were determined. This result reflects the two different climate zone covered by MRB (Figure 5.6)

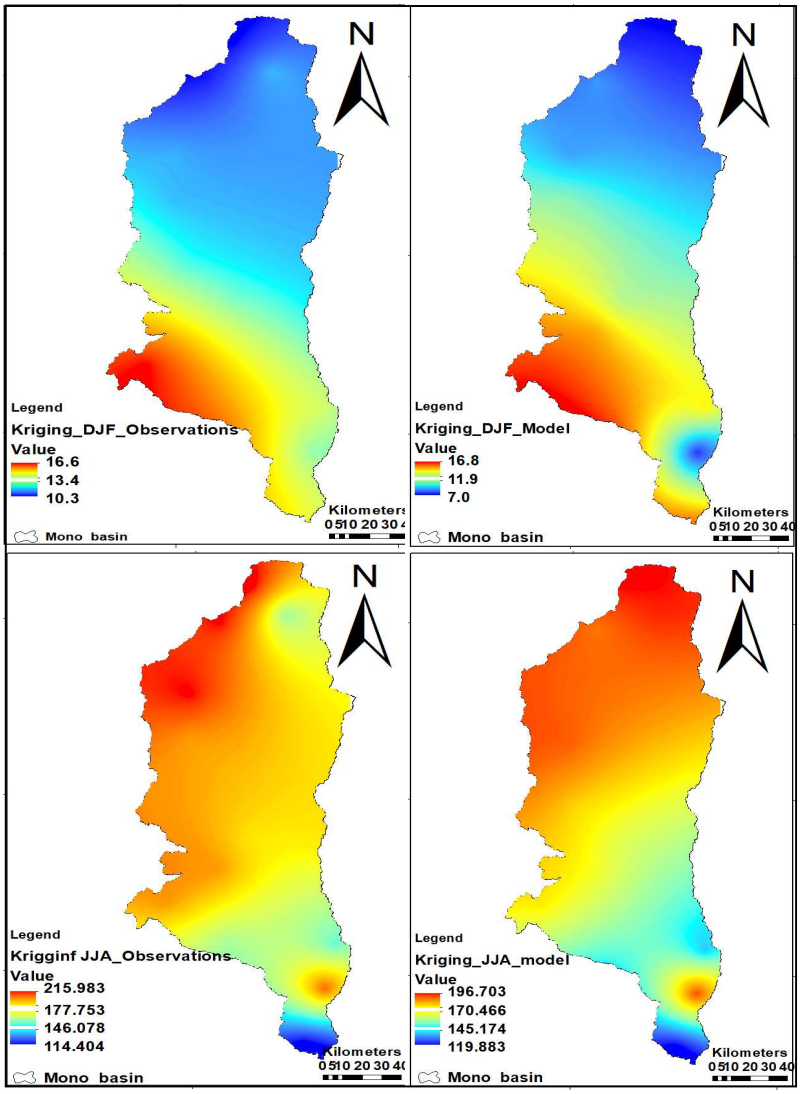

Figure 5.6: Spatial distribution of rainfall of model and observations data

5.6: Temperature and precipitations future scenarios extreme indices

The trend analysis results for RCP4.5 and RCP8.5 in three climatic stations of MRB are summarized in Table 5.7. The values in bold indicate the significant trend at 0.05 confidence level. The results show significant negative, positive or no trend for annual scale at some station from 2020 to 2045. Depending on the scenarios and the selected extremes indices such as: the monthly maximum value of daily temperature indices (TNn), 1-day maximum rainfall indices (RX1day), simple daily index (SDII), number of heavy precipitation days (R10), number of very heavy precipitation days (R20), number of days above 25mm of precipitation (R25) and consecutive dry days (CDD). The result do not present significant trend in the three stations listed below, but positive or negative slope is present, reflects an increase or decrease of annual rainfall in RCP4.5 or RCP8.5.Rainfall intensity indices like annual precipitation amount (PRCPTOT)show no significant increase or decrease trend at Sokode of 6.014mm/year (5.269mm/year) of RCP4.5 (RCP8.5) respective-

ly, positive trend of 5.635mm/year of RCP4.5 and 6.159mm/year of RCP8.5 at Atakpame while 5.469mm/year of RCP4.5 and 5.975mm/year of RCP8.5 at Tabligbo. These results show an increase of rainfall at two stations of MRB.

Indices (R99p) increase significantly at Tabligbo for RCP8.5 whereas not significant at Atakpame and Sokode stations. The consecutive wet days (CWD) for RCP8.5 are significantly increasing at Sokode and Atakpame while not significant at Tabligbo. The maximum 5-day precipitation amount (RX5day) is only significant for RCP4.5 at Sokode with a slope of 3.18mm.

Table 5.7: Annual extremes indices of temperature and precipitation (2020 – 2045)

Zone	North of the basin						Center of the basin						South of the basin					
	Sokode						Atakpame						Tabligbo					
Indices	Slope		Sen of slope		p value		Slope		Sen of slope		*p* value		Slope		Sen of slope		*p* value	
	RCP4.5	RCP8.5	RCP4.5	RCP8.5	RCP4.5	RCP8.5	RCP4.5	RCP8.5	RCP4.5	RCP8.5	RCP4.5	RCP8.5	RCP4.5	RCP8.5	RCP4.5	RCP8.5	RCP4.5	RCP8.5
TXx	-0.021	0.078	0.03	0.034	0.502	**0.03**	0.105	0.133	0.033	0.061	**0.004**	**0.040**	-0.023	0.102	0.04	0.039	0.575	**0.015**
TNx	0.018	0.073	0.015	0.015	0.228	**0.000**	0.005	0.065	0.011	0.016	0.676	**0.00**	0.043	0.075	0.009	0.011	**0.00**	**0.00**
TXn	-0.005	0.045	0.012	0.015	0.686	**0.007**	0.001	0.057	0.01	0.016	0.925	**0.002**	0.014	0.037	0.01	0.009	0.16	**0.001**
TNn	0.002	0.005	0.023	0.025	0.943	0.855	0.01	0.02	0.02	0.022	0.619	0.371	0.024	0.009	0.035	0.035	0.488	0.805
TX90p	-0.116	0.359	0.075	0.091	0.135	**0.001**	0.374	0.399	0.163	0.297	**0.031**	0.192	-0.05	0.724	0.186	0.115	0.79	**0.00**
TN90p	0.312	0.741	0.069	0.09	**0.000**	**0.00**	0.417	0.813	0.09	0.103	**0.00**	**0.00**	0.446	1.128	0.073	0.12	**0.00**	**0.00**
WSDI	-0.086	0.163	0.065	0.082	0.196	0.058	0.301	0.504	0.298	0.568	0.323	0.384	-0.09	0.618	0.325	0.158	0.785	**0.001**
DTR	-0.025	-0.008	0.008	0.01	**0.006**	0.409	0.015	0.023	0.013	0.026	0.271	0.376	-0.021	0.007	0.01	0.01	0.053	0.48
SDII	0.026	-0.05	0.049	0.054	0.598	0.358	-0.016	0.061	0.05	0.068	0.746	0.38	0.057	-0.018	0.057	0.054	0.321	0.737
R10	0.369	-0.035	0.214	0.197	0.098	0.862	0.144	-0.016	0.149	0.162	0.344	0.92	0.279	0.082	0.154	0.198	0.083	0.681
R25	0.122	-0.046	0.107	0.104	0.263	0.659	0.109	-0.041	0.1	0.09	0.286	0.65	0.072	-0.061	0.103	0.097	0.494	0.538
CDD	0.846	0.748	0.781	0.753	0.289	0.331	0.439	1.233	0.798	0.637	0.587	0.065	-0.068	0.713	0.574	0.484	0.906	0.154
CWD	0.138	0.061	0.056	0.049	**0.02**	0.226	0.121	-0.087	0.039	0.039	**0.005**	**0.034**	0.09	-0.023	0.058	0.041	0.132	0.582
R95p	2.251	-4.055	4.096	4.519	0.588	0.378	-1.02	3.843	3.825	5.779	0.792	0.512	4.345	2.479	2.986	4.292	0.158	0.569
R99p	1.721	-0.766	2.431	2.634	0.486	0.774	-1.674	4.875	2.33	3.666	0.48	0.196	5.24	1.798	2.367	2.677	**0.037**	0.508
PRCPTOT	10.638	-1.632	6.014	5.269	0.09	0.759	3.341	1.433	5.635	6.159	0.559	0.818	9.327	4.182	5.469	5.975	0.101	0.491

Note: Significant trends are in bold (p value < 0.05), negative slope shows a decreasing trend while positive shows an increasing trend.

Moreover, the monthly maximum of daily maximum temperature (TXx), the monthly minimum of maximum temperature (TXn) and monthly maximum value of daily minimum temperature (TNx) for RCP8.5show a significant trend in Sokode, Atakpame and Tabligbo representative stations respectively in about -0.03 °C, 0.012°C and 0.015°C at Sokode while 0.061°C, 0.016°C, 0.06°C at Atakpame and 0.039°C; 0.009°C and 0.011°C at Tabligbo.

The diurnal temperature (DTR) indices are only significant at Sokode for RCP4.5 with positive slope showing the increase of monthly mean difference TX and TN. Temperature

indices cool days (TX10p) and warm days (TX90p) show positive and negative trend at 0.05 level of confidence for the Scenarios RCP8.5 in the north of the basin at Sokode station, positive significant trend of RCP4.5 and RCP8.5 at Atakpame station while at Tabligbo station in the south the significant trend is negative. This reveals that cool and warm days annually trend depend from station and also from RCP scenarios in Mono River basin from 2020 to 2045. Nevertheless, cool nights (TN10p) and warm night (TN90p) are all showing significant trend at Tabligbo, Atakpame and Sokode at 0.05 significant levels and for the two considered RCP4.5 and RCP8.5. A particularly TN10p slope is negative while positive for TN90p. The warm spell duration indicator (WSDI) show only a significant RCP8.5 negative trend at Tabligbo while cold spell duration indicator (CSDI) reveals RCP4.5 negative trend at Tabligbio, Atakpame and Sokode stations of 0.147, 0.253 and 0.289 days respectively. The significant maps of climate extremes indices are displayed in Appendix 5

5.7: Discussion

In this study, trend analysis of discharge, rainfall, temperature and potential evapotranspiration are analyzed for historical period of 1961 -2016. The historical period is used for validation of an ensemble model from four different climate models between 1980 and 2005. Afterwards, extremes climate indices are computed for RCP4.5 & RCP8.5 for near future (2020 – 2045) over MRB (Togo) are used for trend analysis.

The temperatures historical trend analysis showed a significant upward of temperature over the whole basin and at each temperature station which is in concordance with most of the previous studies investigated in this region (IPCC, 2014). As illustration (Lawin et al., 2019b, 2019a) reported a low and high increase of temperature over MRB from 1961-2010.Dashkhuu et al.(2015); Halimatou et al.(2017); Oguntunde and Abiodun(2013) observed a highest increase of temperature of 3°C around 14°N in May –June and low increase of 0.5°C below 8°N over West Africa. Over the basin, negative significant trend of precipitation at annual and seasonal scale whereas positive and negative significant trend are observed in PET at annual and seasonal. The last forty years, West African countries have experienced very driest years with drought and extremes temperature. As consequence, there are drastically impacts on local communities activities such as agriculture, water resource, biodiversity and economy (Kasei et al., 2010; Oguntunde et al., 2011, 2006; Tabari et al., 2012).

Ensemble Climate model underestimates observations from 1980 to 2005 with a coefficient of determination higher than 0.9 in almost most of the climate stations over the basin. The uncertainties associated with model are minimized in about less than ± 25% bias at most of rainfall stations.

The spatial coefficient of correlation between observations and model outputs is over 0.6 during the extreme's values of rainfall (1980-2005). This value may be explained by the weakness of the equation systems used during climate model generations; because they consider just a few factors, but in reality it is difficult to reproduce all the process of the earth (Lahsen, 2005; Reichler and Kim, 2008).

Climate trend analysis and extremes indices have been tested recently in West Africa. Most of the results show an increase of extremes events like flooding and drought. Also, West African countries have experienced historical warm extreme temperatures (1961-2000) with or not a significant decrease trend of rainfall (New et al., 2006). For example, Akinsanola and Zhou (2018) used RCMs CORDEX to compute Consecutive Cool Days (CDD), CWD, R10mm, R20mm, PRCPTOT, R95pTOT, RX5day, and SDII extreme rainfall indices under middle and high Representative Concentration Pathway (RCPs) scenarios RCP4.5 and RCP8.5 over West Africa. The results show a significant decrease of total rainfall, increase of consecutive dry and extreme events for the future period of 2070-2099. In Benin, Yabi and Afouda (2012) found an increase of rainfall and drought between 1922 to 2005 with a very dry period noticed between 1970s and 1980s. The study results therefore confirmed the rainfall variability and positive trend of mean temperature over MRB. In previous analysis using REMO model for historical period of 1980-2010 and RCP4.5 and RCP8.5 future emission scenarios (2018-2050), it has been showed over the entire watershed an increase of rainfall and temperature for historical data and high variability of rainfall during the future scenarios (Lawin et al., 2019a). For the analysis using different regional climate model during the baseline of 1961-2010 and with high emission scenarios of RCP8.5 from 2051-2100 of temperature, shows high extreme trends of temperature between 1961-2010 and concerning future change there is an increase in temperature almost in more stations of the river with increase of extreme indices of TX90p, TX10p, TN90p and TN10p (Lawin et al., 2019b).

In the case of MRB population growth have an essential impacts on land use and land cover changes as proved by Koubodana et al.(2019a). The same authors have showed that MRB is characterized by deforestation and savanna decrease and will continue to decrease in the next 30 years if nothing is done.

Also, since the major hydrological components such as rainfall, potential evapotranspiration/temperature are varying considerably in MRB, this has impacts on runoff at upstream-downstream stations of the basin (Corrokopé and Athiémé). The results display over the basin and during the rainy period considerable changes. Thus in JJA and SON there is an increase of temperature, decrease of rainfall and increase (JJA), decrease (SON) of PET which are involving decrease of discharge at Corrokopé and Athiémé

5.8: Partial conclusion

The objective of this study was to understand the seasonal and annual hydro-climatic variable changes using Mann Kendall trend over the whole MRB as for individual station in the past (1961-2011). Afterward, an ensemble climate model was used for 16 ETCCDI climate extreme indices annual trend analysis of RCP4.5 and RCP8.5 in near future (2020-2045). Results can be highly summarized as follows:

- Negative rainfall variability index between 1961 and 2012
- A positive trend of aridity index revealing driest years during of the years 1981-1982-1983-1984-1986-1990-1992-2000
- A positive seasonal and annual trend of historical mean temperature and potential evapotranspiration is observed over the MRB and at selected gauged stations at 99% or 95% significant level
- Positive and negative trends in discharge and rainfall over the entire basin and at selected gauged stations at 99% or 95% significant level.
- Over validation period (1980-2005) ensemble climate model underestimates the observations globally but with spatial and temporal coefficient of correlation between observations and ensemble model higher than 0.60
- Mann Kendall test detected significant annual trend at 95% levels of PRCPTOT, SDII, CDD, R25 rainfall indices and TXn, TXx, DTR and WSDI temperature indices of RCP4.5 and RCP8.5 future scenarios at the mains station between 2020 and 2045

The results of the study can be used for future analysis on modeling the impacts of climate change on streamflow in MRB in order to provide a decision support package for water resource management in this basin. By incorporating and utilizing the finding of this analysis, one can bring positive results in implementation of water management policies.

Chapter 6:Discharge prediction and comparison using two lumped models

Introduction

Water resource management is a key domain in the society, economy, and industry and hydro-electricity production over the world. Therefore, to know spatially and temporally the availability and storage of water, study about rainfall-runoff relationship is useful for hydrological system operation. Many hydrological tools are developed for integrated river basin systems analysis and predictions for environmental resources managements (Jayakrishnan et al., 2005; Kepner et al., 2004; Vilaysane et al., 2015) The use of these models depend strongly on topography, geology, soil, vegetation, land use and climate variable of the region. Therefore, from the spatial consideration of the model there are lumped, semi-distributed and distributed models (Cornelissen et al., 2013; Perrin et al., 2003; Zhang et al., 2014). Specifically lumped model have the ability to consider the spatial variability of the catchment as the same proprieties and estimate the runoff at the considered outlet. Lumped models have a simple structure, less parameters, inputs data and quick methods of calibration and validation. Lumped models give the understanding of the hydrological mechanism in the catchment without taking into account all the structure of the catchment. Therefore lumped hydrological model is an appropriate alternative tools for understanding hydrological regime in an area with limited data (Dye and Croke, 2003). Semi-distributed and distributed model are more complicated and take the real system of the river, more parameters, time consuming, integrating many components and inputs data but more and less realistic in the implementation (Abbaspour et al., 2007; Lørup et al., 1998). Conceptual model have been known to perform better on larger and smaller catchments than drier catchments (Van Esse et al., 2013). These models have been used in many studies for water resource management and planning over the world (Le Lay et al. 2007; Badjana 2015; Renard et al. 2010; Niel, Paturel, and Servat 2003).

Two lumped conceptual hydrological models are selected among many models. They are GR4J (Génie Rural à 4 paramètres Journaliers) and IHACRES (identification of unit hydrographs and component flows from rainfall, evapotranspiration and stream flow data).The selection was based on their easy use, simplicity, popularity, operation, efficiency, reliability, less input data and performances according to previous studies (Andréassian et al., 2004; Andrews et al., 2011; Dye and Croke, 2003; Krysanova et al., 2011; Perrin et al., 2003; Tegegne et al., 2017; Vaze et al., 2011).. Previous studies have demonstrated that lumped models can perform well runoff and extremes low flow simulation in the wa-

tershed than a model which is more complicated such as distributed model (Kling and Gupta, 2009; Vansteenkiste et al., 2014).

6.1: Results of hydrological modeling using two lumped models

6.1.1: Calibration -validation and model performances

6.1.1.1: GR4J model

The results of simulated discharge at Athiémé station are displayed in Figure.6.1 for GR4J model calibration and validation periods. The runoff analysis was evaluated between 1964 and 1973 (Figure. 6.1) and between 1989 and 1997(Figure. 6.2) over the two sub-periods. The results show that the observed and simulated runoff values follow exactly the areal rainfall patterns but present some small differences. The simulated high runoff is underes-timated compared to the observed runoff at Athiémé (1965 -1973) and (1989 – 1997) by GR4J model with a right shift between 1989 and 1997.

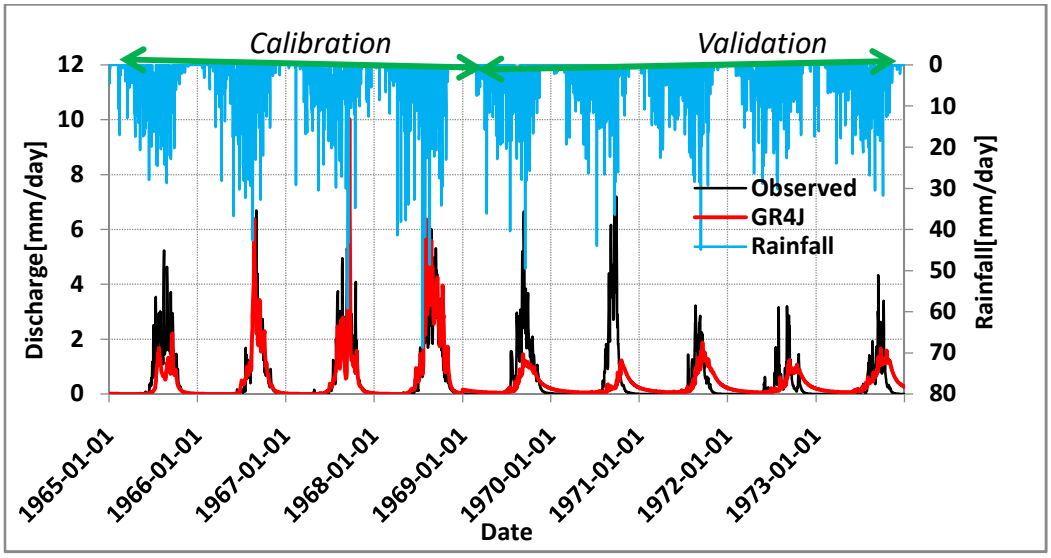

Figure 6.1: GR4J calibrated and validated discharge at Athiéme outlet(1965-1973)

The analysis of Figure 6.1 calibrated and validated runoff variability is similar to a real rainfall dynamic but there are the periods from 1970 to 1973and 1993 to 1997which present a lowest runoff which can be explained by the period of drought in Togo and in West Africa (Koubodana et al., 2019b; Oguntunde et al., 2011, 2006). Specifically, the simulated runoff follow exactly observed runoff during low flow from December to May and matches correctly observations between Junes to October. The runoff reaches the max-imum in August-September during calibration and validation periods.

During the second sub period (1989-1997), the situation is seen to be different **(**Figure.6.2**).** Indeed the simulated flow variability has right shifts with observed runoff. The model underestimates observation during the low flow from January to June. The simulated runoff follows the observed discharge for the period of pre-dam and more and less acceptable for the post -dam. The performances values KGE, NSE, R^2, RMS and PBIAS value after daily calibration and validation are summarized in Table 6.1. The acceptable values of KGE, NSE, R^2 and RMSE are in bolt.

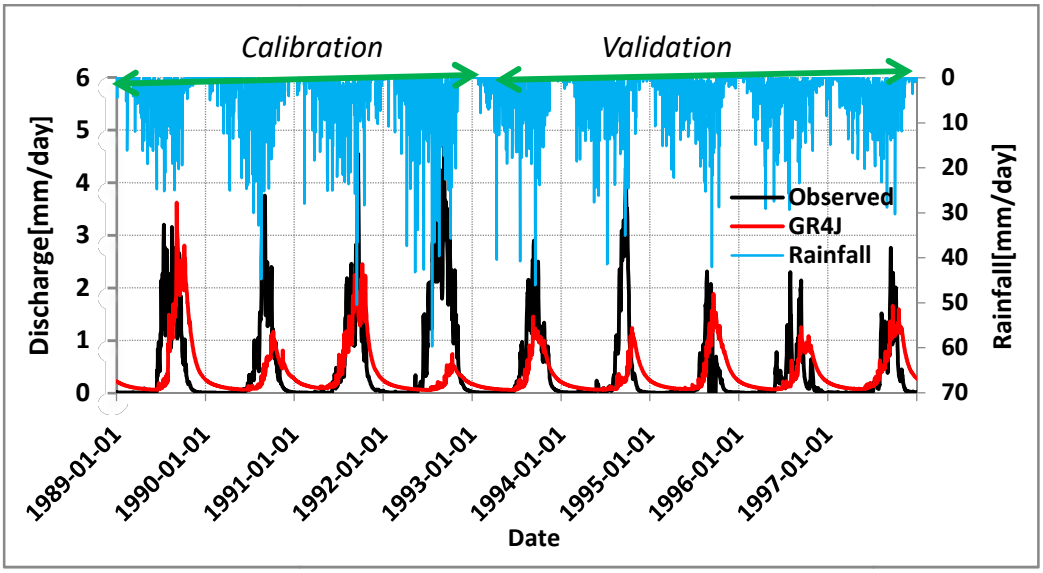

Figure 6.2: GR4J calibrated and validated discharge at Athiémé outlet(1989-1997)

The result shows that GR4J model is able to capture more and less the long-term daily runoff for the whole MRB. Nerveless the calibration and validation of GR4J model between pre-dam periods is better from the post-dam period. Post dam runoff maybe influenced by additional factor which maybe the dam management.

Table 6.1: GR4J model performance results and optimal parameters

GR4J: Performances	KGE	NSE	R^2	PBIAS[%]
Calibration 1965-1968	**0.94**	**0.88**	**0.83**	**13.38**
Validation 1969-1973	**0.82**	**0.80**	**0.90**	20.03
Calibration 1989-1992	**0.70**	**0.58**	0.33	30.11
Validation 1993-1997	0.38	0.28	0.39	**-3.99**
Parameters	X1	X2	X3	X4
Period 1964-1973	290.04	-2.18	41.26	7.40
Period 1988-1997	432.68	-4.64	307.96	1.03

Optimal values are in bolt

6.1.1.2: IHACRES model

The calibrated discharge over the two sub-periods at Athiémé is shown in Figure 6.3. The simulated and observed discharge extremes correspond also to the maximum and minimum areal rainfall. The simulated runoff follows exactly the observed discharge. Following the methodology of calibration and validation over the sub period at Athiémé gauged station, we found that according to the availability of the data, over many years the validated discharge is matching the observed ones. Particularly at Athiémé before dam installment the validated discharge followed the observed discharge with the wet (1969) and dry (1972, 1973) period as in MRB. The model validated well the timing, dry and wet periods at Athiémé during the periods of calibration and validation in the pre-dam as the post-dam periods. However, the simulated runoff underestimates high discharge over the whole period (1965-1973). IHACRES simulates better the dynamic of runoff at Athiémé with the plot of daily flow duration curve of simulated close to observed flow between 1965 and 1973 validation, simulation and the whole period. Moreover, during low flow the simulated exceeds observed flow while the opposite situation is observed during high flow (Figure. 6.3 & Figure. 6.4).

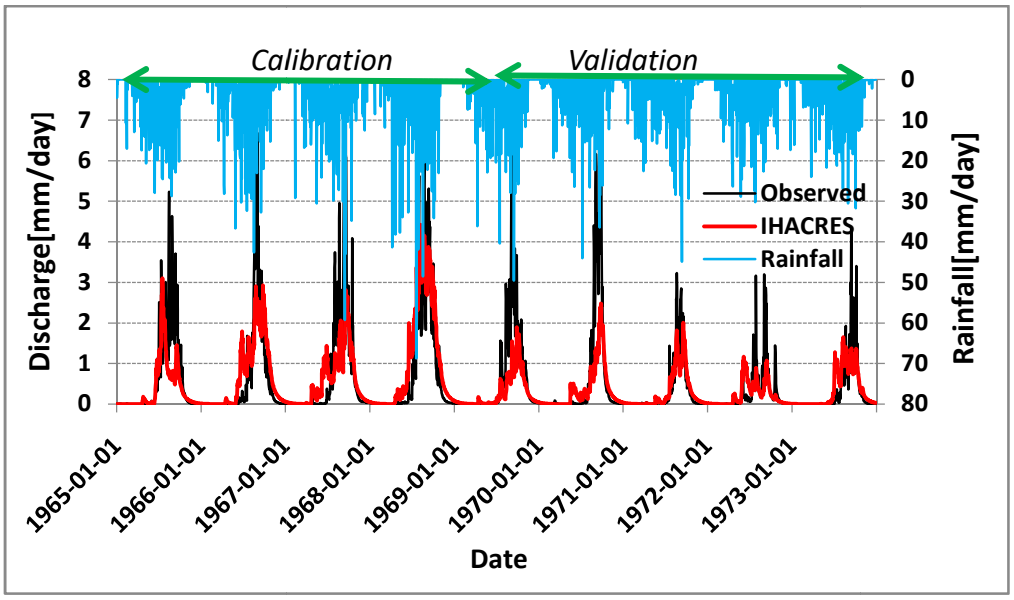

Figure 6.3: IHACRES observed and simulated discharge between 1965 and 1973

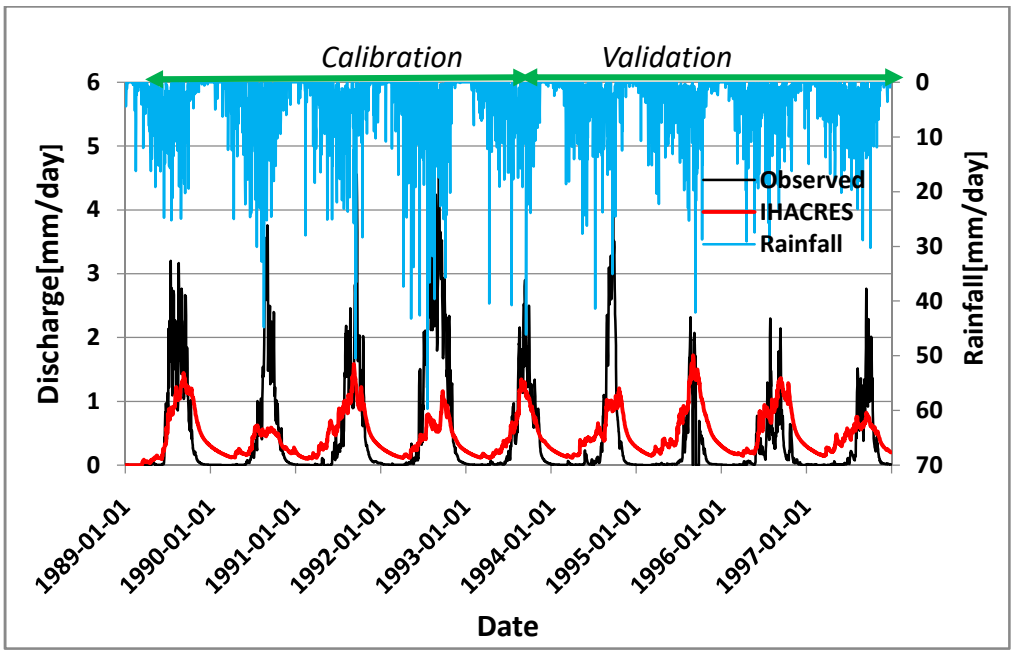

Figure 6.4: IHACRES observed and simulated discharge between 1989 and 1997

IHACRES model performance analysis, uncertainties and optimal values are shown in Table 6.2. IHACRES model during pre-dam have reliable value of KGE, NSE and R^2 higher than 0.5 whereas the errors RMSE and Rel.bias are minimized in the same period. During the second period of Post-dam KGE, NSE and R^2 are only acceptable on the calibration (1989-1992) period while poor during the validation period (1993-1997) model performances criterions are insignificant.

The parameters after optimization of the model respect the range at 95% significant level as the value plotted in Table 6.2.

Table 6.2: IHACRES model performance results and optimal parameters

IHACRES: Performance	KGE	NSE	R^2	PBIAS[%]	RMSE
Calibration 1965-1968	0.41	**0.65**	**0.90**	**1.85**	**0.44**
Validation 1969-1972	**0.55**	**0.90**	**0.75**	-15.71	**0.45**
Calibration 1989-1992	0.36	0.32	**0.74**	**4.10**	0.5
Validation 1993-1996	**0.80**	**0.26**	**0.63**	38.50	0.72
Optimized parameters	tw	τ_s	τ_q	f	ϑ_s
Period 1964-1973	58.53	71.3	1.98	0.36	
Period 1988-1997	100.00	82	2.10	5.86	

Optimal values are in bolt

6.1.2: Intra-annual runoff variability and statistics of GR4J and IHACRES models

Figure 6.5 shows the scatter plot and intra-annual variability of observed, GR4J, IHACRES and simulated Ensemble Mean runoff (EM) runoff for the two sub period of the

study. It reveals that the low simulated flow matches correctly with observations. During high runoff (August to October), IHACRES, GR4J and EM under estimate observations over the two sub-periods. In fact the ensemble model is better representative of stream flow evolution between 1964-1986 en opposite, the period of 1988-2010 where the EM model underestimates and more closer to observations. Scatter plot between observed and simulated runoff shows a promising results with coefficient of correlation bigger than 0.5.

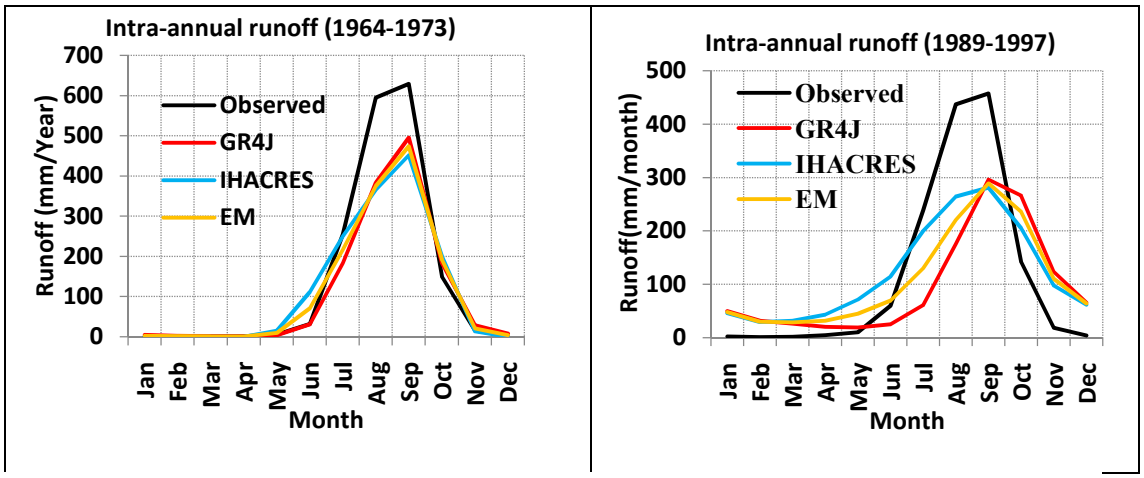

Figure 6.5: Intra-annual runoff at Athiémé (a) for pre-dam and (b) for post-dam periods.

An evaluation of daily statistics from GR4J, IHACRES and EM models are displayed in Table 6.3.

Table 6.3: GR4J and IHACRES model statistics

	1964-1973				1989-1997			
	Observed	GR4J	IHACRES	EM	Observed	GR4J	IHACRES	EM
Max	7.21	10.03	4.47	6.51	4.91	3.62	1.72	2.56
Mean	0.53	0.42	0.44	0.43	0.43	0.36	0.45	0.40
STD	1.08	0.87	0.75	0.78	0.79	0.45	0.37	0.38
Summ	1734.11	1366.5	1449.75	1408.15	1418.33	1183.12	1473.93	1328.52

High values are in red

6.2: Discussion

In thus study, we tested and assessed the performance of two lumped conceptual models: GR4J and IHACRES using the same inputs data to simulate the runoff at Athiémé outlet of MRB. However, the models don't have the same computation system, routing and parame-

ters for rainfall-runoff generation at Athiémé (Perrin and Andre 2003; Dye and Croke 2003).

The study has divided the whole period into two sub periods according to previous studies results in the basin (Koubodana et al., 2019a; Koubodana et al., 2019b)on rainfall trend analysis and past and future land cover change scenarios: The pre-dam period is between 1964 and 1986. During this period the watershed is considered to be natural because any artificial installation doesn't affect the runoff generation over the whole catchment. The only factors that can impact the runoff are soil proprieties, land cover and climate condition (Dubreuil, 1985). The post-dam period cover 1988 to 2010, the dam was installed in 1987 for hydropower electricity generation and irrigation for farmers (PANGIRE, 2016; PCCP, 2008; Rossi, 1996). The calibrated and validated period depend on the wet and dry period and confirmed the drought periods in the West Africa region as proved by (Koubodana et al., 2019b).

According to the results, during the pre-dam period predicted runoff and areal rainfall dynamic are similar and the simulated runoff from IHACRES and GR4J models matches the observed runoff during calibration (1965-1968) and validation (1969-1973) periods with R^2, NSE and KGE coefficient between 0.6 and 0.87. The performances of GR4J models are seen to be more reliable and robust than IHACRES model between 1964 and 1986. This can be explained by model parameterization, assumptions and number of the parameters in the models. Indeed GR4J model has four parameters while IHACRES model has five parameters (Perrin and Andre 2001; Andrews, Croke, and Jakeman 2011). GR4J model overestimates high discharge during this period while IHACRES model is underestimating high discharge over the same period.

Between 1988 and 2010, the calibrated and validated runoff at Athiémé is less reliable than the first period. Thus, R^2, NSE and KGE don't exceed 0.67 and the IHACRES model underestimates observation while GR4J model present a shift of simulated runoff. The results can be due to dam impacts on runoff generation, response time of the soil. Others factors like input data, model structures, and model parameters suggested by Tian et al. (2014).

Difference between the hydrograph of the two sub periods (1964-1986) and (1988-2010) maybe due to many factors responsible of runoff generation in tropical zone. According to (Dubreuil, 1985) , the generation of runoff and subsurface runoff depends on spatial variation of rainfall, soil surface formations, texture and structure, vegetation cover, geological layers, drainage density, weathered material and climate and even on Nangbéto dam management. The results are consistent with those obtained by Badjana et al.(2017a) who has investigated the performance of lumped conceptual IHACRES model at three nested sta-

tion of Kara river basin. Their results show acceptable mean modified Nash-Sutcliffe efficiency measure of 0.6 and the authors' argument that parameters controlling rainfall transformation to effective rainfall are more sensitive than those routing the stream flow in Kara river basin. Amoussou et al.(2014) has used GR4J model between 1988 and 2010 to simulate runoff and note a better performance of the model for short period of calibration or validation length. The same author concluded that there poor performances of model for long period for model evaluation.

The overestimation of runoff during high discharge has also been observed in many rivers in West Africa by Mbaye et al.(2015) ; Speth et al.(2010); Varado et al.(2006). According to (Speth et al., 2010) , the overestimation of runoff is explained by infiltration of surface runoff during high rainfall in the valley bottom or in the dry riverbed at the beginning of the rainy season. However this process is not incorporate in lumped conceptual model such as IHACRES or GR4J. This need further analysis with semi or distributed model taking in account spatial variation of soil, land use, top and down processes and incorporating the reservoir management.

The shift of runoff observed in GR4J model between 1988 and 2010 can be explained by the delay time in the model or the response of the model to transform areal rainfall in surface runoff (Pedinotti et al., 2012). The maximum flow observed and simulated reached their pick in August, September or October. However , the extremes rainfall event that are causing flood in the area occur usually during these months and depending of the season (Amoussou et al., 2016, 2014; Koubodana et al., 2019b). Particularly, the year with high hydrographs are 1969-1980-1981-2000-2010 and this can be related to the year with flooding in Togo and Benin as mentioned by Oguntunde and Abiodun (2013) and Yabi and Afouda(2012).

6.3: Partial conclusion

This study gives a better understanding of Mono River Basin hydrologic system using two rainfall-runoff models for two sub periods. The lumped rainfall-runoff IHACRES and GR4J models are successfully calibrated and validated over the two sub-periods. The results show that the runoff generation is not linear to rainfall variability in the basin and maybe influenced by anthropogenic and natural factors. Dam management has influences on runoff generation after 1987 year. At daily time step GR4J model overestimates the observations whereas IHACRES model underestimates observations during pre-dam (1964-1986). However, during post-dam period (1988-2010), there is a weak prediction of observation with a shift by GR4J model while IHACRES model is underestimating obser-

vations. We have tested a mean ensemble model at intra annual scale over MRB, and results shows that mean ensemble model can probably simulate better runoff at Athiémé between 1964 and 1986. Meanwhile, runoff process of the whole MRB is affected by soil proprieties, geological layers, landscape, climate change, and dam management.

As conclusion, the response of MRB streamflow depends strongly on the model used for parameterization and also if the period of simulation is before or after Nangbéto dam installation. All these factors must be incorporated into semi–distributed or distributed model for further accurate integrated land and water resource evaluation in MRB.

Chapter 7: Land cover change, climate change and dam management impacts on water balance components

Introduction

Water resource management is becoming more and more important face to climate change (CC). CC is resulting from anthropogenic and natural factors (IPCC, 2014; Koubodana, 2015). Water is a source of sustainable and economic developments because it insures safety and supply of the basics resource in a society and ecosystems. Water resource is linked to different sectors of activities such as agriculture, industry, domestic water use and sanitation, hydropower generation, health and environmental security (Hanjra and Qureshi, 2010). Among these sectors, agriculture is the largest user of water followed by hydropower dam for electricity generation and agricultural land irrigation. Water subject to pollution and river hydrology system is modified at the downstream of a reservoir. For instance, dam installation can lead to flooding downstream. All these impacts on water taken together shows that in water resource management we are mostly dealing with a complex system under several interactions between natural, socio-economic and political issues (PCCP, 2008) and elements. Today many challenges that we face are increase water demand in water scarcity, water pollution, flood and drought arena and era. As proved by IPCC (2014) IPPC, global climate change; demographic and economic changes will be felt more in particular regions such as tropic and sub-tropical regions of the World. In several cases, water resource management is much linked with land use and climate variability and changes. Thus, climate variability and human activities are two major driving factors in hydrological processes and spatial-temporal distribution of water balance components.

As originality in this works, we use two different scenarios of land use, climate data and reservoir on two different periods at daily levels. Moreover, SWAT model was calibrated and validated for different upstream downstream discharge station for different period and for the whole basin at Athiéme. We also estimated water balance component for the whole basin upstream-downstream and over different periods.

7.1: Hydrological modeling performances and parameters

Figure 7.1 and Figure 7.2 illustrate the results of calibration and validation of the simulated discharge at the downstream of Nangbéto (Athiémé, Tététou) and upstream (Corrokopé) gauging stations. SUFI-2 calibration technique was used for different sub-periods SIM1 and SIM2 with different land use and climate conditions. The hydrographs globally indi-

cate a good fit of daily discharge dynamics by SWAT model during SIM1 sub-period while during SIM2 sub-period the fit a looking different with the perturbation on hydrograph dynamic.

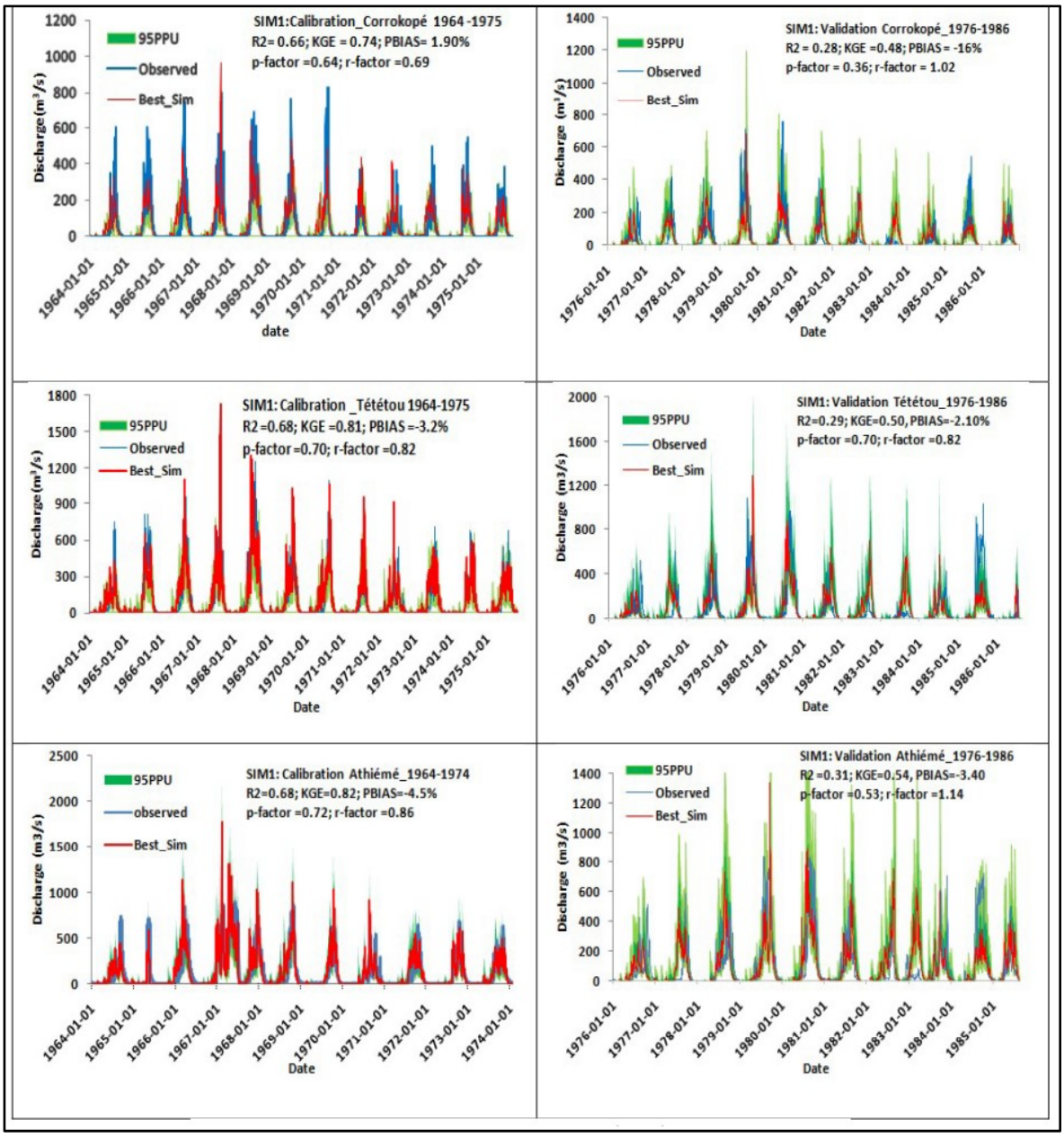

Figure 7.1: SIM1 calibration and validation hydrographs

The SIM1 quality of simulated and observed discharge evolution at each gauging stations is in concordance with the performance statistics in Table 7.1. Meanwhile, high discharge is underestimated in the upstream station (Corrokopé) whereas being overestimated for the downstream stations (Tététou and Athiémé) considering the first simulation SIM1. Indeed the performance over calibration period shows a very good objective function of KGE ≥0.75, acceptable NSE and R^2 and very good PBIAS values (Table 7.1) in the upstream-

downstream stations. In opposite SIM1 validation period displays satisfactory KGE, unsatisfactory NSE, R^2 and good PBIAS values except at Corrokopé station (PBIAS > ±15%). Within the calibration and validation periods, the uncertainties values of R-factor at almost in all stations are acceptable whereas poor in some station for P-factor values.

The periods of low and high discharge related to the periods of flooding and drought in the region are also revealed. For example the period of 1970s-1980s, well know in West Africa as the drought (Kasei et al., 2010; Oguntunde et al., 2006) period is exaltedly predicted by the model over calibration and validation in all discharge gauging stations with low discharge. At the same time, high discharges which involve flood in the region are seen during the years of 1967, 1968, and 1980 in the downstream at Athiémé gauge station with highest discharge. The model overestimates discharge at Tététou and Athiémé station during the calibration period whereas it underestimates over the rest of the period and stations.

Table 7.1 displays the fitted value of model parameters which are in the ranges

Table 7.1: First SWAT model performances statistics (SIM1)

	Station	p-factor	r-factor	R^2	NSE	KGE	PBIAS[%]
SIM1: Pre-dam period 1964-1986							
Calibration: 1964-1975	Corrokope	**0.64**	**0.69**	**0.66**	**0.66**	**0.74**	**1.90**
	Tététou	**0.70**	**0.82**	**0.68**	**0.66**	**0.81**	**-3.20**
	Athiéme	**0.72**	**0.86**	**0.68**	**0.66**	**0.82**	**-4.50**
Validation: 1976-1986	Corrokope	0.36	**1.02**	0.28	0.17	0.48	**-16.00**
	Tététou	**0.53**	**0.97**	0.29	0.20	**0.50**	**-2.10**
	Athiéme	**0.53**	**1.14**	0.31	0.20	0.54	**-3.40**
SIM2: Post-dam period 1988-2010							
Calibration: 1988-2000	Corrokope	0.19	0.48	**0.60**	**0.59**	**0.60**	-16.30
	Nangbéto	0.48	**0.85**	0.37	0.25	**0.61**	-0.30
	Tététou	**0.64**	**1.00**	0.44	0.33	**0.60**	20.80
	Athiémé	**0.55**	**1.06**	0.26	-0.23	0.46	5.90
Validation: 2001-2011	Corrokope	0.21	0.48	0.40	0.38	0.47	-16.60
	Nangbéto	0.42	**0.76**	0.06	-0.31	0.24	-6.80
	Tététou	**0.62**	**0.82**	**0.53**	0.50	**0.62**	17.20
	Athiémé	0.46	**1.06**	0.20	-0.24	0.42	-4.50

[P-factor is the percentage of measured data covered by the 95PPU uncertainty band, R-factor is the relative width (thickness) of the 95PPU uncertainty band, R^2 is the coefficient of determination, NSE is the Nash–Sutcliffe efficiency, PBIAS is the percent bias, and KGE is the Kling–Gupta efficiency].

Table 7.2 displays the details of sensitive parameters and their final value fitted after calibration process. The most sensitivity parameters are SLSUBBSN, OV_N, ESCO,

CANMX, CN2, GW_REVAP, ALPHA_BF, GW_DELAY, GWQMN, SOL_AWC, SOL_BD, and SOL_K.

Table 7.2: First SWAT model parameters fitted values (SIM1)

SIM1:1964-1986			Calibration_1964-1975	Validation_1976-1986
Parameter_Name	Min_value	Max_value	Fitted_Value	Fitted_Value
1:R__SLSUBBSN.hru	0.048305	0.553955	0.302141	0.455859
2:V__OV_N.hru	7.759764	17.312553	9.613006	15.994268
3:R__ESCO.hru	-0.544062	0.015872	-0.072598	-0.430955
4:R__ESCO.hru	0.213044	0.724513	0.432976	0.480031
5:R__ESCO.hru	-0.399236	0.374294	0.270641	0.199476
6:R__ESCO.hru	-0.148037	0.161503	-0.069414	-0.039698
7:R__ESCO.hru	-0.995179	0.288611	-0.730718	0.275773
8:R__EPCO.hru	-0.345453	0.433603	0.129771	0.223258
9:R__CANMX.hru	-0.490572	0.146394	0.089067	-0.303304
10:R__CN2.mgt	-0.125409	0.149695	0.022597	-0.044528
11:R__CN2.mgt	-0.463151	0.019815	-0.44673	-0.050698
12:R__CN2.mgt	-0.748341	0.183689	-0.560071	-0.187259
13:R__CN2.mgt	-0.768212	0.152798	-0.339021	-0.095875
14:R__BIO_INIT.mgt	-0.391095	0.033749	-0.167627	-0.058867
15:R__BIO_MIN.mgt	-0.483204	0.020132	-0.037248	-0.268783
16:V__GW_REVAP.gw	0.131277	0.242543	0.152418	0.236535
17:V__ALPHA_BF.gw	-0.154298	0.418684	0.085208	0.273147
18:V__GW_DELAY.gw	190.199997	400	303.911591	273.700409
19:V__GWQMN.gw	2359.2356	4120.9331	3758.023438	2996.970215
20:R__SOL_AWC(..).sol	0.015184	0.487874	0.320542	0.052054
21:R__SOL_AWC(..).sol	0.219595	0.791475	0.753731	0.717131
22:R__SOL_AWC(..).sol	-0.126935	0.128225	0.014424	-0.058042
23:R__SOL_BD(..).sol	-0.311506	0.41342	-0.211466	0.02341
24:R__SOL_BD(..).sol	-0.940049	0.246487	0.10173	0.172922
25:R__SOL_K(..).sol	-0.429402	0.048336	-0.050078	-0.424625
26:R__SOL_K(..).sol	-0.409317	0.023431	-0.025902	-0.02244
27:V__SOL_ALB(..).sol	0.191331	0.376303	0.359655	0.26199
28:V__SURLAG.bsn	-1.103754	10.478876	4.386413	10.177728

Figure 7.2 shows the graph of simulated discharge over calibration and validation period for SIM2. The result reveals that the upstream Corrokopé gauging station where the dynamic of the hydrograph exhibits a good fit of streamflow. This is explained by the performance statistics value at Corrokope in Table 7.1with satisfactory NSE, R^2 and KGE ≥ 0.60 in calibration period and poor and unsatisfactory performances over validation period.

At upstream station of Corrokopé, high discharge is well simulated, with overestimation of baseflow and underestimation of high discharge during calibration and validation periods.

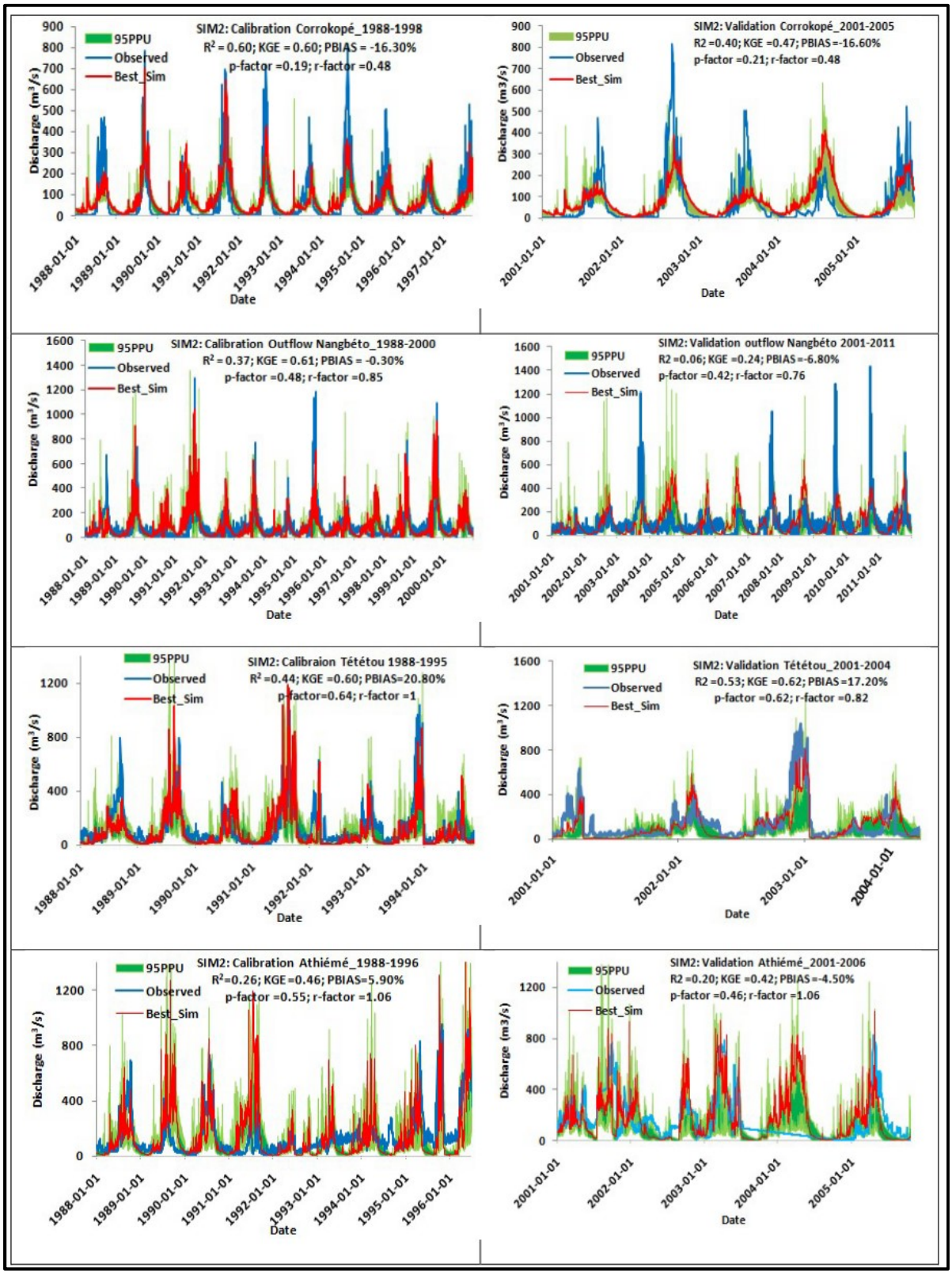

Figure 7.2: Second SWAT model parameters fitted values (SIM 2)

SIM2:1988-2011			Calibration_1988-2000	Validation_2001-2010
Parameter_Name	Min_value	Max_value	Fitted_Value	Fitted_Value
1:R__SLSUBBSN.hru	0.143569	0.445495	0.248035	0.430399
2:V__OV_N.hru	-5.842884	9.059104	7.717925	3.366545
3:R__HRU_SLP.hru	0.300686	1.120598	0.518783	0.54174
4:R__ESCO.hru	0.009828	0.264076	0.094747	0.225939
5:R__ESCO.hru	-0.205156	0.6753	0.117091	0.169918
6:R__ESCO.hru	0.045765	0.289153	0.220518	0.187417
7:R__EPCO.hru	-0.364279	0.147383	-0.187244	-0.295716
8:R__CANMX.hru	-0.118788	0.7309	0.470895	-0.066107
9:R__CN2.mgt	-1.734496	0.518664	-0.864776	-0.837738
10:R__CN2.mgt	0.182399	0.469551	0.403506	0.459788
11:R__BIO_INIT.mgt	-0.103291	0.166169	-0.081195	0.044912
12:R__BIO_MIN.mgt	0.534876	1.46488	1.042658	0.767377
13:V__GW_REVAP.gw	-0.049228	0.874	0.05602	0.008012
14:V__ALPHA_BF.gw	0.417879	0.827577	0.508832	0.657962
15:V__GW_DELAY.gw	-33.974213	68.400246	3.904336	12.503791
16:V__REVAPMN.gw	80.037712	209.99045	195.175827	117.204193
17:V__GWQMN.gw	1084.77991	2482.8376	1305.672974	1915.226196
18:R__RCHRG_DP.gw	-0.2147	0.71676	0.12994	0.673913
19:R__SOL_AWC(..).sol	-0.2408	0.200396	0.06539	-0.118148
20:R__SOL_BD(..).sol	-0.244667	0.28523	-0.016811	0.207865
21:R__SOL_BD(..).sol	-0.428739	0.4671	0.454558	0.006639
22:R__SOL_BD(..).sol	-0.155897	0.217463	0.012115	-0.093919
23:R__SOL_K(..).sol	-0.224561	0.18961	-0.028244	0.02477
24:R__SOL_K(..).sol	0.65142	1.342764	0.940402	0.813195
25:V__SURLAG.bsn	16.159155	21.388464	19.83013	20.72957
26:R__ALPHA_BNK.rte	-0.0614	0.14457	0.052707	0.047764
27:R__CH_K1.sub	-0.697278	0.72386	0.516374	-0.205564
28:R__RES_ESA.res	-0.577215	0.24095	-0.349765	-0.425036

In the opposite, for the downstream stations of Tététou and Athiémé during the second period of simulation SIM2 the simulated discharges are completely different. Therefore the observed discharge at Nangbéto, tététou and Athiémé is totally perturbed by Nangbéto reservoir. Consequently, the outflow, and discharge at Tététou and Athiémé do not respect the climatic dynamic. The situation is confirmed by calibration and validation performance and uncertainties of the SIM2. Therefore over calibration and validation periods, the value of R^2, NSE, KGE and uncertainty of PBIAS are globally unsatisfactory. The management of Nangbéto reservoir has considerably affected the outflow at Nangbéto and the runoff of Tététou and Athiémé after the year 1987.The presence of a large floodplain between

Tététou and Athiémé, the exploitation of the perimeter of Dévé which exploits the waters of the river for agriculture irrigation impacts on surface runoff of the downstream stations.

7.2:Inter-annual and intra-annual mean simulated discharge (1964 -1986)

Figure 7.3 shows the graphs of inter-annual simulated discharge between1964-1986

a

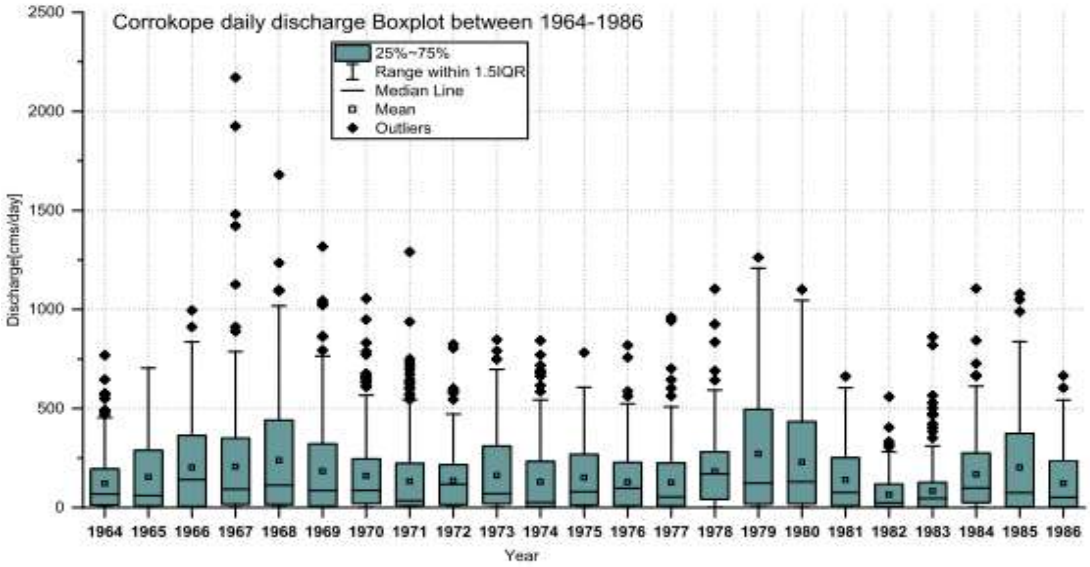

b

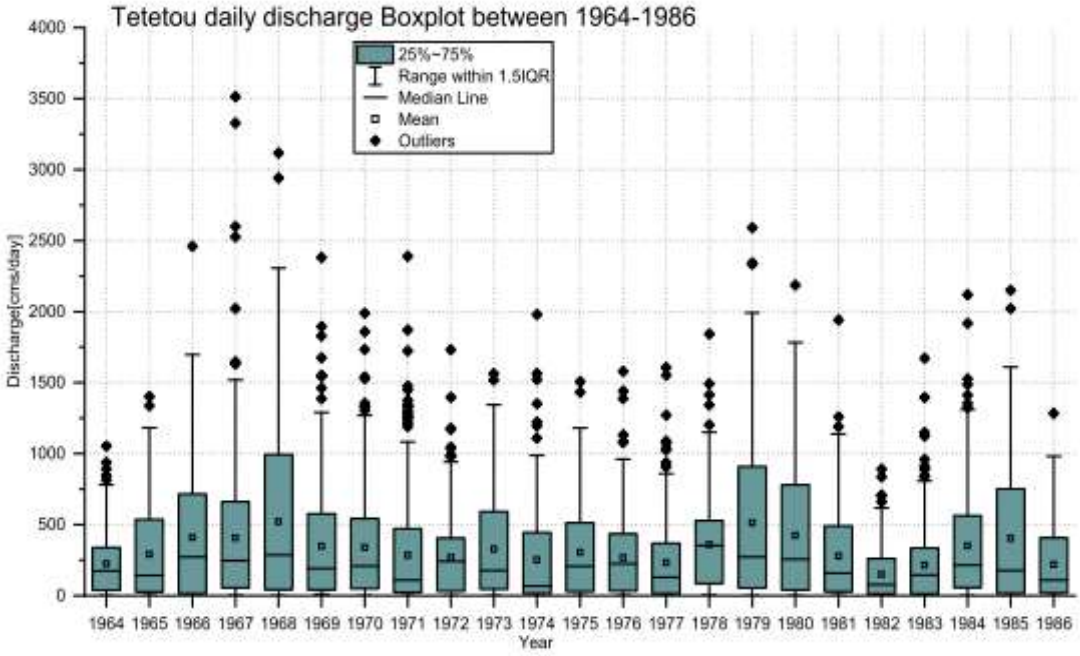

c

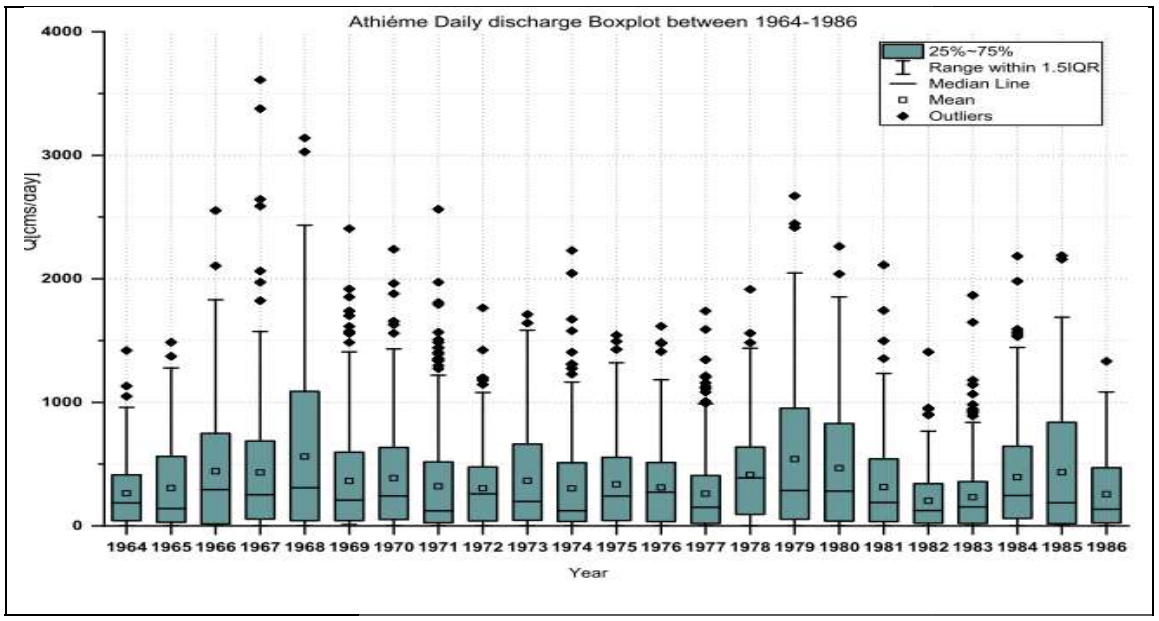

*Upstream station (a) Corrokopé and downstream stations (**b**) Tététou and (**c**) Athiémé.*

Figure 7.3 Inter-annual simulated discharge during first periods (1964-1986)

Discharge at Corrokope upstream station is characterized by an excellent same behavior for calibration validation periods. At inter-annual scale, the high discharges are observed in 1697 or 1968 and the lowest in 1964 during calibration period at the station. During validation periods, the highest discharge occurs in 1979 and 1980 and the lowest discharge in 1983. At monthly scale, observation and simulated discharge peaks are reached in September corresponding to the maximum of rainfall in the region. Meanwhile, at the station of Tététou and Athiémé, there is a peak shift between observed and simulated discharges. At the three gauged stations at Corrokope, Tététou and Athiémé, there is similarity between the maximum discharge over the basin and annual rainfall variability. Indeed the negative rainfall variability (1964, 1965, 1970; 1971, 1972, 1974, 1975, 1976, 1977; 1981, 1982, 1983, 1984, 1986) computed in section 5.2 corresponds in figure 4.2 to the low annual discharge. These years are the dry year over the period between 1964 and 1986 in the (MRB). The outliers are more observed in 1967, 1971, 1974, 1977 and 1983. The highest daily discharge is observed at Athiémé, Tététou and Corrkope (Table 7.4) and show that the final outlet at Athiémé runoff depends on the upstream sub-basin.

Figure 7.4 shows the graphs of intra-annual simulated discharge between1964-1986. Seasonal boxplots at Corrokopé, Tététou and Athiéme stations shows that the maximum discharge are observed between august and October corresponding to the maximum rainfall in the basin while the lowest are between January to april which is the dry season. Athiéme

station has the highest mean discharge and Corrokope station the lowest mean values (Table 7.4). There is distinction between the dry and wet season at each discharge station.

Table 7.4. Daily and monthly statics of simulated discharge between 1964 and 1986

	Athieme		Tetetou		Corrokope	
	Daily	**Monthly**	**Daily**	**Monthly**	**Daily**	**Monthly**
Max	3610.43	1142.80	3514.17	1025.09	2170.86	545.53
Mean	356.69	356.19	321.58	378.97	160.51	160.28
STD	315.95	291.48	286.40	260.81	152.21	142.11
VAR	162986.05	110990.98	137262.32	86408.82	38318.42	26006.52
CV[%]	0.01	0.01	0.01	0.01	0.01	0.01

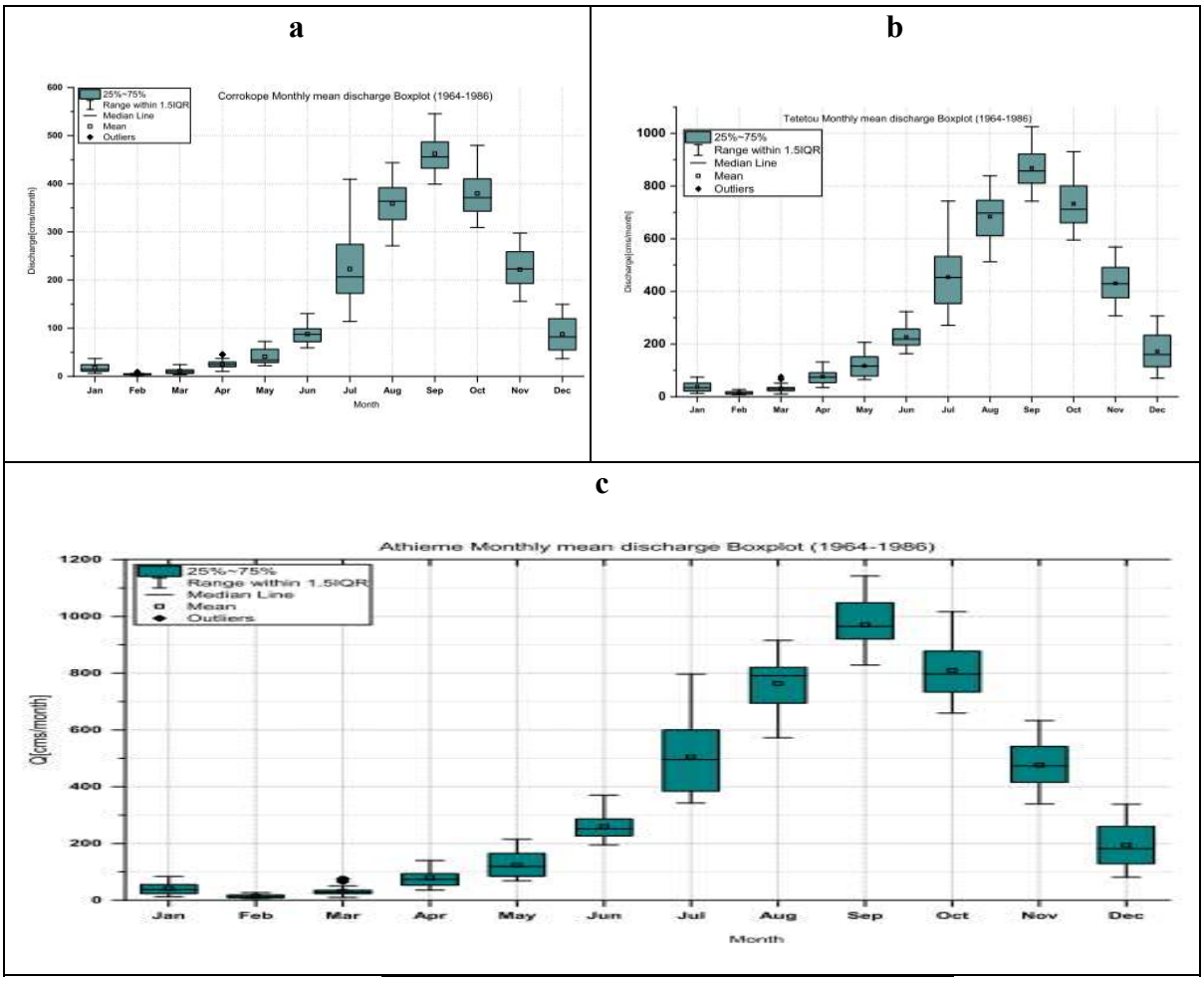

*Upstream station (**a**) Corrokopé ; downstream stations (**b**) Tététou and (**c**) Athiémé.*

Figure 7.4: Intra-annual simulated discharge boxplot during first periods(1964-1986)

7.3: Intra-anual and inter-annual simulated discharge between 1988 and 2010

Inter-annual and intra-annual box plots of discharge with distinction of wet and dry season and years are displayed in Figure 7.5 & Figure 7.6 It is clear that the highest discharges

occurring in the basin station are 1989, 1991, 2008 and 2010 while the driest years are seen in 1992 and 2001 as reported by Yabi and Afouda (2012). In the other side, Figure 7.6 there separation of dry and rainy season. The rainy season peak is in September/ October

a

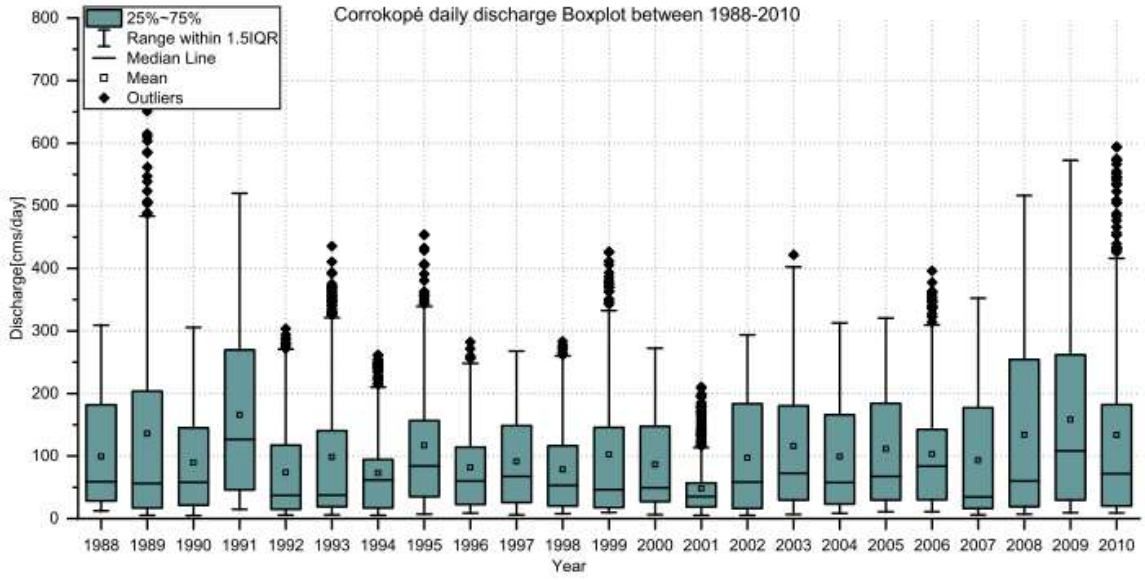

b

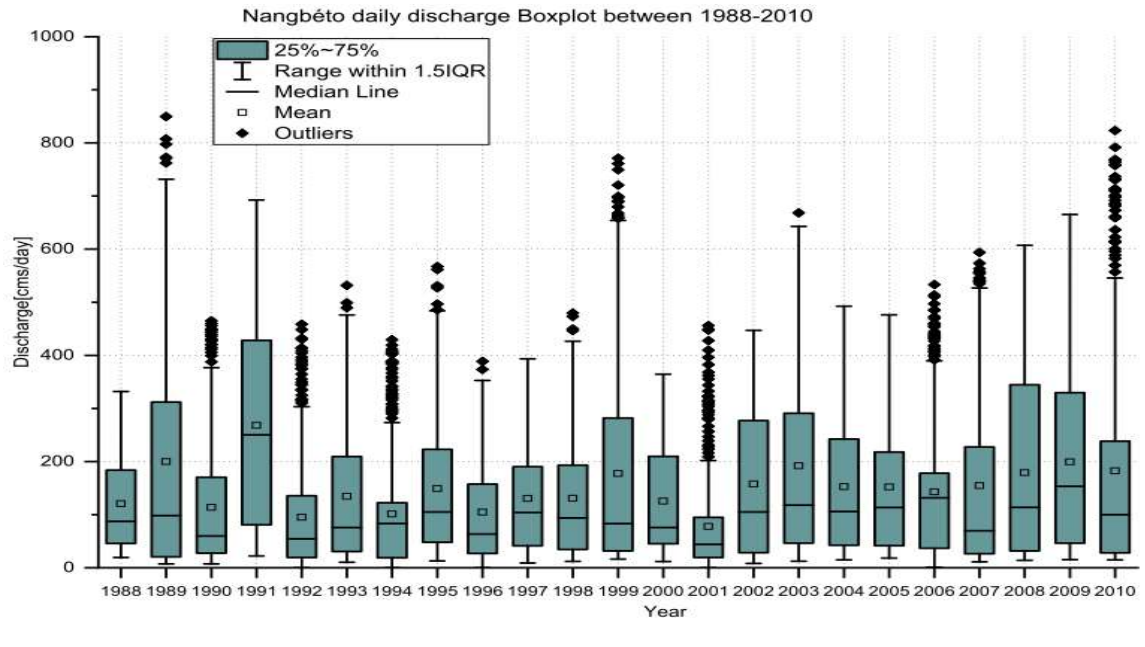

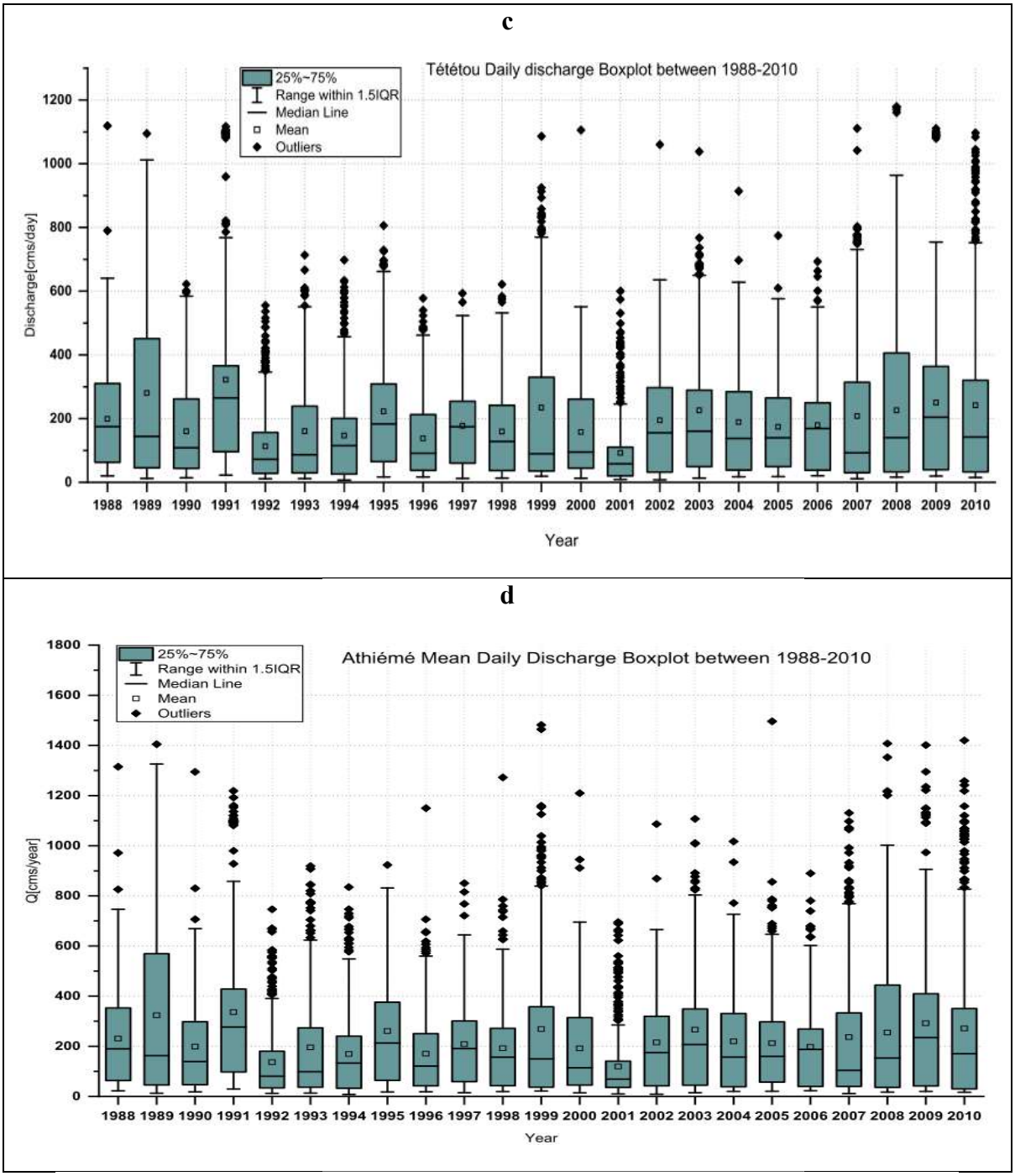

Figure 7.5: Inter-annual simulated discharge during calibration and validation periods for SIM2

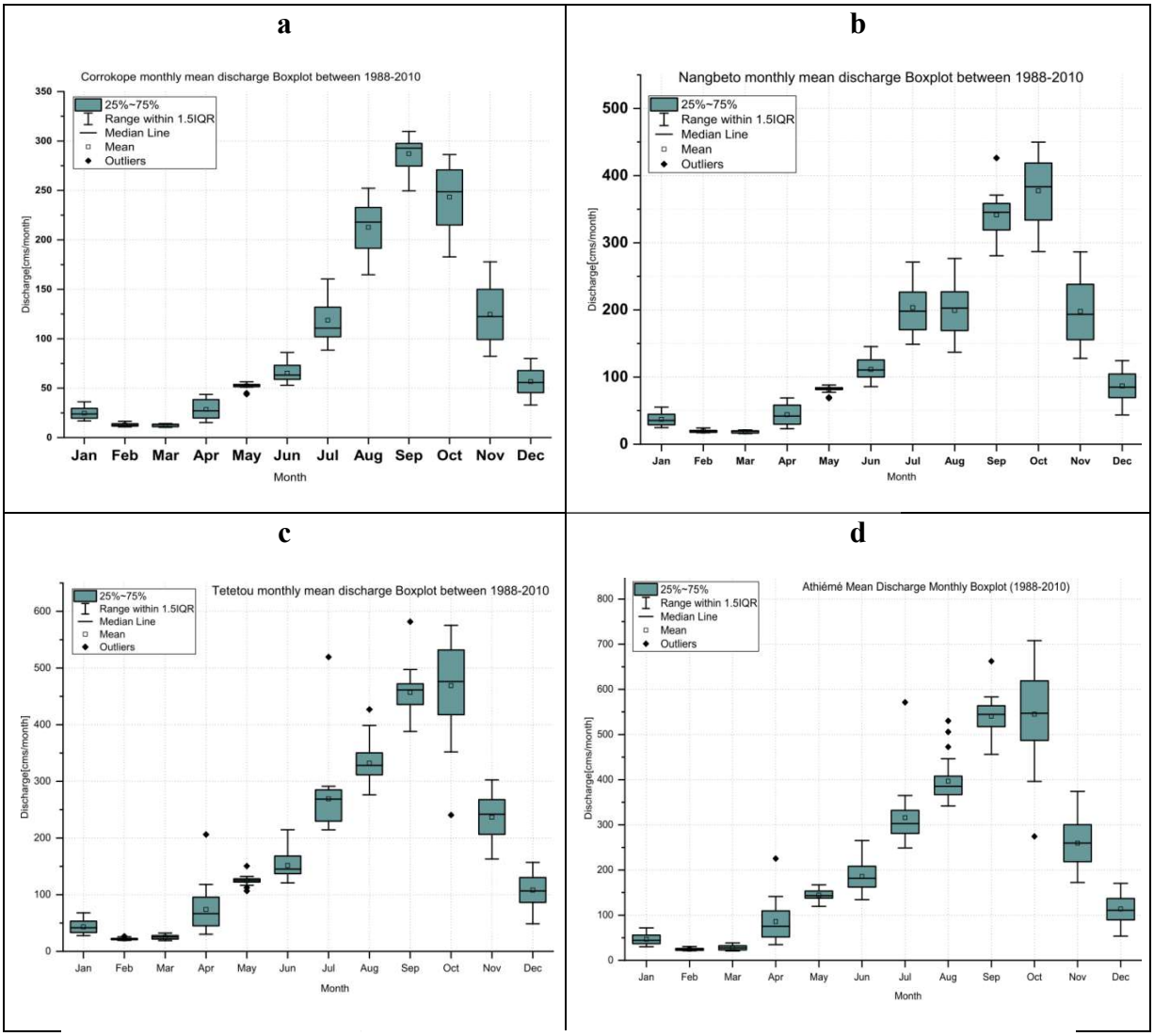

Figure 7.6: Intra-annual simulated discharge during calibration and validation periods

Table 7.5: Daily and monthly statics of simulated discharge between 1988 and 2010

	Athiémé		Tetetou		Nangbeto		Corrokope	
	Daily	Monthly	Daily	Monthly	Daily	Monthly	Daily	Monthly
Max	1496.13	707.98	1178.84	581.72	849.70	449.91	650.98	309.67
Mean	224.74	224.40	193.52	193.23	149.70	143.53	103.74	103.59
STD	174.32	157.97	149.08	134.00	118.29	100.86	84.30	79.29
VAR	51521.60	34543.21	37972.04	24643.63	22329.44	14445.96	11546.06	8670.90
CV[%]	128.93	142.05	129.81	144.20	126.55	142.30	123.06	130.66

7.4: Spatial and temporal analysis of hydrological component

In order to come up with sustainable for water management understanding, it is important to analyze and quantify the spatio-temporal repartition of different components of hydro-logical processes which govern the hydrological system of Mono river basin

7.4.1: Water balance components variability between 1964 and 1986

Figure 7.7 and Figure 7.8 displays the mean inter-annual and intra-annual (seasonal) variability of water balance components. The most important component of water balance selected are precipitation-evapotranspiration-percolation-groundwater-surface runoff-water yield-lateral flow (Begou et al., 2016; Obuobie et al., 2010) and values summarized in Appendix 7.7 and 7.8.

The reported average annual values over MRB of water balance component appearance in Appendix 7.7 and maps in Figure 7.7 show that actual evapotranspiration (31.33%) and water yield (25.95%) have more than 50% of the total average annual water cycle component between 1964 and 1986. The high actual evapotranspiration rate can be explained by the type of land cover and the high temperature in the study area. Lateral flow contribution is the lowest (0.40%) process occurring in the study area in annual average (Figure 7.7b). The total water yield is the net amount of water that leaves the basin and contributes to streamflow annually is important after evapotranspiration in the basin. The mean water that percolates past the root zone during annually as percolation represents 17.67%; groundwater contribution to streamflow is 14.71% and surface runoff is about 9.94% annually.

Inter-annual average value of water components presented in Figure 7.7a the variability of these components for each year. Indeed, lateral flow contribution is very low for during each year whereas the others components such as actual evapotranspiration, water yield, percolation, groundwater and surface runoff decrease respectively. During the year of 1968, 1978 and 1980 the annual contribution of water yield is higher that actual evapotranspiration. There are high values of surface runoff in the year 1968, 1979 and 1980 while maximum actual evapotranspiration is observed in 1967, 1975, 1978 and 1984. The same year of high evapotranspiration were also known to have negative annual rainfall variability index (chapter 5). The change in water cycle components from year to year are due to the variation of climate condition such as temperature, relative humidity and surface land condition which have impacts on any watershed hydrological system (Badjana et al., 2017a; Golmohammadi et al., 2014).

An intra annual mean of water cycle components are displayed in Appendix 7.8 and the graphs of the temporal changes are observed in Figure 7.8-a&b. It appears that actual evapotranspiration has 51.02% of the global while percolation, water yield, surface runoff, groundwater and lateral flow represent respectively 17.53%, 15.93%, 9.43%; 5.67% and

0.42% of total. The peak of actual evapotranspiration, surface runoff, percolation and water yield are obtained in September and corresponding to the maximum of rainfall which coincides with the rainy season in the region. The lateral flow which depends specifically of the slope of the basin is not important and could be explained the elevation range in the basin. Seasonally (Figure 7.8), the maximum of rainfall is ranged from May to October and represent 51.02% of the water balance components.

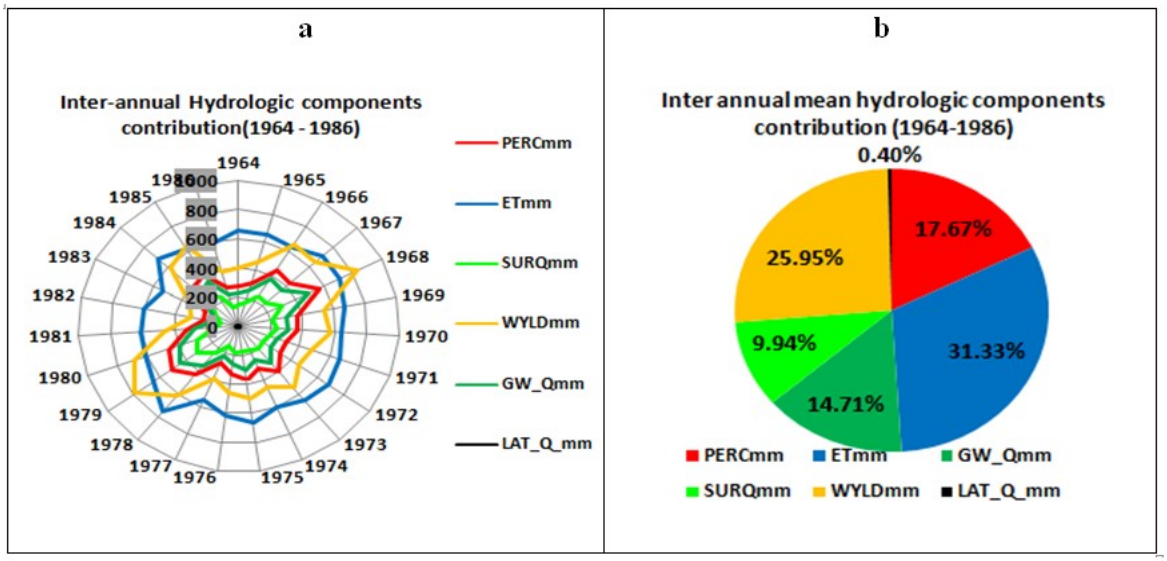

Figure 7.7: Inter-annual variability of hydrological components between 1964 and 1986

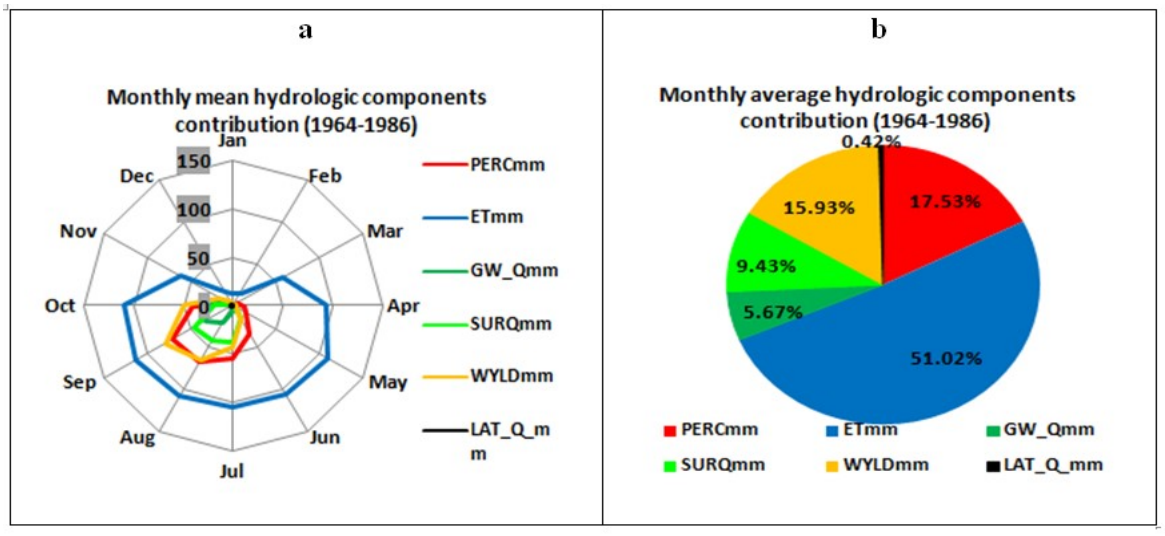

Figure 7.8: Intra-annual variability of hydrological component between 1964 and 1986

7.4.2: Water balance components variability between 1988 and 2010

The simulation of SWAT model between 1988 and 2010 has incorporated a dam management in formations and considering the land use map of 2000. Land use and land cover

change between 1975 and 2000 is essentially deforestation, decrease of savanna, increase of cropland and settlements (Koubodana et al., 2019a). Figure 7.9 and Figure 7.10 show the inter-annual and intra-annual evolution of water cycle components over MRB. The maximum runoff value is displayed in 1991, 1993, 1997, 1999, 2002, 2005 and 2009.

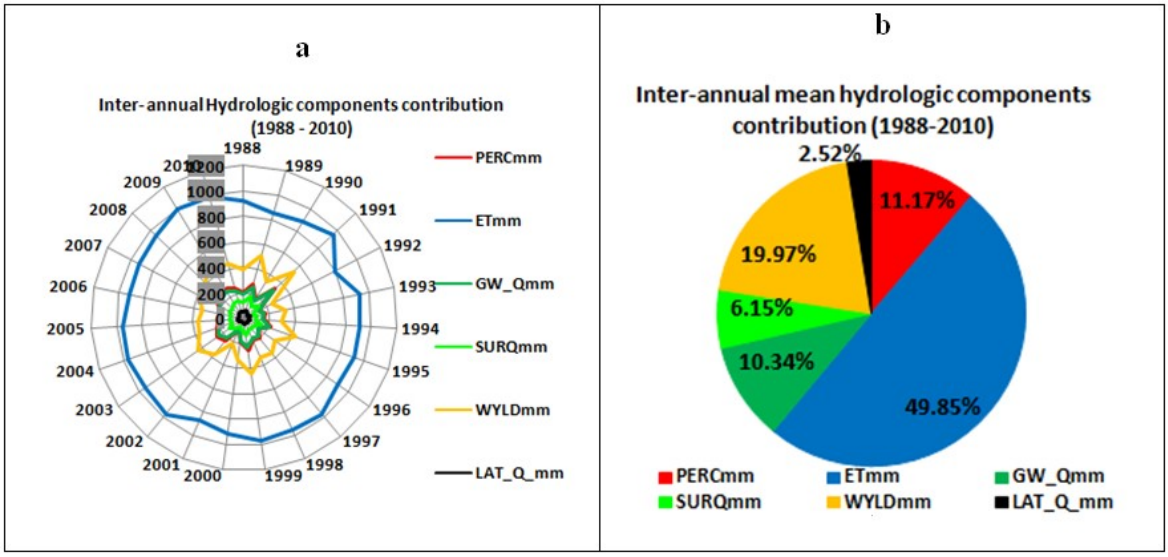

Figure 7.9: Inter-annual variability of hydrological component between 1988 and 2010

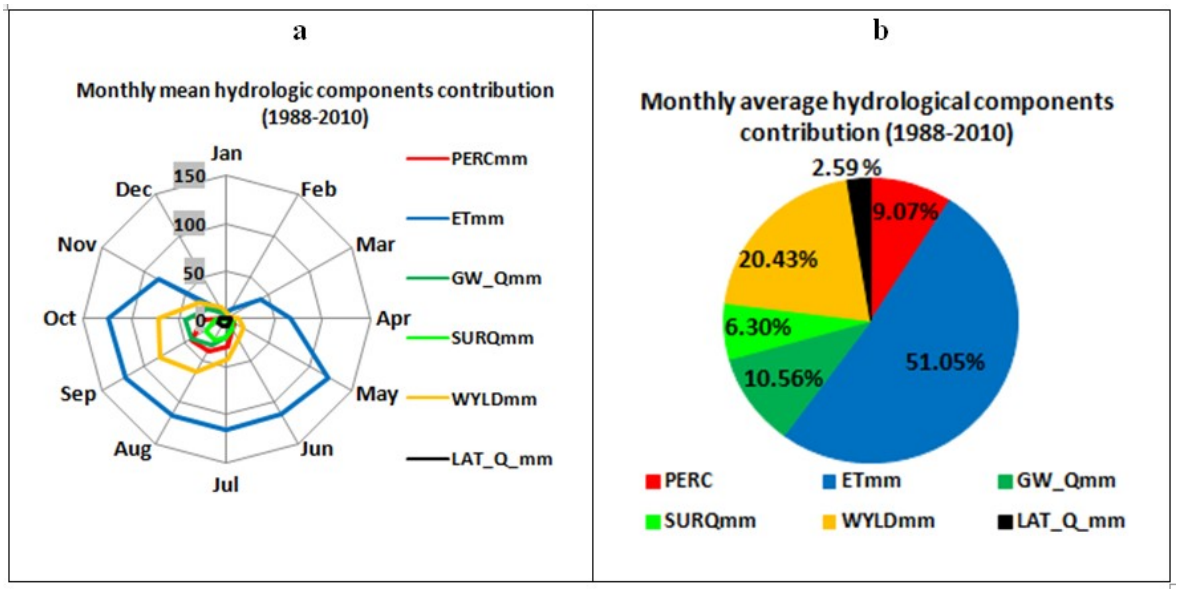

Figure 7.10: Intra-annual variability of hydrological component between 1988 and 2010

The percentages of each water cycle components for inter-annual and intra-annual scale are actual evapotranspiration (49.85%), water yield (19.97%), percolation (11.17%), ground-

water (10.34%), surface runoff (6.15%) and lateral flow (2.52%). Consequently, actual evapotranspiration and water yield components represent more than 60% of the total. The average actual evapotranspiration between 1988 and 2010 is around 900mm/year. Annual mean percolation and groundwater have similar to high value displayed in 1991, 1995, 1999, 2003 and 2008.

By comparison of inter-annual components in the second simulation, there is an increase of actual evapotranspiration and lateral flow whereas a decrease of water yield, surface runoff groundwater and percolation. Contrary to the intra-annually observations there is decrease of percolation, surface runoff and increase of groundwater, lateral flow and actual evapo-transpiration.

7.4.3: Spatial distribution and changes of precipitation

Precipitation is the main parameters in hydrological processes (Rössler et al., 2012; Tuo et al., 2016). Therefore precipitation spatial and temporal distribution impacts considerably other hydrologic component particularly runoff at the outlet. Figure 7.11 shows precipitation spatial repartition at sub-basin levels over the first and second period of simulation.

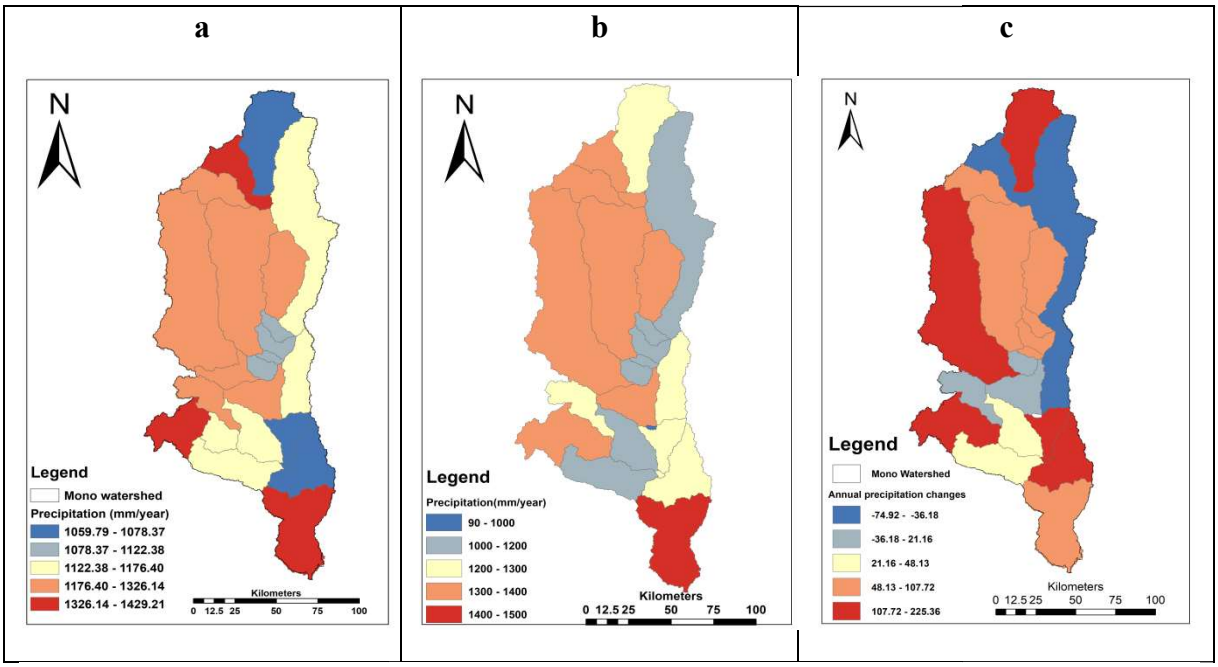

*(**a**), 1988-2010 (**b**) and (**c**) change from (1964-1986) and (1988-2010) periods*

Figure 7.11: Average rainfall spatial distribution between 1964-1986

The results exhibit that the maximum annual rainfall is between 1450 and 1550mm/year and the minimum between 1050 and 1200 mm/year and confirm the conclusion from the observation analysis and others studies implemented in sub-tropical zones (Koubodana et al., 2019b; Oguntunde et al., 2011). The highest amounts of precipitation are observed in

the north-western and the southern basin where there are highest mountains. The south basin of Athiémé sub-basin maximum precipitation is due to the accumulation of the amount of the upstream stations. The lowest annual amount of precipitation (84mm/year) is located in the reservoir sub-basin. Figure 7.11c exhibits annual changes in precipitation from 1988 to 2010 and from 1964 to 1986. This underlines that there are negative changes in precipitation in the east and center sub-basins. Contrariwise, a positive change of precipitation is displayed in rest sub-basin but the changes intensity is more remarkable in the south and west-center sub-basins.

Figure 7.12 underlines the distinction of wet and dry season and showing the monthly rainfall pattern for the whole basin between 1964 and 1986 (a) and between 1988 and 2010 (b). The rainy season begins in May/June and ends in September/October for SIM1 and October/November for SIM2.

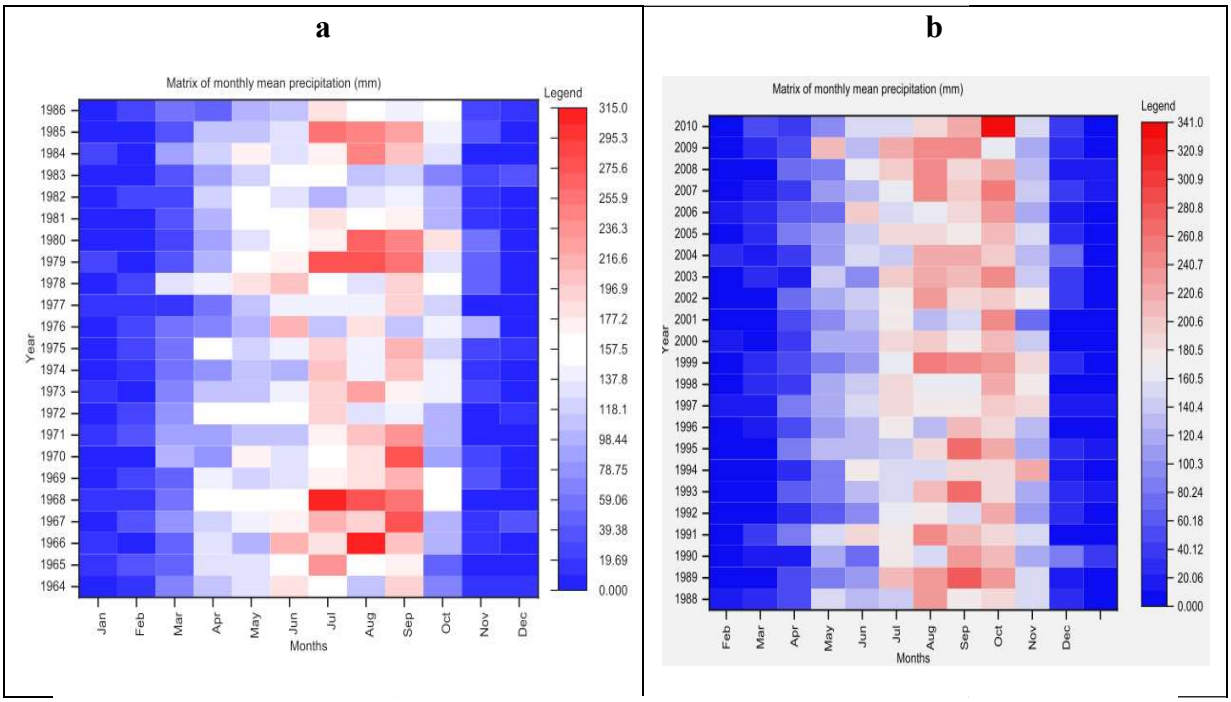

Figure 7.12: Average rainfall spatial and temporal evolution for SIM (a), SIM2 (b)

The peak of rainfall is reached in June, August or September during SIM1 and June, August, September or October during SIM2. The dry season always starts from November/December to March/ April of the following year in the two simulations. There is alteration of unimodal years (1966, 1968, 1979, 1980, 1985 & 1989, 1991, 1993 1995, 1999, 2002, 2003, 2010) and bimodal years (1964, 1974, 1976, 1978& 2007, 2009). Rainfall magnitude between 1988 and 2010 was considerably decrease compare of the intensity between 1964 and 1986 while there is the inverse situation in term of frequency.

7.4.4:Spatial distribution of water balance components(1964-1986)

Figure 7.13(a-f) illustrates the contribution of an individual water balance components in a given sub-basin. The spatial repartition of percolation range between [441 -130mm/year], groundwater [771 -615mm/year] and water yield [654 -330mm/year] (Figure 7.13a-d-e) show a high contribution from the north sub-basins compared to the contribution of the south sub-basins.

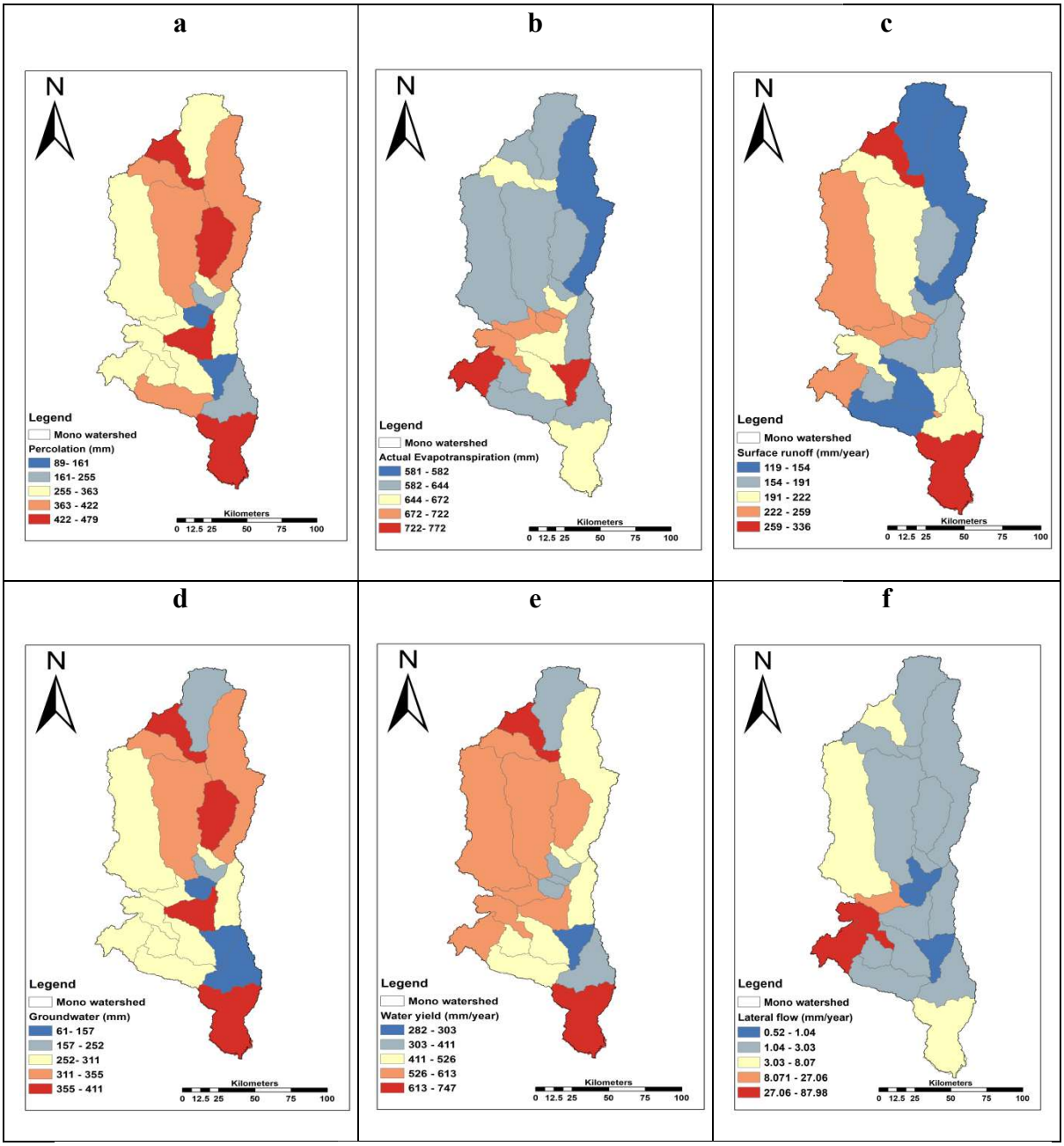

(a) *percolation, (**b**) actual evapotranspiration, (**c**) surface runoff, and (**d**) groundwater contribution (**e**) water yield and (**f**) lateral flow.*

Figure 7.13. Average value of water balance components between1964 and 1986

The very low contribution of water yield and groundwater is located in the south-west where there are the highest mountains. The contribution of actual evapotranspiration (Figure 7.13b) displays a high amount of evapotranspiration in the mountains (South-west) and low in the north sub-basin. In the northern mountains, the potential evapotranspiration is seen to be high. Lateral flow (Figure 7.13f) shows a spot of maximum contribution in the south-west sub-basin whereas in the others sub-basins the annual mean contribution is between 1.30 and 12.89mm/year. Surface runoff contribution (Figure 7.13c) presents some disparities of surface runoff distribution over the sub-basins. Meanwhile, the lowest annual surface runoff is located in the north-east sub-basins whereas the maximum surface runoff located in the south sub-basin.

7.4.5: Spatial distribution of water balance components (1988-2010)

The contribution of a single water cycle component over a sub-basin during the second period of simulation (1988-2010) is displayed in Figure 7.14. From this graph is t clear that water cycle component annual mean amount depends considerably on the sub-basin locations. There are many similarities in the spatial reparation of percolation and groundwater contributions in streamflow in Figure 7.14(a-d). The maximum values of percolation or groundwater are observed in the north-west, center and south of the basin whereas the mean values are detected over the west and center-east sub-basins. The patterns of actual evapotranspiration (Figure 7.14b) show a contradictory situation in many sub-basins. The highest values of actual evapotranspiration are noted in the center and south-west sub-basins. The surface runoff (Figure 7.14c) displays an average amounts in the north, south and south-east sub-basins while the maximum are located at some sub-basins in the north and center of the basin

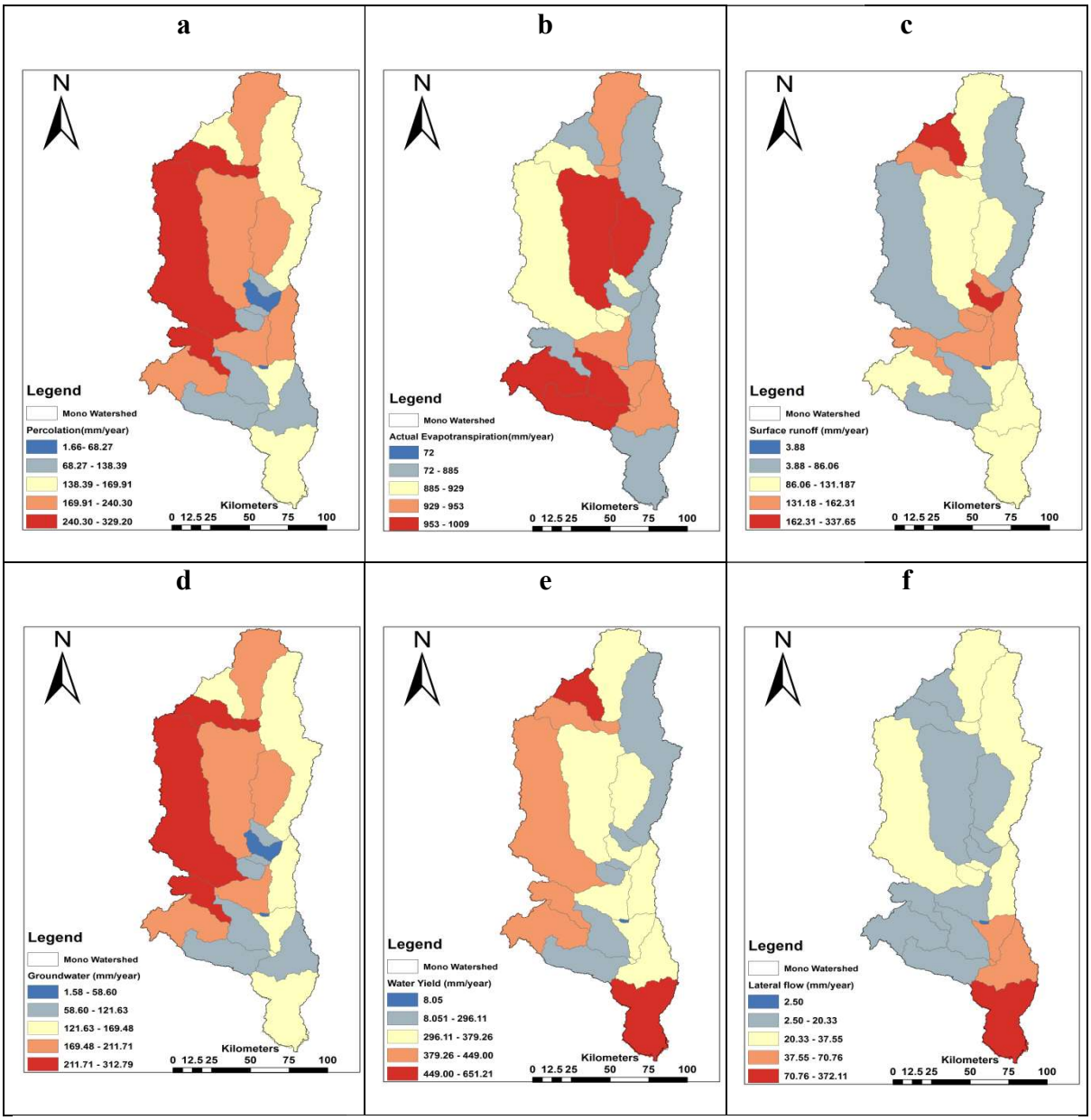

*(**a**) percolation, (**b**)actual evapotranspiration, (**c**) surface runoff, and (**d**) groundwater contribution (**e**) water yield and (**f**) lateral flow*

Figure 7.14: Annual average value in water balance components (in mm/year) between 1988 and 2010

7.4.6: Matrix illustration of hydrological components between 1964 and 1986

Figure 7.15(a-f) exhibits the influence of individual water cycle components between 1964 and 1986. These figures show the distinction between wet and dry months and years over the entire basin. Particularly, actual evapotranspiration (Figure 7.15-**b**) ranges between 3.5 and 135mm/year and the maximum is observed for each year between April and October corresponding to the rainy season. Contrariwise, the minimum of actual evapotranspiration is displayed between November and March which is the dry season. For the other water

cycle components such as percolation, surface runoff, groundwater water yield and lateral flow (Figure 7.15a, c-f), the maximum value are observed between August and October which is the period of peak of rainfall over the study area. Some year underlines the pronounced lowest value of these variables during this season. For example in 1984,1982, 1981, 1977, 1976,1973,1972 and 1964 known in the previous analysis as drought year with negative annual rainfall variability index (Descroix et al., 2009; Yabi and Afouda, 2012).

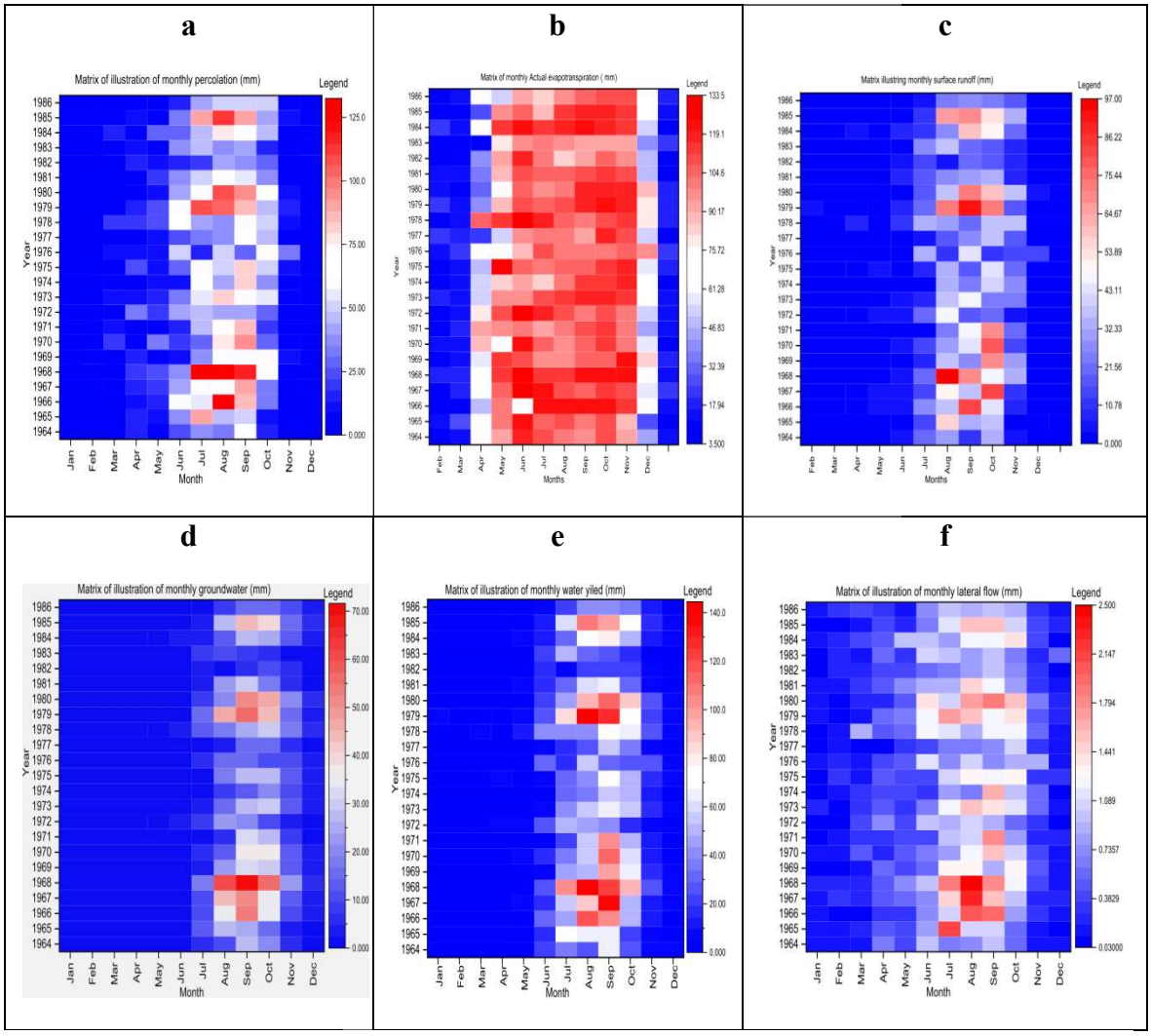

*(**a**) Percolation, (**b**) actual evapotranspiration, (**c**) surface runoff, (**d**) groundwater, (**e**) water yield and (**f**) lateral flow*

Figure 7.15: Matrix illustration of water balance components between 1964 and 1986

7.4.7: Matrix illustration of water balance components between 1988 and 2010

Over the second period of simulation between 1988 and 2010, water cycle component monthly variability per year is presented in Figure 7.16(a-f). This figure reveals that the high values of actual evapotranspiration are seen between May and October of the year and the others months (November to April) are characterized by the low actual evapotranspiration. The others components of hydrological cycle, the maximum is obtained between July

and October. There are years with lowest surface runoff over the year of 1988, 1992, 1996, 1997, 2000, 2001, 2002, 2004 and 2005 which are the year of drought in the region.

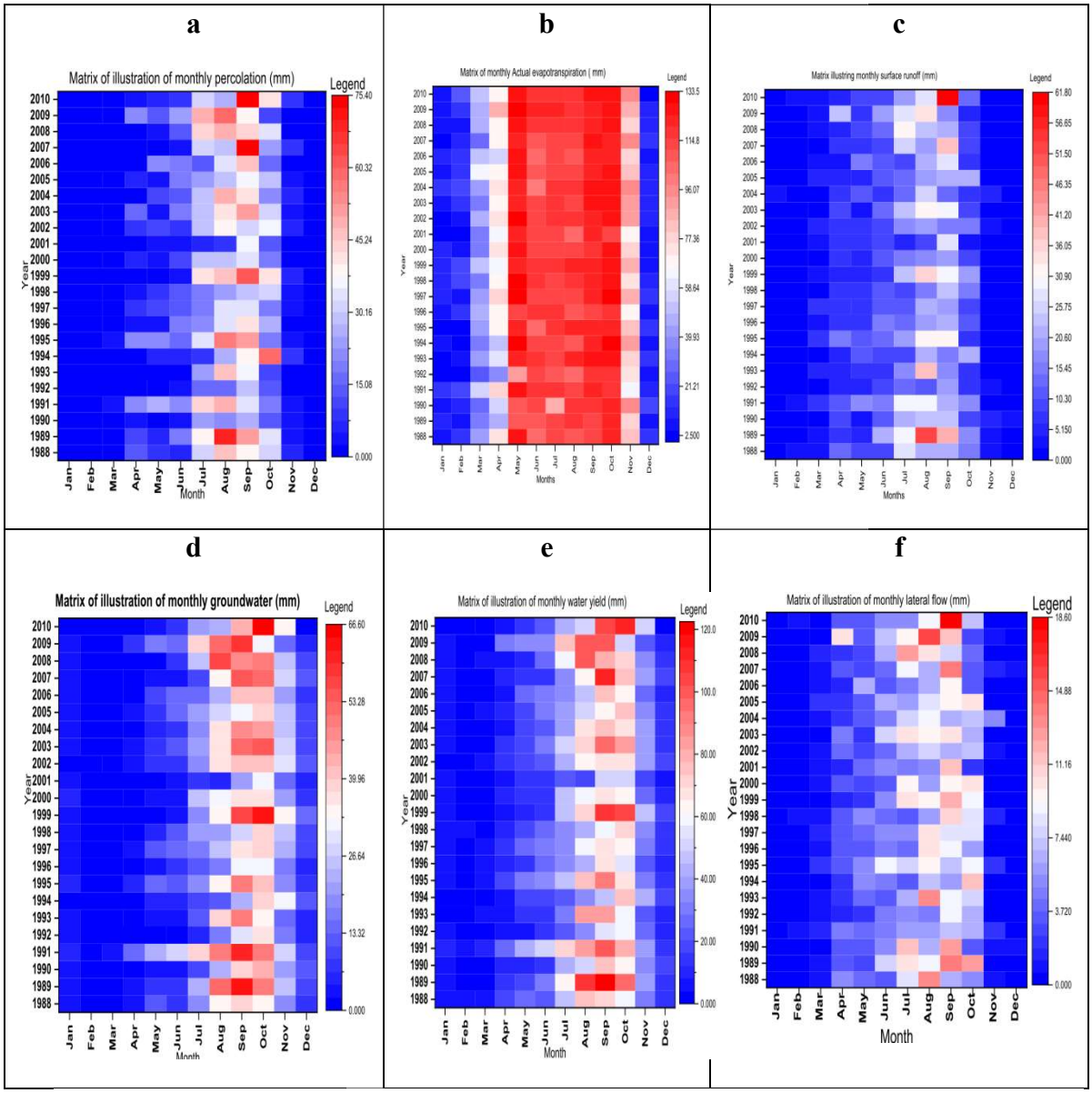

(a) *Percolation, (**b**) actual evapotranspiration, (**c**) surface runoff, (**d**) groundwater, (**e**) water yield and (**f**) lateral flow.*

Figure 7.16: Matrix ilustration of water balance components between 1988 and 2010

7.5: Land cover, climate change and dam management impacts on water resource

Knowledge about land use and land cover (LULC) dynamics is of high importance for a complete water resource management at a given watershed. Therefore land use and land cover change was estimated between 1975 and 2000. The major land use changes are observed in savanna; forest, agriculture and cropland (Table 7.6). Between 1975 and 2000; there is 12.27% of decrease of savanna estimated at 2701.08 Km^2 of losses savanna, 2.35% (517.32 Km^2) of decrease of forest, 15.35% (3379.10 Km^2) increase of agriculture land,

1.29% (283.98 Km^2) increase of Cropland and fallow with oil palms as majors land cover over Mono river basin. The results confirmed the analysis of (Koubodana et al., 2019a) over the basin. Figure 7.17 shows land use and land cover changes between 1975 and 2000 and water components annual mean for (1964-1986) and (1988-201 0) sub-periods.

Forest and savanna are decreased and could be explained by agriculture expansion, bush fire, timber extraction and linked by population growth (Atsri et al., 2018; Koglo et al., 2018; Kokou et al., 2005; Koubodana et al., 2019a), Togo and Benin countries are characterized by an exponential increase of population which involve need of land for agriculture activities and for habitation, people use wood as an energy source, another cause of deforestation.

Table 7.6: Land use and land cover area and changes area for the period 1975-2000

Code	Land use/ cover name	Land use area 1975		Land use area 2000		Change area 1975-2000	
		[Km^2]	[%]	[Km^2]	[%]	[Km^2]	[%]
FRST	Forest	1184.34	5.38	667.02	3.03	-517.32	-2.35
RNGE	Savanna	16737.02	76.03	14035.94	63.76	-2701.08	-12.27
WETN	Wetland-floodplain	4.40	0.02	72.65	0.33	68.24	0.31
AGRR	Plantation/Agriculture	1426.49	6.48	4805.59	21.83	3379.10	15.35
WATR	Water bodies	4.40	0.02	114.47	0.52	110.07	0.50
URBN	Settlements	68.24	0.31	107.87	0.49	39.62	0.18
FRSE	Gallery and riparian forest	1144.71	5.20	942.19	4.28	-202.53	-0.92
RNGB	degraded forest	860.74	3.91	435.87	1.98	-424.86	-1.93
FRSD	Woodland	94.66	0.43	59.44	0.27	-35.22	-0.16
OILP	Cropland and fallow with oil palms	488.70	2.22	772.68	3.51	283.98	1.29
Total	-	22013.70	100.00	22013.70	100.00	0.00	0.00

The land use and land cover changes between 1975 and 2000 have repercussion on water balance components of 1964-1986 and 1998-2010 over the study area. Consequently, the results show that there are significant decreases of forest, savanna and increases of agricultural land involve an increase of precipitation, actual evapotranspiration and lateral flow over the second period of simulation compared to the first period of simulation. The other component displayed a decrease in the second period of simulation. According to (Verstraeten et al., 2008) ET is the process whereby water originating from a wide range of sources is transferred from the soil compartment and/or vegetation layer to the atmosphere. Therefore, any change in land cover (leaf index area) or land use will affect ET intensity.

Soil characteristics and climate condition also impact on water balance components variation (Sciuto and Diekkrüger, 2010).

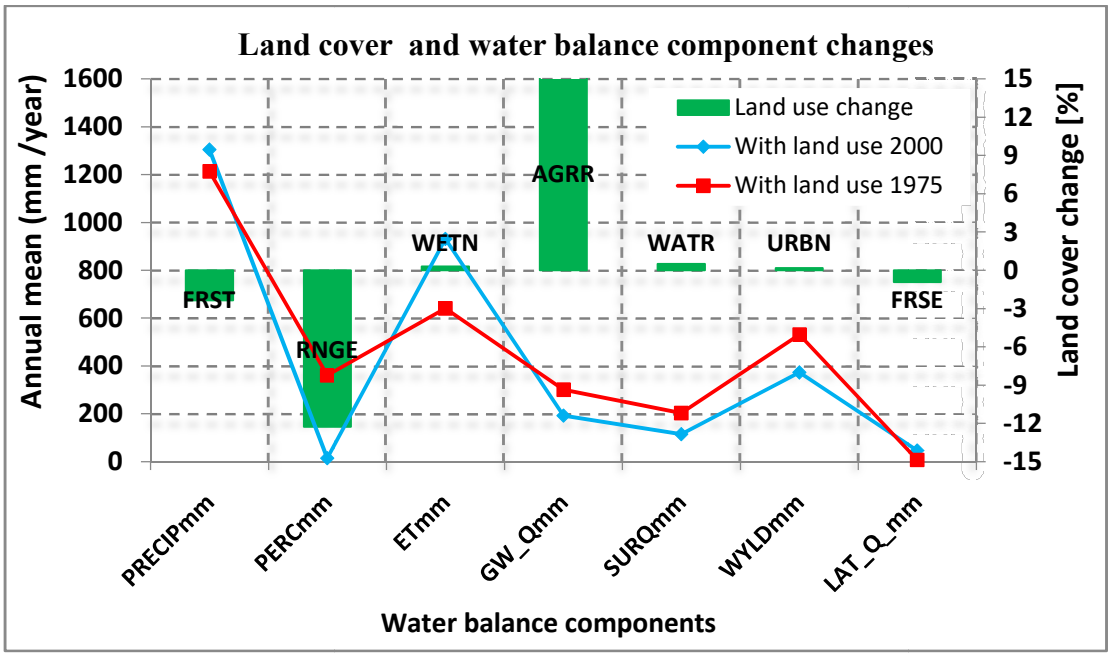

Figure 7.17: Land cover and water balance components contribution changes

Figure 7.18 displays the intra-annual average change of a single water balance component between 1964-1986 and 1988-2010 sub-periods. Except percolation which change is totally negative over a year, the other water balance components changes are significant and depending on the season or the months. Nevertheless, surface runoff and percolation decrease are important (Figure 7.18-a&b) between June and November which is the rainy season in the Mono river basin. Groundwater change is positive at each month and very significant between July and November whereas, actual evapotranspiration change is negative between December and April and positive between the rests of the year. Lateral flow and water yield change are positive over year except some month where it is negative. Figure 7.18-**b** reveals the intensity of water balance change in absolute values is ranged from percolation (31.94%) to actual evapotranspiration (6.88%).

Finally, Figure 7.19 exposes the individual water balance components annual average spatial changes at sub-basin level of annual percolation (Figure 7.19-**a**), water yield (Figure 7.19-**b**), surface runoff (Figure 7.19-**c**), groundwater (Figure 7.19-**d**), water yield (Figure 7.19-**e**) and lateral flow (Figure 7.19-**f**).

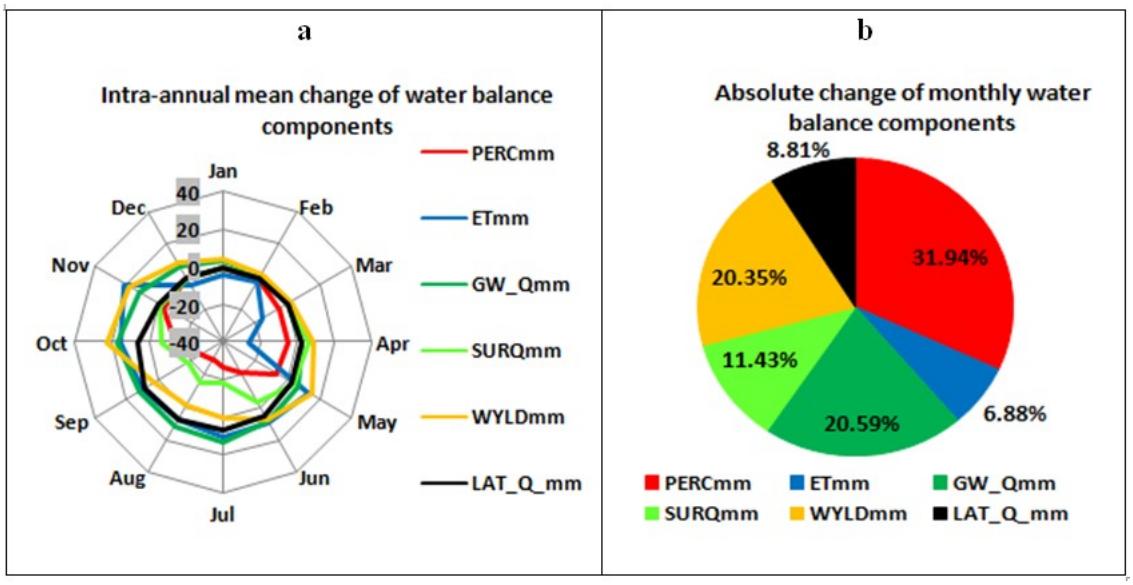

Figure 7.18: Monthly average changes of hydrological components contribution between (1964 -1986) and (1988-2010) sub-periods

In concrete terms, groundwater, percolation, water yield and surface runoff contributions show a decreasing trend in almost all the sub-basin over the whole basin (See Table 7.7). Particularly, the trend intensity is high in the location where there are significant change trend of forest to savanna, forest to cropland and savanna to cropland between 2000 and 2013 (Figure 4.3). ET and Lateral flow present a positive change in most of the sub-basins. Meanwhile, ET positive change intensity is more important in center and south-west sub-basin where lateral flow changes are completely negative. Many sub-basins in the mountain located in the western of the basin with forest and where the soils are with subsurface accumulation of low activity clays and high base saturation (Table 2.3) are characterized by significant negative change of percolation, groundwater, water yield and a positive change of ET.

Table 7.7: Water balance components contribution for different temporal scales

Scale	**Inter-annual average**		**Intra-annual average**	
Period	1964-1986	1988-2010	1964-1986	1988-2010
PERCmm	17.67	11.17	17.53	9.07
ETmm	31.33	49.85	51.02	51.05
GW_Qmm	14.71	10.34	5.67	10.56
SURQmm	9.94	6.15	9.43	6.30
WYLDmm	25.95	19.97	15.93	20.43
LAT_Q_mm	0.40	2.52	0.42	2.59
Total	100.00	100.00	100.00	100.00

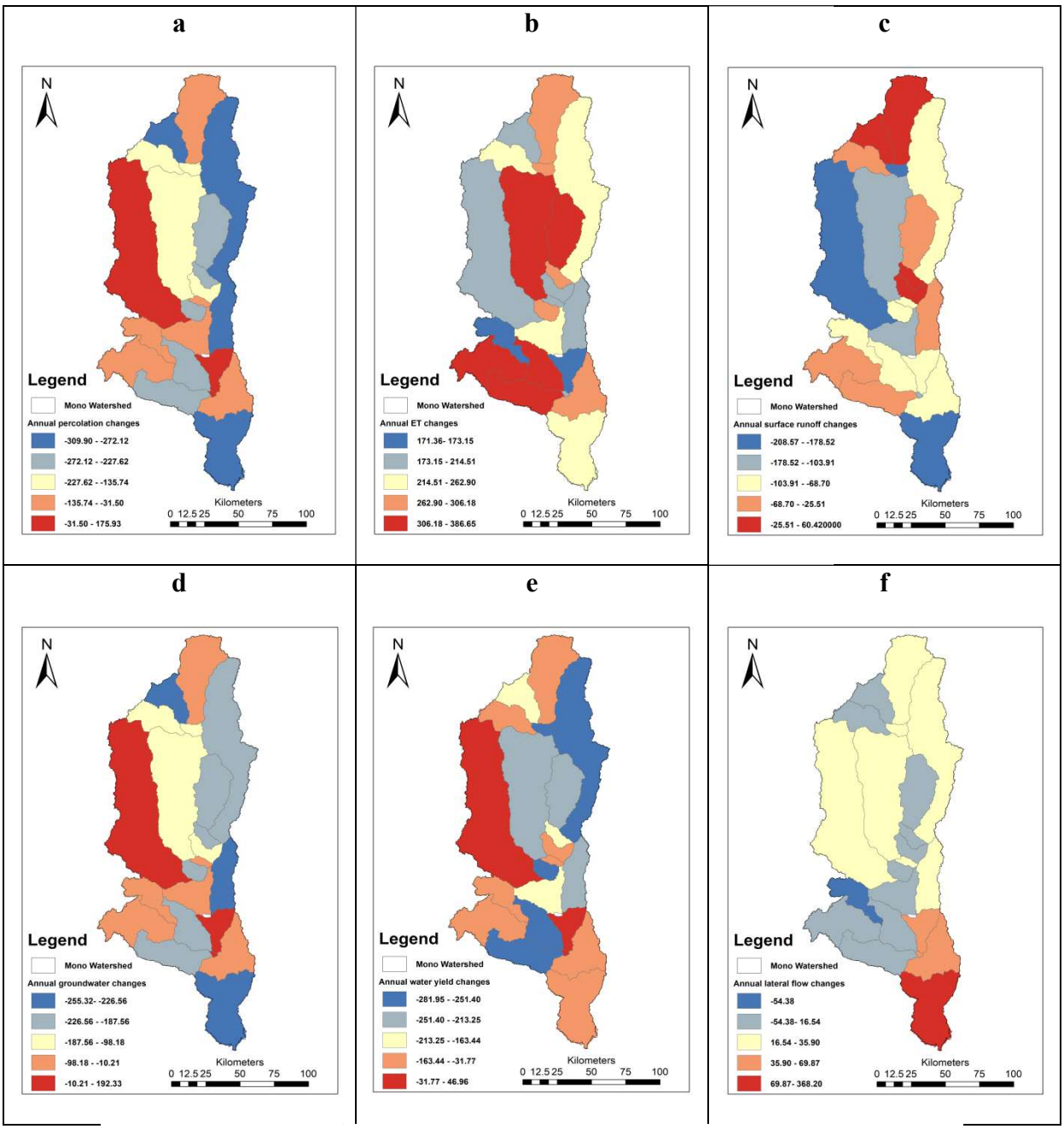

Figure 7.19: Annual average spatial changes of water balance components contribution between (1964-1986) and (1988-2010)

7.6: Discussion

7.6.1: Model evaluation and spatio-temporal analysis of water balance components

SWAT model was set up, calibrated and validated at four discharge gauged stations and for two different periods: Periods of pre-dam installation (1964-1986) and period of post-dam installation (1988-2011). Model performances and uncertainties depend strongly on the period of simulation and the location of the discharge gauge stations (upstream or down-stream of the reservoir). The method used for model performance and uncertainty is Se-

quential Uncertainty Fitting procedure (SUFI-2) (Abbaspour et al., 2004). This method was chosen because of the comparative studies using the methodologies such as Parameters Solution (ParaSol) (Van Griensven and Meixner, 2006), Generalized Likelihood Uncertainty Estimation method (GLUE) (Beven and Binley, 1992)and Particule Swarm Optimization (PSO) (Kennedy and Everhart, 1995).

Indeed, Figure 7.1 displays the hydrographs over pre-dam period observed and simulated discharge at Corrokopé, Tététou and Athiémé stations and Table 7.1 model performances statistics. The results indicate very good KGE ≥0.75 and PBIAS< ± 10; acceptable NSE and R^2 (0.50<NSE or R^2<0.65) in most of the station except at Corrokope validation periods. This can be explained by the capability of the SWAT model to well reproduce hydrological process in tropical region as in many studies (Bossa et al., 2012; Hiepe and Diekkrüger, 2007; Näschen et al., 2018; Obuobie and Diekkrüger, 2008; Poméon et al., 2018). Over the second period of simulation (1988-2011), there is a weakness of the model to simulate discharge particularly in the downstream station of Tététou and Athiémés justified by performance statistics and hydrographs (Table 7.1 and Figure 7.2). The implementation of Nangbéto reservoir constructed in 1987 has significantly modified the river from natural to artificial hydro-sedimentary system in the downstream as concluded by many studies in the Mono river basin (Amoussou et al., 2014, 2012; Rossi, 1996). SWAT model calibration, validation and uncertainties were applied by following SWAT-CUP techniques (Abbaspour, 2015) and keeping the model parameterizations with a reasonable value compared to the others analysis using SWAT model in surrounding watersheds (Hounkpè et al., 2015; Poméon et al., 2018). Although, thirteen parameters were known to be more sensitivity (Table 7.2), calibration and validation processes were performed for all gauged station considering a specific land use and soil texture in order to increase performance results. These parameters are average slope length (SLSUBBSN), Manning's "n" value for overland flow (OV_N), soil evaporation compensation factor (ESCO), Maximum canopy storage (CANMX), SCS runoff curve number (CN2), groundwater "revap" coefficient (GW_REVAP), baseflow alpha factor (ALPHA_BF), groundwater dalay (GW_DELAY), treshold depth of water in the shallow aquifer (GWQMN), Available water capacity of the soil layer (SOL_AWC), moist bulk density (SOL_BD), and saturated hydraulic conductivity (SOL_K) which govern the lateral, horizontal and vertical water flow (Cornelissen et al., 2013; Schuol et al., 2008).With the acceptable results of SWAT model prediction, it was possible to analyze at different temporal scale of simulated discharge in the basin.

The inter-annual graphs (Figure 7.3 and Figure 7.7) of simulated discharge reveal the periods of high and low discharge. For example over the years of 1967, 1968, 1989, 1991, 1998 and 2010, it is displayed the highest discharge related to the year flooding whereas the years from 1970 to 1980, 1992 and 2002 show the lowest value of discharge involving drought years. The results confirmed the past conclusions in the zone. As illustration Amoussou et al. (2014) used GR4J model and a Frechet-type generalized extreme value (GEV) distribution to determine peaks flow in the upstream-downstream of Nangbéto dam. And results have shown that the installation of Nangbéto dam in 1987 has modified the hydrological system of the basin particularly for the lower Mono. Koubodana et al. (2019b) performed a trend analysis over long period of hydro-climate variables and deduced that the same years were characterized by negative and positive rainfall variability index over MRB. The intra-annual graphs of discharge of Figure 7.4 and Figure 7.9 exhibits that simulated discharge reaches it maximum in the months of September and October which exactly correspond to the maximum rainfall in subtropical regions (Amoussou, 2010; Djaman et al., 2017; Koubodana et al., 2019b). Figure 7.8a and Figure 7.10a demonstrate that the maximum of some water balance components is reached between May and October as summarized values in Appendix 7.7 and Appendix 7.8. This season coincides with the rainy season in the sub-tropical zone. Consequently, the contribution of the others components strongly depends on precipitation variations which is the main driver in hydrology process (Tuo et al., 2016).

7.6.2: Spatio-temporal analysis of water cycle components

Section 7.4 comments on the spatial and temporal results of water cycle components between 1964 and 1986 and between 1988 and 2010 sub-periods. For water management strategy planning, analysis of individual water balance component contribution at temporal and spatial scales is required. Sathian and Symala (2009) indicate that precipitation, actual evapotranspiration, percolation, groundwater, surface runoff, water yield and lateral flow are the most important components of water balance in a watershed. Within these components, precipitation is an input variable in hydrological models such as SWAT and the others need to be predicted because of inexistent observation data (Ghoraba, 2015). Actual evapotranspiration and water yield components contribution are important over the two periods of inter-annual and intra-annual scales as displayed in Figure 7.7, Figure 7.8, Figure 7.9 and Figure 7.10. Actual evapotranspiration is the highest amount of water loss by the watershed in annual and monthly mean scale. The high amount of actual evapotranspiration can be explained by the various type of vegetation and also by the increase of tem-

perature in the study area (Koubodana et al., 2019b; Lawin et al., 2019). Meanwhile, it is important to note that actual evapotranspiration has increased from 31.33% (1964-1986) to 49.85% (1988-2010) in inter-annual time scale and from 51.02% (1964-1986) to 51.05% (1988-2010) for intra-annual period. This increase of water actual evapotranspiration from the pre-dam period to post-dam period is due to the increasing CO_2 concentrations in the atmosphere, land-use and land cover changes or decreasing wind speed (Koubodana et al., 2019a, 2019b). The second major water component is water yield which is net amount of water that leaves the sub-basin or the basin and contributes to streamflow in the reach during the time step. It is computed as WYLD = SURQ + LATQ + GWQ – TLOSS – pond abstractions. Therefore, an important amount of precipitation percentage received by the watershed of all case is lost as streamflow. The amount percentage is ranging from 0.40% (1964-1986) to 2.52% (1988-2010). According to Figure 7.7b and Figure 7.9b, water yield decreases from 25.95% between 1964 and 1986 to 19.97% between 1988 and 2010 at inter-annual scale whereas Figure 7.8b and Figure 7.10b show in intra-annually the amount has decreased from 15.93% (1964-1986) to 20.43% (1988-2010). Lateral flow is the lowest (1988-2010) for inter-annual average and from 0.42% (1964-1986) to 2.59% (1988-2010) for intra-annual average. This can be due to the low infiltration rate and also that lateral flow depends on the watershed local slope (Cornelissen et al., 2013) which is not uniform in the basin and ranges from 12 to 948m. The results of water cycle components contribution confirmed most analysis performed in West Africa (Akpovi et al., 2016; Awotwi et al., 2015; Begou, 2016; Hounkpè, 2016). Over inter-annual analysis of the two sub-periods, many years are associated with high and low contribution of surface runoff compared to the average over the period. For example 1968, 1979, 1980, 1995, 1999 and 2003 runoff contribution is higher and with positive rainfall index in section 5.2 (Koubodana et al., 2019b). The years of 1977, 1982, 1983, 1986, 1990 and 2002 present the period with lowest surface runoff and associated with negative rainfall variability index in section 5.2 and confirmed the years of drought in West Africa (Koubodana et al., 2019b; Oguntunde et al., 2006; Yabi and Afouda, 2012).

The spatial analysis of water balance components in sections 7.4.4 and 7.4.5 reveals that its contribution depend strongly on the sub-basin, sub-basin position and the sub-period of simulation. In particular, the greatest amount of precipitation falls in the north-western and the southern sub-basin of mountainous area and is also located in the sub-basin of Athiémé over the two sub-periods. This is explained by evaporation and convection caused by the thermal inertia of this mass of water significantly increases moisture cloud of orographic

lift. (Robert) 2013 by modeling the pond slope in the Mono River basin reveals that average of the annual rainfall is about 1340 mm with a maximum of 1700 mm in mountains regions.

Rainfall matrix of Figure 7.12 shows the monthly precipitation average from 1964 to 1986 sub-period and also from 1988 to 2010. The results confirmed that in the Mono river basin, the climate is unimodal and bimodal according to the past studies (Amoussou et al., 2014). Figure 4.4.4 exhibits the low contribution of water yield and groundwater in the south-west, and the actual evapotranspiration seems important in the south-west where there are high mountains.

Figure 7.15 and Figure 7.16 show the matrix illustration of water cycle components between 1964 and 1986 and from 1988 and 2010 sub-periods. These figures illustrate the dry and wet months and years over the entire basin. It displays also the nature of the season assigned in the basin. The results reported that most of water balance components reach their peak between July and October which is exactly the period of rainy season in sub-tropical zone (Djaman et al., 2017; Giertz and Diekkrüger, 2003; Laux et al., 2009). The period of 1964, 1984,1982, 1981, 1977, 1976,1973, 1972, 1988, 1992, 1996, 1997, 2000, 2001, 2002 and 2004 characterized by a very low amount of surface runoff and precipitation are justified by the year where drought occurred in West Africa (Laux et al., 2009; Louvet et al., 2016; Omotosho and Abiodun, 2007).

7.6.3: Climate, land use changes and dam management impacts on water resources

A reclassified data from CILSS database results indicates that land use change significantly between 1975 and 2000 and justified by drivers such as population growth. It must be noticed that, the results could be better if land use data were collected from a supervised classification of remote sensing data such as LANDSAT 7, 8 or sentinels-2 with high spatial resolution (Ahmad and Sufahani, 2012; Pereira et al., 2016; Pontius and Millones, 2011). Nevertheless, we concluded that decrease of forest and savanna flowed by an increase of cropland and settlements has occurred in Mono River basin between 1975 and 2000 (Koubodana et al., 2019a). And this is really what is occurring in the study area. The uncertainties can be found in the statistics along with LULC maps.

Globally, SWAT model performed reasonable results over MRB despite several limitations found in the model application and data availability which need to be taken into consideration in future hydrological modeling in MRB. The main issue in this study in the limitation

of data accessibility like daily relative humidity, solar radiation, wind speed and reservoir inputs data (Bormann, 2005; Giertz et al., 2006). Further, SWAT simulation in MRB must be taken into consideration the elevation bands due to the topography and high relief in order to account for orographic precipitation patterns, as well as altitudinal temperature change (Neitsch et al., 2011.).

The combined impacts of land use changes and climate variability induce the increase of precipitation, actual evapotranspiration and lateral flow whereas decrease in percolation, groundwater, surface runoff and water yield were found. One of the reason of this situation is that the conversion of forest and savanna in cropland caused the change in surface soil layer and vegetation canopy(Wagner et al., 2009). These confirms that land use and land cover play an important role in local water cycle components changes, water infiltration, evaporation and movement (Hagemann et al., 2014).

7.7: Partial Conclusion

This study focuses on the prediction and comparison of streamflow based on different land use scenarios and climate conditions. Afterward predicted water balance components contribution were assessed over the two sub-periods to develop sustainable adaptation measures to mitigate with the possible impacts of climate and land use changes in the the Mono river basin. The analysis has been achieved by simulating a semi-distributed SWAT hydrological model interfaced with Window GIS software, a well-documented tool for effective water management. For a successful model setup, calibration and validation, soil, DEM, topography, land use, weather daily data and hydrological database are necessary. The model simulation outputs discharge were compared with daily measured datasets at Athiémé, Tététou, Nangbéto and Corrokopé gauge stations for both calibration (1964-1975 & 1988-2000) and validation(1976-1986 & 2001-2011) over the two periods of model simulation. A good model performances and uncertainties (R^2> 0.60; KGE ≥ 0.60 and PBIAS ≤ ±4.5) at daily scale show acceptable parameters values range during the first simulation period and poor performances (R^2<0.50; KGE <0.50 and PBIAS ≥ ±25) during the second simulation period. The calibrated model was used to detect the intra-annual and inter-annual variability of runoff at gauged station and then to assess the impacts of climate, land use change and dam management on water balance component contribution over the two sub-periods. The results show that at intra-annual scale runoff reaches its peak between September and October corresponding to the maximum of rainfall in the area whereas the intern-annual analysis displays the years of drought and floods in the wa-

tershed determined by the highest and lowest runoff simulated. Concerning water balance component contribution, the runoff, evapotranspiration and water yield evolution depend strongly on different land-use type change, climate conditions and also on the presence or not of reservoir in the watershed. These outputs have revealed that the implementation of the dam in the MRB in 1987 has affected consequently the hydrological system of the river. Land use land cover change with the amplification of climate change and the others drivers have accelerated water resource fluctuation in the Mono river basin.

Overall modeling results suggest that SWAT model is a potential tool for studying runoff and water balance components response under different land cover geo-data and climate conditions of a watershed. The results indicate that GIS-based SWAT model implementation is a highly valuable tool to support policies and decision-making by relevant authorities in West Africa for a sustainable water resource management at watershed level.

Finally, there is a strong need to develop sustainable adaptation measures in future studies, particularly at a local scale where the impact is happening, to mitigate the possible impacts of the projected change in climate.

The performance of semi-distributed or distributed model can be enhanced in further analysis by integrating more climate data such as solar radiation, relative humidity and wind. These studies can investigate in more detail future scenarios land use and climate impacts on water balance components.

Chapter 8: General conclusion, recommendations and perspectives

This chapter presents the general conclusion regarding all the findings of the study, emphasizing on the significance of the results for sustainable decision making processes, the limitations of the study and giving some recommendations for future studies.

Mono River Basin, the major border river shared between Togo and Benin Republics and which host the Nangbéto dam for electro-electricity production is of upmost importance for the two countries. The second roles of the reservoir are promotion of agriculture irrigation area at Dévé location and fishery and the regulation of the streamflow at the downstream. The river will continue to experience irrigation expansion and rising domestic and industrial water demands due to population growth and urbanization in sub-tropical region. Actually, the major challenge in this river basin is the global climate change (CC) coupled with land use/cover change, rapid population growth, urbanization, increase of food demand, need of water for agriculture, energy for households and industries. Therefore, a sustainable and participatory investigation on these real challenges can enable the appropriate measures for efficient and sustainable integral land use, land cover changes (LULCC) and dam management for water resources control of the river basin. This will be important for local communities and for understanding the impacts of CC and LULCC on the water balance components.

The present study is the first attempt of modeling the impacts of climate change, land use change and dam management on water balance components in the MRB and the methodology adopted is structured on:

- Land use and land cover datasets evaluation trough accuracy assessment, land cover prediction (2020 and 2027) using the tool of land change modeler of TerrSet IDRISI software,
- Mann Kendall trend analysis to detect climate change on historical hydro-climate data sets and RclimDex was used for extreme climate indices computation of two future scenarios between 2020 and 2045
- Two lumped model calibration and validation over two sub-periods (pre-dam and post-dam installation) and evaluation of models performances analysis/ uncertainty analysis for discharge prediction in the basin
- Finally, a semi-distributed model of SWAT was used to integrated dam management information, land use, soil, relief and climate data to predict discharge at four

gauging stations and over the two sub-periods. And then, Sequential Uncertainty Fitting procedure (SUFI-2) was used for the sensitivity analysis, model calibration and validation of daily discharge. Furthermore, the calibrated model was used to investigate the impacts of land use land cover dam management and climate change on water balance components for the two sub-periods.

The conclusions and recommendations drawn from findings of the present study are as follows.

8.1: Land use/cover datasets evaluation and prediction over Mono River Basin

To evaluate the accuracy of CILSS (2 km resolution), ESA-CCI (300 m) and Globeland (30 m) datasets and select the best for further analysis, land cover reclassification, land cover assessment and Validation were performed using reference points in the watershed derived from satellite images. The most accurate data set of CILSS among all shows a decrease of savanna and forest in the period 1975 to 2013 and an increase of cropland. The increase of cultivated surface area of 30.97% from 1975 to 2013 can be related to the increase in population and their food demand, while the losses of forest area and the decrease of savanna are further amplified by using wood as energy sources and the lack of forest management. The three datasets were used to predict future land cover change using the Terrset Land Change Modeler. The validation of the model using CILSS data for 2013 showed a quality of 50.94%, it is only 40% for ESA-CCI and 20% for Globeland30. The good performance of CILSS data allows the predictions of the land cover for the years 2020 and 2027. The results show that a high spatial resolution is not a guarantee of high quality. However land use and land cover change is not the only cause which impacts water resource management. It is also important to look at the climate variable usually by trend analysis. Many studies in West African have displayed similar conclusions in the watershed around Mono river basin. But since a hydrological system is not only affected by land use and land cover change, it is also important to look climate variables trend trends over a long period in the basin.

8.2: Climate change detection and future extremes indices determination

To analyze the climate variability, non-parametric Mann Kendall (MK) trend analysis have been used on historical hydro-climatic data (1961-2016), an ensemble climate model developed was selected for a computation of 16 Expert Team on Climate Change Detection and Indices (ETCCDI) temperature and rainfall extremes indices. The climate indices are

evaluated using MK test and annual trend analysis for two Representative Concentration Pathways (RCP4.5 & RCP8.5) future scenarios from 2020 to 2045 over Mono River Basin (MRB). The results indicate a positive and negative trend of hydro-climatic data over MRB from 1961 to 2016. Particularly, mean temperatures increase significantly in the watershed whereas a negative non-significant trend is remarkable in rainfall. Furthermore discharge in the gauging stations presents a significant seasonal and annual positive or negative trend. The Despite the ensemble climate model under-estimates slightly observations climate datasets with a linear regression and spatial correlation coefficients higher than 0.6, it has been used to compute extreme climatic indices under RCP4.5 and RCP8.5 scenarios. The computed extreme indices indicate a significant annual trend of some extreme climatic indices of rainfall and temperature at selected stations between 2020 and 2045 in the MRB Previous studies showed an increasing trend in temperature at many available synoptic stations of the basin. This indicates the evidence of global warming at local scale and it probable effect on rainfall patterns. Because climate data are the main drivers in hydrological process, an investigation of surface runoff response with lumped model can be done to understand its variability over time.

8.3: Discharge prediction and comparison with lumped hydrological models

To test and to assess runoff variability performance at Athiémé outlet of Mono River Basin (West Africa), two lumped models: GR4J (Génie Rural à 4 paramètres Journaliers) and IHACRES (Identification of unit Hydrographs and Component flows from Rainfall, Evapotranspiration and Stream data) were used over two different periods. The models use less inputs data with easy computation to predict runoff at the downstream of the river. The lumped models performances of discharge predictions of the two models are statically acceptable for the pre-dam period (1964 – 1986) and more and less acceptable during post-dam period (1988-2011). Two lumped model under-estimates extreme high while IHACRES presents a shift of runoff with observations. Therefore the robustness of the predicted runoff depends of the period of simulation and also on the type of model used. Truly, additional affects of land cover, soil proprieties, geological layers, climate conditions and dam managements are also impacting the runoff generation and evolution of the whole basin. This is the reason why a distributed model which considers all above parameters cited in the modeling was used to give in detail Mono river hydrology system mechanism and their effects on water balance components.

8.4: Hydrological modeling and impacts on water balance components

To understand the impacts of climate change, land-use changes and reservoir management on streamflow and water balance components can allow the development of sustainable water resources strategies. Thus a semi- distributed hydrological of Water Assessment Tool (SWAT) was applied over two baseline scenarios with different land use, climate conditions. Two baselines are considered during SWAT model simulation of water component in the basin (pre-dam and post-dam). Using Sequential Uncertainty Fitting procedure (SUFI-2) for the sensitivity analysis, model calibration and validation at daily time step over the two periods, the hydrologic components over the two periods are simulated and compared. There are good model performances with acceptable parameters values range during the first simulation and poor performances during the second simulation. Results indicate that the surface runoff, evapotranspiration and water yield evolution depends to different land-use type change, climate conditions and also to the implementation of Nangbéto reservoir in the watershed.

8.5: Final conclusion

As conclusion, the SWAT model can be used for water management assessment in the region and for the future prediction of water availability under different climate scenarios. The study has proposed effective strategies for better planning and management of water resources under climate change issues in West African basin or in the world. Therefore, relevant governmental politics are needed to elaborate strategies and measures to cope with projected climate changes impacts in the country.

In general, if the methods used in study have allowed obtaining reliable and useful results, it is important to underline their limitations for further research and uncertainties reduction in the estimations and predictions.

8.6: Limits of the study

Despites the interesting outputs, some limitation faced must be enumerate for the new future analysis in the basin.

- The use of reclassified land use and land cover data has some repercussions on the results; therefore classification of high resolution remote sensing data can be more accurate.

- In addition SWAT model needs several reservoir data which were difficult to access therefore future analysis need the all reservoir data
- During SWAT modeling elevation band were not considered for precipitation and temperature adjustment according the elevation changes
- SWAT model have several parameters and this impact on model calibration and validation, for future analysis model developed such tropical catchment is needed.
- The directives of "Plan National de developpement (PND)" in Togo/Benin were not considered in the study and need to be take in account in the future to improve the results of this thesis.

8.7: Recommendations

The following recommendations are made for sustainable the management of the Mono River Basin and further research:

To decision makers:

- Sensitization of local communities on the impacts of deforestation, no structural agriculture practice which accelerate the changes of land use and land cover with consequences in the hydrology system of the basin
- Restoration and supervision of hydro-climatic station in the basin in order to have regular and good data for an accurate analysis in the future
- Increase the budget of universities in order to work on national and specific topic needed for county development
- Create more institute of research in the country or sub-region for a precise mission
- Integrate climate change studies in the high school and universities for vulgarization of negatives impacts of climate change at all social levels
- Necessity to create new incomes-generating activities is urging to reduce the economic vulnerability of the local communities because of the high poverty level of the local population in the Basin.

To the researchers

- The impacts of the Nangbéto dam and the future Adjaralala dam in the basin should be investigated in conjunction with the effects of climate change on the stream flows and water balance component. Additionally, the impact of the Nangbéto dam

on river bank erosion coupled with the impact of climate change and land use changes should be investigated.

- The impacts of land use/cover and climate change on hydro-electricity production should be investigated
- Extend this study to many other rivers are poorly or not studied in the region
- The development of methods and tools for assessment, estimation and predictions of discharge for other basins
- Further application of integrated and multidisciplinary approaches in environmental assessments in order to identify sustainable solutions

To the local communities:

- Local population need to reconsider their actions such deforestation and type of energy used
- Awareness of the population

8.8: Perspectives

As this study, is the first analysis in the basin incorporating land cover/use , climate change and dam management for water resource variability assessment, it is important for future investigation in the basin to consider the limitation from this study to have robust results. These investigations which constitute the next tasks of this study will encompass:

- To integrate the impact of climate change, land use change, and dam management for flood risk scenarios analysis and mapping in the Lower Mono river basin
- To analyze flood frequency and magnitude for future scenarios considering climate change, land use change, and dam management impacts.
- To implement climate sensitive adaptation strategies to reduce current and future flood risk in the Lower Mono river basin

- To assess the impact of climate change, land use change and dam management using distributed hydrological models and for future scenarios at sub basin levels;

- To evaluate of human and climate impacts on water quality and quantity in the basin

- Investigate the impacts of land use/cover and climate change on hydro-electricity variability and evaluate the future scenarios

Annex 1:liste of appedixes

Appendix 4.1: Accuracy assessment reports

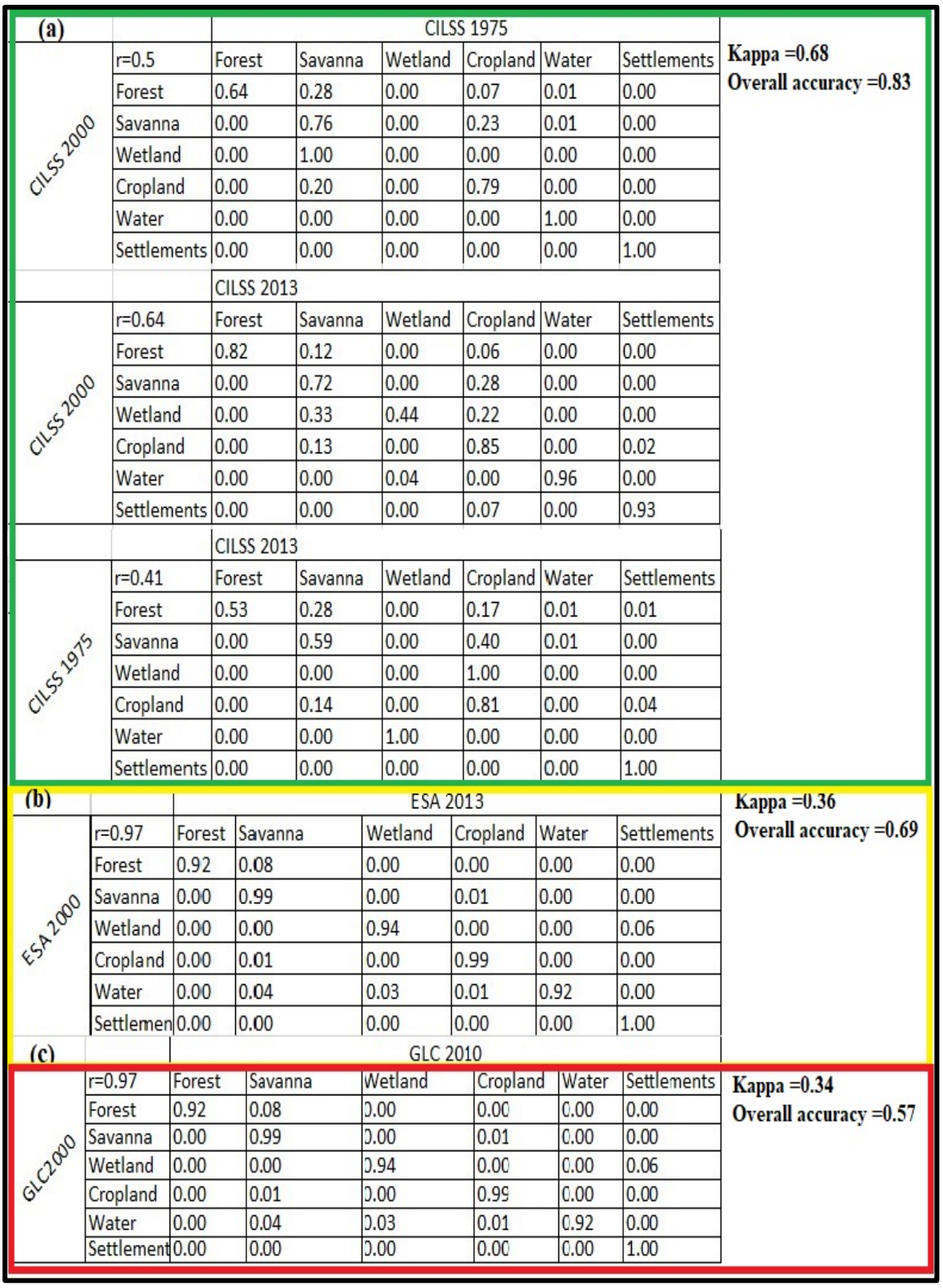

(a)

		CILSS 1975					
	r=0.5	Forest	Savanna	Wetland	Cropland	Water	Settlements
CILSS 2000	Forest	0.64	0.28	0.00	0.07	0.01	0.00
	Savanna	0.00	0.76	0.00	0.23	0.01	0.00
	Wetland	0.00	1.00	0.00	0.00	0.00	0.00
	Cropland	0.00	0.20	0.00	0.79	0.00	0.00
	Water	0.00	0.00	0.00	0.00	1.00	0.00
	Settlements	0.00	0.00	0.00	0.00	0.00	1.00

Kappa =0.68
Overall accuracy =0.83

		CILSS 2013					
	r=0.64	Forest	Savanna	Wetland	Cropland	Water	Settlements
CILSS 2000	Forest	0.82	0.12	0.00	0.06	0.00	0.00
	Savanna	0.00	0.72	0.00	0.28	0.00	0.00
	Wetland	0.00	0.33	0.44	0.22	0.00	0.00
	Cropland	0.00	0.13	0.00	0.85	0.00	0.02
	Water	0.00	0.00	0.04	0.00	0.96	0.00
	Settlements	0.00	0.00	0.00	0.07	0.00	0.93

		CILSS 2013					
	r=0.41	Forest	Savanna	Wetland	Cropland	Water	Settlements
CILSS 1975	Forest	0.53	0.28	0.00	0.17	0.01	0.01
	Savanna	0.00	0.59	0.00	0.40	0.01	0.00
	Wetland	0.00	0.00	0.00	1.00	0.00	0.00
	Cropland	0.00	0.14	0.00	0.81	0.00	0.04
	Water	0.00	0.00	1.00	0.00	0.00	0.00
	Settlements	0.00	0.00	0.00	0.00	0.00	1.00

(b)

		ESA 2013					
	r=0.97	Forest	Savanna	Wetland	Cropland	Water	Settlements
ESA 2000	Forest	0.92	0.08	0.00	0.00	0.00	0.00
	Savanna	0.00	0.99	0.00	0.01	0.00	0.00
	Wetland	0.00	0.00	0.94	0.00	0.00	0.06
	Cropland	0.00	0.01	0.00	0.99	0.00	0.00
	Water	0.00	0.04	0.03	0.01	0.92	0.00
	Settlemen	0.00	0.00	0.00	0.00	0.00	1.00

Kappa =0.36
Overall accuracy =0.69

(c)

		GLC 2010					
	r=0.97	Forest	Savanna	Wetland	Cropland	Water	Settlements
GLC2000	Forest	0.92	0.08	0.00	0.00	0.00	0.00
	Savanna	0.00	0.99	0.00	0.01	0.00	0.00
	Wetland	0.00	0.00	0.94	0.00	0.00	0.06
	Cropland	0.00	0.01	0.00	0.99	0.00	0.00
	Water	0.00	0.04	0.03	0.01	0.92	0.00
	Settlement	0.00	0.00	0.00	0.00	0.00	1.00

Kappa =0.34
Overall accuracy =0.57

Appendix 4.2: Land use changes (transitions)

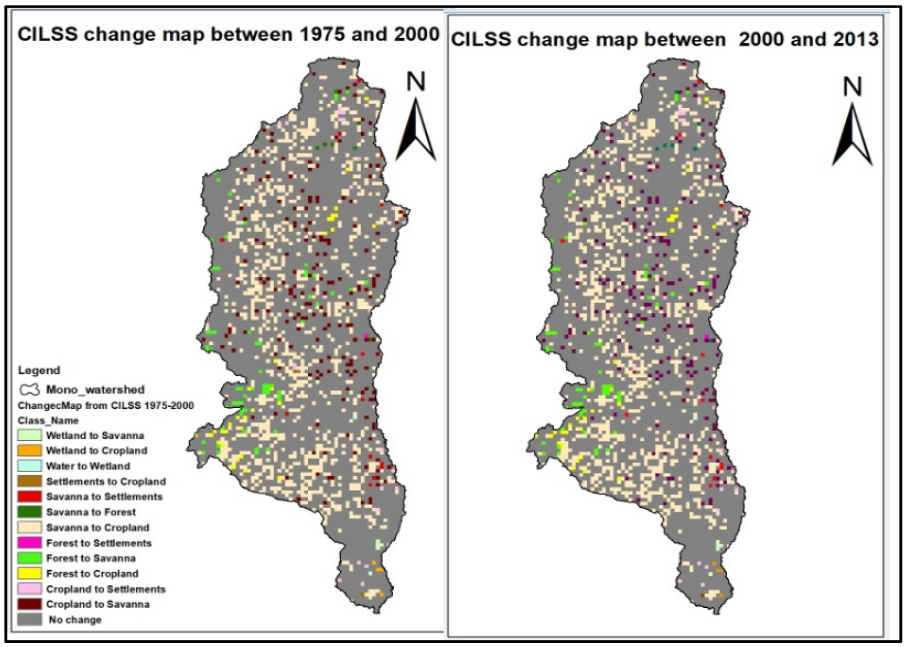

Appendix 4.4: Validation of CILSS LULC in 2013

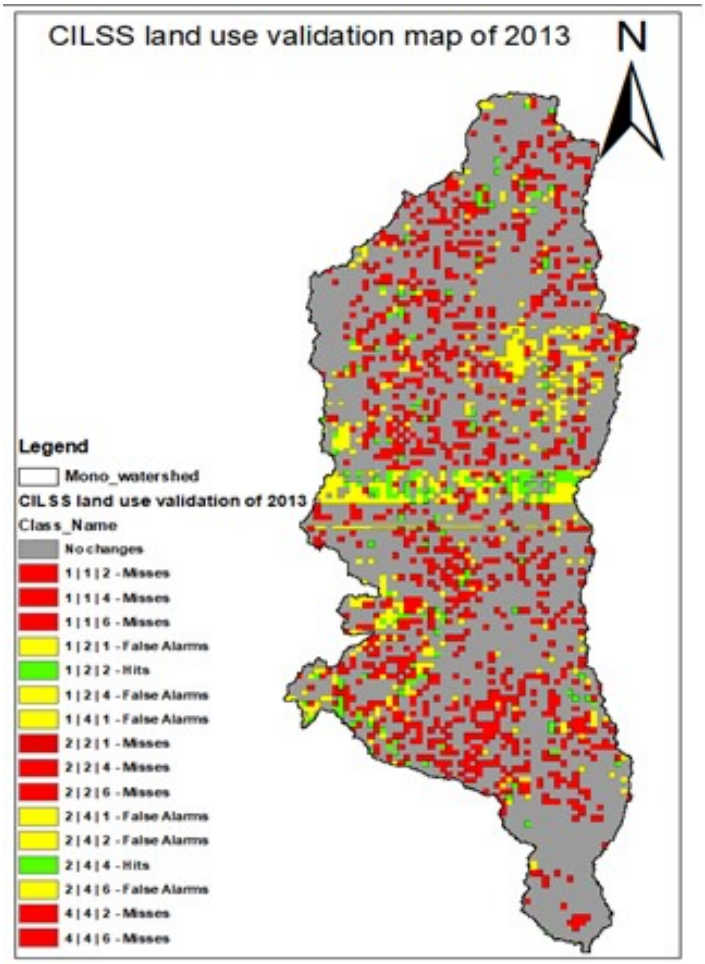

Appendix 4.4: Land use cells and area transitions in 2020 and 2027

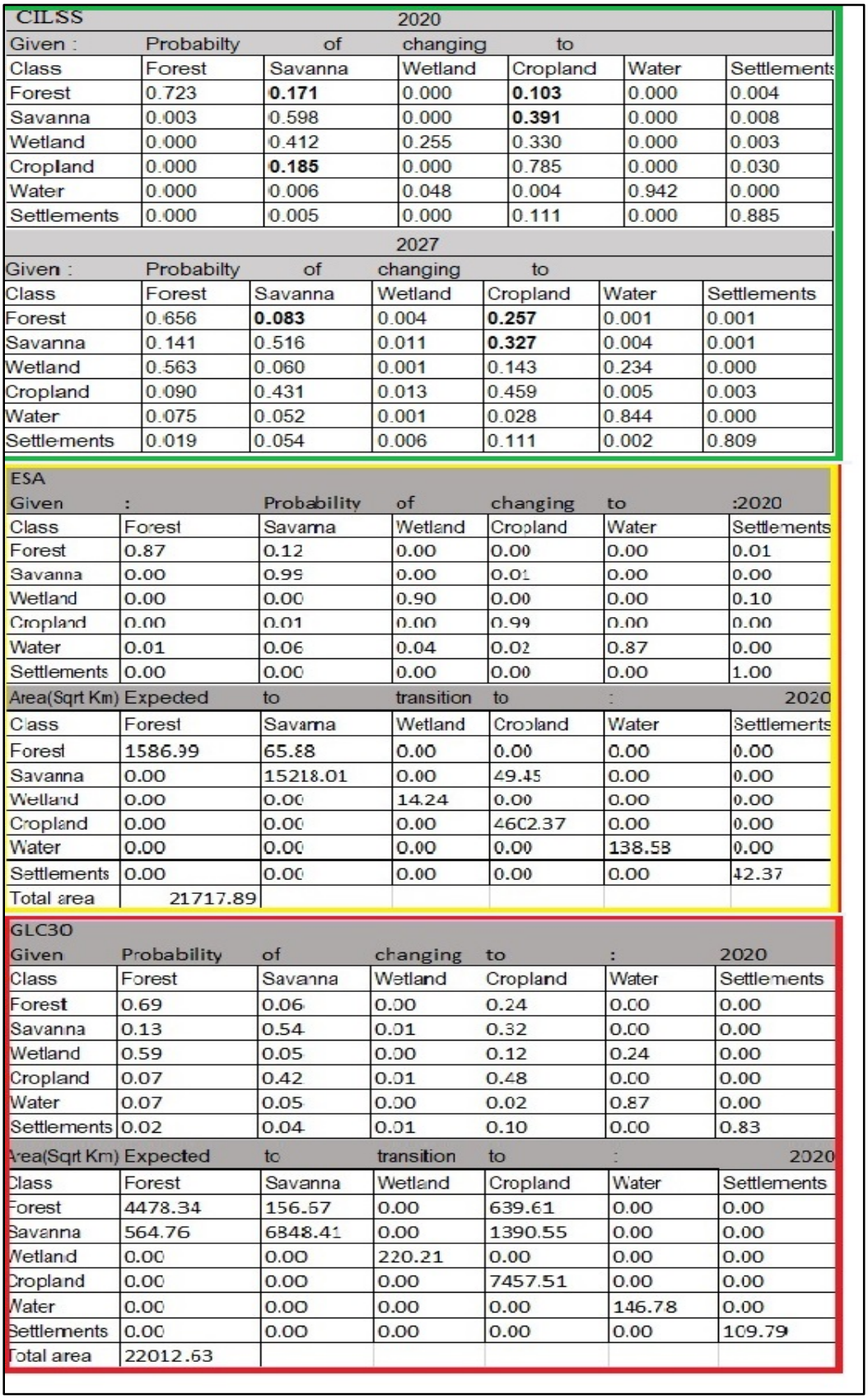

CILSS			2020			
Given :	Probabilty	of	changing	to		
Class	Forest	Savanna	Wetland	Cropland	Water	Settlements
Forest	0.723	**0.171**	0.000	**0.103**	0.000	0.004
Savanna	0.003	0.598	0.000	**0.391**	0.000	0.008
Wetland	0.000	0.412	0.255	0.330	0.000	0.003
Cropland	0.000	**0.185**	0.000	0.785	0.000	0.030
Water	0.000	0.006	0.048	0.004	0.942	0.000
Settlements	0.000	0.005	0.000	0.111	0.000	0.885

			2027			
Given :	Probabilty	of	changing	to		
Class	Forest	Savanna	Wetland	Cropland	Water	Settlements
Forest	0.656	**0.083**	0.004	**0.257**	0.001	0.001
Savanna	0.141	0.516	0.011	**0.327**	0.004	0.001
Wetland	0.563	0.060	0.001	0.143	0.234	0.000
Cropland	0.090	0.431	0.013	0.459	0.005	0.003
Water	0.075	0.052	0.001	0.028	0.844	0.000
Settlements	0.019	0.054	0.006	0.111	0.002	0.809

ESA						
Given	:	Probability	of	changing	to	:2020
Class	Forest	Savanna	Wetland	Cropland	Water	Settlements
Forest	0.87	0.12	0.00	0.00	0.00	0.01
Savanna	0.00	0.99	0.00	0.01	0.00	0.00
Wetland	0.00	0.00	0.90	0.00	0.00	0.10
Cropland	0.00	0.01	0.00	0.99	0.00	0.00
Water	0.01	0.06	0.04	0.02	0.87	0.00
Settlements	0.00	0.00	0.00	0.00	0.00	1.00

Area(Sqrt Km)	Expected	to	transition	to	:	2020
Class	Forest	Savanna	Wetland	Cropland	Water	Settlements
Forest	1586.99	65.88	0.00	0.00	0.00	0.00
Savanna	0.00	15218.01	0.00	49.45	0.00	0.00
Wetland	0.00	0.00	14.24	0.00	0.00	0.00
Cropland	0.00	0.00	0.00	4602.37	0.00	0.00
Water	0.00	0.00	0.00	0.00	138.58	0.00
Settlements	0.00	0.00	0.00	0.00	0.00	42.37
Total area	21717.89					

GLC30						
Given	Probability	of	changing	to	:	2020
Class	Forest	Savanna	Wetland	Cropland	Water	Settlements
Forest	0.69	0.06	0.00	0.24	0.00	0.00
Savanna	0.13	0.54	0.01	0.32	0.00	0.00
Wetland	0.59	0.05	0.00	0.12	0.24	0.00
Cropland	0.07	0.42	0.01	0.48	0.00	0.00
Water	0.07	0.05	0.00	0.02	0.87	0.00
Settlements	0.02	0.04	0.01	0.10	0.00	0.83

Area(Sqrt Km)	Expected	to	transition	to	:	2020
Class	Forest	Savanna	Wetland	Cropland	Water	Settlements
Forest	4478.34	156.57	0.00	639.61	0.00	0.00
Savanna	564.76	6848.41	0.00	1390.55	0.00	0.00
Wetland	0.00	0.00	220.21	0.00	0.00	0.00
Cropland	0.00	0.00	0.00	7457.51	0.00	0.00
Water	0.00	0.00	0.00	0.00	146.78	0.00
Settlements	0.00	0.00	0.00	0.00	0.00	109.79
Total area	22012.63					

Appendix 5: Plot significant scenarios extremes indices trend (RCP4.5)

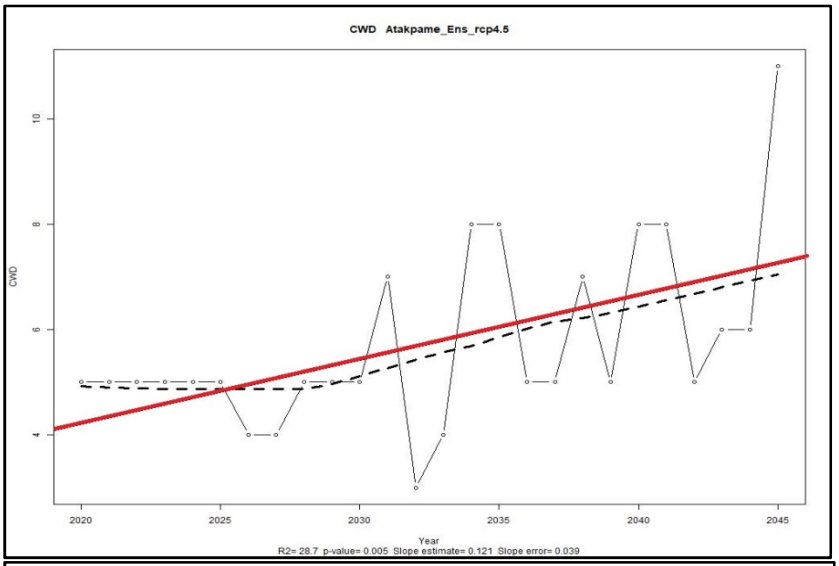
CWD Atakpame_Ens_rcp4.5
CWD
Year
R2= 28.7 p-value= 0.005 Slope estimate= 0.121 Slope error= 0.039

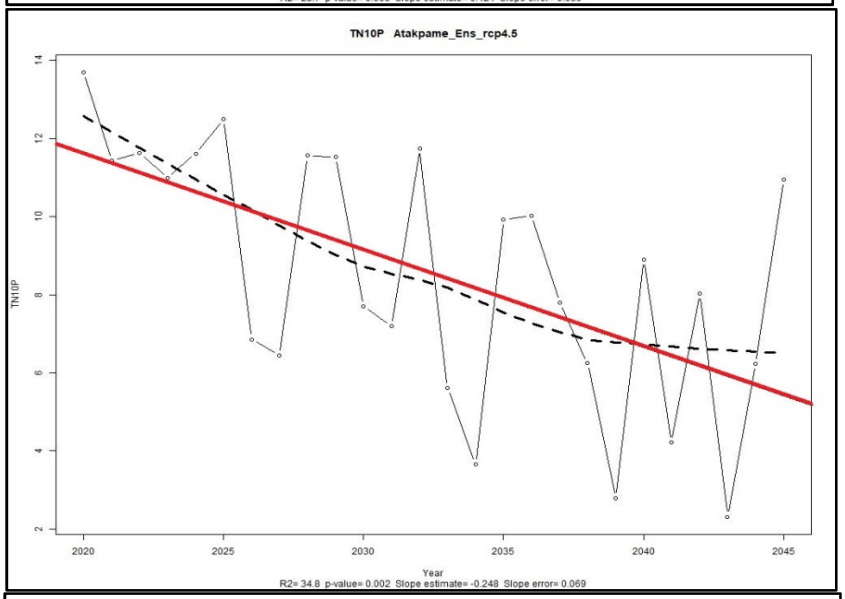
TN10P Atakpame_Ens_rcp4.5
TN10P
Year
R2= 34.8 p-value= 0.002 Slope estimate= -0.248 Slope error= 0.069

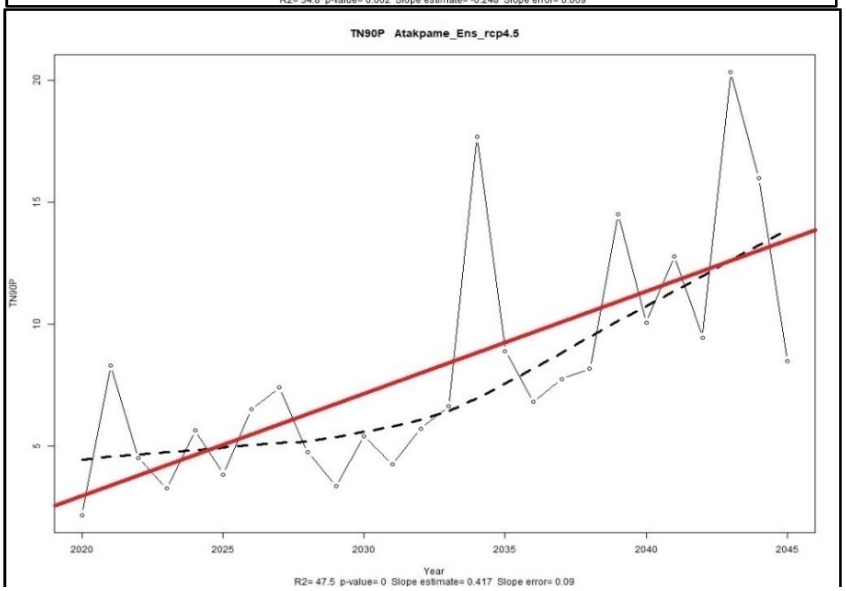
TN90P Atakpame_Ens_rcp4.5
TN90P
Year
R2= 47.5 p-value= 0 Slope estimate= 0.417 Slope error= 0.09

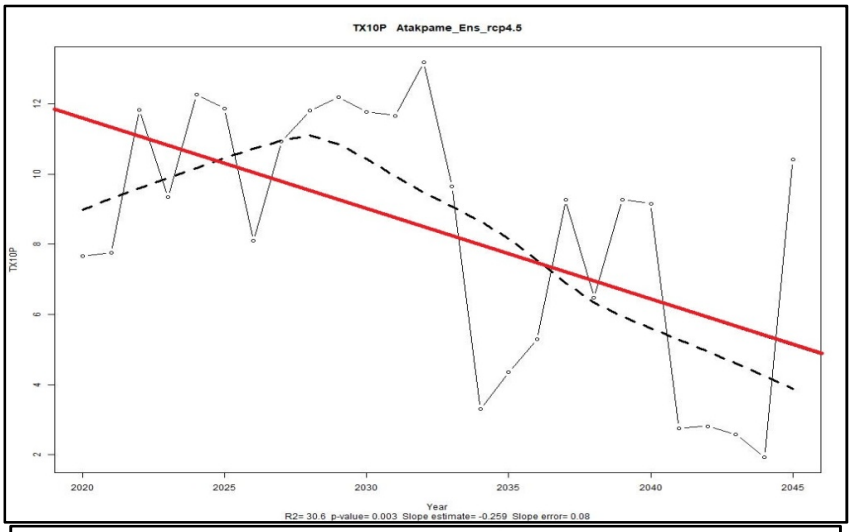
TX10P Atakpame_Ens_rcp4.5
TX10P
Year
R2= 30.6 p-value= 0.003 Slope estimate= -0.259 Slope error= 0.08

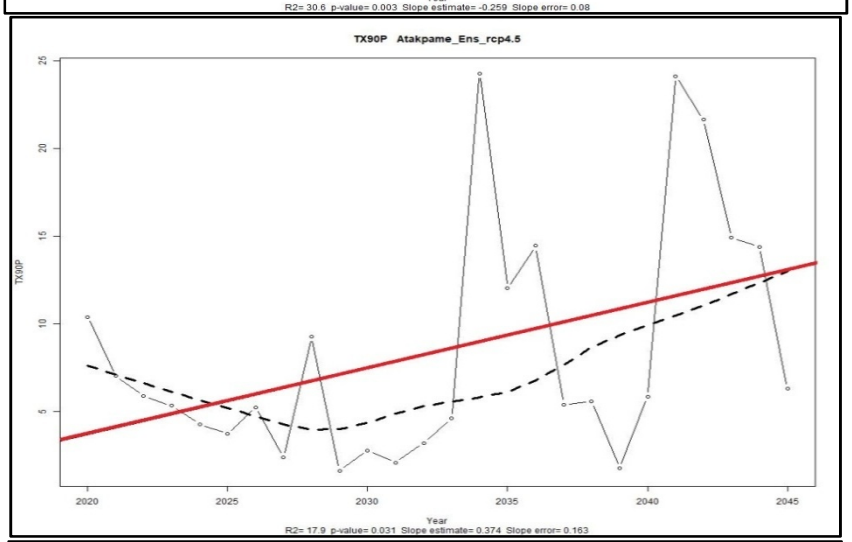
TX90P Atakpame_Ens_rcp4.5
TX90P
Year
R2= 17.9 p-value= 0.031 Slope estimate= 0.374 Slope error= 0.163

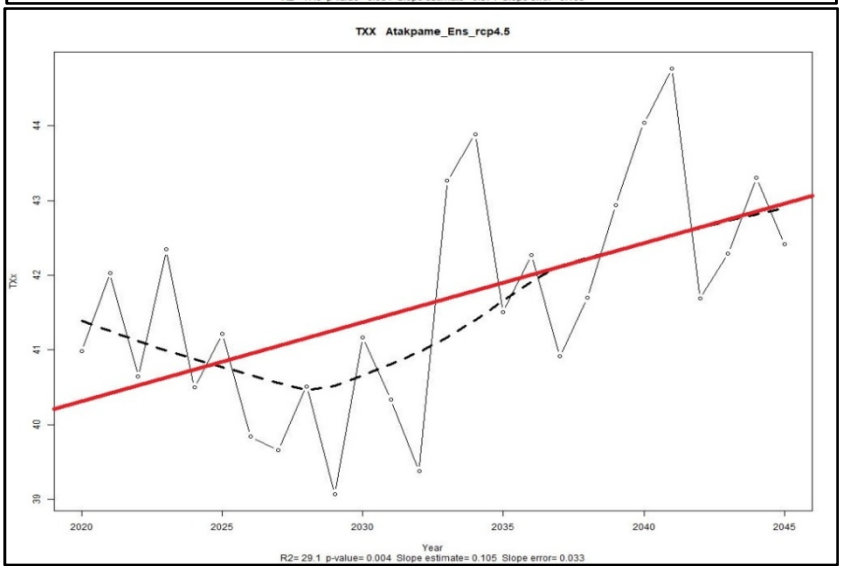
TXX Atakpame_Ens_rcp4.5
TXx
Year
R2= 29.1 p-value= 0.004 Slope estimate= 0.105 Slope error= 0.033

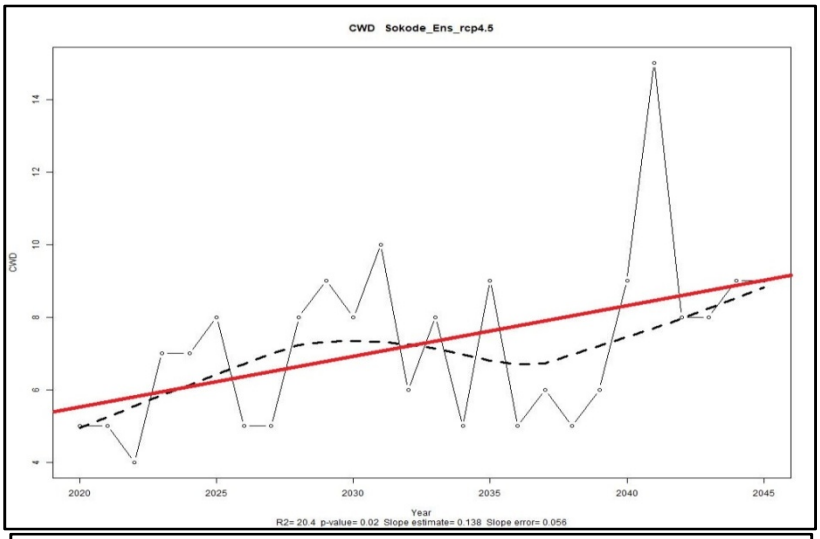
CWD Sokode_Ens_rcp4.5
CWD
Year
R2= 20.4 p-value= 0.02 Slope estimate= 0.138 Slope error= 0.056

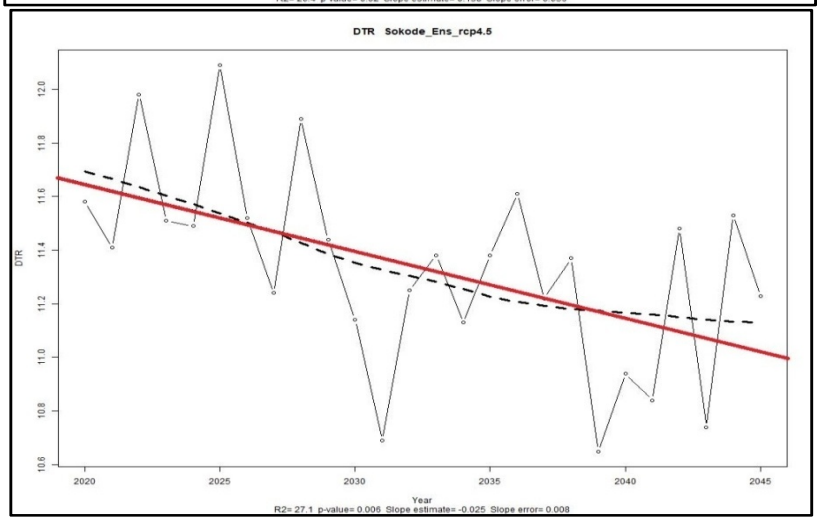
DTR Sokode_Ens_rcp4.5
DTR
Year
R2= 27.1 p-value= 0.006 Slope estimate= -0.025 Slope error= 0.008

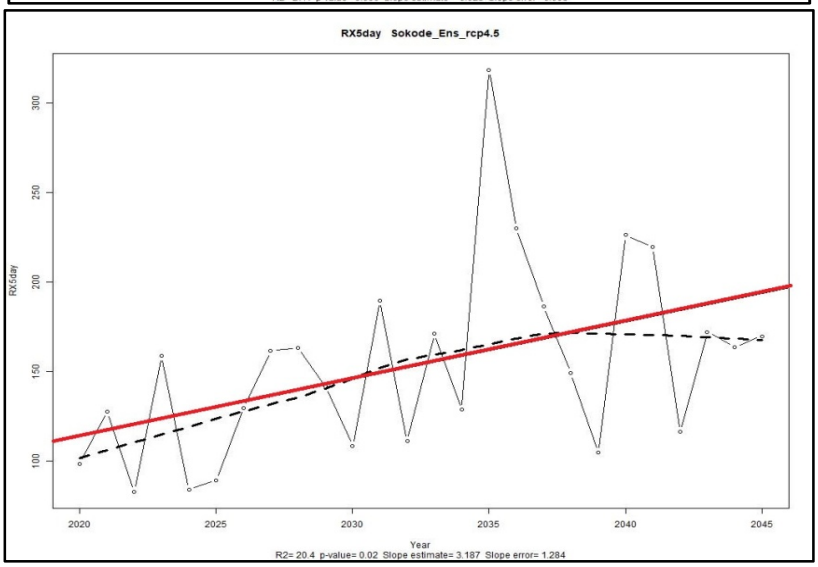
RX5day Sokode_Ens_rcp4.5
RX5day
Year
R2= 20.4 p-value= 0.02 Slope estimate= 3.187 Slope error= 1.284

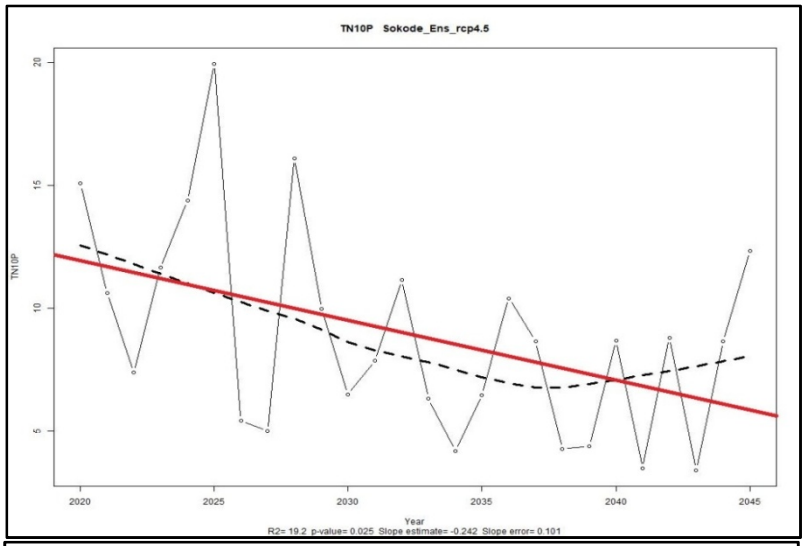
TN10P Sokode_Ens_rcp4.5
TN10P
Year
R2= 19.2 p-value= 0.025 Slope estimate= -0.242 Slope error= 0.101

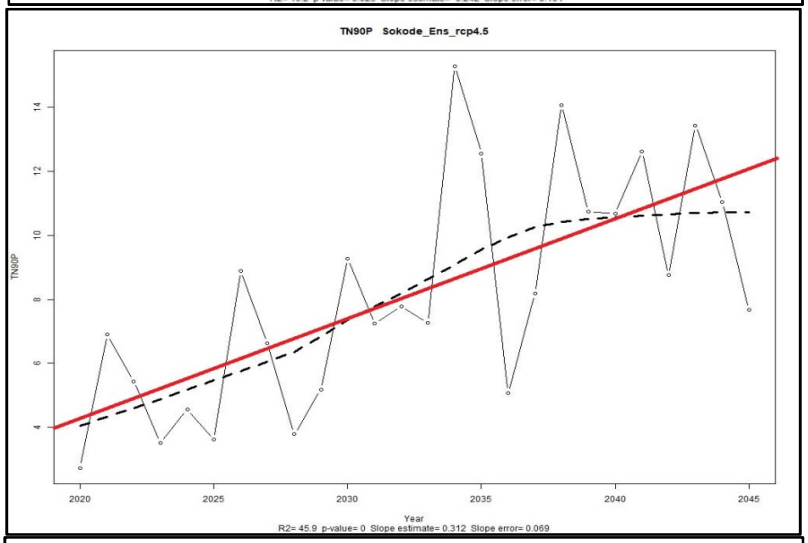
TN90P Sokode_Ens_rcp4.5
TN90P
Year
R2= 45.9 p-value= 0 Slope estimate= 0.312 Slope error= 0.069

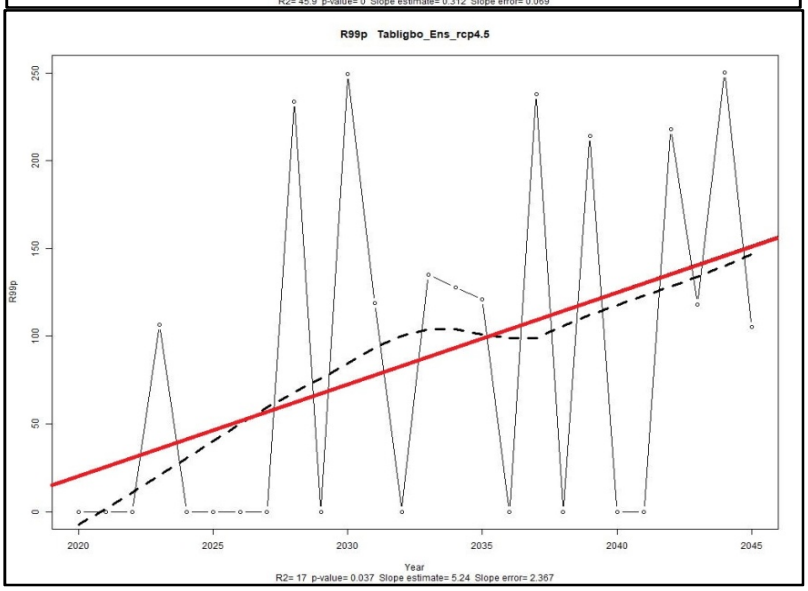
R99p Tabligbo_Ens_rcp4.5
R99p
Year
R2= 17 p-value= 0.037 Slope estimate= 5.24 Slope error= 2.367

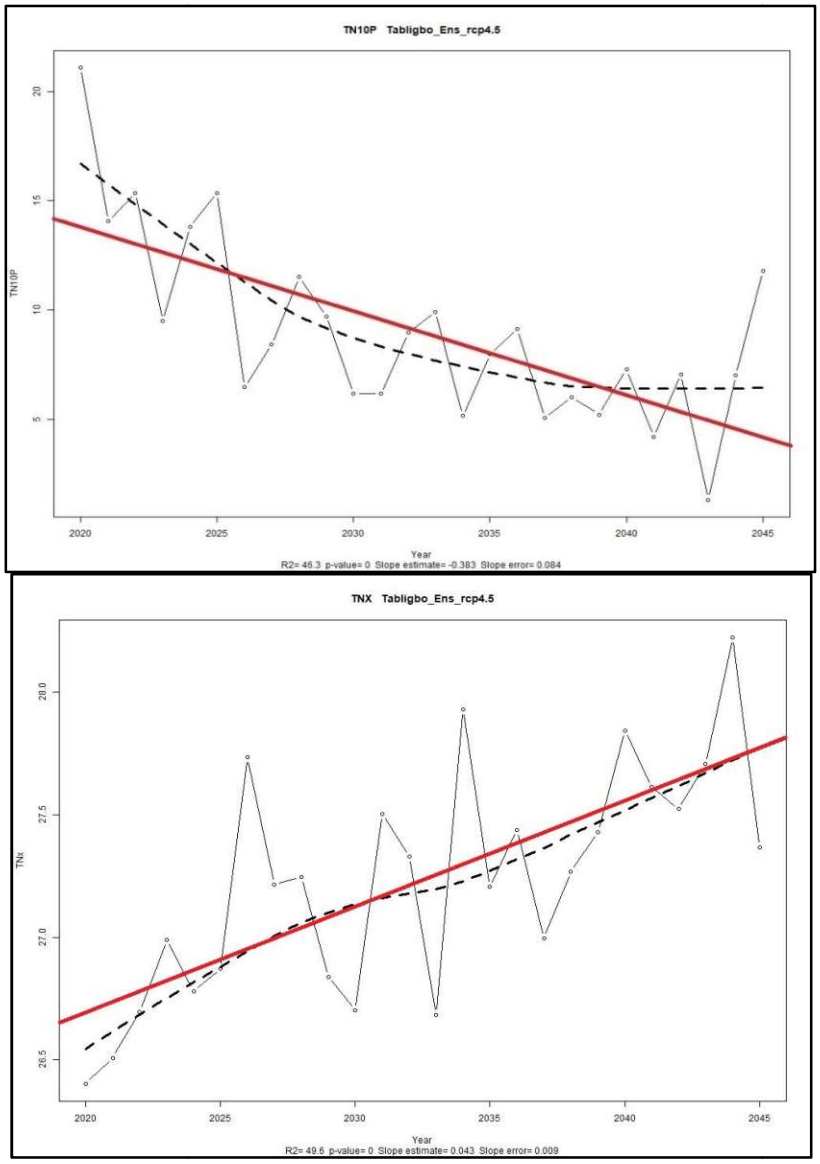

Appendix 7.1: Annual simulated and observed discharge in MRB gauge station

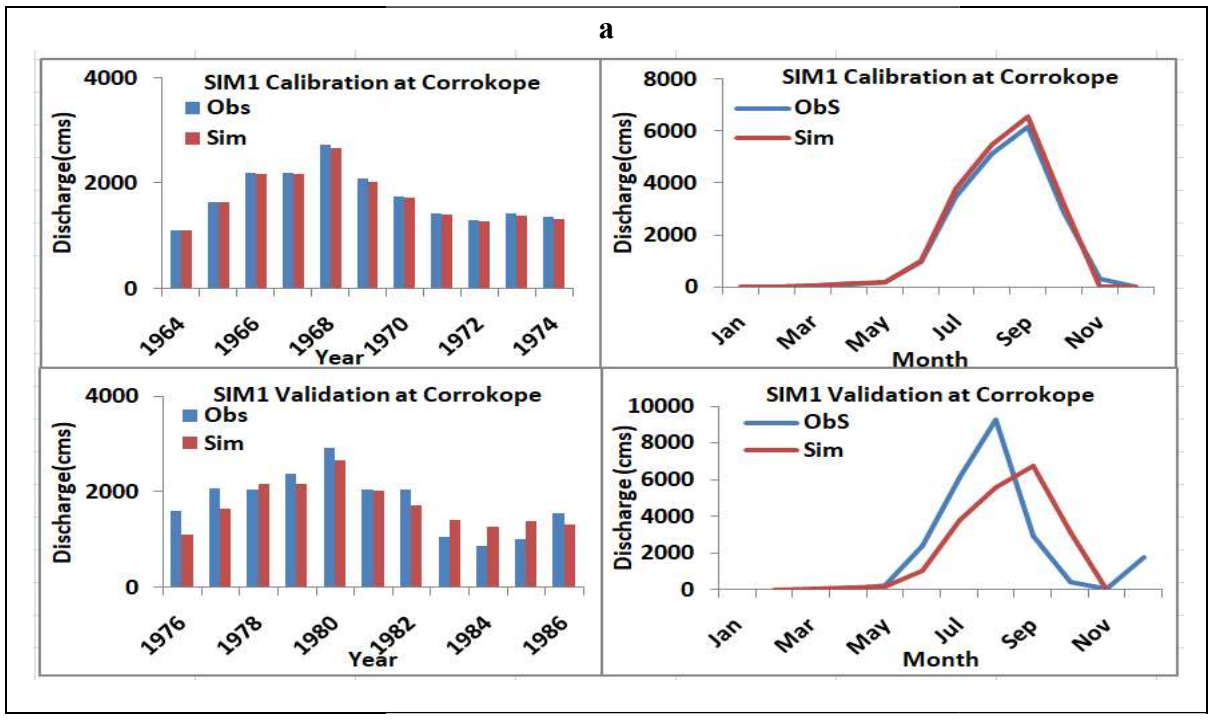

b

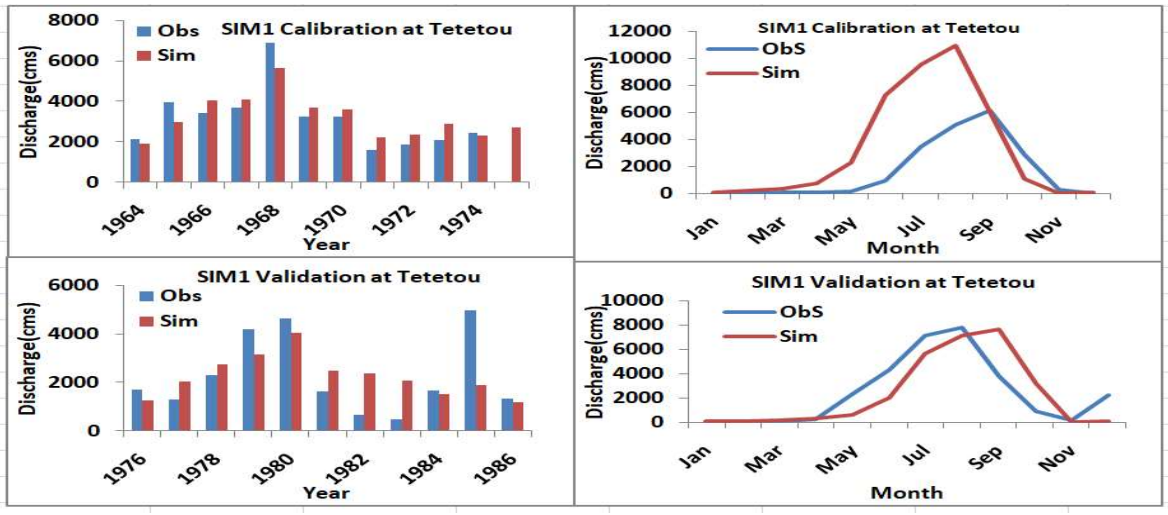
SIM1 Calibration at Tetetou
Obs
Sim
Discharge(cms)
Year
SIM1 Calibration at Tetetou
ObS
Sim
Discharge(cms)
Month
SIM1 Validation at Tetetou
Obs
Sim
Discharge(cms)
Year
SIM1 Validation at Tetetou
ObS
Sim
Discharge(cms)
Month

c

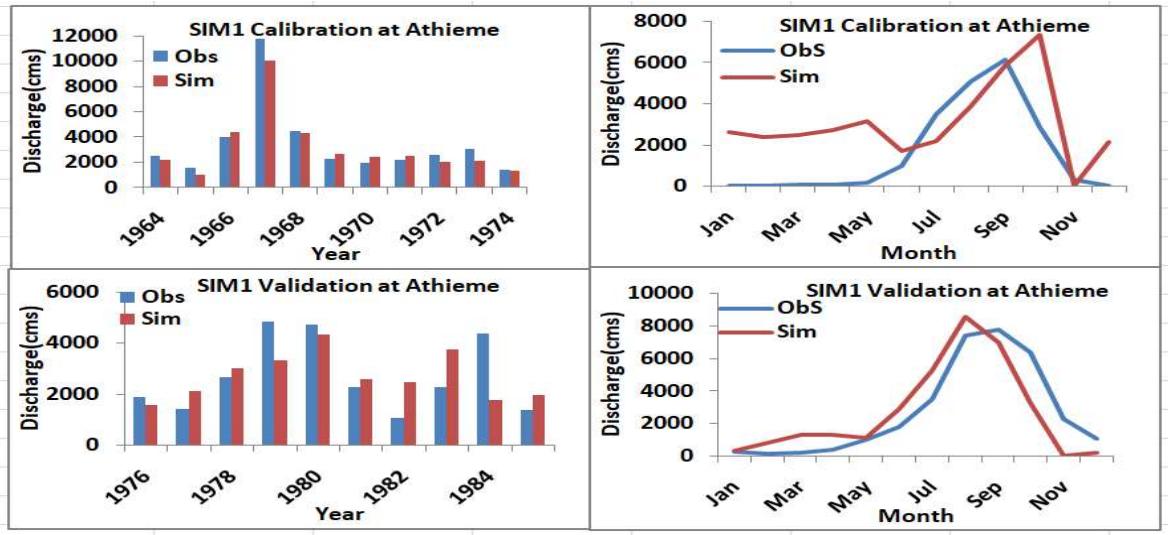
SIM1 Calibration at Athieme
Obs
Sim
Discharge(cms)
Year
SIM1 Calibration at Athieme
ObS
Sim
Discharge(cms)
Month
SIM1 Validation at Athieme
Obs
Sim
Discharge(cms)
Year
SIM1 Validation at Athieme
ObS
Sim
Discharge(cms)
Month

a

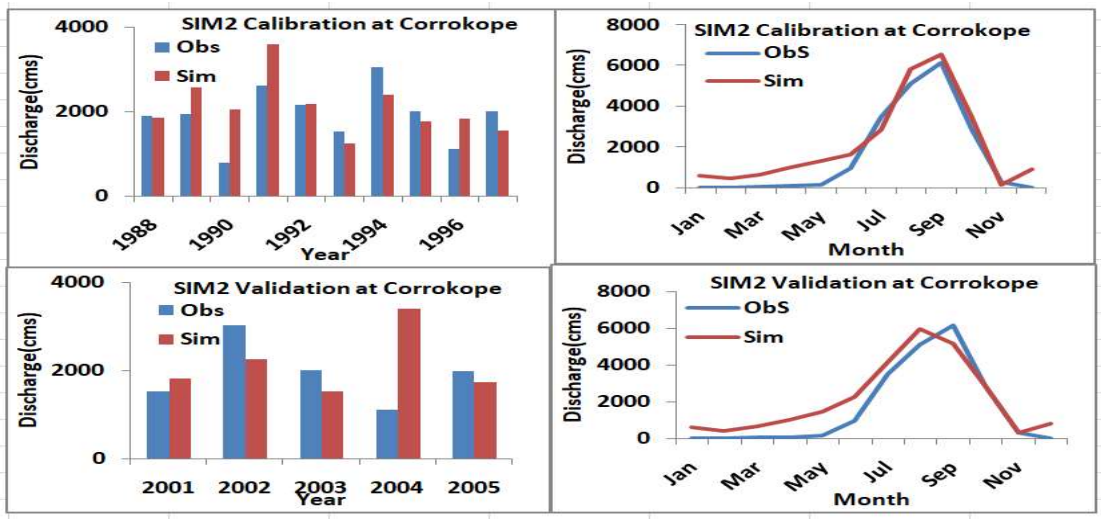
SIM2 Calibration at Corrokope
Obs
Sim
Discharge(cms)
Year
SIM2 Calibration at Corrokope
ObS
Sim
Discharge(cms)
Month
SIM2 Validation at Corrokope
Obs
Sim
Discharge(cms)
Year
SIM2 Validation at Corrokope
ObS
Sim
Discharge(cms)
Month

b

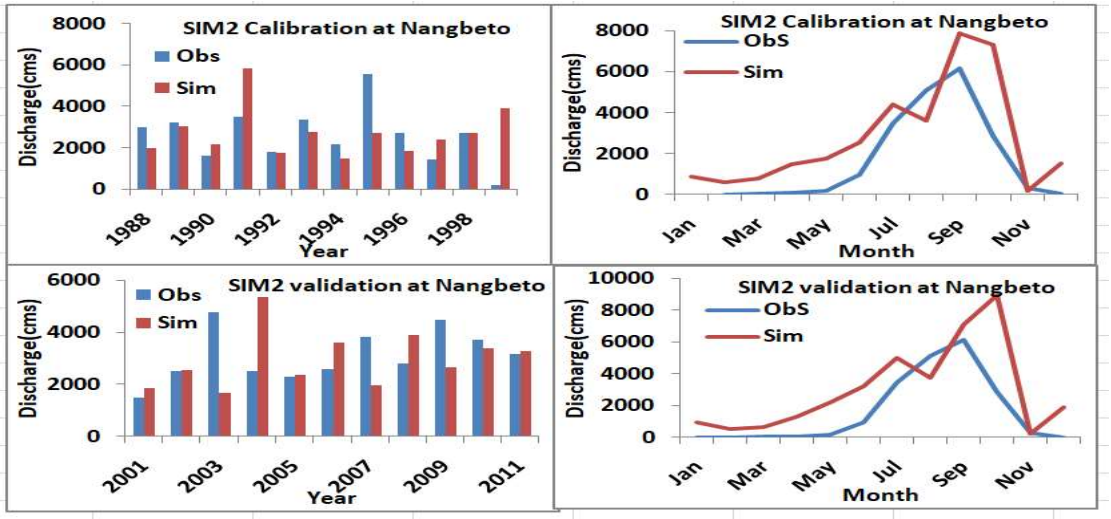
SIM2 Calibration at Nangbeto
Obs
Sim
Discharge(cms)
Year
SIM2 Calibration at Nangbeto
ObS
Sim
Discharge(cms)
Month
SIM2 validation at Nangbeto
Obs
Sim
Discharge(cms)
Year
SIM2 validation at Nangbeto
ObS
Sim
Discharge(cms)
Month

c

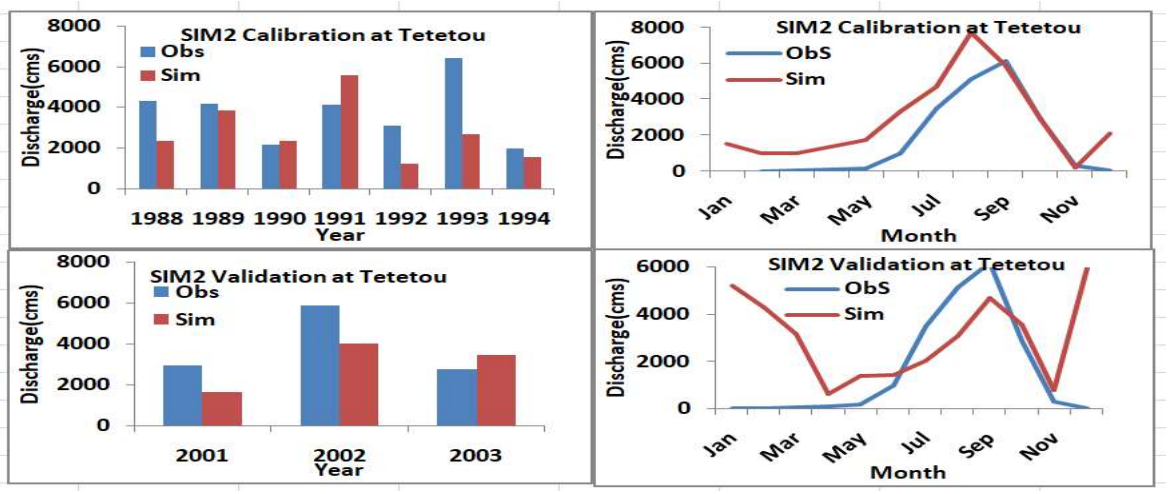
SIM2 Calibration at Tetetou
Obs
Sim
Discharge(cms)
Year
SIM2 Calibration at Tetetou
ObS
Sim
Discharge(cms)
Month
SIM2 Validation at Tetetou
Obs
Sim
Discharge(cms)
Year
SIM2 Validation at Tetetou
ObS
Sim
Discharge(cms)
Month

d

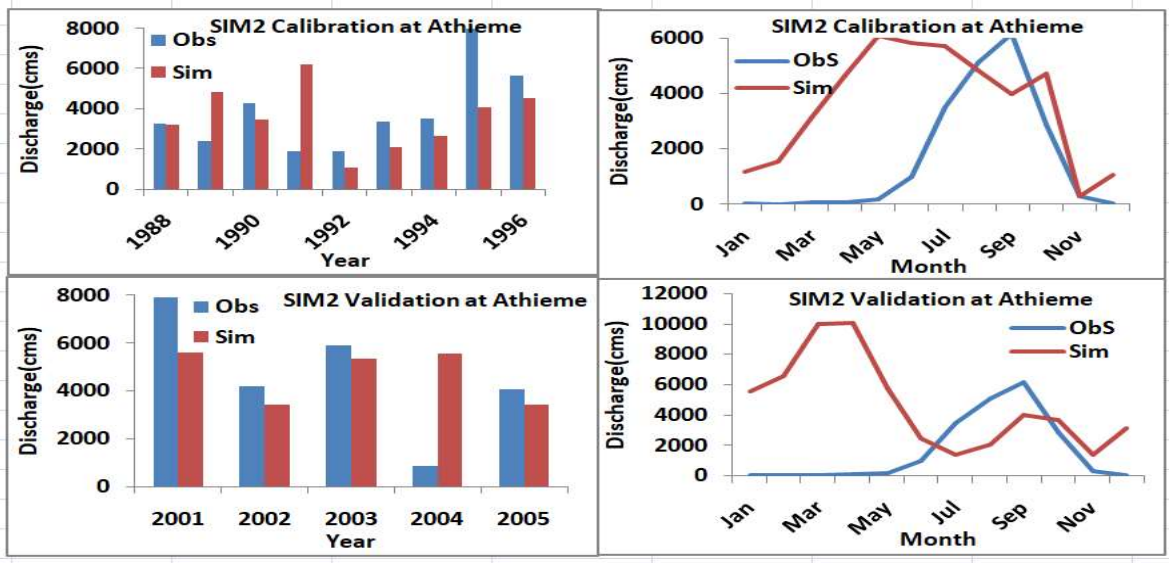
SIM2 Calibration at Athieme
Obs
Sim
Discharge(cms)
Year
SIM2 Calibration at Athieme
ObS
Sim
Discharge(cms)
Month
SIM2 Validation at Athieme
Obs
Sim
Discharge(cms)
Year
SIM2 Validation at Athieme
ObS
Sim
Discharge(cms)
Month

Appendix 7.7: Annual water balance components average value (1964-1986)

Year	PRECIPmm	PERCmm	ETmm	GW_Qmm	SURQmm	WYLDmm	LAT_Q_mm
1964	1095.87	276.00	662.38	226.32	146.30	398.35	6.77
1965	1142.35	309.52	652.84	256.21	178.73	458.67	7.83
1966	1344.08	453.06	639.01	383.44	239.91	651.74	8.85
1967	1397.29	434.11	710.56	369.74	236.84	638.27	9.91
1968	1573.00	562.07	708.79	489.86	298.70	825.13	11.03
1969	1253.66	368.26	668.23	305.45	207.78	542.58	8.22
1970	1243.48	367.18	634.08	310.32	235.86	573.14	7.83
1971	1186.22	309.77	664.77	251.60	202.83	478.43	7.62
1972	1183.55	310.27	679.3	251.13	180.78	455.66	7.71
1973	1232.17	388.01	648.99	323.03	191.52	540.93	8.78
1974	1088.39	308.60	598.41	252.48	175.09	451.47	7.58
1975	1215.85	366.21	666.52	303.98	171.06	500.68	8.12
1976	1134.48	323.37	620.04	259.76	181.09	465.29	7.93
1977	967.42	271.75	545.92	222.65	149.02	391.8	5.49
1978	1408.35	420.05	746.42	351.10	229.45	608.61	9.21
1979	1475.48	508.76	643.85	444.23	315.51	793.4	9.74
1980	1349.55	459.02	608.97	387.04	270.40	690.17	10.01
1981	1095.76	323.37	604.84	278.39	162.12	468.67	8.13
1982	941.43	222.32	600.34	171.97	115.34	306.61	6.60
1983	936.13	235.10	530.95	176.23	155.82	350.98	6.89
1984	1310.84	387.41	683.12	323.41	236.46	584.79	8.76
1985	1311.47	423.54	621.16	357.03	256.06	640.97	7.85
1986	1020.05	280.04	594.89	225.58	135.28	384.51	7.19
Average	1213.34	361.21	640.63	300.91	203.13	530.47	8.18

Appendix 7.8: Monthlywater balance components average value (1964-1986)

Month	PRECIPmm	PERCmm	ETmm	GW_Qmm	SURQmm	WYLDmm	LAT_Q_mm
Jan	8.79	0.75	11.85	0.47	0.37	1.72	0.12
Feb	17.80	1.72	14.77	0.01	0.50	1.18	0.17
Mar	58.63	5.72	56.33	0.03	1.10	1.76	0.27
Apr	108.87	12.00	92.96	0.04	1.93	2.74	0.44
May	133.87	15.26	109.07	0.10	3.87	4.24	0.46
Jun	153.75	33.53	104.51	1.03	15.52	16.78	0.80
Jul	189.09	55.14	104.40	6.36	37.85	42.68	1.09
Aug	188.00	67.31	107.76	20.40	41.28	64.60	1.28
Sep	200.05	69.65	112.59	30.92	43.87	77.46	1.28
Oct	120.72	40.34	108.91	26.24	18.18	48.40	1.01
Nov	25.06	6.35	61.24	11.15	1.47	14.62	0.39
Dec	8.70	1.41	15.52	3.28	0.37	4.77	0.18
Average	101.11	25.77	74.99	8.34	13.86	23.41	0.62

Appendix 7.9: Annual water balance components average value (1986-2010)

Year	PRECIPmm	PERCmm	ETmm	GW_Qmm	SURQmm	WYLDmm	LAT_Q_mm
1988	1307.39	15.31	924.24	185.77	128.44	382.65	49.48
1989	1368.94	19.54	860.80	248.95	181.69	513.57	60.73
1990	1254.41	8.39	886.35	158.41	115.18	335.04	48.73
1991	1455.88	18.60	963.66	313.31	150.94	536.66	43.15
1992	1041.31	6.97	802.29	121.20	75.93	244.36	35.03
1993	1277.69	10.26	928.50	162.55	106.75	331.14	48.15
1994	1214.70	12.90	913.71	141.31	95.17	289.12	39.92
1995	1333.73	18.93	916.92	209.37	139.80	424.52	55.20
1996	1174.34	12.32	902.47	134.53	103.22	294.81	42.76
1997	1357.94	11.88	969.33	186.70	99.45	351.30	48.25
1998	1252.96	11.24	949.08	170.30	95.58	326.56	44.16
1999	1416.30	17.03	967.61	230.54	133.49	436.39	50.90
2000	1221.45	11.13	915.72	175.79	87.19	326.82	45.01
2001	1065.31	6.38	867.83	95.34	71.31	211.80	35.53
2002	1370.83	14.30	966.46	201.75	100.23	361.09	40.86
2003	1365.31	16.35	947.15	233.30	125.29	432.91	53.07
2004	1349.95	14.15	969.99	205.27	96.19	368.04	47.06
2005	1296.39	12.71	956.75	185.37	104.91	355.86	49.28
2006	1248.13	12.97	925.06	180.16	100.27	335.39	37.44
2007	1348.53	14.34	929.30	203.55	120.97	390.15	46.58
2008	1356.92	15.97	950.47	232.86	115.03	418.09	48.42
2009	1469.81	18.41	1002.87	245.21	140.88	469.82	61.33
2010	1455.72	16.73	992.65	217.59	153.16	440.94	53.10
Average	1304.52	13.78	930.84	193.01	114.83	372.91	47.14

Appendix 7.10: Monthlywater balance components average value (1988-2010)

Month	PRE-CIPmm	PERCmm	ETmm	GW_Qmm	SURQmm	WYLDmm	LAT_Q_mm
Jan	7.53	0.04	7.70	3.40	0.44	5.79	0.10
Feb	18.43	0.08	11.51	1.16	1.14	2.93	0.24
Mar	53.25	0.60	41.15	0.72	3.16	4.31	0.96
Apr	111.88	7.02	66.66	2.58	8.21	11.51	3.35
May	137.59	7.84	122.72	7.10	8.11	19.16	3.60
Jun	173.50	11.60	113.23	8.92	11.51	24.13	5.21
Jul	200.02	27.62	114.29	18.85	18.70	42.60	7.28
Aug	206.49	37.68	114.58	31.63	25.05	63.54	8.68
Sep	216.75	42.59	122.07	42.66	25.06	79.82	9.82
Oct	143.18	26.08	124.00	43.09	11.50	71.32	6.93
Nov	27.33	3.88	82.49	23.43	1.35	33.55	0.84
Dec	8.90	0.30	10.51	9.26	0.62	13.92	0.14
Aver-age	108.74	13.78	77.58	16.07	9.57	31.05	3.93

Annex 2: List of publications-Conferences and Workshop

List of publications

i. **Koubodana, H.D**., Diekkrüger, B., Näschen, K., Adounkpe, J., Atchonouglo, K. 2019a. Impact of the Accuracy of Land Cover Data Sets on the Accuracy of Land Cover Change Scenarios in the Mono River Basin, Togo, West Africa. Int. J. Adv. Remote Sens. GIS 8, 3073–3095. https://doi.org/10.23953/cloud.ijarsg.422

ii. **Koubodana, H.D.,** Tall, M., Amoussou, E., Mumtaz, M., Adounkpe, J., Atchonouglo, K. 2019b. Trend Analysis of Hydroclimatic Historical Data and Future Scenarios of Climate Extreme Indices over Mono River Basin in West Africa. Preprint June, 22. https://doi.org/10.20944/preprints201906.0267.v1 (*Under review in American Journal of Rural Development)*

Conferences Processing

(i) **Koubodana, H.D**.; Diekküger, B.; Adounkpe, J.; Atchonouglo, K , Land Use Change, Climate Change And Dam Management Impacts On Hydrological Cycle Components in The Mono River Basin, Togo (West Africa**) ,**Quatrième édition des Journées Scientifiques du CAMES (JSDC-4), **2 - 5 Décembre 2019, Ouidah, Bénin** (http://www.lecames.org/programme-des-4es-journees-scientifiques-du-cames/) *Oral presentation*

(ii) **Koubodana, H.D**.; Diekküger, B.; Amoussou, E.; Adounkpe, J.; Atchonouglo, K. Runoff Prediction and Comparison in West Africa using IHACRES and GR4J Lumped Models : case of Mono River Basin (Togo , West Africa). In Proceedings of the Water Security and Climate Change Conference, 28. - 30.10.2019 | San Luis Potosí, Mexiko; Unpublished, 2019; p. 152. (https://watersecurity.info/#19-about) *Poster presentation*

(iii) **Koubodana, H.D**.; Diekküger, B.; Adounkpe, J.; Atchonouglo, K, Land Use, Land Cover, Climate Changes and Dam Management Impacts on Runoff in the Mono River Basin, West Africa Tropical Atlantic Climate and COastal VARiability (TACCOVAR) Conference, **23-27 Septembre 2019, Cotonou, Benin**(https://taccovar-2017-79.webself.net/) *Oral presentation*

(iv) **Koubodana, H.D**.; Diekkrüger, B.; Näschen, K.; Adounkpe, J.; Atchonouglo, K. Impact of the Accuracy of Land Cover Data Sets on the Accuracy of Land Cover Change Scenarios in the Mono River Basin, Togo, West Africa. *2nd Asian Population Forum* ***October 11-12, 2019, University of Shanghai,*** *China* (http://www.asianmc.org/the-second-asian-population-forum/)- *Poster presentation*

Workshop and training

1. Training workshop "Methods and Models for Spatial Analysis on Population and Climate Change", **October. 5-9, 2019, University of Shanghai, China**.

2. Feed the Future Innovation Lab for Small Scale Irrigation IDSS Workshop (Kumasi-Ghana), **July24-28th, 2017.**

3. Inter-displinary Remote sensing, Modeling and Validation of Environmental Processes, COSPAR capacityBuildingWorkshop**,Kumasi,Ghana-12-23June 2017**

4. Hydro-climate and remote sensing training opportunity for west Africa students & early career scientists,CompetenceCenter,**12-21March2017,Ouagadougou; Burkina Faso**

5. International climate change research methodology workshop and networking sessions**, 27th February-12thof March,2017,Cotonou-Benin**

6. Training on Geographic Information System (GIS): applications to marine and coastal domain IODE/OTGA/CRODT/ISRA**, January2017, Dakar, Senegal**

References

Abbaspour, K.C., 2015. SWAT-CUP 2012. SWAT Calibration and Uncertainty Programs.

Abbaspour, K.C., Johnson, C.A., van Genuchten, M.T., 2004. Estimating Uncertain Flow and Transport Parameters Using a Sequential Uncertainty Fitting Procedure. Soil Soc. Am. 1352, 1340–1352.

Abbaspour, K.C., Vaghefi, S.A., Srinivasan, R., 2017. A Guideline for Successful Calibration and Uncertainty Analysis for Soil and Water Assessment: A Review of Papers from the 2016 International SWAT Conference. Water 10, 1–18. https://doi.org/10.3390/w10010006

Abbaspour, K.C., Yang, J., Maximov, I., Siber, R., Bogner, K., Mieleitner, J., Zobrist, J., Srinivasan, R., 2007. Modelling hydrology and water quality in the pre-alpine/alpine Thur watershed using SWAT. J. Hydrol. 333, 413–430. https://doi.org/10.1016/j.jhydrol.2006.09.014

Abdalla, C.W., 2001. The industrialization of agriculture: Implications for public concern and environmental consequences of intensive livestock operations. Penn St. Envtl. L. Rev. 10, 175.

Adamowski, K., 2000. Regional analysis of annual maximum and partial duration flood data by nonparametric and L-moment methods. J. Hydrol. 229, 219–231.

Adeaga, O., Mahe, G., Dieulin, C., Elbaz-poulichet, F., Rouche, N., Seidel, J.-L., Servat, E., 2012. Rainfall-Runoff Simulation in Part of Lower Niger Basin. J. Environ. Sci. Eng. 1, 812–819.

Affaton, P., 1990. Le bassin des Volta (Afrique de l'Ouest): une marge passive, d'âge protérozoïque supérieur, tectonisée au Panafricain (600 plus ou moins 50 Ma).

Ago, E.E., Petit, F., Pierre, O., 2005. Analyse des inondations en aval du barrage de Nangbeto sur le fleuve Mono (Togo et Bénin) Analysis of flood downstream from the Nangbeto dam on the. Geo. Eco. Trop. 29, 1–14.

Ahmad, A., Sufahani, S.F., 2012. Analysis of Landsat 5 TM Data of Malaysian Land Covers Using ISODATA Clustering Technique.

Ahmed, K.F., Wang, G., You, L., Yu, M., 2016. Potential impact of climate and socioeconomic changes on future agricultural land use in West Africa. Earth Syst. Dyn. 7, 151–165. https://doi.org/10.5194/esd-7-151-2016

Akinsanola, A.A., Zhou, W., 2018. Projections of West African summer monsoon rainfall extremes from two CORDEX models. Clim. Dyn. 12pp. https://doi.org/10.1007/s00382-018-4238-8

Akinyemi, F.O., Pontius, R.G., Braimoh, A.K., 2017. Land change dynamics : insights from Intensity Analysis applied to an African emerging city. J. Spat. Sci. 62, 69–83. https://doi.org/10.1080/14498596.2016.1196624

Akpagana, K., 1989. Recherches sur les forêts denses humides du Togo.

Akpovi, K., Antwi, E.O., Kabo-bah, A., 2016. Impacts of Rainfall Variability , Land Use and Land Cover Change on Stream Flow of the Black Volta. Hydrology 3, 1–24. https://doi.org/10.3390/hydrology3030026

Ali, R., Mcfarlane, D., Varma, S., Dawes, W., Emelyanova, I., Hodgson, G., Charles, S., 2012. Potential climate change impacts on groundwater resources of south-western Australia. J. Hydrol. 475, 456–472. https://doi.org/10.1016/j.jhydrol.2012.04.043

Allchin, M.I., Déry, S.J., 2017. A spatio-temporal analysis of trends in Northern Hemisphere snow-dominated area and duration, 1971–2014. Ann. Glaciol. 58, 21–35.

Amisigo, B.A., Mccluskey, A., Swanson, R., 2015. Modeling Impact of Climate Change on Water Resources and Agriculture Demand in the Volta Basin and other Basin Systems in Ghana. Sustainability 7, 6957–6975. https://doi.org/10.3390/su7066957

Amoussou, E., 2010. Variabilité pluviométrique et dynamique hydro-sédimentaire du bassin versant du complexe fluvio-lagunaire Mono-Ahémé-Couffo. These de doctorat de l'Université de Bourgogne - Centre de Recherches de Climatologie (CRC) CNRS – UMR 5210, soutenu le 11 mai 2010.

Amoussou, E., Camberlin, P., Mahé, G., 2012. Impact de la variabilité climatique et du barrage Nangbéto sur l'hydrologie du système Mono- Couffo (Afrique de l'Ouest). Hydrol. Sci. J. 57, 805–817. https://doi.org/10.1080/02626667.2011.643799

Amoussou, E., Camberlin, P., Totin, H.S. V, Tramblay, Y., Houndenou, C., Paturel, J.E., Boko, M., 2016. Évolution des précipitations extrêmes dans le bassin versant du Mono (Bénin-Togo) en contexte de variabilité/ changement, in: XXVIIe Colloque de l'Association Internationale de Climatologie. Dijon (France).

Amoussou, E., Osseni, A.A., Totin, H.S. V, Lange, U., Preuss, S., 2017. Hydroclimatic variability and flood risk on Naglanou and Akissa forests areas in Mono River Delta (West Africa). Int. J. Biodivers. Conserv. 9, 212–223. https://doi.org/10.5897/IJBC2016.1061

Amoussou, E., Tramblay, Y., Totin, H.S. V, Mahé, G., Camberlin, P., 2014. Dynamique et modélisation des crues dans le bassin du Mono à Nangbéto (Togo / Bénin). Hydrol. Sci. J. 59, 2060–2071. https://doi.org/10.1080/02626667.2013.871015

Anderson, J.R., Hardy, E.E., Roach, J.T., Witmer, R.E., 1976. A Land Use and Land Cover Classification System for Use with Remote Sensor Data, US Government Printing Office.

Andréassian, V., Bourgin, F., Oudin, L., Mathevet, T., Perin, C., Lerat, J., Coron, L., Berthet, L., 2014. Seeking genericity in the selection of parameter sets: Impact on hydrological model efficiency. Water Resour. Res. 50, 1–17. https://doi.org/10.1002/2013WR014333.Received

Andréassian, V., Perrin, C., Michel, C., 2004. Impact of imperfect potential evapotranspiration knowledge on the efficiency and parameters of watershed models. J. Hydrol. 286, 19–35. https://doi.org/10.1016/j.jhydrol.2003.09.030

Andrews, F.T., Croke, B.F.W., Jakeman, A.J., 2011. An open software environment for hydrological model assessment and development. Environ. Model. Softw. 26, 1171–

1185. https://doi.org/10.1016/j.envsoft.2011.04.006

Arnold, J.G., Allen, P.M., Muttiah, R., Bernhardt, G., 1995. Automated base flow separation and recession analysis technicues. Ground Water 33, 1010–1018. https://doi.org/10.1111/j.1745-6584.1995.tb00046.x

Arnold, J.G., Kiniry, J.R., Srinivasan, R., Williams, J.R., Haney, E.B., Neitsch, S.L., 2012. Soil & Water Assessment Tool-Input/Output Documentation Version 2012. Texas Water Resources Institute.

Arnold, J.G., Srinivasan, R., Muttiah, R.S., Williams, J.R., Arnold, J.G., Bednarz, S.T., Srinivasan, R., 1998. Large Area Hydrologic Modeling and Assessment Part I : Model Development. J. Am. Water Resour. Assoc. 34, 73–89. https://doi.org/10.1111/j.1752-1688.1998.tb05961.x

Arsanjani, J.J., Helbich, M., Kainz, W., Boloorani, D.A., 2013. Integration of logistic regression, Markov chain and cellular automata models to simulate urban expansion. Int. J. Appl. Earth Obs. Geoinf. 21, 265–275. https://doi.org/10.1016/j.jag.2011.12.014

Atsri, K.H., Konko, Y., Cuni-Sanchez, A., Abotsi, K.E., 2018. Changes in the West African forest-savanna mosaic , insights from central Togo. PLoS One 13, 10. https://doi.org/10.1371/journal.pone.0203999

Attogouinon, A., Lawin, A.E., M'Po, Y.N.T., Houngue, R., 2017. Extreme Precipitation Indices Trend Assessment over the Upper Oueme River Valley-(Benin). Hydrology 4, 36. https://doi.org/10.3390/hydrology4030036

Awotwi, A., Kumi, M., Jansson, P.E., Yeboah, F., Nti, I.K., 2015. Predicting Hydrological Response to Climate Change in the White Volta Catchment, West Africa. Earth Sci. Clim. Chang. 6, 1–7. https://doi.org/10.4172/2157-7617.1000249

Badjana, H.M., 2016. River Basins Assessment and Hydrologic Processes Modeling for Integrated Land and Water Resources Management (ILWRM) in West Africa. PhD Thesis, Graduate Research Program on Climate Change and Water Resources ,University of Abomey Calavi, Benin; defense date: december 11,02016.

Badjana, H.M., Fink, M., Helmschrot, J., Diekkrüger, B., Kralisch, S., Afouda, A.A., Wala, K., 2017a. Hydrological system analysis and modelling of the Kara River basin (West Africa) using a lumped metric conceptual model. Hydrol. Sci. J. 62, 1094–1113. https://doi.org/10.1080/02626667.2017.1307571

Badjana, H.M., Hounkpè, K., Kpérkouma, W., Batawila, K., Akpagana, K., Edjamé, K.S., 2014. Analyse de la variabilité temporelle et spatiale des séries climatiques du nord du Togo entre 1960 et 2010. Eur. Sci. J. 10, 257–275.

Badjana, H.M., Olofsson, P., Woodcock, C.E., Helmschrot, J., Wala, K., 2017b. Mapping and estimating land change between 2001 and 2013 in a heterogeneous landscape in West Africa: Loss of forestlands and capacity building opportunities. Int. J. Appl. Earth Obs. Geoinf. 63, 15–23. https://doi.org/10.1016/j.jag.2017.07.006

Badou, D.F., 2016. Multi-Model Evaluation of Blue and Green Water Availability Under Climate Change in Four-Non Sahelian Basins of the Niger River Basin. Doctor of Philosophy (Ph.D) thesis in Climate Change and Water Resources at University of

Abomey Calavi (Benin Republic), Defence date: September 09,.

Bárdossy, A., Schmidt, F., 2009. GIS approach to scale issues of perimeter-based shape indices for drainage basins. Hydrol. Process. 47, 931–942. https://doi.org/10.1080/02626660209493001

Begou, J.C., 2016. Hydrological Modeling of the Bani Basin in West Africa: Uncertainties and Parameters Regionalization. PhD of Graduate Research Program on Climate Change and Water Resources (GRP-CCWR) of the University of Abomey-Calavi (Benin Republic), Public defense on: 26/10/2016.

Begou, J.C., Jomaa, S., Benabdallah, S., Bazie, P., Afouda, A., Rode, M., 2016. Multi-Site Validation of the SWAT Model on the Bani Catchment: Model Performance and Predictive Uncertainty. Water (Switzerland) 8, 1–23. https://doi.org/10.3390/w8050178

Bennett, N.D., Croke, B.F.W., Guariso, G., Guillaume, J.H.A., Hamilton, S.H., Jakeman, A.J., Marsili-libelli, S., Newham, L.T.H., Norton, J.P., Perrin, C., Pierce, S.A., Robson, B., Seppelt, R., Voinov, A.A., Fath, B.D., 2013. Environmental Modelling & Software Characterising performance of environmental models q. Environ. Model. Softw. 40, 1–20. https://doi.org/10.1016/j.envsoft.2012.09.011

Berg, P., Feldmann, H., Panitz, H.-J., 2012. Bias correction of high resolution regional climate model data. J. Hydrol. 448–449, 80–92. https://doi.org/10.1016/j.jhydrol.2012.04.026

Beven, K., Binley, A., 1992. The future of distributed models: model calibration and uncertainty prediction. Hydrol. Process. 6, 279–298.

Biao, I.E., Gaba, C., Alamou, A.E., Afouda, A., 2015. Influence of the uncertainties related to the Random Component of Rainfall Inflow in the Ouémé River Basin (Benin , West Africa). Int. J. Curr. Eng. Technol. 5, 1618–1629.

Bilotta, G.S., Brazier, R.E., Haygarth, P.M., 2007. The impacts of grazing animals on the quality of soils, vegetation, and surface waters in intensively managed grasslands. Adv. Agron. 94, 237–280.

Bogena, H.R., Herbst, M., Huisman, J. a., Rosenbaum, U., Weuthen, a., Vereecken, H., 2010. Potential of Wireless Sensor Networks for Measuring Soil Water Content Variability. Vadose Zo. J. 9, 1002. https://doi.org/10.2136/vzj2009.0173

Bormann, H., 2005. Evaluation of hydrological models for scenario analyses: signal-to-noise-ratio between scenario effects and model uncertainty. Adv. Geosci. 5, 43–48.

Bormann, H., Ahlhorn, F., Klenke, T., 2012. Adaptation of water management to regional climate change in a coastal region – Hydrological change vs . community perception and strategies. J. Hydrol. 454–455, 64–75. https://doi.org/10.1016/j.jhydrol.2012.05.063

Bossa, A.Y., Diekkrüger, B., Giertz, S., Steup, G., Sintondji, L.O., Agbossou, E.K., Hiepe, C., 2012. Modeling the effects of crop patterns and management scenarios on N and P loads to surface water and groundwater in a semi-humid catchment (West Africa). Agric. Water Manag. 115, 20–37. https://doi.org/10.1016/j.agwat.2012.08.011

Bossa, A.Y., Diekkrüger, B., Igué, A.M., Gaiser, T., 2012. Analyzing the effects of different soil databases on modeling of hydrological processes and sediment yield in Benin (West Africa). Geoderma 173–174, 61–74. https://doi.org/10.1016/j.geoderma.2012.01.012

Bossio, D., Geheb, K., Critchley, W., 2010. Managing water by managing land: addressing land degradation to improve water productivity and rural livelihoods. Agric. Water Manag. 97, 536–542.

Breuer, L., Huisman, J.A., Willems, P., Bormann, H., Bronstert, A., Croke, B.F.W., Frede, H.-G., Gräff, T., Hubrechts, L., Jakeman, A.J., Kite, G., Lanini, J., Leavesley, G., Lettenmaier, D.P., Lindström, G., Seibert, J., Sivapalan, M., Viney, N.R., 2009. Assessing the impact of land use change on hydrology by ensemble modeling (LUCHEM). I: Model intercomparison with current land use. Adv. Water Resour. 32, 129–146. https://doi.org/10.1016/j.advwatres.2008.10.003

Brink, A.B., Eva, H.D., 2009. Monitoring 25 years of land cover change dynamics in Africa: A sample based remote sensing approach. Appl. Geogr. 29, 501–512. https://doi.org/10.1016/j.apgeog.2008.10.004

Brirhet, H., Benaabidate, L., 2016. Comparison Of Two Hydrological Models (Lumped And Distributed) Over A Pilot Area Of The Issen Watershed In The Souss Basin , Morocco. uropean Sci. J. 12, 347–358. https://doi.org/10.19044/esj.2016.v12n18p347

Butt, A., Shabbir, R., Ahmad, S.S., Aziz, N., 2015. Land use change mapping and analysis using Remote Sensing and GIS: A case study of Simly watershed , Islamabad , Pakistan. Egypt. J. Remote Sens. Sp. Sci. 18, 251–259. https://doi.org/10.1016/j.ejrs.2015.07.003

Camacho Olmedo, M.T., Pontius, R.G., Paegelow, M., Mas, J.F., 2015. Comparison of simulation models in terms of quantity and allocation of land change. Environ. Model. Softw. 69, 214–221. https://doi.org/10.1016/j.envsoft.2015.03.003

CEB, 2014. Barrage hydroélectrique d'Adjarala Avis sur l'examen de qualité de l'EIES. Cotonou, Benin.

Chen, D., Stow, D.A., Gong, P., 2004. Examining the effect of spatial resolution and texture window size on classification accuracy: an urban environment case. Int. J. Remote Sens. 25, 2177–2192. https://doi.org/10.1080/01431160310001618464

Chen, J., Cao, X., Peng, S., Ren, H., 2017. Analysis and Applications of GlobeLand30 : A Review. Int. J. Geo-information 3, 1–16. https://doi.org/10.3390/ijgi6080230

Chen, J., Chen, J., Liao, A., Cao, X., Chen, L., Chen, X., He, C., Han, G., Peng, S., Lu, M., Zhang, W., Tong, X., Mills, J., 2015. Global land cover mapping at 30 m resolution: A POK-based operational approach. ISPRS J. Photogramm. Remote Sens. 103, 7–27. https://doi.org/10.1016/j.isprsjprs.2014.09.002

Cho, K.H., Pachepsky, Y.A., Kim, J.H., Kim, J.-W., Park, M.-H., 2012. The modified SWAT model for predicting fecal coliforms in the Wachusett Reservoir Watershed, USA. water Res. 46, 4750–4760.

Ciais, P., Sabine, C., Bala, G., Bopp, L., Brovkin, V., Canadell, J., Chhabra, A., DeFries, R.,

Galloway, J., Heimann, M., 2013. Climate change 2013: the physical science basis. Contribution of Working Group I to the Fifth Assessment Report of the Intergovernmental Panel on Climate Change. K., Tignor, M., Allen, SK, Boschung, J., Nauels, A., Xia, Y., Bex, V., Midgley, PM, Eds.

CILSS, 2016. Landscapes of West Africa- A Window on a Changing World. 47914 252nd St, Garretson, SD 57030, UNITED STATES.

Congalton, R.G., 1991. A review of assessing the accuracy of classifications of remotely sensed data. Remote Sens. Environ. 37, 35–46. https://doi.org/10.1016/0034-4257(91)90048-B

Cornelissen, T., Diekkrüger, B., Giertz, S., 2013. A comparison of hydrological models for assessing the impact of land use and climate change on discharge in a tropical catchment. J. Hydrol. 498, 221–236. https://doi.org/10.1016/j.jhydrol.2013.06.016

Cotillon, S., 2017. The landscapes of West Africa—40 years of change. U.S. Geo- Log. Surv. Fact Sheet 4p. https://doi.org/10.3133/fs20173005

Da Costa, P.Y.D., Johnson, A.K.C., Affaton, P., 2013. Les terrains paléozoïques et mésozoïques du bassin côtier togolais: Stratigraphie et Paléogéographie. Stand. Sci. Res. Essays 1, 415–429.

Dashkhuu, D., Pil, J., Ahn, J., Lee, W., 2015. Long-term trends in daily temperature extremes over Mongolia. Weather Clim. Extrem. 8, 26–33. https://doi.org/10.1016/j.wace.2014.11.003

Descroix, L., Mahé, G., Lebel, T., Favreau, G., Galle, S., Gautier, E., Olivry, J.-C., Albergel, J., Amogu, O., Cappelaere, B., Dessouassi, R., Diedhiou, A., Le Breton, E., Mamadou, I., Sighomnou, D., 2009. Spatio-temporal variability of hydrological regimes around the boundaries between Sahelian and Sudanian areas of West Africa: A synthesis. J. Hydrol. 375, 90–102. https://doi.org/10.1016/j.jhydrol.2008.12.012

Devi, G.K., Ganasri, B.P., Dwarakish, G.S., 2015. A Review on Hydrological Models. Aquat. Procedia 4, 1001–1007. https://doi.org/10.1016/j.aqpro.2015.02.126

DGSCN-MPDAT, 2014. Quatrième Recensement Général de la Population et de l' Habitat au Togo. Direction Générale de la statistique et de la Comptabilité Nationale (DGSCN), Ministère Auprès du Président de la République, Chargé de la Planification, du Développement et de l'Aménagement du Territoire (MPDAT), Lomé-Togo.

Diallo, I., Sylla, M.B., Camara, M., Gaye, A.T., 2012. Interannual variability of rainfall over the Sahel based on multiple regional climate models simulations. Theor. Appl. Climatol. 12. https://doi.org/10.1007/s00704-012-0791-y

Diwediga, B., Wala, K., Folega, F., Dourma, M., Woegan, Y.A., Akpagana, K., Bao, Q., 2015. Biophysical and anthropogenous determinants of landscape patterns and degradation of plant communities in Mo hilly basin (Togo). Ecol. Eng. 85, 132–143. https://doi.org/10.1016/j.ecoleng.2015.09.059

Djaman, K., Sharma, V., Daran, R.R., Koudahe, K., Irmak, S., Amouzou, K.A., Rudnick, D.R., Sogbedji, J.M., 2017. Spatial and Temporal Variation in Precipitation in Togo. Int. J. Hydrol. 1, 1–10. https://doi.org/10.15406/ijh.2017.01.00019

Du, J., Qian, L., Rui, H., Zuo, T., Zheng, D., Xu, Y., Xu, C., 2012. Assessing the effects of urbanization on annual runoff and flood events using an integrated hydrological modeling system for Qinhuai River basin, China. J. Hydrol. 464–465, 127–139. https://doi.org/10.1016/j.jhydrol.2012.06.057

Dubreuil, P.L., 1985. Review of Field Observations of Runoff generation in the Tropics. J. Hydrol. 80, 237–264.

Dye, P.J., Croke, B.F.W., 2003. Evaluation of streamflow predictions by the IHACRES rainfall- runoff model in two South African catchments. Environ. Model. Softw. 18, 705–712. https://doi.org/10.1016/S1364-8152(03)00072-0

Eastman, J.R., 2006. IDRISI Andes, Guide to GIS and Image Processing, IDRISI Andes Guide to GIS and Image Processing. Clark Labs Clark University,950 Main Street Worcester, MA 01610-1477 USA.

Eisfelder, C., Kuenzer, C., Dech, S., 2012. Derivation of biomass information for semi-arid areas using remote-sensing data. Int. J. Remote Sens. 33, 2937–2984. https://doi.org/10.1080/01431161.2011.620034

Eshtawi, T., Evers, M., Tischbein, B., Diekkrüger, B., 2016. Integrated hydrologic modeling as a key for sustainable urban water resources planning. Water Res. 101, 411–428. https://doi.org/10.1016/j.watres.2016.05.061

FAO-ONU, 2016. Map Accuracy Assessment and Area Estimation: A Practical Guide. Organization of the United Nations Rome, Italia.

FAO-UNESCO, 1974. Legend of the soil map of the world. FAO Rome, Italy.

FAO, 2012. FAO Statistical Yearbook 2012 Africa: Food and Agriculture. Food and Agriculture Organization of the United Nations Regional Office for Africa Accra.

Faure, P., 1985. Les sols de la Kara, Nord-Est-Togo: relations avec l'environnement: carte pédologique à 1/50 000. IRD Editions.

Faure, P., Volkoff, B., 1998. Some factors affecting regional differentiation of the soils in the Republic of Benin (West Africa). Catena 32, 281–306. https://doi.org/10.1016/S0341-8162(98)00038-1

Ficchì, A., Perrin, C., Andréassian, V., 2016. Impact of temporal resolution of inputs on hydrological model performance: An analysis based on 2400 flood events. J. Hydrol. 538, 454–470. https://doi.org/10.1016/j.jhydrol.2016.04.016

Fitzgerald, R.W., Lees, B.G., 1994. Assessing the Classification Accuracy of Multisource Remote Sensing Data. Remote Sens. Environ. 47, 362–368.

Fohrer, N., Haverkamp, S., Frede, H.G., 2005. Assessment of the effects of land use patterns on hydrologic landscape functions: Development of sustainable land use concepts for low mountain range areas. Hydrol. Process. 19, 659–672. https://doi.org/10.1002/hyp.5623

Foody, G.M., 2002. Status of land cover classification accuracy assessment. Remote Sens. Environ. 80, 185–201. https://doi.org/10.1016/S0034-4257(01)00295-4

Gaba, O.U.C., Biao, I.E.E., Alamou, A.E., Afouda, A.A., 2015. An Ensemble Approach Modelling to Assess Water Resources in the Mékrou Basin , Benin. Hydrology 3, 22–32. https://doi.org/10.11648/j.hyd.20150302.11

Gan, T.Y., Dlamini, E.M., Biftu, G.F., 1997. Effects of model complexity and structure, data quality, and objective functions on hydrologic modeling. J. Hydrol. 192, 81–103.

Gardner, M.W., Dorling, S.R., 1998. Artificial neural networks (the multilayer perceptron) - A review of applications in the atmospheric sciences. Atmos. Environ. 32, 2627–2636.

Gassman, P.W., Reyes, M.R., Green, C.H., Arnold, J.G., 2007. The soil and water assessment tool: historical development, applications, and future research directions. Trans. ASABE 50, 1211–1250.

Gayibor, N., 1986. Écologie et histoire: les origines de la savane du Bénin. Cah. Etud. Afr. 26, 13–41.

Gbobaniyi, E., Sarr, A., Sylla, B., Diallo, I., Lennard, C., Dosio, A., Dhiediou, A., Kamga, A., Klutse, N.A.B., Hewitson, B., Nikulin, G., Lamptey, B., 2013. Climatology, annual cycle and interannual variability of precipitation and temperature in CORDEX simulations over West Africa. Int. J. Climatol. 1–17. https://doi.org/10.1002/joc.3834

Gérard-Marchant, P., Hively, W.D., Steenhuis, T.S., 2005. Distributed hydrological modelling of total dissolved phosphorus transport in an agricultural landscape, part I: distributed runoff generation. Hydrol. Earth Syst. Sci. Discuss. 2, 1537–1579. https://doi.org/10.5194/hessd-2-1537-2005

Gessner, U., Machwitz, M., Esch, T., Tillack, A., Naeimi, V., Kuenzer, C., Dech, S., 2015. Multi-sensor mapping of West African land cover using MODIS, ASAR and TanDEM-X/TerraSAR-X data. Remote Sens. Environ. 164, 282–297. https://doi.org/10.1016/j.rse.2015.03.029

Gessner, U., Niklaus, M., Kuenzer, C., Dech, S., 2013. Intercomparison of Leaf Area Index Products for a Gradient of Sub-Humid to Arid Environments in West Africa. Remote Sens. 5, 1235–1257. https://doi.org/10.3390/rs5031235

Ghoraba, S.M., 2015. Hydrological modeling of the Simly Dam watershed (Pakistan) using GIS and SWAT model. Alexandria Eng. J. 54, 583–594. https://doi.org/10.1016/j.aej.2015.05.018

Giertz, S., Diekkrüger, B., 2003. Analysis of the hydrological processes in a small headwater catchment in Benin (West Africa). Phys. Chem. Earth 28, 1333–1341. https://doi.org/10.1016/j.pce.2003.09.009

Giertz, S., Diekkrüger, B., Steup, G., 2006. Physically-based modelling of hydrological processes in a tropical headwater catchment in Benin (West Africa) – process representation and multi-criteria validation. Hydrol. Earth Syst. Sci. 3, 595–651. https://doi.org/10.5194/hessd-3-595-2006

Giertz, S., Junge, B., Diekkrüger, B., 2005. Assessing the effects of land use change on soil physical properties and hydrological processes in the sub-humid tropical environment of West Africa. Phys. Chem. Earth, Parts A/B/C 30, 485–496.

Gilbert, R.O., 1987. Statistical Methods for Environmental Pollution Monitoring. John Wiley & Sons, Inc, 605 Third Avenue, New York NY 10158M12. (212)850-6011, Fax (212) 850-6008.

Giorgetta, M.A., Jungclaus, J., Reick, C.H., Legutke, S., Bader, J., Böttinger, M., Brovkin, V., Crueger, T., Esch, M., Fieg, K., 2013. Climate and carbon cycle changes from 1850 to 2100 in MPI-ESM simulations for the Coupled Model Intercomparison Project phase 5. J. Adv. Model. Earth Syst. 5, 572–597.

Gocic, M., Trajkovic, S., 2013. Analysis of changes in meteorological variables using Mann-Kendall and Sen ' s slope estimator statistical tests in Serbia. Glob. Planet. Change 100, 172–182. https://doi.org/10.1016/j.gloplacha.2012.10.014

Golmohammadi, G., Prasher, S., Madani, A., Rudra, R., 2014. Evaluating Three Hydrological Distributed Watershed Models: MIKE-SHE, APEX, SWAT. Hydrology 1, 20–39. https://doi.org/10.3390/hydrology1010020

Gosling, S.N., Taylor, R.G., Arnell, N.W., Todd, M.C., 2011. A comparative analysis of projected impacts of climate change on river runoff from global and catchment-scale hydrological models. Hydrol. Earth Syst. Sci. 15, 279–294. https://doi.org/10.5194/hess-15-279-2011

Grimaldi, S., Petroselli, A., Arcangeletti, E., Nardi, F., 2013. Flood mapping in ungauged basins using fully continuous hydrologic – hydraulic modeling. J. Hydrol. 487, 39–47. https://doi.org/10.1016/j.jhydrol.2013.02.023

Gudmundsson, L., Seneviratne, S.I., 2016. Observation-based gridded runoff estimates for Europe (E-RUN version 1.1). Earth Syst. Sci. Data 8, 279–295. https://doi.org/10.5194/essd-8-279-2016

Gupta, H. V., Kling, H., Yilmaz, K.K., Martinez, G.F., 2009. Decomposition of the mean squared error and NSE performance criteria: Implications for improving hydrological modelling. J. Hydrol. 377, 80–91. https://doi.org/10.1016/j.jhydrol.2009.08.003

Haddeland, I., Heinke, J., Biemans, H., Eisner, S., Flörke, M., Hanasaki, N., Konzmann, M., Ludwig, F., Masaki, Y., Schewe, J., Stacke, T., Tessler, Z.D., Wada, Y., Wisser, D., 2014. Global water resources affected by human interventions and climate change. Proc. Natl. Acad. Sci. U. S. A. 111, 3251–6. https://doi.org/10.1073/pnas.1222475110

Haerter, J.O., Hagemann, S., Moseley, C., Piani, C., 2011. Climate model bias correction and the role of timescales. Hydrol. Earth Syst. Sci. 15, 1065–1079. https://doi.org/10.5194/hess-15-1065-2011

Hagemann, S., Blome, T., Saeed, F., Stacke, T., 2014. Perspectives in Modelling Climate-Hydrology Interactions. Surv. Geophys. 35, 739–764. https://doi.org/10.1007/s10712-013-9245-z

Halimatou, T., Kakifa, T., Kyei-baffour, N., 2017. Assessment of changing trends of daily precipitation and temperature extremes in Bamako and Segou in Mali from 1961- 2014. Weather Clim. Extrem. J. 18, 8–16. https://doi.org/10.1016/j.wace.2017.09.002

Hamilton, R.A., Archbold, J.W., Douglas, C.K.M., 1945. Meteorology of Nigeria and adjacent territory. Q. J. R. Meteorol. Soc. 71, 231–264.

Hanjra, M.A., Qureshi, M.E., 2010. Global water crisis and future food security in an era of climate change. Food Policy 35, 365–377. https://doi.org/10.1016/j.foodpol.2010.05.006

Hargreaves, G.H., Samani, Z.A., 1982. Estimating potential evapotranspiration. J. Irrig. Drain. Div. 108, 225–230.

Herbst, M., Casper, M.C., Grundmann, J., Buchholz, O., 2009. Comparative analysis of model behaviour for flood prediction purposes using Self-Organizing Maps. Nat. Hazards Earth Syst. Sci. 9, 373–392. https://doi.org/10.5194/nhess-9-373-2009

Herbst, M., Diekkrüger, B., Vereecken, H., 2006. Geostatistical co-regionalization of soil hydraulic properties in a micro-scale catchment using terrain attributes. Geoderma 132, 206–221. https://doi.org/10.1016/j.geoderma.2005.05.008

Heuzé, C., Heywood, K.J., Stevens, D.P., Ridley, J.K., 2013. Southern Ocean bottom water characteristics in CMIP5 models. Geophys. Res. Lett. 40, 1409–1414. https://doi.org/10.1002/grl.50287

Hiepe, C., 2008. Soil degradation by water erosion in a sub-humid West-African catchment: a modelling approach considering land use and climate change in Benin.

Hiepe, C., Diekkrüger, B., 2007. Modelling soil erosion in a sub-humid tropical environment at the regional scale considering land use and climate change. 4th Int. SWAT Conf. 73–80.

Houessou, S., 2016. Les inondataions et les risques prévisionnels liés aux barrages hydroéléctriques dans la basse vallée du Mono. These de doctorant, Universite d'Abomey Calavi, Benin, Soutenu publiquement le 11 Octobre 2016.

Houngue, N.R., 2018. Assessment of mid-century climate change impacts on Mono river's downstream inflows. Master thesis, Department of Geography, Université de Lomé, Togo, defended in January, 2018.

Hounkpè, J., 2016. Assessing the climate and land use changes impacts on flood hazard in Ouémé River Basin, Benin (West Africa). Doctor of Philosophy (Ph.D) thesis in Climate Change and Water Resources at University of Abomey Calavi (Benin Republic); Date of defense: 05 September 2016.

Hounkpè, J., Afouda, A.A., Diekkrüger, B., Hountondji, F., 2015. Modelling extreme streamflows under non-stationary conditions in the Ouémé River basin, Benin, West Africa. Hydrol. Sci. Water Secur. 366, 143–144. https://doi.org/10.5194/piahs-366-143-2015

Huang, H., Ouyang, W., Guo, B., Shi, Y., Hao, F., 2014. Vertical and horizontal distribution of soil parameters in intensive agricultural zone and effect on diffuse nitrogen pollution. Soil Tillage Res. 144, 32–40. https://doi.org/10.1016/j.still.2014.07.006

Huth, J., Kuenzer, C., Wehrmann, T., Gebhardt, S., Tuan, V.Q., Dech, S., 2012. Land Cover and Land Use Classification with TWOPAC:towards Automated Processing for Pixel- and Object-Based Image Classification. Remote Sens. 4, 2530–2553. https://doi.org/10.3390/rs4092530

Idrissou, M., Ngom, D.F., Malou, R., Vayssade, B., Courbis, A.-L., 2015. Water balance simulation for resource evaluation at watershed scale: application to the Nema (Sudano-Sahelian zone, Senegal). Hydrol. Sci. J. 60, 1620–1630. https://doi.org/10.1080/02626667.2014.932055

INDC-Togo, 2015. Intended Nationally Determined Contribution (INDC) Within The Framework Of The United Nations Framework Convention On Climate Change (UNFCCC).

IPCC, 2014. Climate Change 2014: Synthesis Report. Contribution of Working Groups I, II and III to the Fifth Assessment Report of the Intergovernmental Panel on Climate Change; Technical Report. IPCC, Geneva, Switzerland.

Jain, S.K., Kumar, V., 2016. Trend analysis of rainfall and temperature data for India. Curr. Sci. 102, 37–49.

Jaiswal, R.K., Lohani, A.., Tiwari, H.., 2015. Statistical Analysis for Change Detection and Trend Assessment in Climatological Parameters. Environ. Process. 2, 729–749. https://doi.org/10.1007/s40710-015-0105-3

Jakeman, A.J., Hornberger, G.M., 1993. How Much Complexity Is Warranted in a Rainfall-Runoff Model? Water Resour. Res. 29, 2637–2649.

Jayakrishnan, R., Srinivasan, R., Santhi, C., Arnold, J.G., 2005. Advances in the application of the SWAT model for water resources management. Hydrol. Process. 19, 749–762. https://doi.org/10.1002/hyp.5624

Jiang, D., Huang, Y., Zhuang, D., Zhu, Y., Xu, X., Ren, H., 2012. A Simple Semi-Automatic Approach for Land Cover Classification from Multispectral Remote Sensing Imagery. PLoS One 7. https://doi.org/10.1371/journal.pone.0045889

Kankam-yeboah, K., Obuobie, E., Amisigo, B., Opoku-ankomah, Y., 2013. Impact of climate change on streamflow in selected river basins in Ghana. Hydrol. Sci. J. 58, 773–788. https://doi.org/10.1080/02626667.2013.782101

Kappelle, M., Van Vuuren, M.M.I., Baas, P., 1999. Effects of climate change on biodiversity: a review and identification of key research issues. Biodivers. Conserv. 8, 1383–1397. https://doi.org/10.1023/A:1008934324223

Kasei, R., Diekkrüger, B., Leemhuis, C., 2010. Drought frequency in the Volta Basin of West Africa. Sustain. Sci. 5, 89–97. https://doi.org/10.1007/s11625-009-0101-5

Kendall, M.G., 1975. Rank Correlation Methods, Charles Griffin, London (1975). Google Sch.

Kennedy, J., Everhart, R.C., 1995. A new optimizer using particle swarm theory. In proceedings of the sixth international symposium on micro machine and human science. Nagoya Japón. IEEE Serv. Cent. Piscataway, NJ.

Kepner, W.G., Semmens, D.J., Bassett, S.D., Mouat, D.A., Goodrich, D.C., 2004. Scenario analysis for the San Pedro River, analyzing hydrological consequences of a future environment. Environ. Monit. Assess. 94, 115–127.

Kharel, G., Zheng, H., Kirilenko, A., 2016. Can land-use change mitigate long-term flood risks in the Prairie Pothole Region? The case of Devils Lake, North Dakota, USA. Reg. Environ. Chang. 1–14. https://doi.org/10.1007/s10113-016-0970-y

Kim, N.W., Lee, J., 2010. Enhancement of the channel routing module in SWAT. Hydrol. Process. An Int. J. 24, 96–107.

Kinnell, P.I.A., 2010. Event soil loss , runoff and the Universal Soil Loss Equation family of models : A review. J. Hydrol. 385, 384–397. https://doi.org/10.1016/j.jhydrol.2010.01.024

Kissi, A.E., Abbey, G.A., Agboka, K., Egbendewe, A., 2015. Quantitative Assessment of Vulnerability to Flood Hazards in Downstream Area of Mono Basin, South-Eastern Togo: Yoto District. J. Geogr. Inf. Syst. 7, 607–619. https://doi.org/10.4236/jgis.2015.76049

Klassou, K.S., 1996. Evolution climato-hydrologique récente et conséquence sur l'environnement: l'exemple du bassin versant du fleuve Mono (Togo-Bénin). Dissertation doctorale, Université de Bordeaux 3, France.

Kleemann, J., Baysal, G., Bulley, H.N.N.N., Fürst, C., 2017. Assessing driving forces of land use and land cover change by a mixed-method approach in north-eastern Ghana, West Africa. J. Environ. Manage. 196, 411–442. https://doi.org/10.1016/j.jenvman.2017.01.053

Kling, H., Gupta, H., 2009. On the development of regionalization relationships for lumped watershed models: The impact of ignoring sub-basin scale variability. J. Hydrol. 373, 337–351. https://doi.org/10.1016/j.jhydrol.2009.04.031

Knauer, K., Gessner, U., Dech, S., Kuenzer, C., 2014. Remote sensing of vegetation dynamics in West Africa. Int. J. ofRemote Sens. 35, 6357–6396. https://doi.org/10.1080/01431161.2014.954062

Kodja, D.J., Mahé, G., Amoussou, E., Boko, M., Paturel, J.-E., 2018. Assessment of the Performance of Rainfall-Runoff Model GR4J to Simulate Streamflow in Ouémé Watershed at Bonou's outlet (West Africa). Preprint 18. https://doi.org/10.20944/PREPRINTS201803.0090.V1

Koglo, Y.S., Agyare, W.A., Diwediga, B., Sogbedji, J.M., Adden, A.K., Gaiser, T., 2018. Remote Sensing-Based and Participatory Analysis of Forests, Agricultural Land Dynamics, and Potential Land Conservation Measures in Kloto District (Togo, West Africa). Soil Syst. 2, 49. https://doi.org/10.3390/soilsystems2030049

Kokou, K.., Adjossou, K., Hamberger, K., 2005. Les Forets Sacrees De L'Aire Ouatchi Au Sud-Est Modes De Gestion Locale Des Ressources Forestieres. VertigO-la Rev. électronique en Sci. l'environnement 6.

Komi, K., Amisigo, B.A., Diekkrüger, B., 2016. Integrated Flood Risk Assessment of Rural Communities in the Oti River Basin, West Africa. Hydrology 3, 42. https://doi.org/10.3390/hydrology3040042

Koubodana, H.D., 2015. Mecanismes de connexions entre les modes de varaibilités internannuelle equatorial et meridien de l'Atlantique tropical. These de Master, Chaire

Internationale en Physique Mathématique et Applications (CIPMA-Chaire UNESCO), Université d'Abomey-Calavi (UAC), Benin, Soutenu en Octobre 2015.

Koubodana, H.D., Diekkrüger, B., Näschen, K., Adounkpe, J., Atchonouglo, K., 2019a. Impact of the Accuracy of Land Cover Data Sets on the Accuracy of Land Cover Change Scenarios in the Mono River Basin, Togo, West Africa. Int. J. Adv. Remote Sens. GIS 8, 3073–3095. https://doi.org/10.23953/cloud.ijarsg.422

Koubodana, H.D., Tall, M., Amoussou, E., Mumtaz, M., Adounkpe, J., Atchonouglo, K., 2019b. Trend Analysis of Hydroclimatic Historical Data and Future Scenarios of Climate Extreme Indices over Mono River Basin in West Africa. Preprint June, 22. https://doi.org/10.20944/preprints201906.0267.v1

Kouchi, D.H., Esmaili, K., Faridhosseini, A., Sanaeinejad, S.H., Khalili, D., Abbaspour, K.C., 2017. Sensitivity of calibrated parameters and water resource estimates on different objective functions and optimization algorithms. Water (Switzerland) 9, 1–16. https://doi.org/10.3390/w9060384

Koutroulis, A.G., Tsanis, I.K., Daliakopoulos, I.N., Jacob, D., 2013. Impact of climate change on water resources status : A case study for Crete Island, Greece. J. Hydrol. 479, 146–158. https://doi.org/10.1016/j.jhydrol.2012.11.055

Krause, P., Boyle, D.P., 2005. Advances in Geosciences Comparison of different efficiency criteria for hydrological model assessment. Adv. Geosci. 5, 89–97. https://doi.org/10.5194/adgeo-5-89-2005

Krysanova, V., Hattermann, F., Huang, S., 2011. Model SWIM for Climate and land use change assessment, Chinese German Summer School.

Krysanova, V., Hattermann, F., Huang, S., Hesse, C., Vetter, T., Liersch, S., Koch, H., Kundzewicz, Z.W., 2015. Modelling climate and land-use change impacts with SWIM: lessons learnt from multiple applications. Hydrol. Sci. J. 60, 606–635. https://doi.org/10.1080/02626667.2014.925560

Lahsen, M., 2005. Seductive Simulations? Uncertainty Distribution Around Climate Models. Soc. Stud. Sci. 35, 895–922. https://doi.org/10.1177/0306312705053049

Lambin, E.F., Geist, H.J., Lepers, E., 2003. Dynamics of Land-Use and Land Cover Change in Tropical Regions. Annu. Rev. Environ. Resour. 28, 205–241. https://doi.org/10.1146/annurev.energy.28.050302.105459

Lamouroux, M., Lamouroux, R., 1969. Carte pédologique du Togo à l'échelle de 1: 1 000 000, Office de. ed. Office de la recherche scientifique et technique outre-mer, Paris, France.

Lamouroux, R., 196AD. Carte pédologique du Togo à l'échelle de 1: 1 000 000. Office de la recherche scientifique et technique outre-mer.

Laurent, H., Jobard, I., Toma, A., 1998. Validation of satellite and ground based estimates of precipitation over the Sahel. Atmos. Res. 47–48, 651–670.

Laux, P., Wagner, S., Wagner, A., Jacobeit, J., B, A., 2009. Modelling daily precipitation features in the Volta Basin of West Africa. Int. J. Climatol. 29, 937–954.

https://doi.org/10.1002/joc

Lawin, A.E., Hounguè, N.R., Biaou, C.A., Badou, D.F., 2019a. Statistical Analysis of Recent and Future Rainfall and Temperature Variability in the Mono River Watershed (Benin, Togo). Climate 7, 8. https://doi.org/10.3390/cli7010008

Lawin, A.E., Lamboni, B., Manirakiza, C., Kamou, H., 2019b. Future Extremes Temperature: Trends and Changes Assessment over the Mono River Basin, Togo (West Africa). J. Water Resour. Prot. 11, 82–98. https://doi.org/10.4236/jwarp.2019.111006

Le Barbé, L., Lebel, T., 1997. Rainfall climatology of the HAPEX-Sahel region during the years 1950–1990. J. Hydrol. 188, 43–73.

Le Lay, M., Galle, S., Saulnier, G.M., Braud, I., 2007. Exploring the relationship between hydroclimatic stationarity and rainfall-runoff model parameter stability: A case study in West Africa. Water Resour. Res. 43, 1–10. https://doi.org/10.1029/2006WR005257

Lebel, T., Ali, A., 2009. Recent trends in the Central and Western Sahel rainfall regime (1990-2007). J. Hydrol. 375, 52–64. https://doi.org/10.1016/j.jhydrol.2008.11.030

Leblanc, M., Tweed, S., Dijk, A. Van, Timbal, B., 2012. A review of historic and future hydrological changes in the Murray-Darling Basin. Glob. Planet. Change 80–81, 226–246. https://doi.org/10.1016/j.gloplacha.2011.10.012

Lee, H., Zehe, E., Sivapalan, M., 2007. Predictions of rainfall-runoff response and soil moisture dynamics in a microscale catchment using the CREW model. Hydrol. Earth Syst. Sci 11, 819–849. https://doi.org/10.5194/hessd-3-1667-2006

Leopold, L.B., 1968. Hydrology for urban land planning: A guidebook on the hydrologic effects of urban land use, US Departm. ed. Citeseer.

Li, H.-Y.Y., Ruby Leung, L., Tesfa, T., Voisin, N., Hejazi, M., Liu, L., Liu, Y., Rice, J., Wu, H., Yang, X., Ruby Leng, L., Testfa, T., Voisin, N., Hejazi, M., Liu, L., Lui, Y., Rice, J., Wu, H., Yang, W., 2014. Modeling stream temperature in the Anthropocene: An earth system modeling approach. J. Adv. Model. Earth Syst. 7, 513–526. https://doi.org/110.1002/2015MS000471

Li, Y., Feng, A., Iu, W., Ma, X., Dong, G., 2017. Variation of Aridity Index and the Role of Climate Variables in the Southwest China. Water 9, 743. https://doi.org/10.3390/w9100743

Lindström, G., Johansson, B., Persson, M., 1997. Development and test of the distributed HBV-96 hydrological model. J. Hydrol. 201, 272–288.

Littlewood, I.G., Down, K., Parker, J.R., Post, D.A., 1997. IHACRES V1.0 User Guide. Centre for Ecology and Hydrology, Wallingford, UK & Integrated Assessment and Management Centre, AUstralian National University, Canberra.

Liu, G., He, Z., Luan, Z., Qi, S., 2018. Intercomparison of a Lumped Model and a Distributed Model for Streamflow Simulation in the. Water 10, 1004. https://doi.org/10.3390/w10081004

Liu, J., 2009. A GIS-based tool for modelling large-scale crop-water relations. Environ.

Model. Softw. 24, 411–422. https://doi.org/10.1016/j.envsoft.2008.08.004

Liu, Y., Chen, Y., 2006. Impact of population growth and land-use change on water resources and ecosystems of the arid Tarim River Basin in Western China. Int. J. Sustain. Dev. World Ecol. 13, 295–305.

Lørup, J.K., Refsgaard, J.C., Mazvimavi, D., 1998. Assessing the effect of land use change on catchment runoff by combined use of statistical tests and hydrological modelling: Case studies from Zimbabwe. J. Hydrol. 205, 147–163. https://doi.org/10.1016/S0168-1176(97)00311-9

Louvet, S., Paturel, J.E., Mahé, G., Rouché, N., Koité, M., 2016. Comparison of the spatiotemporal variability of rainfall from four different interpolation methods and impact on the result of GR2M hydrological modeling-case of Bani River in Mali, West Africa. Theor. Appl. Climatol. 123, 303–319. https://doi.org/10.1007/s00704-014-1357-y

Lunetta, R.S., Knight, J.F., Ediriwickrema, J., Lyon, J.G., Dorsey, L., 2006. Land-Cover Change Detection Using Multi-Temporal MODIS NDVI Data. Remote Sens. Environ. 105, 142–154.

Ma, L., Ascough Ii, J.C., Ahuja, L.R., Shaffer, M.J., Hanson, J.D., Rojas, K.W., 2000. Root zone water quality model sensitivity analysis using Monte Carlo simulation. Trans. ASAE 43, 883.

Mango, L.M., Melesse, A.M., Mcclain, M.E., Gann, D., Setegn, S.G., Melesse, A.M., Mcclain, M.E., Gann, D., Setegn, S.G., 2011. Land use and climate change impacts on the hydrology of the upper Mara River Basin, Kenya: results of a modeling study to support better resource management. Hydrol. Earth Syst. Sci. 15, 2245–2258. https://doi.org/10.5194/hess-15-2245-2011

Mann, H.B., 1945. Nonparametric tests against trend. Econom. J. Econom. Soc. 245–259.

Maraun, D., 2013. Bias Correction, Quantile Mapping, and Downscaling: Revisiting the Inflation Issue. J. Clim. 26, 2137–2143. https://doi.org/10.1175/JCLI-D-12-00821.1

Maraun, D., Wetterhall, F., Ireson, A.M., Chandler, R.E., Kendon, E.J., Widmann, M., Brienen, S., Rust, H.W., Sauter, T., Al., E., Themeßl, M., Venema, V.K.C., Chun, K.P., Goodess, C.M., Jones, R.G., Onof, C., Vrac, M., Thiele-Eich, I., 2010. Precipitation downscaling under climate change. Recent developments to bridge the gap between dynamical models and the end user. Rev. Geophys. 48, 1–39. https://doi.org/10.1029/2009RG000314.

Maria, R., Omrani, H., Charif, O., Gerber, P., 2014. Land use changes modelling using advanced methods : Cellular automata and arti fi cial neural networks . The spatial and explicit representation of land cover dynamics at the cross-border region scale. Appl. Geochemistry 53, 160–171. https://doi.org/10.1016/j.apgeog.2014.06.016

Martinez-Casanovas, A., 2003. A spatial information technology approach for the mapping and quantification of gully erosion. Catena 50, 293–308.

Mas, J.F., Kolb, M., Paegelow, M., Camacho Olmedo, M.T., Houet, T., 2014. Inductive pattern-based land use/cover change models: A comparison of four software packages.

Environ. Model. Softw. 51, 94–111. https://doi.org/10.1016/j.envsoft.2013.09.010

Mbaye, M.L., Hagemann, S., Haensler, A., Stacke, T., Gaye, A.T., Afouda, A.A., 2015. Assessment of Climate Change Impact on Water Resources in the Upper Senegal Basin (West Africa). Am. J. Clim. Chang. 04, 77–93. https://doi.org/10.4236/ajcc.2015.41008

Memarian, H., Balasundram, S.K., Talib, J.B., Sood, A.M., Abbaspour, K.C., 2012. Trend analysis of water discharge and sediment load during the past three decades of development in the Langat basin, Malaysia Trend analysis of water discharge and sediment load during the past. Hydrol. Sci. J. 57, 1207–1222.

MERF, 2015. Troisième communication national sur les changements climatiques. Ministere de l'environnements et des ressources forestières (MERF), Lomé, Togo.

Michel, C., 1989. Un modèle pluie-débit journalier à trois paramètres. La Houille Blanche 113–122.

Mikemina, P., 2013. Climate chan ge impact on Togo's agriculture performance: a ricardian analysis based on time series data. Ethiop. J. Environ. Stud. Manag. Vol. 6, 390–397.

Mishra, A.K., Singh, V.P., 2010. A review of drought concepts. J. Hydrol. 391, 202–216. https://doi.org/10.1016/j.jhydrol.2010.07.012

Mishra, V.N., Rai, P.K., Mohan, K., 2014. Prediction of land use changes based on land change modeler (LCM) using remote sensing: a case study of Muzaffarpur (BIHAR), India. J. Geogr. Institute'Jovan Cvijic'SASA 64, 111–127. https://doi.org/10.2298/IJGI1401111M

Mohammed, Y.S., Mustafa, Mw., Bashir, N., Mokhtar, A.S., 2013. Renewable energy resources for distributed power generation in Nigeria: a review of the potential. Renew. Sustain. Energy Rev. 22, 257–268.

Monteith, J.L., 1965. Evaporation and environment, in the state and movement of water in living organisms, in: Symp. Soc. Exp. Biol. Academic Press, pp. 205–234.

Montenegro, S., Ragab, R., 2012. Impact of possible climate and land use changes in the semi arid regions : A case study from North Eastern Brazil. J. Hydrol. 434–435, 55–68. https://doi.org/10.1016/j.jhydrol.2012.02.036

Moriasi, D.N., Arnold, J.G., Van Liew, M.W., Binger, R.L., Harmel, R.D., Veith, T.L., Liew, M.W. Van, Bingner, R.L., Harmel, R.D., Veith, T.L., 2007. Model evaluation guidelines for systematic quantification of accuracy in watershed simulations. Am. Soc. Agric. Biol. Eng. 50, 885–900. https://doi.org/10.13031/2013.23153

Moriasi, D.N., Wilson, B.N., Arnold, J.G., Gowda, P.H., 2012. Hydrologic and water quality models: use, calibration, and validation. Am. Soc. Agric. Biol. Eng. 55, 1241–1247. https://doi.org/10.13031/2013.42265

Muleta, M.K., Nicklow, J.W., 2005. Sensitivity and uncertainty analysis coupled with automatic calibration for a distributed watershed model. J. Hydrol. 306, 127–145.

Näschen, K., Diekkrüger, B., Leemhuis, C., Steinbach, S., Seregina, L.S., Thonfeld, F., van der Linden, R., 2018. Hydrological modeling in data-scarce catchments: The

Kilombero floodplain in Tanzania. Water (Switzerland) 10, 28. https://doi.org/10.3390/w10050599

Nash, J.E., Sutcliffe, J. V, 1970. River flow forecasting through conceptual models part I— A discussion of principles. J. Hydrol. 10, 282–290.

Navarro-Racines, C.E., Tarapues-Montenegro, J.E., Ramírez-Villegas, J.A., 2015. Bias-correction in CCAFS Climate poral: Description of methodologies. Cali, Colombia.

Ndomba, P., Mtalo, F., Killingtveit, A., 2008. SWAT model application in a data scarce tropical complex catchment in Tanzania. Phys. Chem. Earth 33, 626–632. https://doi.org/10.1016/j.pce.2008.06.013

Ndulue, E.L., Mbajiorgu, C.C., Ugwu, S.N., Ogwo, V., Ogbu, K.N., 2015. Assessment of land use/cover impacts on runoff and sediment yield using hydrologic models: A review. J. Ecol. Nat. Environ. 7, 46–55.

Neitsch, S.L., Arnold, J.G., Kiniry, J.R., Williams, J.R., 2011. Soil and water assessment tool theoretical documentation version 2009. Texas Water Resources Institute, Texas Water Resources Institute: Temple, TX, USA, 2011.

New, M., Hewitson, B., Stephenson, D.B., Tsiga, A., Kruger, A., Manhique, A., Gomez, B., Coelho, C.A.S., Masisi, D.N., Kululanga, E., Mbambalala, E., Adesina, F., Saleh, H., Kanyanga, J., Adosi, J., Bulane, L., Fortunata, L., Mdoka, M.L., Lajoie, R., Town, C., Town, C., Africa, S., Town, C., 2006. Evidence of trends in daily climate extremes over southern and west Africa. J. Geophys. Res. 111, 1–11. https://doi.org/10.1029/2005JD006289

Nicholson, S.E., 2013. The West African Sahel: A Review of Recent Studies on the Rainfall Regime and Its Interannual Variability. ISRN Meteorol. 2013, 32 pages.

Niel, H., Paturel, J., Servat, E., 2003. Study of parameter stability of a lumped hydrologic model in a context of climatic variability. J. Hydrol. 278, 213–230. https://doi.org/10.1016/S0022-1694(03)00158-6

Ntajal, J., 2015. Flood Disaster Risk Mapping in the Lower Mono River Basin in Togo. Master Degree thesis in Climate Change and Human Security,Department of Geography, University of Lome, Togo; Defense dat: October.

Ntajal, J., Lamptey, B.L., Mahamadou, I.B., Nyarko, B.K., 2017. Flood Disaster Risk Mapping in the Lower Mono River Basin in Togo, West. Int. J. Disaster Risk Reduct. 23, 93–103. https://doi.org/10.1016/j.ijdrr.2017.03.015

Obuobie, E., Diekkrüger, B., 2008. Using SWAT to Evaluate Climate Change Impact on Water Resources in the White Volta River Basin, West Africa, in: Conference on International Research on Food Security, Natural Resource Management and Rural Development. Tropentag,University of Hohenheim, October 7-9, 2008 Conference, pp. 1–4.

Obuobie, E., Diekkrüger, B., Reichert, B., 2010. Use of chloride mass balance method for estimating the groundwater recharge in northeastern Ghana. Int. J. River Basin Manag. 8, 245–253. https://doi.org/10.1080/15715124.2010.505895

Oguntunde, P.G., Abiodun, B.J., 2013. The impact of climate change on the Niger River Basin hydroclimatology, West Africa. Clim. Dyn. 40, 81–94. https://doi.org/10.1007/s00382-012-1498-6

Oguntunde, P.G., Abiodun, B.J., Lischeid, G., 2011. Rainfall trends in Nigeria , 1901 – 2000. J. Hydrol. 411, 207–218. https://doi.org/10.1016/j.jhydrol.2011.09.037

Oguntunde, P.G., Friesen, J., Giesen, N. Van De, Savenije, H.H.G., 2006. Hydroclimatology of the Volta River Basin in West Africa: Trends and variability from 1901 to 2002. Phys. Chem. Earth, Parts A/B/C 31, 1180–1188. https://doi.org/10.1016/j.pce.2006.02.062

Olofsson, P., Foody, G.M., Stehman, S. V, Woodcock, C.E., 2013. Making better use of accuracy data in land change studies: Estimating accuracy and area and quantifying uncertainty using stratified estimation. Remote Sens. Environ. 129, 122–131. https://doi.org/10.1016/j.rse.2012.10.031

Omotosho, J.B., Abiodun, B.J., 2007. A numerical study of moisture build-up and rainfall over West Africa. Meteorol. Appl. 225, 209–225. https://doi.org/10.1002/met.11

ONU-SOFRELEC, 1964. Rapport final d'Aménagement du bassin du Mono. Société Française d'Etudes et de Réalisations d'Equipements Electriques (SOFRELEC).19, Rue de Passy Paris, France.

Onyutha, C., Tabari, H., Rutkowska, A., Nyeko-Ogiramoi, P., Willems, P., 2016. Comparison of different statistical downscaling methods for climate change rainfall projections over the Lake Victoria basin considering CMIP3 and CMIP5. J. hydro-environment Res. 12, 31–45.

Osorio, J.D.G., Galiano, S.G.G., 2012. Non-stationary analysis of dry spells in monsoon season of Senegal River Basin using data from Regional Climate Models (RCMs). J. Hydrol. 450–451, 82–92. https://doi.org/10.1016/j.jhydrol.2012.05.029

Ouedraogo, I., Tigabu, M., Savadogo, P., Compaoré, H., Odén, P.C., Ouadba, J.M., 2010. Land cover change and its relation with population dynamics in Burkina Faso, West Africa. L. Degrad. Dev. 21, 453–462.

Ouyang, Y., 2012. A potential approach for low flow selection in water resource supply and management. J. Hydrol. 454, 56–63. https://doi.org/10.1016/j.jhydrol.2012.05.062

Owusu, K., Waylen, P., Qiu, Y., 2008. Changing rainfall inputs in the Volta basin: implications for water sharing in Ghana. GeoJournal 71, 201–210. https://doi.org/10.1007/s10708-008-9156-6

Oyerinde, G.T., Hountondji, F.C.C., Wisser, D., Diekkrüger, B., Lawin, A.E., Odofin, A.J., Afouda, A., Diekkruger, B., Lawin, A.E., Odofin, A.J., Afouda, A., 2015. Hydro-climatic changes in the Niger basin and consistency of local perceptions. Reg. Environ. Chang. 15, 1627–1637. https://doi.org/10.1007/s10113-014-0716-7

Oyerinde, G.T., Wisser, D., Hountondji, F.C.C., Odofin, A.J., Lawin, A.E., Afouda, A.A., Diekkrüger, B., 2016. Quantifying Uncertainties in Modeling Climate Change Impacts on Hydropower Production. Climate 4, 1–15. https://doi.org/10.3390/cli4030034

Pachauri, R.K., Allen, M.R., Barros, V.R., Broome, J., Cramer, W., Christ, R., Church, J.A., Clarke, L., Dahe, Q., Dasgupta, P., 2014. Climate change 2014: synthesis report. Contribution of Working Groups I. II III to fifth Assess. Rep. Intergov. Panel Clim. Chang. 151.

Paeth, H., Thamm, H.P., 2007. Regional modelling of future African climate north of 15°S including greenhouse warming and land degradation. Clim. Change 83, 401–427. https://doi.org/10.1007/s10584-006-9235-y

PANGIRE, 2016. Plan d'Action National de Gestion Intégrée des Ressources en Eaux - TOGO. Lomé, Togo.

Panthou, G., Vischel, T., Lebel, T., Blanchet, J., Quantin, G., Ali, A., 2012. Extreme rainfall in West Africa: A regional modeling. Water Resour. Res. 48, 1–19. https://doi.org/10.1029/2012WR012052

PCCP, 2008. PROGRAMME PCCP -From Potential Conflict to Cooperation Potential: cas du basin du Mono (Togo-Benin). Lomé-Togo.

Pedinotti, V., Boone, A., Decharme, B., Cr, J.F., 2012. Evaluation of the ISBA-TRIP continental hydrologic system over the Niger basin using in situ and satellite derived datasets. Hydrol. Earth Syst. Sci. 16, 1745–1773. https://doi.org/10.5194/hess-16-1745-2012

Penman, H.L., 1956. Estimating evaporation. Eos, Trans. Am. Geophys. Union 37, 43–50.

Penman, J., Gytarsky, M., Hiraishi, T., Krug, T., Kruger, D., Pipatti, R., Wagner, F., 2003. Good practice guidance for land use, land use change and forestry. Institute for Global Environmental Strategies (IGES) for the IPCC, 2108 -11, Kamiyamaguchi Hayama, Kanagawa Japan, 240-0115.

Pereira, D.R., Martinez, M.A., Pruski, F.F., da Silva, D.D., 2016. Hydrological simulation in a basin of typical tropical climate and soil using the SWAT model part I: Calibration and validation tests. Biochem. Pharmacol. 7, 14–37. https://doi.org/10.1016/j.ejrh.2016.05.002

Perrin, C., Michel, C., Andre, V., 2003. Improvement of a parsimonious model for streamflow simulation. J. Hydrol. 279, 275–289. https://doi.org/10.1016/S0022-1694(03)00225-7

Perrin, C., Michel, C., Andre, V., 2001. Does a large number of parameters enhance model performance ? Comparative assessment of common catchment model structures on 429 catchments. J. Hydrol. 242, 275–301.

PNSET, 2012. Programme National de Suivi de l'Environnement au TOGO (PNSET). Lomé, Togo.

Poff, N.L., Allan, J.D., Palmer, M.A., Hart, D.D., Richter, B.D., Arthington, A.H., Rogers, K.H., Meyer, J.L., Stanford, J.A., 2003. River flows and water wars : emerging science for environmental decision making. Ecol. Soc. Am. 298–306.

Polo-akpisso, A., Wala, K., Soulemane, O., Foléga, F., Akpagana, K., Tano, Y., 2019. Assessment of Habitat Change Processes within the Oti-Keran-Mandouri Network of

Protected Areas in Togo (West Africa) from 1987 to 2013 Using Decision Tree Analysis. Sci 1, 9. https://doi.org/10.3390/sci1010009.v1

Poméon, T., Diekkrüger, B., Springer, A., Kusche, J., Eicker, A., 2018. Multi-Objective Validation of SWAT for Sparsely-Gauged West African River Basins—A Remote Sensing Approach. Water 10, 1–22. https://doi.org/10.3390/w10040451

Poméon, T., Jackisch, D., Diekkrüger, B., 2017. Evaluating the performance of remotely sensed and reanalysed precipitation data over West Africa using HBV light. J. Hydrol. 547, 222–235. https://doi.org/10.1016/j.jhydrol.2017.01.055

Pontius, R.G., Cornell, J.D., Hall, C.A.S., 2001. Modeling the spatial pattern of land-use change with GEOMOD2: application and validation for Costa Rica. Agric. Ecosyst. Environ. 85, 191–203.

Pontius, R.G., Malanson, J., 2014. Comparison of the structure and accuracy of two land change models. Int. J. Geogr. Inf. Sci. 19, 243–265. https://doi.org/10.1080/13658810410001713434

Pontius, R.G., Millones, M., 2011. Death to Kappa: Birth of quantity disagreement and allocation disagreement for accuracy assessment. Int. J. Remote Sens. 32, 4407–4429. https://doi.org/10.1080/01431161.2011.552923

Pontius, R.G., Neeti, N., 2010. Uncertainty in the difference between maps of future land change scenarios. Sustain. Sci. 5, 39–50. https://doi.org/10.1007/s11625-009-0095-z

Pontius, R.G., Spencer, J., 2005. Uncertainty in extrapolations of predictive land-change models. Environ. Plan. B Plan. Des. 32, 211–230. https://doi.org/10.1068/b31152

Priestley, C.H.B., Taylor, R.J., 1972. On the assessment of surface heat flux and evaporation using large-scale parameters. Mon. Weather Rev. 100, 81–92.

Rana, A., Foster, K., Bosshard, T., Olsson, J., Bengtsson, L., 2014. Regional Studies Impact of climate change on rainfall over Mumbai using Distribution-based Scaling of Global Climate Model projections. J. Hydrol. Reg. Stud. 1, 107–128. https://doi.org/10.1016/j.ejrh.2014.06.005

Regh, T., Bossa, A.Y., Diekkrüger, B., 2014. Scenario-based simulations of the impacts of rainfall variability and management options on maize production in Benin. African J. Agric. Res. 9, 3393–3410. https://doi.org/10.5897/AJAR2014.8757

Reichler, T., Kim, J., 2008. Uncertainties in the climate mean state of global observations , reanalyses , and the GFDL climate model. J. Geophys. Res. 113, 1–13. https://doi.org/10.1029/2007JD009278

Reid, R.S., Kruska, R.L., Muthui, N., Taye, A., Wotton, S., Wilson, C.J., Mulatu, W., 2000. Land-use and land-cover dynamics in response to changes in climatic, biological and socio-political forces: the case of southwestern Ethiopia. Landsc. Ecol. 15, 339–355.

Ren, H., Cai, G., Zhao, G., Li, Z., 2018. Accuracy Assessment of the GlobeLand30 dataset in Jiangxi Province. Remote Sens. Spat. Inf. Sci. 42, 1481–1487. https://doi.org/10.5194/isprs-archives-XLII-3-1481-2018 %7C

Renard, B., Kavetski, D., Kuczera, G., Thyer, M., Franks, S.W., 2010. Understanding predictive uncertainty in hydrologic modeling: The challenge of identifying input and structural errors. Water Resour. Res. 46, 1–22. https://doi.org/10.1029/2009WR008328

Reuter, H.I., Nelson, A., Jarvis, A., 2007. An evaluation of void-filling interpolation methods for SRTM data. Int. J. Geogr. Inf. Sci. 21, 983–1008.

Rientjes, T.H.M., Muthuwatta, L.P., Bos, M.G., Booij, M.J., Bhatti, H. a. A., 2013. Multi-variable calibration of a semi-distributed hydrological model using streamflow data and satellite-based evapotranspiration. J. Hydrol. 505, 276–290. https://doi.org/10.1016/j.jhydrol.2013.10.006

Ritchie, J.T., 1972. Model for predicting evaporation from a row crop with incomplete cover. Water Resour. Res. 8, 1204–1213.

Robert, H., 2013. Modeling the pond slope of Mono River with an equivalent electric scheme for flood forecasting in Nagbeto. Int. J. Sci. Eng. Res. 4, 5pp.

Robson, A.J., Kundzewicz, Z.W., Robson, A.J., 2004. Change detection in hydrological records - a review of the methodology. Hydrol. Sci. Journal-journal Des Sci. Hydrol. 49, 7–19. https://doi.org/10.1623/hysj.49.1.7.53993

Rodriguez, J.L.G., Suarez, M.C.G., 2012. Methodology for estimating the topographic factor LS of RUSLE3D and USPED using GIS. Geomorphology 175–176, 98–106. https://doi.org/10.1016/j.geomorph.2012.07.001

Rosenbaum, U., Bogena, H.R., Herbst, M., Huisman, J.A., Peterson, T.J., Weuthen, A., Western, A.W., Vereecken, H., 2012. Seasonal and event dynamics of spatial soil moisture patterns at the small catchment scale. Water Resour. Res. 48, 1–22. https://doi.org/10.1029/2011WR011518

Rossi, G., 1996. L'impact des barrages de la vallée du Mono (Togo-Benin). La gestion de l'incertitude. Géomorphologie Reli. Process. Environ. 2, 55–68. https://doi.org/10.3406/morfo.1996.878

Rössler, O., Diekkrüger, B., Löffler, J., 2012. Potential drought stress in a Swiss mountain catchment — Ensemble forecasting of high mountain soil moisture reveals a drastic decrease, despite major uncertainties. Water Resour. Res. 48, 1–19. https://doi.org/10.1029/2011WR011188

Rounsevell, M.D.A., Reginster, I., Araujo, M.B., Carter, T.R., Dendoncker, N., Ewert, F., House, J.I., Kankaanpää, S., Leemans, R., Metzger, M.J., Schmit, C., Smith, P., Tuck, G., 2006. A coherent set of future land use change scenarios for Europe. Agric. Ecosyst. Environ. 114, 57–68. https://doi.org/10.1016/j.agee.2005.11.027

Ruelland, D., Dezetter, A., Puech, C., Ardoin-Bardin, S., 2008. Long-term monitoring of land cover changes based on Landsat imagery to improve hydrological modelling in West Africa. Int. J. Remote Sens. 29, 3533–3551.

Sahin, S., 2012. An aridity index defined by precipitation and specific humidity. J. Hydrol. 444–445, 199–208. https://doi.org/10.1016/j.jhydrol.2012.04.019

Salmi, T., Määttä, A., Anttila, P., Ruoho-Airola, T., Amnell, T., 2002. Detecting trends of

annual values of atmospheric pollutants by the Mann-Kendall test and Sen's slope estimates-the Excel template application MAKESENS. Finnish Meteorological Institute (FMI): Helsinki, Finland.

Sanogo, S., Fink, A.H., Omotosho, J.A., Ba, A., Redl, R., Ermert, V., 2015. Spatio-temporal characteristics of the recent rainfall recovery in West Africa. Int. J. Climatol. 35, 4589–4605.

Sathian, K., Symala, P., 2009. Application of GIS integrated SWAT model for basin level water balance. Indian J. Soil Cons 37, 100–105.

SAWES, 2011. Etudes relatives a la promotion de trois (3) nouvelles organisations de bassins transfrontaliers en Afrique de l'ouest Cas du schéma du Bassin du Mono. Aougadougou, Burkina Faso.

Schewe, J., Heinke, J., Gerten, D., Haddeland, I., Arnell, N.W., Clark, D.B., Dankers, R., Eisner, S., Fekete, B.M., Colón-González, F.J., Gosling, S.N., Kim, H., Liu, X., Masaki, Y., Portmann, F.T., Satoh, Y., Stacke, T., Tang, Q., Wada, Y., Wisser, D., Albrecht, T., Frieler, K., Piontek, F., Warszawski, L., Kabat, P., 2014. Multimodel assessment of water scarcity under climate change. Proc. Natl. Acad. Sci. U. S. A. 111, 3245–3250. https://doi.org/10.1073/pnas.1222460110

Schneider, L.C., Pontius, R.G., 2001. Modeling land-use change in the Ipswich watershed, Massachusetts, USA. Agric. Ecosyst. Environ. 85, 83–94. https://doi.org/10.1016/S0167-8809(01)00189-X

Schoof, J.T., Robeson, S.M., 2016. Projecting changes in regional temperature and precipitation extremes in the United States. Weather Clim. Extrem. 11, 28–40. https://doi.org/10.1016/j.wace.2015.09.004

Schuol, J., Abbaspour, K.C., Srinivasan, R., Yang, H., Schuol, J., Abbaspour, K.C., Srinivasan, R., Yang, H., 2008. Estimation of freshwater availability in the West African sub-continent using the SWAT hydrologic model. J. Hydrol. 352, 30–49. https://doi.org/10.1016/j.jhydrol.2007.12.025

Sciuto, G., Diekkrüger, B., 2010. Infl uence of Soil Heterogeneity and Spatial Discretization on Catchment Water Balance Modeling. VadoseZoneJournal 9, 955–969. https://doi.org/10.2136/vzj2009.0166

Sen, A.K., Niedzielski, T., 2010. Statistical Characteristics of Riverflow Variability in the Odra River Basin , Southwestern Poland. Polish J. environement Stud. 19, 387–397.

Setegn, S.G., Srinivasan, R., Melesse, A.M., Dargahi, B., 2010. SWAT model application and prediction uncertainty analysis in the Lake Tana Basin, Ethiopia. Hydrol. Process. An Int. J. 24, 357–367.

Sintondji, L.O.C., 2005. Modelling the Rainfall Runoff Process in the Upper Ouémé Catchment (Terou in Bénin Republic) in a Context of Global Change: Extrapolation from the Local to the Regional Scale. Shaker, Shaker Publisher, Aachen.

Sintondji, L.O.C., Zokpodo, B., Ahouansou, D.., Vissin, W.E., Agbossou, K.E., 2014. Modelling the water balance of Ouémé catchment at the Savè outlet in Benin: contribution to the sustainable water resource management. Int. J. AgriScience 4, 74–

88.

Sitthi, A., Nagai, M., Dailey, M., Ninsawat, S., 2016. Exploring Land Use and Land Cover of Geotagged Social-Sensing Images Using Naive Bayes Classifier. Sustainability 8, 921. https://doi.org/10.3390/su8090921

Soil Survey Staff USA, 1975. Soil taxonomy: A basic system of soil classification for making and interpreting soil surveys. US Government Printing Office.

Soro, G., Noufé, D., Goula Bi, T., Shorohou, B., 2016. Trend Analysis for Extreme Rainfall at Sub-Daily and Daily Timescales in Côte d'Ivoire. Climate 4, 37. https://doi.org/10.3390/cli4030037

Speth, P., Christoph, M., Diekkrüger, B., 2010. Impacts of Global Change on the Hydrological Cycle in West and Northwest Africa, Springer S. ed. Springer Heidelberg, Germany. https://doi.org/10.1007/978-3-642-12957-5_1

Stehman, S. V., 2009. Sampling designs for accuracy assessment of land cover. Int. J. Remote Sens. 30, 5243–5272. https://doi.org/10.1080/01431160903131000

Stocker, T., 2014. Climate change 2013: the physical science basis: Working Group I contribution to the Fifth assessment report of the Intergovernmental Panel on Climate Change. Cambridge University Press.

Sun, B., Robinson, D., 2018. Comparison of Statistical Approaches for Modelling Land-Use Change. land 7, 144. https://doi.org/10.3390/land7040144

Sutton, P., 1997. Modeling population sensity with night-timed satellite imagery and GIS. Comput. Environ. Urban Syst. 21, 227–244.

Sylla, M.B., Giorgi, F., Coppola, E., Mariotti, L., 2013. Uncertainties in daily rainfall over Africa: Assessment of gridded observation products and evaluation of a regional climate model simulation. Int. J. Climatol. 33. https://doi.org/10.1002/joc.3551

Sylla, M.B., Pinghouinde, M.K., Gibba, P., Kebe, I., Klutse, N.A.B., Nikiema, P.M., Gibba, P., Kebe, I., Ama, N., Klutse, B., 2016. Climate Change over West Africa: Recent Trends and Future Projections, in: Hesselberg, J.A.Y. and J. (Ed.), Adaptation to Climate Change and Variability in Rural West Africa. Springer International Publishing, pp. 25–40. https://doi.org/10.1007/978-3-319-31499-0

Tabari, H., Aeini, A., Talaee, P.H., Some, B.S., 2012. Spatial distribution and temporal variation of reference evapotranspiration in arid and semi-arid regions of Iran. Hydrol. Process. 26, 500–512. https://doi.org/10.1002/hyp.8146

Tairou, M.S., Affaton, P., Anum, S., Fleury, T.J., 2012. Pan-African paleostresses and reactivation of the Eburnean basement complex in Southeast Ghana (West Africa). J. Geol. Res. 2012, 15. https://doi.org/10.1155/2012/938927

Tall, M., Sylla, M.B., Diallo, I., Pal, J.S., 2016. Projected impact of climate change in the hydroclimatology of Senegal with a focus over the Lake of Guiers for the twenty-first century. Theor. Appl. Climatol. 1–12. https://doi.org/10.1007/s00704-016-1805-y

Tan, M.L., Ibrahim, A.L., Yusop, Z., Duan, Z., Ling, L., 2015. Impacts of land-use and

climate variability on hydrological components in the Johor River basin, Malaysia. Hydrol. Sci. J. 60, 873–889. https://doi.org/10.1080/02626667.2014.967246

Tan, M.L., Samat, N., Chan, N.W., Lee, A.J., Li, C., 2019. Analysis of precipitation and temperature extremes over the Muda River Basin, Malaysia. Water (Switzerland) 11, 1–16. https://doi.org/10.3390/w11020283

Tegegne, G., Park, D.K., Kim, Y., 2017. Comparison of hydrological models for the assessment of water resources in a data-scarce region , the Upper Blue Nile River Basin. J. Hydrol. Reg. Stud. 14, 49–66. https://doi.org/10.1016/j.ejrh.2017.10.002

Teutschbein, C., Seibert, J., 2012. Bias correction of regional climate model simulations for hydrological climate-change impact studies: Review and evaluation of different methods. J. Hydrol. 456–457, 12–29. https://doi.org/10.1016/j.jhydrol.2012.05.052

Thenmozhi, M., Kottiswaran, S.S., 2016. Aalysis of rainfall trend using Mann-Kendall test and the Sen's slope estimation in Udumalpet of future district in Tamil Nadu. Int. J. Agric. Sci. Res. 6, 131–138.

Théveniaut, H., Thiéblemont, D., 2016. Geological mapping for mining development in West Africa. Geosciences pp-22.

Thibaut, A., Tchuenté, K., Roujean, J., Jong, S.M. De, 2011. Comparison and relative quality assessment of the GLC2000, GLOBCOVER, MODIS and ECOCLIMAP land cover data sets at the African continental scale. Int. J. Appl. Earth Obs. Geoinf. 13, 207–219. https://doi.org/10.1016/j.jag.2010.11.005

Thiessen, A.H., 1911. Precipitation averages for large areas. Mon. Weather Rev. 39, 1082–1089.

Thompson, J.R., Green, A.J., Kingston, D.G., 2014. Potential evapotranspiration-related uncertainty in climate change impacts on river flow: An assessment for the Mekong River basin. J. Hydrol. 510, 259–279. https://doi.org/10.1016/j.jhydrol.2013.12.010

Tian, Y., Booij, M.J., Xu, Y.P., 2014. Uncertainty in high and low flows due to model structure and parameter errors. Stoch. Environ. Res. Risk Assess. 28, 319–332. https://doi.org/10.1007/s00477-013-0751-9

Trambauer, P., Maskey, S., Winsemius, H., Werner, M., Uhlenbrook, S., 2013. A review of continental scale hydrological models and their suitability for drought forecasting in (sub-Saharan) Africa. Phys. Chem. Earth Parts A/B/C 66, 16–26. https://doi.org/10.1016/j.pce.2013.07.003

Tramblay, Y., Amoussou, E., Dorigo, W., Mahé, G., 2014. Flood risk under future climate in data sparse regions: Linking extreme value models and flood generating processes. J. Hydrol. 519, 549–558. https://doi.org/10.1016/j.jhydrol.2014.07.052

Tuo, Y., Duan, Z., Disse, M., Chiogna, G., 2016. Evaluation of precipitation input for SWAT modeling in Alpine catchment: A case study in the Adige river basin (Italy). Sci. Total Environ. 573, 66–82. https://doi.org/10.1016/j.scitotenv.2016.08.034

Turner, B.L., Meyer, W.B., Skole, D.L., 1994. Global land-use/land-cover change: towards an integrated study. Ambio. Stock. 23, 91–95.

Václavík, T., Rogan, J., 2009. Identifying Trends in Land Use/ Land Cover Changes in the Context of Post-Socialist Transformation in Central Europe: A Case Study of the Greater Olomouc Region, Czech Republic. GIScience Remote Sens. 46, 54–76. https://doi.org/10.2747/1548-1603.46.1.54

Van Esse, W.R., Perrin, C., Booij, M.J., Augustijn, D.C.M., Fenicia, F., Kavetski, D., Lobligeois, F., Esse, W.R. Van, Perrin, C., Booij, M.J., Augustijn, D.C.M., Fenicia, F., Kavetski, D., Lobligeois, F., 2013. The influence of conceptual model structure on model performance: A comparative study for 237 French catchments. Hydrol. Earth Syst. Sci. 17, 4227–4239. https://doi.org/10.5194/hess-17-4227-2013

Van Griensven, A., Bauwens, W., 2003. Multiobjective autocalibration for semidistributed water quality models. Water Resour. Res. 39, 1–9. https://doi.org/10.1029/2003WR002284

Van Griensven, A., Meixner, T., 2006. Methods to quantify and identify the sources of uncertainty for river basin water quality models. Water Sci. Technol. 53, 51–59.

van Griensven, A. van, Meixner, T., Grunwald, S., Bishop, T., Diluzio, M., Srinivasan, R., 2006. A global sensitivity analysis tool for the parameters of multi-variable catchment models. J. Hydrol. 324, 10–23.

Vansteenkiste, T., Tavakoli, M., Van Steenbergen, N., De Smedt, F., Batelaan, O., Pereira, F., Willems, P., 2014. Intercomparison of five lumped and distributed models for catchment runoff and extreme flow simulation. J. Hydrol. 511, 335–349. https://doi.org/10.1016/j.jhydrol.2014.01.050

Varado, N., Braud, I., Galle, S., Lay, M. Le, 2006. Multi-criteria assessment of the Representative Elementary Watershed approach on the Donga catchment (Benin) using a downward approach of model complexity. Hydrol. Earth Syst. Sci. 10, 427–442.

Vaze, J., Jordan, P., Beecham, R., Frost, A., Summerell, G., 2011. Guidelines for Rainfall-Runoff Modelling: Towards Best Practice Model Application. Innovation Centre, Building 22 University Drive South Bruce, ACT, 2617, Australia2617.

Veldkamp, A., Lambin, E.F., 2001. Predicting land-use change. Agric. Ecosyst. Environ. 85, 1–6. https://doi.org/10.1016/S0167-8809(01)00199-2

Verburg, P.H., Veldkamp, A., 2002. Modeling the Spatial Dynamics of Regional Land Use: The CLUE-S Model. Environ. Manage. 30, 391–405. https://doi.org/https://doi.org/10.1007/s00267-002-2630-x

Vereecken, H., Huisman, J.A., Pachepsky, Y., Montzka, C., van der Kruk, J., Bogena, H.R., Weihermüller, L., Herbst, M., Martinez, G., Vanderborght, J., 2013. On the spatio-temporal dynamics of soil moisture at the field scale. J. Hydrol. https://doi.org/10.1016/j.jhydrol.2013.11.061

Verstraeten, W., Veroustraete, F., Feyen, J., 2008. Assessment of Evapotranspiration and Soil Moisture Content Across Different Scales of Observation. Sensors 8, 70–117.

Vilaysane, B., Takara, K., Luo, P., Akkharath, I., 2015. Hydrological stream flow modelling for calibration and uncertainty analysis using SWAT model in the Xedone river basin ,

Lao PDR. Procedia Environ. Sci. 28, 380–390. https://doi.org/10.1016/j.proenv.2015.07.047

Wagener, T., Boyle, D.P., Lees, M.J., Wheater, H.S., Gupta, H. V, Sorooshian, S., 2001. A framework for development and application of hydrological models. Hydrol. Earth Syst. Sci. 5, 13–26. https://doi.org/10.5194/hess-5-13-2001

Wagner, S., Kunstmann, H., Bárdossy, A., Conrad, C., Colditz, R.R., 2009. Water balance estimation of a poorly gauged catchment in West Africa using dynamically downscaled meteorological fields and remote sensing information. Phys. Chem. Earth 34, 225–235. https://doi.org/10.1016/j.pce.2008.04.002

Watanabe, S., Hajima, T., Sudo, K., Nagashima, T., Takemura, T., Okajima, H., Nozawa, T., Kawase, H., Abe, M., Yokohata, T., 2011. MIROC-ESM 2010: Model description and basic results of CMIP5-20c3m experiments. Geosci. Model Dev. 4, 845.

White, K.L., Chaubey, I., 2005. Sensitivity analysis, calibration, and validations for a multisite and multivariable SWAT model 1. JAWRA J. Am. Water Resour. Assoc. 41, 1077–1089.

Wilson, D., Hisdal, H., Lawrence, D., 2010. Has streamflow changed in the Nordic countries? – Recent trends and comparisons to hydrological projections. J. Hydrol. 394, 334–346. https://doi.org/10.1016/j.jhydrol.2010.09.010

Wisser, D., Frolking, S., Douglas, E.M., Fekete, B.M., Schumann, A.H., Vörösmarty, C.J., 2010. The significance of local water resources captured in small reservoirs for crop production – A global-scale analysis. J. Hydrol. 384, 264–275. https://doi.org/10.1016/j.jhydrol.2009.07.032

Wösten, J.H.M., Pachepsky, Y.A., Rawls, W.J., 2001. Pedotransfer functions: bridging the gap between available basic soil data and missing soil hydraulic characteristics. J. Hydrol. 251, 123–150.

Wu, H., Chen, B., 2015. Evaluating uncertainty estimates in distributed hydrological modeling for the Wenjing River watershed in China by GLUE, SUFI-2, and ParaSol methods. Ecol. Eng. 76, 110–121.

Wu, T., Song, L., Li, W., Wang, Z., Zhang, H., Xin, X., Zhang, Y., Zhang, L., Li, J., Wu, F., 2014. An overview of BCC climate system model development and application for climate change studies. J. Meteorol. Res. 28, 34–56. https://doi.org/10.1007/s13351-014-3041-7

Xie, H., Longuevergne, L., Ringler, C., Scanlon, B.R., 2012. Calibration and evaluation of a semi-distributed watershed model of Sub-Saharan Africa using GRACE data. Hydrol. Earth Syst. Sci. 16, 3083–3099. https://doi.org/10.5194/hess-16-3083-2012

Yabi, I., Afouda, F., 2012. Extreme rainfall years in Benin (West Africa). Quat. Int. 262, 39–43. https://doi.org/10.1016/j.quaint.2010.12.010

Yamba, F.D., Walimwipi, H., Jain, S., Zhou, P., Cuamba, B., Mzezewa, C., 2011. Climate change/ variability implications on hydroelectricity generation in the Zambezi River Basin. Mitig. Adapt. Strateg. Glob. Chang. 16, 617–628. https://doi.org/10.1007/s11027-011-9283-0

Yan, T., Bai, Z., 2017. Spatial and Temporal Changes in Temperature, Precipitation, and Streamflow in the Miyun Reservoir Basin of China. Water 9, 78. https://doi.org/10.3390/w9020078

Yang, T., Li, H., Wang, W., Xu, C., Yu, Z., 2012. Statistical downscaling of extreme daily precipitation , evaporation , and temperature and construction of future scenarios. Hydrol. Process. 26, 3510–3523. https://doi.org/10.1002/hyp.8427

Yira, Y., Diekkrüger, B., Steup, G., Bossa, A.Y., 2016. Modeling land use change impacts on water resources in a tropical West African catchment (Dano , Burkina Faso). J. Hydrol. 537, 187–199. https://doi.org/10.1016/j.jhydrol.2016.03.052

Youssef, A.M., Pradhan, B., Hassan, A.M., 2010. Flash flood risk estimation along the St . Katherine road , southern Sinai , Egypt using GIS based morphometry and satellite imagery. Environ. Earth Sci. 63, 611–623. https://doi.org/10.1007/s12665-010-0551-1

Zargar, A., Sadiq, R., Naser, B., Khan, F.I., 2011. A review of drought indices. Environ. Rev. 19, 333–349.

Zhang, L., O'Neill, A.L., Lacey, S., 1996. Modelling approaches to the prediction of soil erosion in catchments. Environ. Softw. 11, 123–133. https://doi.org/10.1016/S0266-9838(96)00023-8

Zhang, W., Wang, Y., Peng, H., Li, Y., Tang, J., Wu, K.B., 2010. A Coupled Water Quantity – Quality Model for Water Allocation Analysis. Water Resour. Manag. 24, 485–511. https://doi.org/10.1007/s11269-009-9456-8

Zhang, X., Feng, Y., Chan, R., 2018. Introduction to RClimDex v1 . 9. Climate Research Division Environment Canada Downsview, Ontario Canada.

Zhang, X., Xu, Y., Fu, G., 2014. Uncertainties in SWAT extreme flow simulation under climate change. J. Hydrol. 515, 205–222. https://doi.org/10.1016/j.jhydrol.2014.04.064

Zoungrana, B.J., Conrad, C., Amekudzi, L.K., Thiel, M., Da, E.D., Forkuor, G., Löw, F., 2015. Multi-Temporal Landsat Images and Ancillary Data for Land Use/Cover Change (LULCC) Detection in the Southwest of Burkina Faso, West Africa. Remote Sens. 7, 12076–12102. https://doi.org/10.3390/rs70912076

http://worldpopulationreview.com/countries/togo-population accessed on 25/09/2018

http://www.worldbank.org accessed on 25/09/2018

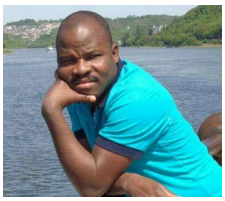

Candidate biography

Mr **Djan'na KOUBODANA HOUTETA** was born in Koka canton (Togo). He attended at Lycee Kpangalam (Sokode, Togo) secondary school where he got his scientific Baccalaureat in 2006. Afterward his baccalaureat he continued his studies at Faculty of Sciences at University of Lomé (Togo) where he received his Master degree (ex-Maîtrise) in theorical physics in 2011. After three years of physic and chemist ry teaching at governmental and private secondary schools at Lomé (Togo), he was granted by IRD &Total French scholarship for his master's degree in environmental science (option physical oceanography and applications) in sandwich between university of Paul Sabatier of Toulouse III (France) and university of Abomey Calavi (UAC) (Benin) and he was graduated in 2015. In 2016, Djan'na was selected within many West African candidates for German government scholarship under the West African Science Service Center on Climate Change and Adapted Land Use (WASCAL) program for his doctoral thesis in Climate change and water resource at UAC in partnership with university of Bonn (Germany) where he stayed eight months for scientific visit within hydrology research group. He is expert in climate change, surface hydrology, extreme events, remote sensing –geographic information system, water resource management, oceanography and physics sciences. He has many articles in peer reviewed international journals.

Abstract: The understanding of the impacts of climate, land-use changes and reservoir management on water cycle components enable the development of sustainable water resources strategies in West Africa. In study objectives were to evaluate three different land cover datasets between 1975 and 2013, to investigate climate change detection on hydro-climatic datasets over the period of 1961 to 2016, to predict and compare discharge using lumped, semi- distributed hydrological model and to assess water balance components changes for two baseline periods with different land use and land cover (LULC), and climate conditions over Mono River Basin in West Africa.

The methodologies approaches consist to land cover reclassification and prediction using the Terrset Land Change Modeler. Afterward, non-parametric Mann Kendall (MK) trend analysis of historical hydro-climatic data which were used as inputs in lumped models, GR4J (Génie Rural à 4 paramètres Journaliers), IHACRES (Identification of unit Hydrographs and Component flows from Rainfall, Evapotranspiration and Stream data) and SWAT (Soil, and Water Assessment Tool SWAT) simulations. The results indicate an increase of cropland area of 30.97% from 1975 to 2013 which is related to the increase in population and their food demand, while the losses of forest area and the decrease of savanna are further amplified by using wood as energy sources and the lack of forest management. The three datasets were used to simulate future LULC changes using the Terrset Land Change Modeler. CILSS data was utilized to predict LULC distribution for the years 2020 and 2027 because of its satisfactory performances. Concerning, climate change detection analysis reveals positive and negative trends of hydro-climatic data over Mono River Basin (MRB) from 1961 to 2016. Mean temperatures increase significantly in most of the stations while a negative non-significant trend is noticed for rainfall. Meanwhile, the discharge presents a significant seasonal and annual trend for three gauge stations investigated and acceptable accuracy of validated ensemble climate models allow the computation of extreme climatic indices under RCP4.5 and RCP8.5 scenarios which shows a significant annual trend of some extreme climatic indices of rainfall and temperature at selected stations between 2020 and 2045. The analysis indicates that the two lumped models discharge predictions are acceptable with evaluation efficiencies over before dam installation period (1964 – 1986) and more and less acceptable during after dam installation period (1988-2010). IHACRES model was found to underestimating extreme high runoff in the downstream of MRB (1964-1986). The simulation of SWAT model performances and uncertainty analysis show that there are good model performances show acceptable parameters values range between 1964 and 1986 and poor performances during the second period. An individual assessment of runoff, evapotranspiration and water yield components shows that its seasonal and annual variability depends to different land-use type change, climate conditions and also of the presence or not of reservoir in the watershed. This implicate that the implementation of the dam in the MRB in 1987 has affected on the hydrological system of the river. Land use land cover change with the amplification of climate change are the others drivers that involve this change. The study has proposed effective strategies for better planning and management of water resources in West African basin.

Keywords: Land covers change; climate change detection; sensitive analysis; dam management; hydrological modeling; Mono River Basin.

PhD	Djan'na. KOUBODANA HOUTETA	MODELING THE IMPACTS OF CLIMATE CHANGE, LAND USE AND DAM MANAGEMENT ON WATER RESOURCES IN WAEST AFRICA: CASE OF THE MONO RIVER BASIN, TOGO-BENIN	GRP/CCWR/INE/WASCAL – UAC 02, 2020